JOURNAL OF THE

Electrochemical Society

ol. 108, No. 6 June 1961

The Electrochemical Society
Founded in Philadelphia 1902
Incorporated 1930

GLC Anodes Are CUSTOM MADE

for

Olin

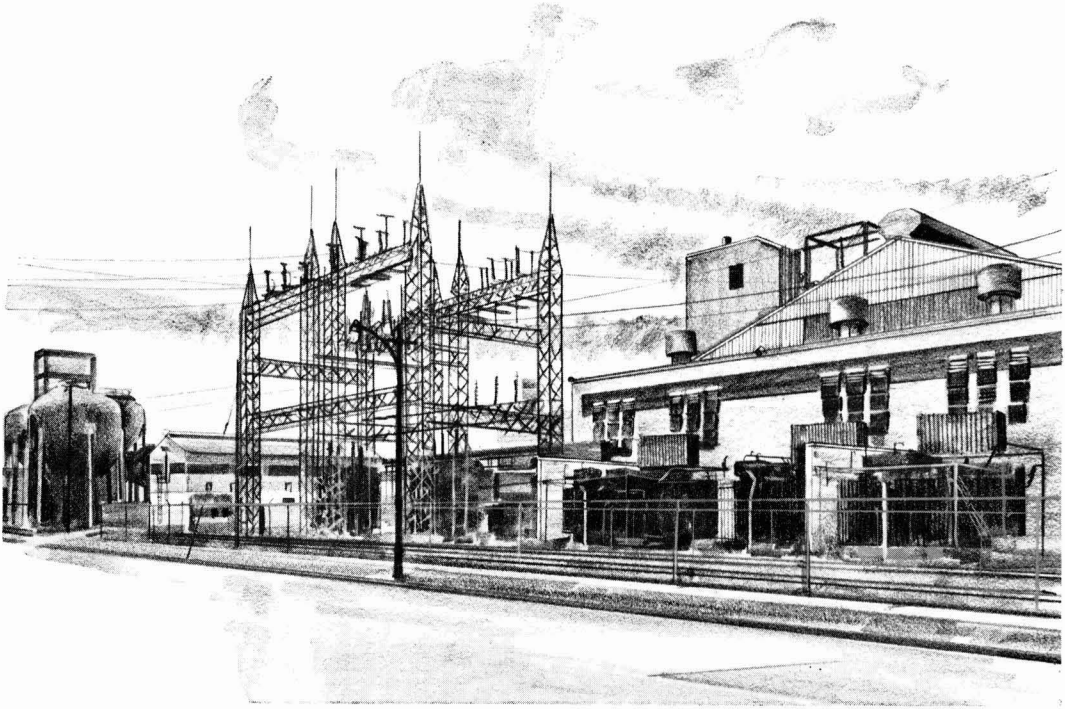

The Olin Mathieson Chlor-Alkali Plant at Niagara Falls, New York

TECHNICAL TEAMWORK with our chlor-alkali customers provides a base for continuing improvements in GLC anode performance. Our program of progress gives GLC anode customers better results now than ever before — seeks still better results in the years ahead.

SHARE THE REWARDS of this program by putting custom made GLC anodes to work now in your electrolytic cells. We can then help you develop the technical information and specifications needed to improve cell efficiency and lower your operating costs.

PRODUCTS YOU CAN TRUST ® ELECTRODE GLC DIVISION

GREAT LAKES CARBON CORPORATION

18 EAST 48TH STREET, NEW YORK 17, N.Y. OFFICES IN PRINCIPAL CITIES

Journal of the
Electrochemical Society

JUNE 1961 VOL. 108 • NO. 6

Manuscripts submitted to the Journal should be sent, in triplicate, to the Editorial Office at 1860 Broadway, New York 23, N. Y. They should conform to the revised Instructions to Authors, last published on pp. 46C-47C of the March 1961 issue. Manuscripts so submitted become the property of The Electrochemical Society and may not be published elsewhere, in whole or in part, unless permission is requested of and granted by the Editor.

The Electrochemical Society does not maintain a supply of reprints of papers appearing in its Journal. A photoprint copy of any particular paper, however, may be obtained by corresponding directly with the Engineering Societies Library, 29 W. 39 St., New York 18, N. Y.

Inquiries re positive microfilm copies of volumes should be addressed to University Microfilms, Inc., 313 N. First St., Ann Arbor, Mich.

Walter J. Johnson, Inc., 111 Fifth Ave., New York 3, N. Y., have reprint rights of out-of-print volumes of the Journal, and also have available for sale back volumes and single issues, with the exception of the current calendar year. Anyone interested in securing back copies should correspond direct with them.

CONTENTS

Published monthly by The Electrochemical Society, Inc., from Manchester, N. H., **Executive Offices, Editorial Office** and **Circulation Dept.**, and **Advertising Office** at 1860 Broadway, New York 23, N. Y., combining the JOURNAL and TRANSACTIONS OF THE ELECTROCHEMICAL SOCIETY. Statements and opinions given in articles and papers in the JOURNAL OF THE ELECTROCHEMICAL SOCIETY are those of the contributors, and The Electrochemical Society assumes no responsibility for them. Subscription to members as part of membership service; subscription to nonmembers $24.00. Single copies $1.70 to members, $2.25 to nonmembers. Entered as second-class matter at the Post Office at Manchester, N. H., under the act of August 24, 1912.

Editorial

The Role of The Electrochemical Society

IN our opinion, it is wise that an organization such as ours should stop periodically and take an inventory to determine just what service we do render to science and industry. The Electrochemical Society is, by nature, considerably different from the American Chemical Society, the American Physical Society, the American Institute of Chemical Engineers, the American Institute of Metallurgical Engineers, etc., since these organizations are considered to be professional in nature, in that we all recognize chemistry as a profession, chemical engineering as a profession, etc.

On the other hand, electrochemistry is not a profession in the same sense and, therefore, it becomes our duty periodically to evaluate our position. What do we do to justify our existence? Do we perform a service for our members that no other organization can perform, or do we better perform services that others also can perform? The record, to a certain extent, speaks for itself. Our Society has had a normal existence up to about ten years ago, at which time the membership increase started in earnest, and we now have about half again as many members as we did then. This would indicate that we are doing something worthwhile.

Let us examine the situation to see if we can determine just what this function can be. We hold technical meetings twice a year which bring together a wide variety of disciplines, physics, chemistry, chemical engineering, metallurgy, electrical engineering, and others, for discussion of common problems. This, if for no other reasons, is a justification for our existence.

Of course, in addition to holding of meetings, we publish the JOURNAL, which is now entering into its fourteenth year. A remarkable record has been set here in the quality of publication. The JOURNAL makes available a medium for papers that are in the "in between" areas generated at the meetings of the several disciplines, which naturally occur with national Society conventions of the nature already discussed. This in no way detracts from the value of the papers. As a matter of fact, it enhances their status since, always, crossbreeding leads to strengthening of the lines. We should always strive to maintain this sounding board for mixed disciplines. We think that this is the strong point of our Society, one that has maintained and nurtured the organization through nearly sixty years, with the last ten being the most vigorous of all.

Your Officers are always busy attempting to be sure that the coverage of areas most appropriate to our organization is complete. Any suggestions that members have to make with respect to the handling of our affairs will always be welcome.

—H. B. LINFORD[1]

[1] President of The Electrochemical Society, 1961-1962; Columbia University, Dept. of Chemical Engineering, New York, N. Y.

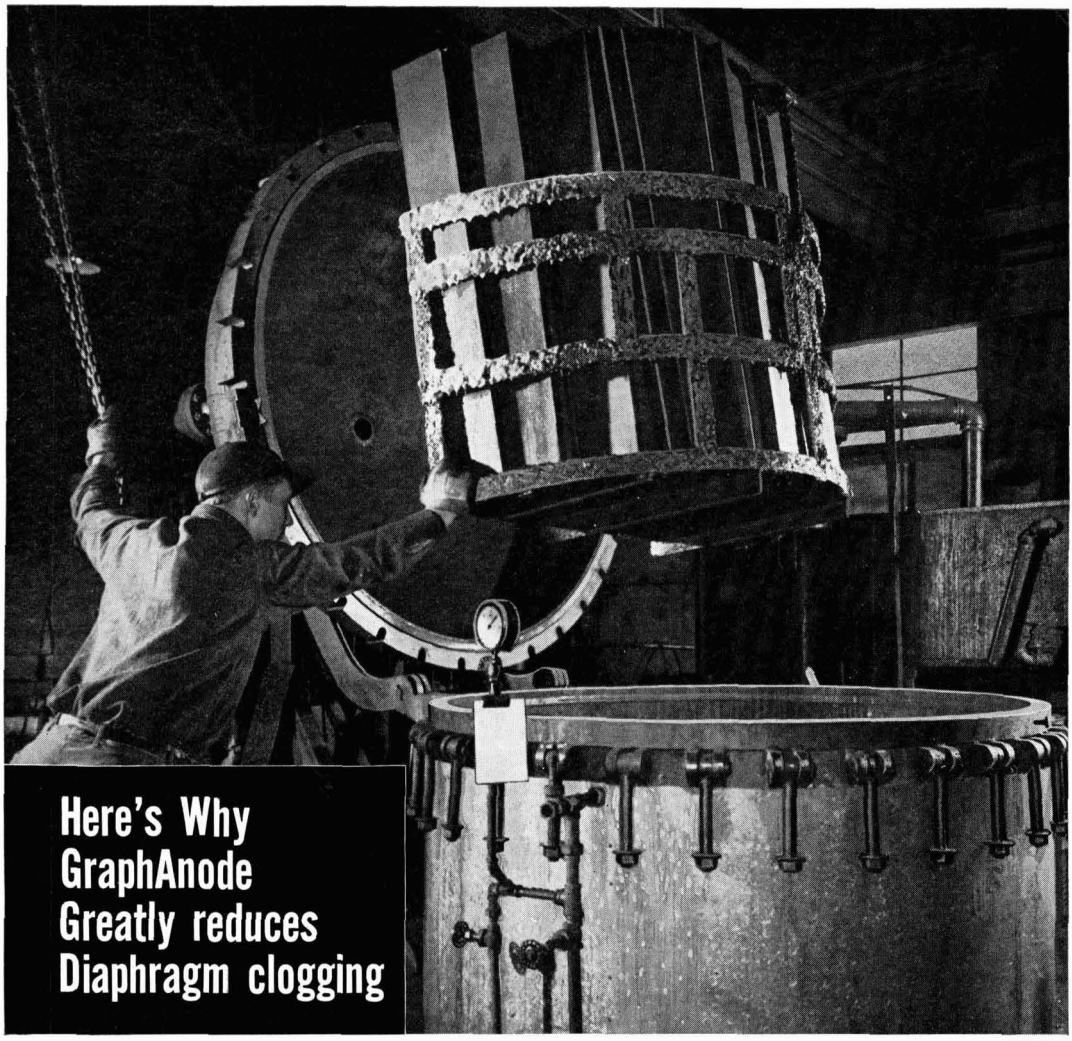

. . . and whack down cell maintenance costs accordingly

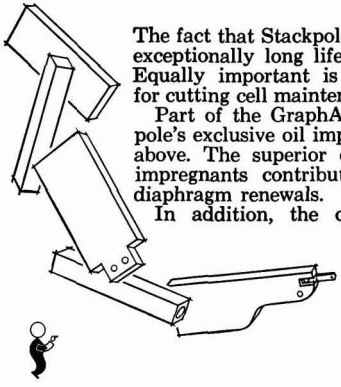

The fact that Stackpole GraphAnode anodes have exceptionally long life is only part of the story. Equally important is their enviable reputation for cutting cell maintenance costs.

Part of the GraphAnode "secret" is in Stackpole's exclusive oil impregnation process pictured above. The superior chemical resistance of the impregnants contributes substantially to fewer diaphragm renewals.

In addition, the carefully-machined GraphAnode anodes present outstandingly uniform, low-porosity surfaces to the electrolyte. The graphite is consumed slowly and evenly. It does not slough off to contaminate the cell.

Inevitably, the result is many more useful cell operating hours — and with the added advantage of low cell voltages. For a convincing demonstration on your own equipment, we suggest you get *in touch with Stackpole now.*

STACKPOLE CARBON CO., St. Marys, Pa.

CATHODIC PROTECTION ANODES • TUBE ANODES • BEARINGS • SEAL RINGS FLUXING & DE-GASSING TUBES • SALT BATH RECTIFICATION RODS • ELECTRODES & HEATING ELEMENTS • POROUS CARBON • WELDING CARBONS • ROCKET NOZZLES • VOLTAGE REGULATOR DISCS • MOLDS & DIES • "CERAMAGNET"® CERAMIC MAGNETS • ELECTRICAL CONTACTS • BRUSHES for all rotating electrical equipment • and many other carbon, graphite and electronic components

STACKPOLE

GraphAnode®

ELECTROCHEMICAL ANODES

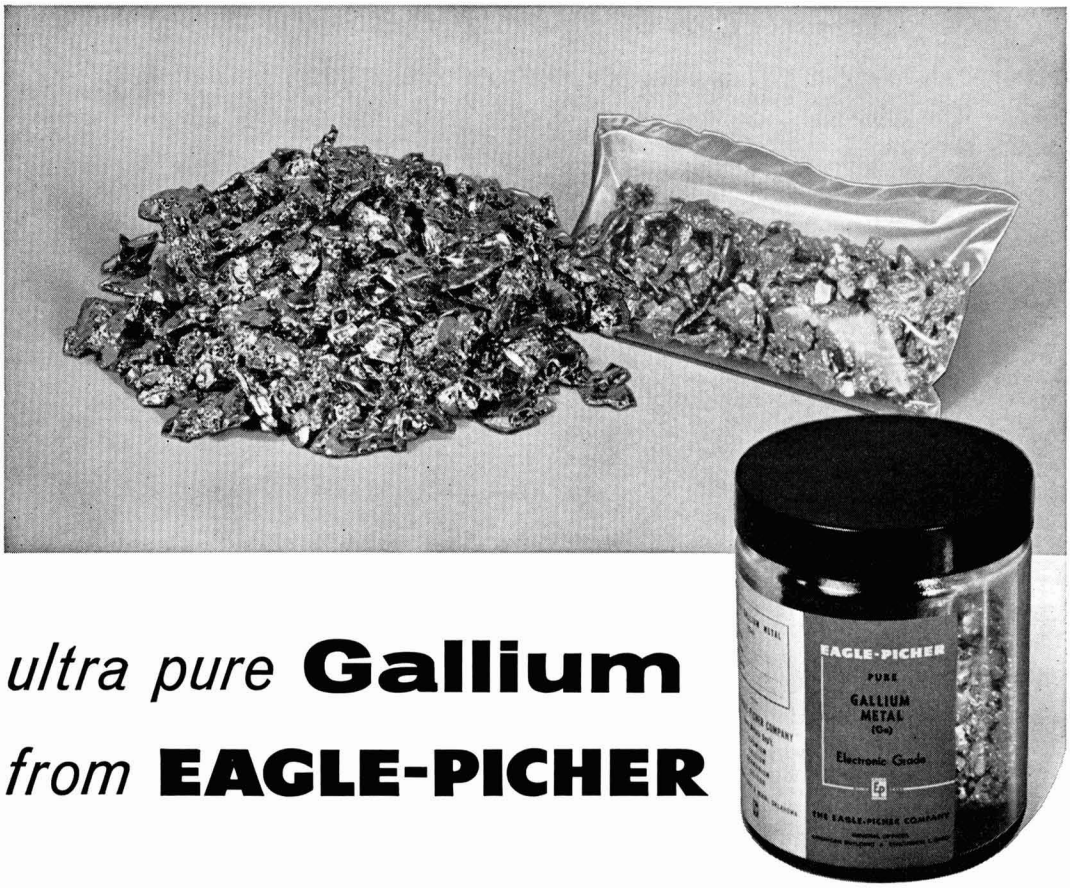

ultra pure **Gallium** *from* **EAGLE-PICHER**

New applications for Gallium are being discovered and to meet the growing demand for this rare metal, Eagle-Picher offers painstaking production and dependable supply. We offer, also, a complete line of Germanium products.

Eagle-Picher Rare Metals and Semiconductors

GALLIUM, ultra pure.
Metallic crystals, minimum purity 99.9999%
Metallic crystals, minimum purity 99.999%

GALLIUM SESQUIOXIDE

—*also immediately available*

CADMIUM SULPHIDE

GERMANIUM DIOXIDE, minimum purity 99.999%

FIRST REDUCTION GERMANIUM METAL, minimum resistivity 5 ohm-cm.

INTRINSIC GERMANIUM METAL, minimum resistivity 40 ohm-cm.

SINGLE CRYSTAL GERMANIUM (undoped) minimum resistivity 30 ohm-cm.

SINGLE CRYSTAL GERMANIUM (doped) to customers' specified resistivity.

SPECIAL SHAPES. Intrinsic Germanium Metal for horizontal or vertical crystal growing. Wide variety in stock, other shapes furnished to customers' specifications.

SCRAP GERMANIUM PLAN. Scrap Germanium may be returned for economical reprocessing under a toll arrangement.

EAGLE EP PICHER

Since 1843
THE EAGLE-PICHER COMPANY
Chemical Division, Dept. JES-661
GENERAL OFFICES: CINCINNATI 1, OHIO

Experiments on the Discharge Mechanism of the Manganese Dioxide Electrode

W. C. Vosburgh and Pao-Soong Lou

Department of Chemistry, Duke University, Durham, North Carolina

ABSTRACT

Complete discharge curves of electrodeposited α- and γ-MnO_2 electrodes in an electrolyte of *p*H 7.5 are compared. Oxide on the electrode at the end of discharge had the composition $MnO_{1.57}$ for γ- and $MnO_{1.66}$ for α-MnO_2. In the later portions of both discharges the rate of increase of Mn^{++} in the electrolyte is equivalent to the current. The effect of larger concentrations of Mn^{++} in the electrolyte on the discharge curve is shown. A method is developed for the dissolving of surface oxides from a partially or wholly discharged electrode and measuring Mn(II) and Mn(III). The amounts recovered were only a small fraction of Mn(IV) reduced even when no Mn^{++} was appearing in solution.

A theory of the discharge mechanism of the MnO_2 electrode has been proposed (1, 2). It is based on the assumption that the polarization is mainly a solid-state concentration polarization (3). In electrolytes of *p*H 7-8 the discharge product remains within the oxide structure in the early part of the discharge causing a decrease in open-circuit potential (2). Some additional experiments in harmony with this theory now are reported.

The theory has been based on experiments with electrodes formed by electrodeposition of MnO_2 on graphite rods. A different theory (4) has been based mainly on experiments with Leclanché cells. An important difference between the discharges of the two types of electrode is pointed out.

Preparation and Discharge of Electrodes

Electrodes were prepared by electrodeposition of MnO_2 on cylindrical graphite rods 0.48 cm in diameter and 5.1 cm exposed length having an apparent area of 8 cm^2 (2, 3, 5). The MnO_2 was deposited at 80°C by a current of 25 ma for 30 min, giving usually about 0.2 millimole. Two baths were used, both 0.33M $MnSO_4$ and 0.67M H_2SO_4 and one of them containing in addition 0.3M $(NH_4)_2SO_4$. It is assumed that the MnO_2 deposited from the bath without $(NH_4)_2SO_4$ was γ-MnO_2 and that the other was α-MnO_2 (5).

The electrodes were washed by allowing them to stand in 0.01M $(NH_4)_2SO_4$ with daily change until no Mn^{++} was detected in the wash solution. Then they were kept either in distilled water or in the wash solution until used.

For discharge an electrode was mounted centrally in a 300-ml tall-form beaker with a clean sheet-Pb electrode lining the inner surface of the beaker. The electrolyte was 1M $(NH_4)_2SO_4$ with NH_3 added to give *p*H 7.5, except as otherwise noted. The volume of electrolyte was 220-240 ml. A Luggin capillary allowed measurement of the MnO_2 electrode potential against a saturated calomel electrode, and a gas inlet tube led in a current of N_2 during discharges. The gas was well washed with the electrolyte before introduction into the cell to prevent removal of NH_3 and *p*H change. Discharges were made at room temperature, which was usually 25° ± 2°C. The electrolyte was stirred mechanically.

A hand-regulated current of 2 ma from 3 No. 6 dry cells in series (with the necessary resistance) was passed between the Pb and MnO_2 electrodes until the potential of the latter had fallen to zero against the calomel electrode. The MnO_2 electrode potential was measured by a recording potentiometer. The *p*H was measured by a *p*H meter.

Discharge curves for γ- and α-MnO_2 are given in Fig. 1. These are average curves for 5 γ-MnO_2 and 3 α-MnO_2 electrodes, respectively. The curves are much like similar ones given by Sam (6), showing that the difference between the two kinds of MnO_2 is reproducible. Previously (5) only the earlier parts of the curves have been shown.

The discharge products.—The Mn^{++} in solution at the end of discharge was determined colorimetrically as MnO_4^-, and the residue on the discharged electrode was analyzed for available oxygen and total Mn. Average results are shown in Table I. The variation among the individual electrodes, though considerable, was much smaller than the differences between the two averages shown.

Sam (6) in attempting the analysis of the residue found that the procedure used to wash it (with Na_2SO_4 solution) caused a loss of Mn. In the present work washing with water was kept to a minimum

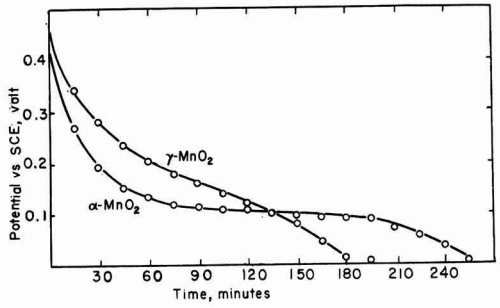

Fig. 1. Discharge curves to zero cut-off against the saturated calomel electrode of γ-MnO_2 and α-MnO_2 electrodes in an electrolyte of 1M $(NH_4)_2SO_4$ and NH_3, pH 7.5.

Table I. Discharge data for γ-MnO_2 and α-MnO_2 electrodes, averages of 5 and 3, respectively; electrolyte 1M $(NH_4)_2SO_4$ and NH_3, pH 7.5, 25° ± 1°C; see curves, Fig. 1

	Discharged electrode					
MnO_2	Avail. oxygen, mmole	Total Mn, mmole	x in MnO_x	Discharge, ma-min	Mn^{++} in solution, mmole	Original x in MnO_x
γ	0.079	0.139	1.57	352	0.056	1.97
α	0.039	0.058	1.66	506	0.152	1.95

and the residue was analyzed by the cold $FeSO_4$ method (7). In this method contamination by $(NH_4)_2SO_4$ does not interfere. The electrodes were always removed from the cell vessels immediately after the end of the discharge.

Although the amount of residue on the discharged electrodes and the Mn^{++} in solution and the electrical capacity varied considerably among the individual electrodes, the composition of the discharged oxide was much less variable. For γ-MnO_2 the extreme values were, for x in MnO_x, 1.55 and 1.58. For α-MnO_2 the corresponding values were 1.61 and 1.70. The difference between the two kinds of electrodes is consistent with the theory (1) that penetration of the lattice by protons is a part of the discharge process (8, 9) and that α-MnO_2 is less penetrable than γ-MnO_2.

In the last column the composition of the original oxide, as calculated from the discharge data assuming 100% current efficiency, is given. The standard deviation for γ-MnO_2 was 0.02. Analysis of 5 undischarged γ-MnO_2 electrodes gave 1.99 ± 0.02 for x. For α-MnO_2 analysis of 2 undischarged electrodes gave 1.95.

The agreement of calculated and observed original compositions is a check on the experimental work and the assumptions of the calculation.

Neumann and Fink (9) found similar agreement and also found that discharged electrodes similar to those of this investigation showed nearly the same x-ray diffraction pattern as the original MnO_2. The composition was $MnO_{1.6}$. They conclude that little change in structure took place during the discharge, other than an expansion of the lattice, in agreement with Brenet (8). On the other hand, Brenet (8) working with electrodes much more nearly like Leclanché cell bobbins found x-ray evidence of a change in phase during the discharge and also of the slow formation of manganite, MnOOH. There can be no doubt of the formation of MnOOH and $Zn(MnO_2)_2$ in the dry-cell bobbin (10, 11). They also can be formed by the reduction of MnO_2 by Mn^{++} (12), and this is considered by Cahoon, Johnson, and Korver (13) to be the mechanism by which they are formed in the Leclanché cell. It seems highly probable that this reaction did not take place to an appreciable extent in the present experiments. This conclusion is based on the observations of Neumann and Fink on the structure of the solid product and on experiments described in the next section.

Formation of Mn^{++} *in solution.*—A number of discharges made as already described were terminated at different times. The Mn^{++} in the electrolyte was determined colorimetrically as MnO_4^- in each case. Results are shown in Fig. 2.

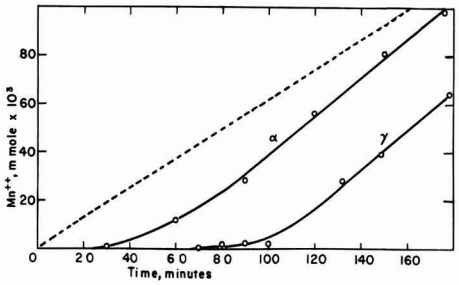

Fig. 2. Formation of Mn^{++} in the electrolyte during a discharge. The dashed line is the theoretical for complete conversion to Mn^{++}; the middle curve is for α-MnO_2 and the right-hand curve for γ-MnO_2.

The amounts of Mn^{++} found in the complete discharges described above (Table I) varied considerably. However, the points in Fig. 2 are close to the smooth curves, indicating good agreement in different discharges. It should be noted that in the complete discharges the time varied, whereas the present experiments show agreement among different electrodes for the same time intervals.

The results for the shorter discharges are in agreement with previous experience (14) that no Mn^{++} is formed in the first part of a discharge at pH 7.5. The curve for γ-MnO_2 in Fig. 2 also agrees with the similar previous curve except that the latter, for pH 8, lies a little below the present one for pH 7.5, as expected.

The curve in Fig. 2 for α-MnO_2 shows that Mn^{++} formation starts earlier in the discharge than for γ-MnO_2. The dashed line shows the theoretical Mn^{++} production if this were the only reduction product. The slope of the α-MnO_2 curve is at first less than that of the theoretical. It increases and becomes larger than the theoretical. Below about 30 min (60 ma-min) practically all of the reduced oxide is retained by the electrode. Between 30 and 60 min some is retained, but much goes into solution as Mn^{++}. For a short distance the Mn^{++} passing into solution equals the theoretical amount produced, since the curve becomes approximately parallel to the theoretical curve. From 100 min on the increase of Mn^{++} is larger than the theoretical. The excess Mn^{++} must come from some of the reduced solid oxide which becomes exposed as the surface oxide reacts with the electrolyte. The γ-MnO_2 curve is similar, except that the amount of Mn^{++} is less, and the excess Mn^{++} in the latter portion is less.

If this interpretation is correct, the reaction of Mn^{++} with MnO_2 to form MnOOH must have been unimportant if it took place at all. It must have been slower than the formation of Mn^{++} in excess of the theoretical.

Comparison of Fig. 1 and 2 shows that, by the time appreciable Mn^{++} had been formed from either type of electrode, the electrode potential had fallen to 0.2 v or below. This is considerably below the potential of a Mn_2O_3 electrode (against a saturated

calomel electrode) (15), and an oxide of such low potential should not be capable of reacting with Mn^{++} to form MnOOH. It may be concluded that this reaction does not take place under the conditions of the experiments of this investigation.

Discharge in the presence of excess Mn^{++}.—It has been shown that in discharge experiments like those of the present investigation the volume of the electrolyte has little or no effect on the formation of Mn^{++} (14). This was interpreted to mean that the Mn^{++} was formed by a slow reaction and the systems were not at equilibrium. However, the smallest volume tried was much too large to approximate conditions in a Leclanché cell. Therefore, some discharges have been made in which $MnSO_4$ was added to the electrolyte to see if much larger concentrations of Mn^{++} would affect the discharge process. Figure 3 shows three discharge curves, in two of which the electrolyte contained excess Mn^{++}. All three electrolytes contained 1M $(NH_4)_2SO_4$ and a buffer of pyridine and H_2SO_4 adjusted to *p*H 5. No Mn^{++} was added to one electrode; the other two were made 0.1M and 1M, respectively, in $MnSO_4$. The discharge (at 2 ma) was begun immediately after the introduction of the electrode to avoid any reaction of Mn^{++} and MnO_2 before the discharge. Discharge curves in the 3 electrolytes are shown in Fig. 3. The upper curve, for no added Mn^{++}, is the average for 6 discharges, the middle curve for 0.1M $MnSO_4$ is the average for 4, and the lower curve for 1M $MnSO_4$ is the average for 6. A few discharges in which the electrode capacity was abnormal were omitted from the averages.

The three curves differ in certain respects. The added Mn^{++} seems to have an effect on the course of the reaction in the first 60 ma-min; this was observed in all discharges with added Mn^{++}. The average capacity seems to be affected by the added Mn^{++}, but the effect is not large. The added Mn^{++} affects the electrode potential. The difference in open-circuit potential for 0.1 and 1M $MnSO_4$ is 0.027 v as compared with 0.0295 v calculated by the Nernst equation. The corresponding closed-circuit potentials differ by about 0.04 v.

That the curves are similar in shape beyond 60 ma-min indicates a similarity in reaction. Evidently in all three electrolytes practically all of the reaction product after 60 ma-min goes into solution. Otherwise the curves would have a more downward trend. Whether some of the Mn^{++} from the larger concentrations reacted with MnO_2 to form MnOOH cannot be ascertained, but analysis of the residues on the electrodes indicated that this reaction could not have been important.

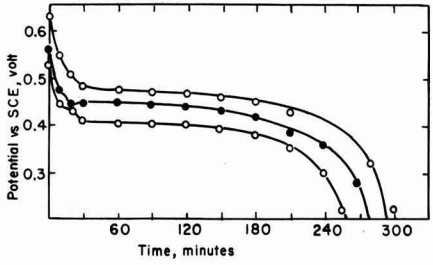

Fig. 3. Effect of added $MnSO_4$ on the discharge of electrodeposited γ-MnO_2 electrodes in 1M (NH_4) SO_4 electrolyte buffered at pH 5; 25° ± 2°C.

With no added Mn^{++} the residue on the electrode had the average composition $MnO_{1.9}$ with an average of 0.02 mmole of available oxygen. The Mn in the other residues was not determined because of the probability of contamination from electrolyte not removed by washing, but the average available oxygen was 0.04 mmole. Thus, only 0.2-0.1 of the original available oxygen remained in the residue. The error in these analyses was large because of the small amount of sample.

The difference between a discharge at *p*H 5 and one at *p*H 7.5 is that more Mn^{++} goes into solution at *p*H 5 and the residue remaining on the electrode is smaller and much richer in available oxygen. The electrical output is correspondingly larger at *p*H 5. The amount of residue on the individual discharged electrodes at *p*H 5 was quite variable and sometimes very small, but never too small to measure, as previously found for more acid solutions (16).

Surface of a Discharging MnO_2 Electrode

It has been shown (17) that a short treatment of a partially discharged MnO_2 electrode with a solution of $Na_2H_2P_2O_7$ has the effect of promoting recovery from polarization. When Mn is titrated in $Na_2H_2P_2O_7$ solution of *p*H 6-7 (18) it passes from a colorless Mn(II) compound (often a white precipitate) to an intensely red Mn(III) complex ion that remains in solution. This change and the color of the Mn(III) complex can be made the basis of the determination of small quantities of both Mn(II) and Mn(III) in the same sample. The method was used for the analysis of the Mn removed from the surface of an electrode by pyrophosphate.

Method.—A solution of 0.1M $Na_4P_2O_7$ was prepared with enough H_2SO_4 to give *p*H 6.0. To test electrodes, 5 ml of this solution was diluted to 10 ml and an electrode immersed in it for a known period of time. The optical absorbence of the solution was measured by a Spectronic 20 colorimeter at wavelength 480μ. The solution was then treated with 0.5 ml of saturated Br_2 water, boiled to remove excess Br_2 (and some H_2O), and diluted to 10 ml. The absorbence was again measured.

The first absorbence was taken as a measure of Mn(III) in the solution and the second as a measure of the total Mn.

To relate absorbence to amount of Mn, portions of a standard $MnSO_4$ solution were added to 5 ml of the stock pyrophosphate, followed by dilution to 10 ml. After oxidation by Br_2 water the absorbence was a linear function of the Mn present.

Samples of the order of magnitude of 10^{-3} mmole of Mn can be analyzed in this way. Too much Mn(II) causes precipitation of a Mn(II) compound which interferes with the measurement of absorbence.

Test of the method.—The method was tested first by the addition of a known small amount of standard $KMnO_4$ solution to 5 ml of stock pyrophosphate, then

a known excess of standard $MnSO_4$ solution. After dilution to 10 ml the Mn(III) and Mn(II) were determined as above. The results were a little low in this test, but never more than 6% low. This was sufficient for the purpose.

Another test was necessary to determine whether a MnO_2 electrode immersed in the diluted pyrophosphate would oxidize Mn(II) present in the solution. If not, it would be concluded that any Mn(III) found in the solution must have been dissolved from the electrode as Mn(III). While MnO_2 should be able to oxidize Mn(II) in pyrophosphate solution, it was found that in the time intervals involved and with the very small concentrations of Mn(II) used the reaction is too slow to be of significance.

Some MnO_2 electrodes were washed until no Mn could be removed from them by treatment with pyrophosphate solution. Some 10-ml solutions containing 5 ml of stock pyrophosphate and 0.1 mg of Mn(II) (1.8×10^{-3} mmole) were prepared. Electrodes were immersed in these solutions for 10, 20, and 30 min periods. No measurable Mn(III) was formed. A considerably longer treatment resulted in measurable Mn(III), but the practical experiments never involved more than a 15-min period of contact of the electrode with a pyrophosphate solution.

Analysis of manganese adsorbed by MnO_2.—As another control experiment some Mn^{++} was deposited on well-washed MnO_2 electrodes by adsorption, and the surface analyzed. A MnO_2 electrode was immersed for 30 min in 100 ml of pH 7.5 electrolyte containing either 1×10^{-4}M or 1.5×10^{-4}M $MnSO_4$, the solution being stirred. Three identical pyrophosphate solutions were prepared from 5 ml of stock solution and 5 ml of water. At the end of 30 min the electrode was quickly washed and immersed in one of the pyrophosphate solutions for 5 min, then it was transferred to another for 10 min, and finally to the third for 15 min. Each of the solutions was analyzed for Mn(III) and Mn(II). The results are given in Table II, each set of data being the average for 4 electrodes. The figures in the last column show how much of the original adsorbed Mn^{++} was recovered. In calculating the recovery it was assumed that half of the Mn(III) came from MnO_2 and half was from the adsorbed Mn^{++}. All of the Mn(II) was taken to represent adsorbed Mn^{++}. The total Mn adsorbed was calculated by difference; the concentration of Mn^{++} in the solution after adsorption by the electrode was determined colorimetrically as MnO_4^-. The amounts of Mn^{++} adsorbed from the two solutions, which contained 0.01 and 0.015 mmole, respectively, were 0.0039 and 0.0042 mmole.

Table II. Recovery of Mn adsorbed by a MnO_2 electrode from 100 ml of a solution 1 or 1.5×10^{-4}M in $MnSO_4$ and 1M in $(NH_4)_2SO_4$, pH 7.5; average data for 4 electrodes for each concentration

$MnSO_4$ M × 10^4	Mn recovered from electrode: Mn(III), mmole × 10^3			Mn(II) mmole × 10^3			Total Mn recovered, %
	5 min	10	15	5 min	10	15	
1	1.1	0.8	0.4	0.6	0.3	0.3	58
1.5	1.7	0.7	0.4	0.5	0.2	0.1	55

Table II shows that more Mn was recovered in the first time interval than in either of the others, and that there was more Mn(III) than Mn(II). Taking account of the formation of half of the Mn(III) from MnO_2, about half of the recovered original Mn^{++} was oxidized. Less than 60% of the Mn adsorbed was recovered.

The experiment was twice repeated with 1×10^{-4}M $MnSO_4$ solution and with all conditions as before except that the electrodes were allowed to stand in a 1M $(NH_4)_2SO_4$, pH 7.5 solution containing no added Mn after the 30 min adsorption period. After 30 min standing there was a little larger proportion in the form of Mn(III) than with no standing, and more Mn(II) was recovered in the later periods than in the first. The total recovery was not much different. However, after 4 days standing all of the recovered Mn was Mn(III) and in amount (average of 6 electrodes) was 1.2, 0.9, and 0.7×10^{-3} mmole in the three time intervals, respectively. This is only a little larger than the Mn(III) recovered in Table II. The percentage recovery was 35%. Thus, the remainder of the recoverable Mn(II) was oxidized on long standing, and less of the original adsorbed Mn could be recovered after long standing. Neither of the two storage solutions contained enough Mn afterward to be detected.

These experiments are useful controls for experiments to be described, and also lead to two conclusions of value in the consideration of the discharge mechanism of the MnO_2 electrode. (*A*) On a MnO_2 surface, and probably also within the lattice, Mn(III) is more stable than Mn(II). (*B*) The decreased availability for recovery of the adsorbed Mn as time goes on is in harmony with the assumption that part of the lower oxide formed in a discharge diffuses toward the interior of the MnO_2 (19-21, 17).

As an additional control experiment well-washed MnO_2 electrodes were immersed successively in 3 portions (10 ml) of $Na_2H_2P_2O_7$ solution for 3, 3, and 10 min, respectively. No Mn could be detected in the solutions.

The lower oxide at the surface of a discharging electrode.—In most of the discharges at pH 7.5 from which the data on the formation of Mn^{++} in solution were obtained, the electrodes were examined as to their surface composition. The discharges were discontinued after 10-100 min for γ-MnO_2, and longer for α-MnO_2, and the electrodes immediately immersed successively in three 10-ml portions of the diluted pyrophosphate for 3, 3, and 10 min, respectively. The solutions then were analyzed for Mn(III) and Mn(II) as above.

Figure 4 shows the total amounts of Mn(III) and Mn(II) extracted by pyrophosphate plotted against the time of discharge. For γ-MnO_2 most of the data are for single electrodes, but the points for 40, 50, and 60 min are averages of 2 each. For α-MnO_2 the points are averages of 3 or more. The Mn extracted was surprisingly small. The largest amount, average for 4 α-electrodes after 60 ma-min of discharge, was about 0.1 of the Mn reduced.

The Mn recovered from the γ-electrode after 10 min discharge was barely detectable. This was con-

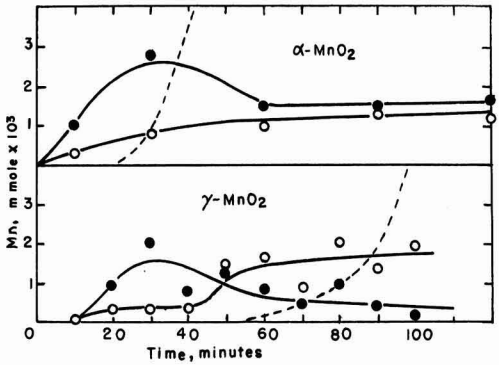

Fig. 4. Mn(III) and Mn(II) recovered from electrodes after different amounts of partial discharge, ● and ○, respectively. The dashed lines give the corresponding Mn^{++} in the electrolyte, from Fig. 2. The upper curves are for α-MnO_2 and the lower for γ-MnO_2.

firmed with a number of other electrodes, provided that they had been washed free from Mn^{++} before discharge. For comparison the Mn(III) recovered in 15 min after adsorption of Mn^{++} by an undischarged γ-electrode was 20 times as large and Mn(II) recovered was 8 times as large. The calculated amount of Mn reduced in 20 ma-min of discharge is 0.012 mmole if the product is Mn(III) or 0.006 mmole if Mn(II). The amount of adsorbed Mn^{++} was 0.004 mmole, which would result in 0.008 mmole of Mn(III) if completely oxidized. Thus, the amounts of lower-valence Mn on the electrodes were not greatly different in the two cases.

For α-MnO_2 both Mn(III) and Mn(II) extracted after 10 min discharge were larger fractions of the Mn recovered in the adsorption experiment, both roughly half. In agreement with the explanation of the shapes of the discharge curves (Fig. 1), α-MnO_2 is found to have more lower-valence Mn on its surface than γ-MnO_2 has in the early part of the discharge.

In Fig. 4 the Mn(III) is shown to increase rapidly at first, then decrease and remain roughly constant for some time. The scattering of the points is probably to be attributed more to the disagreement of different electrodes than to errors in analysis. The Mn(II) increases more slowly. The curves represent total Mn(III) and Mn(II) recovered at the time in question. By far the greater part of the Mn(III) recovered from both types of electrode came in the 10-min, or third, extraction by $H_2P_2O_7^{=}$. However, Mn(II) recovery was usually as large in the second 3-min period as in the 10-min period. In the adsorption experiment more of the adsorbed Mn was recovered in the first 5-min period than in the subsequent 10-min period. Thus, the lower-valence Mn resulting from discharge differs in reactivity from that placed on an electrode by adsorption.

The dashed curves in Fig. 4 are small portions of the curves of Fig. 2 showing the increase in Mn^{++} in solution as the discharge proceeds. These emphasize how little Mn was recovered from the electrodes and also indicate when Mn^{++} begins to appear in the electrolyte. In γ-MnO_2 especially it is apparent that no Mn^{++} goes into solution when the Mn(II) recoverable from the surface is small. The Mn(II) recoverable is roughly constant after the appearance of Mn^{++}.

At the end of a discharge about equal amounts of Mn(III) and Mn(II) were extracted from the electrode. An average of 2 x 10^{-3} mmole of each was extracted from 7 γ-electrodes. The total lower-valence Mn extracted was 2.5 mole-% of the residue on the electrode. For α-MnO_2 the corresponding figures were 3 x 10^{-3} mmole of each and 8 mole-% of the residue.

Discussion

The experiments on the surface analysis give information on the location of the primary electrode reaction. Brenet (8) has concluded from x-ray experiments on partially discharged MnO_2 that the reaction takes place below the surface of the MnO_2, causing an expansion of the lattice. The expansion was less in α-MnO_2 than in γ-MnO_2. The results of the surface analysis are in agreement with Brenet. The reduction product of the electrode reaction is much less accessible to extraction by pyrophosphate than Mn^{++} adsorbed by MnO_2.

The decrease in recoverability of the adsorbed Mn with time is best explained as a diffusion, which may involve the movement of only protons and electrons (19, 20). The diffusion is too slow to be consistent with the hypothesis that the electrolytic reduction of MnO_2 takes place entirely on the surface, followed by diffusion. It is more probable that the larger part of the reduction takes place below the surface. In α-MnO_2 there is more reaction at or near the surface than in γ-MnO_2. Diffusion may still be assumed to play a part in the electrode process, as the recovery from polarization in the early part of a discharge at *p*H 7.5 is best explained in terms of solid-state diffusion (20, 2, 21).

Acknowledgment

This work was supported in part by the Office of Ordnance Research.

Manuscript received Dec. 16, 1960.

Any discussion of this paper will appear in a Discussion Section to be published in the December 1961 JOURNAL.

REFERENCES

1. W. C. Vosburgh, *This Journal*, **106**, 339 (1959).
2. W. C. Vosburgh and J. H. DeLap, *ibid.*, **107**, 255 (1960).
3. A. M. Chreitzberg, Jr. and W. C. Vosburgh, *ibid.*, **104**, 1 (1957).
4. N. C. Cahoon, R. S. Johnson, and M. P. Korver, *ibid.*, **105**, 296, (1958).
5. A. Kozawa and W. C. Vosburgh, *ibid.*, **105**, 59 (1958).
6. A. Sam, Ph.D. Thesis, Duke University (1958). *Univ. Microfilms* (Ann Arbor, Mich.) *L. C. Card* No. **Mic.** 58-2295, 127 pp.; Dissertation Abstr., **19**, 37 (1958).
7. A. Kozawa and W. C. Vosburgh, *This Journal*, **105**, 235 (1958).
8. J. Brenet, *Proc. Intern. Comm. Electrochem. Thermodynam. and Kinetics*, 8th Meeting, Madrid, 1956, p. 394.
9. K. Neumann and W. Fink, *Z. Elektrochem.*, **62**, 114 (1958).
10. N. C. Cahoon, *Trans. Electrochem. Soc.*, **92**, 159 (1947).
11. L. C. Copeland and F. S. Griffith, *ibid.*, **89**, 495 (1946).

12. H. F. McMurdie, D. N. Craig, and G. W. Vinal, *ibid.*, **90**, 509 (1946).
13. N. C. Cahoon, R. S. Johnson, and M. P. Korver, *This Journal*, **105**, 296 (1958).
14. W. C. Vosburgh, M. J. Pribble, A. Kozawa, and A. Sam, *ibid.*, **105**, 1 (1958).
15. A. Kozawa, *ibid.*, **106**, 79 (1959).
16. S. Hills, Ph.D. Thesis, Duke University (1956).
17. A. M. Chreitzberg, Jr., D. R. Allenson, and W. C. Vosburgh, *This Journal*, **102**, 557 (1955).
18. J. J. Lingane and R. Karplus, *Ind. Eng. Chem. Anal. Ed.*, **18**, 191 (1946).
19. J. J. Coleman, *Trans. Electrochem. Soc.*, **90**, 545 (1946).
20. D. T. Ferrell, Jr. and W. C. Vosburgh, *This Journal*, **98**, 334 (1951).
21. A. B. Scott, *This Journal*, **107**, 941 (1960).

High-Temperature Oxidation of Fe-Cr Base Alloys with Particular Reference to Fe-Cr-Y Alloys

Edward J. Felten

Research Laboratory, General Electric Company, Schenectady, New York

ABSTRACT

The oxidation kinetics of iron-chromium alloys containing 25 and 37.5% chromium and small additions of yttrium and various other rare earth metals have been measured between 700° and 1200°C. Agreement with the parabolic rate law is generally observed for all alloys. Iron-chromium binary alloys have good oxidation resistance, but lose their protective oxide film due to spalling above 1000°C. Alloys containing yttrium, lanthanum, dysprosium, gadolinium, and erbium exhibit both good oxidation resistance and scale retention. Enhanced scale retention for alloys containing yttrium and the rare earth metals is attributed to the formation of internal as well as external oxide.

Previous investigations (1-3) have shown that iron-chromium alloys containing about 20% or more chromium are oxidation resistant at elevated temperatures. Aluminum (4-7) and more recently yttrium (8) have been found to improve the oxidation resistance of these alloys. The purpose of this investigation was to examine the behavior of iron-chromium alloys containing either 25 or 37.5% chromium to which small additions of yttrium or various other rare earth metals had been made. Alloys of these chromium contents were selected since they exhibit good oxidation resistance while still retaining the good mechanical properties not found in alloys of higher chromium content. The kinetics of oxidation and the structures of the oxides formed and their relation to the type and concentration of the additive have been studied.

Experimental Procedures

Alloy preparation.—All alloys were prepared from vacuum-melted electrolytic iron and hydrogen deoxidized electrolytic chromium. The alloys were prepared as 50-100 g buttons in an inert arc furnace employing a purified argon atmosphere. The buttons were forged at 1000°C, then rolled at 600°C to a thickness of about 0.015 in. A representative portion of the sheet stock was submitted for chemical analysis (see Table I).

Iron-chromium alloys containing 25 and 37.5% chromium were prepared both with and without 1% yttrium. Another group of alloys was prepared with several other rare earth metals in which the additive concentration was equal (atom-wise) to that of the yttrium alloys. Alloys with 0.5-2.0% yttrium and 25% chromium were prepared to study the cumulative effect of yttrium.

Specimens for the oxidation experiments were 13 mm wide by 20 mm long and were surface abraded through 600-grit wet emery paper immediately before use. After abrading they were degreased with toluene and then acetone. The surface area of the specimens was close to 5 cm^2.

Kinetic measurements.—Experiments were conducted in an atmosphere of dry oxygen at a partial pressure of 100 mm, unless noted differently. Two types of balance were used for kinetic measurements. For temperatures to 1000°C a microbalance of the "Gulbransen type" (9) was used. This balance has a sensitivity of about 0.1 μg and a reproducibility of approximately $\pm$ 1 μg.

Measurements above 1000°C were made using a quartz-spring balance which was obtained from the Microchemical Specialties Company, Berkeley, Cal-

Table I. Analysis of alloys tested

Alloy No.	Alloy composition	Chemical analysis	
20	Fe-25% Cr	% Cr-24.7	
759	Fe-37.5% Cr	% Cr-37.1	
22	Fe-25% Cr-1% Y	% Cr-24.9	% Y-0.83
758	Fe-37.5% Cr-1% Y	% Cr-37.3	% Y-0.96
6	Fe-37.5% Cr-1% Y	% Cr-37.7	% Y-0.75
8	Fe-25% Cr-0.3% Al	% Cr-24.8	% Al-0.18
4	Fe-25% Cr-0.78% Ga	% Cr-24.4	% Ga-0.56
14	Fe-25% Cr-1.56% La	% Cr-25.0	% La-1.88
29	Fe-25% Cr-1.77% Gd	No analysis performed	
30	Fe-25% Cr-1.83% Dy	No analysis performed	
31	Fe-25% Cr-1.88% Er	No analysis performed	
5	Fe-37.5% Cr-0.3% Al	% Cr-37.6	% Al-0.28
10	Fe-37.5% Cr-0.78% Ga	% Cr-34.5	% Ga-0.72
15	Fe-37.5% Cr-1.56% La	% Cr-37.1	% La-1.66
21	Fe-25% Cr-0.5% Y	% Cr-24.7	% Y-0.50
23	Fe-25% Cr-1.5% Y	% Cr-24.8	% Y-1.32
24	Fe-25% Cr-2% Y	% Cr-24.9	% Y-1.89

ifornia. This balance is capable of accommodating the greater weight gains observed at elevated temperatures, where the beam balance is inadequate. The spring balance has a sensitivity of about 10 μg.

The experimental procedure was the same for either type of balance. The specimen was suspended in the center of a uniform hot zone of a Nichrome wound furnace and the system evacuated. In order to bring the specimen up to temperature rapidly, the furnace was arranged so that it could be raised or lowered along the furnace tube. The furnace was heated to the temperature desired while in the lowered position; this allowed the specimen to remain at or near room temperature. The furnace was then raised, and after the specimen had attained the desired temperature, the system was filled with oxygen to the desired partial pressure. Balance readings were begun as soon as possible following the addition of oxygen.

Scale identification.—To determine the nature of the scale formed, specimens oxidized in the Gulbransen type thermal balance were examined by x-ray and electron diffraction techniques. The extremely thin, adherent oxides were examined *in situ*. Additional specimens were oxidized between 1000° and 1300°C in flowing oxygen in order to obtain larger amounts of oxide.

Two methods have been used for descaling specimens, *i.e.*, by mechanical means and by the dissolution of the unoxidized metal with a 10% bromine in methanol solution, followed by recovery of the oxide which is unattacked. The oxide obtained by the bromine method consists of internal as well as external oxide.

The elemental composition of the detached oxide was determined by x-ray fluorescence spectroscopy. This method was selected because only small amounts of sample are required. Very often only 5 mg or less of oxide were obtained after heat treatment of the metal.

The solutions obtained after the bromine-methanol treatment of the oxidized alloys were analyzed by conventional methods to determine the composition of the unattacked metal after oxidation.

Before microscopic examination the oxidized specimens were treated in the following manner to minimize loss of oxide during the polishing operation. Initially, a thin film of silver (~0.0001 in.) was vacuum deposited on the specimen. A thin film of copper and a fairly thick (~0.005 in.) layer of nickel were electroplated over the silver. The specimens were then polished perpendicular to their flat surface.

A short study was made of the solubility of yttrium oxide in chromium oxide. Oxide mixtures were prepared by ball milling slurries of the previously weighed components in alcohol. After evaporation of the alcohol, the mixtures were compacted and fired for 2 hr at 1800°C in hydrogen, saturated with water vapor at room temperature. Compacts fired in this manner become sufficiently dense for polishing and microscopic examination. Portions of the specimens were also examined by x-ray diffraction methods.

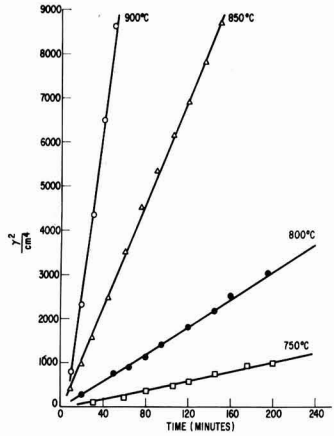

Fig. 1. (Weight-gain)^2-time at 750°, 800°, 850° and 900°C for an Fe-37.5% Cr-1% Y alloy in 100mm O_2.

Experimental Data

Kinetic measurements.—Kinetic measurements indicate that the alloys generally obey the parabolic law as written in the following form

$$\Delta M^2/cm^4 = k_p\ (t - t_o)$$

where $\Delta M/cm^2$ is the weight gain per unit area t, and t_o is time, and k_p is parabolic rate constant.

In Fig. 1 are representative results obtained at 750°, 800°, 850°, and 900°C using the Fe-37.5% Cr-1% Y alloy. Here γ^2/cm^4 (weight gain/cm^2, squared) *vs.* time yields a straight line as required by the parabolic rate law. Similar data for Fe-37.5% Cr is found in Fig. 2.

In some of the γ^2/cm^4 *vs.* t curves a change in slope takes place within the first 100 min of the experiment. This initial slope was disregarded and the parabolic rate constant calculated from the slope between 100 and 400 min, at which time most runs were terminated. The rate constants obtained appear

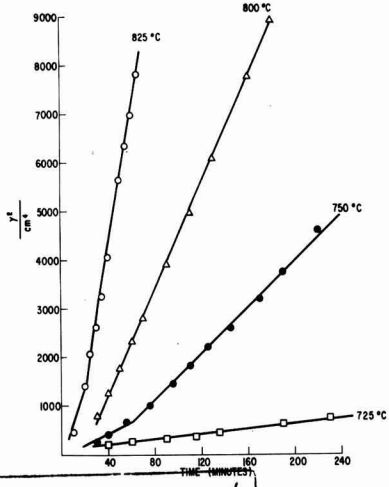

Fig. 2. (Weight-gain)^2-time at 725°, 750°, 800° and 825°C for Fe-37.5 Cr in 100mm O_2.

Table II. Oxidation rate (g cm^{-4} sec^{-1}) as a function of temperature for iron-chromium and iron-chromium-yttrium alloys

Temp, °C	Fe-25Cr	Fe-37.5Cr	Fe-25Cr-1Y	Fe-37.5Cr-1Y
650	1.3×10^{-13}			5×10^{-14}
700	1.3×10^{-13}	4.4×10^{-14}	1.2×10^{-14}	8.4×10^{-14}
				8.1×10^{-14}
725		2.5×10^{-13}		
750	1.7×10^{-13}	4.5×10^{-13}	2.0×10^{-14}	8.8×10^{-14}
775		9.2×10^{-13}		1.5×10^{-13}
800	3.0×10^{-13}	9.2×10^{-13}	1.4×10^{-13}	2.0×10^{-13}
		1.6×10^{-12}	1.7×10^{-13}	2.6×10^{-13}
		2.6×10^{-12}		9.8×10^{-14}
				1.1×10^{-13}
				2.8×10^{-13}
825		1.7×10^{-12}		7.5×10^{-13}
850	6.7×10^{-13}		4.4×10^{-13}	1.1×10^{-12}
				9.5×10^{-13}
				1.3×10^{-12}
875				2.0×10^{-12}
900	7.2×10^{-13}		2.5×10^{-12}	4.1×10^{-12}
925	1.3×10^{-12}			
950	6.3×10^{-12}			
1100	2.5×10^{-10}	7.6×10^{-11}	2.9×10^{-10}	3.1×10^{-10}
1200	9.5×10^{-10}	2.4×10^{-10}	6.1×10^{-10}	6.1×10^{-10}

in graphs relating rate constants to temperature.

Fe-25% Cr, Fe-37.5% Cr and these alloys with 1% yttrium.—As shown in Table II at temperatures between 700° and 1000°C the Fe-25% Cr alloy oxidizes at a slower rate than does the Fe-37.5% Cr alloy. The addition of 1% yttrium results in some increase in oxidation resistance. Between 1000° and 1200°C the oxidation rates for all four alloys are nearly the same, at least for short oxidation times. In 48 hr tests in oxygen at 1000°C, a weight gain of 1.15 x 10^{-3} g/cm^2 was observed for the Fe-25% Cr alloy as compared to a 2.4 x 10^{-4} g/cm^2 gain for the Fe-25% Cr-1% Y alloy.

The parabolic rate constants for the alloys containing yttrium obey Arrhenius' equation:

$$k_p = Ae^{-Q/RT}$$

where Q is the activation energy and A is a constant (see Fig. 3). The average activation energy obtained from the two curves is about 70 kcal/mole. Greater scatter of the experimental points in the k_p *vs.* $1/T$ relationship is noted for the binary alloys (see Fig. 4). However, the activation energy for these alloys

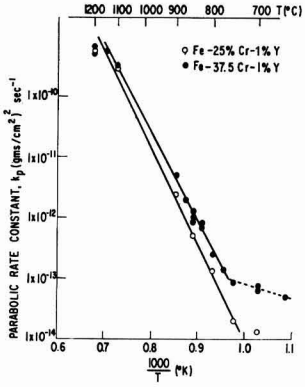

Fig. 3. Temperature dependence of parabolic rate constant for Fe-25% Cr-1% Y and Fe-37.5% Cr-1% Y.

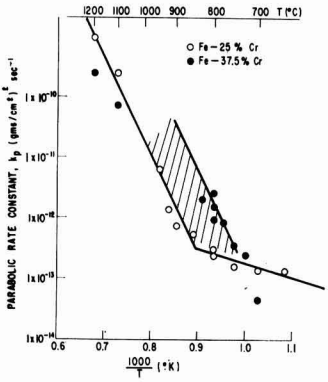

Fig. 4. Temperature dependence of parabolic rate constant for Fe-25% Cr and Fe-37.5% Cr alloys in 100 mm O^2.

is probably close to that determined for those containing yttrium.

Fe-Cr alloys containing other rare earth metal additives.—Iron-chromium alloys were prepared containing lanthanum, gadolinium, dysprosium, and erbium of equal atom concentrations to that of the 1% yttrium. In 48 hr service tests in flowing oxygen between 1000° and 1200°C these alloys were comparable in oxidation resistance to those containing yttrium as seen in Table III.

Fe-Cr *alloys with varying amounts of yttrium.*—Alloys containing 0.5-2.0% yttrium and 25% chromium were compared with regard to cumulative effects of the yttrium. These alloys were examined at 800°C in thermal balance experiments and above 1000°C in 48 hr service tests. As seen in Table IV, oxidation resistance is independent of yttrium content. Data presented earlier for Fe-25% Cr-1% Y adequately describes these alloys.

Spalling behavior of Fe-Cr alloys.—The Fe-25% Cr and Fe-37.5% Cr alloys when heated at 1000°C for 48 hr lose scale due to spalling on cooling. Only limited spalling is detectable on cooling from specimens containing 1% yttrium or an equivalent amount of the other rare earth metals heated to 1200° or 1300°C for 48 hr. The scale obtained from all the Fe-Cr base alloys was uniformly blue-gray in color in bulk, but was deep green after grinding.

Results of diffraction experiments.—Some specimens

Table III. Weight gain data for Fe-25% Cr alloys with various rare earth metal additions heated 48 hr at 1000° or 1100°C in flowing oxygen

Experiment No.	Additive	Temp, °C	Wt gain, avg unit area, g/cm^2	Parabolic rate constant, (g/cm^2)^2 sec^{-1}
146-149	1% Y	1000	2.4×10^{-4}	3.3×10^{-13}
192-193	1.6% La	1000	4.2×10^{-4}	1.0×10^{-12}
269-269A	1.8% Gd	1000	1.3×10^{-4}	9×10^{-14}
270-270A	1.8% Dy	1000	1.9×10^{-4}	2.1×10^{-13}
271-271A	1.9% Er	1000	1.7×10^{-4}	1.7×10^{-13}
199-199A	1% Y	1100	9.0×10^{-4}	4.7×10^{-12}
209-209A	1.6% La	1100	5.4×10^{-4}	1.7×10^{-12}
272-272A	1.8% Gd	1100	4.9×10^{-4}	1.4×10^{-12}
273-273A	1.8%Dy	1100	7.1×10^{-4}	2.9×10^{-12}
274-274A	1.9% Er	1100	4.6×10^{-4}	1.2×10^{-12}

Table IV. Weight gain data for Fe-25% Cr alloys of varying yttrium content in; A, thermal balance experiments, and B, 48 hr oxidation tests

Experiment No.	% Y in alloy	Temp, °C	Parabolic rate constant, $(g/cm^2)^2\ sec^{-1}$
	A. Thermal balance experiments		
132	0.5	800	1.0×10^{-13}
131	1.0	800	1.4×10^{-13}
237	1.0	800	1.7×10^{-13}
136	1.5	800	1.3×10^{-13}
125	2.0	800	1.1×10^{-13}
	B. 48 hr oxidation tests		
160-161	None	1000	7.6×10^{-12}
142-145	0.5	1000	4.2×10^{-13}
146-149	1.0	1000	3.3×10^{-13}
150-153	1.5	1000	3.2×10^{-13}
162-163	2	1000	7.1×10^{-13}
198-198A	0.5	1100	3.8×10^{-12}
199-199A	1.0	1100	4.7×10^{-12}
200-200A	1.5	1100	4.8×10^{-12}
201-201A	2	1100	8.3×10^{-12}

oxidized in the thermal balance were examined by reflection by means of electron diffraction or with the x-ray diffractometer (G.E. X RD-5). In all cases the oxide phase in contact with the metal was found to be Cr_2O_3.

The oxide obtained by bromine-methanol treatment of oxidized yttrium-containing alloys was often of the same shape and size of the subdivided specimen and was sandwich-like in appearance, see Fig. 5. The surface oxides were blue-gray in color between which a gray or sometimes light green oxide exists. The x-ray diffraction results of the oxides obtained in this manner indicate the presence of Cr_2O_3, Y_2O_3, and $CrYO_3$ depending on the oxidation temperature. As seen in Table V, oxides recovered by the bromine-methanol method from the alloys containing La, Gd, Dy, and Er are similar in composition.

Scale analysis.—Initially x-ray fluorescence spectroscopic experiments on Fe-Cr-Y alloys were run without removing the oxide. The intensities of the

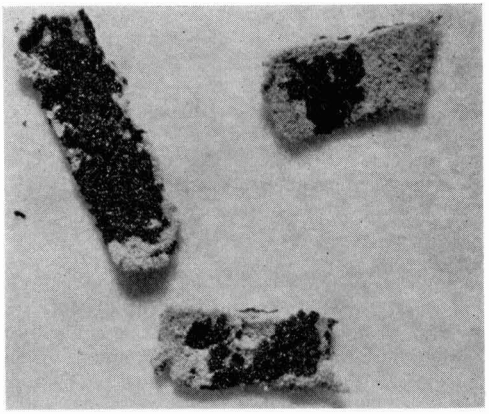

Fig. 5. Oxide removed from Fe-37.5% Cr-1% Y oxidized 90 hours in O_2 at 1000°C. (X 15)

Table V. X-ray data for oxides recovered from Fe-Cr-rare earth alloys by bromine-methanol method

Alloy composition	Temp, °C	Phases found
Fe-25% Cr-1% Y	1000	Cr_2O_3, Y_2O_3
Fe-25% Cr-1% Y	1100	Cr_2O_3, Y_2O_3, and $YCrO_3$ (10)
Fe-25% Cr-1% Y	1200	Cr_2O_3, $YCrO_3$
Fe-37.5% Cr-1% Y	1000	Cr_2O_3, Y_2O_3, and trace $YCrO_3$
Fe-37.5% Cr-1% Y	1200	Cr_2O_3, $YCrO_3$
Fe-25% Cr-1.6% La	1100	Cr_2O_3, La_2O_3, and $LaCrO_3$[a]
Fe-25% Cr-1.6% La	1200	Cr_2O_3, La_2O_3, and $LaCrO_3$
Fe-25% Cr-1.8% Gd	1000	Cr_2O_3, Gd_2O_3
Fe-25% Cr-1.8% Gd	1100	Cr_2O_3, Gd_2O_3
Fe-25% Cr-1.8% Dy	1000	Cr_2O_3, Dy_2O_3
Fe-25% Cr-1.8% Dy	1100	Cr_2O_3, Dy_2O_3
Fe-25% Cr-1.9% Er	1000	Cr_2O_3, Er_2O_3
Fe-25% Cr-1.9% Er	1100	Cr_2O_3, Er_2O_3

[a] High-temperature pseudocubic form (A_o = 3.933A, α = 90°22) (11).

iron, chromium, and yttrium K_α lines emitted from one surface of a polished specimen were measured. The K_α lines were remeasured at regular intervals as the specimen was oxidized at 1000°C. As seen in Table VI, the most striking trend in the measurements is the large increase in the intensity of the chromium line accompanied by a simultaneous decrease in the intensity of the iron line. The intensity of the yttrium K_α line remained constant throughout the test.

More definitive results may be obtained by the x-ray fluorescence analysis of the detached scale. Therefore, the powdered scale was spread uniformly on mylar film and the intensities of the metal K_α lines determined. Synthetic Cr_2O_3-Fe_2O_3 and Cr_2O_3-Y_2O_3 mixtures were used to establish intensity ratio-oxide concentration curves. The results show the oxide to be primarily Cr_2O_3 with 1-3% Fe_2O_3 and 0.2-0.5% Y_2O_3 also present.

The bromine-methanol solutions of the alloys containing yttrium were analyzed to determine the metal composition after oxidation. The results for several yttrium-containing alloys show a preferential depletion of both chromium and yttrium during oxidation at 1000°C or above (see Table VII).

Table VI. Fe-25% Cr-1% Y oxidized at 1000°C in oxygen

Line intensity, cts/sec \ t, hr	0	1	2	5	25	100
Fe K_α	31,900	19,900	17,700	15,400	12,000	7,200
Cr K_α	7,900	10,800	11,300	11,700	12,000	13,300
Y K_α	713	735	730	730	723	717

Fe-37.5% Cr-1% Y oxidized at 1000°C in oxygen

Line intensity, cts/sec \ t, hr	0	1	2	5	25	100
Fe K_α	23,800	15,400	13,700	12,000	9,000	5,800
Cr K_α	10,700	13,000	13,400	13,700	14,200	14,400
Y K_α	625	657	655	658	664	677

Table VII. Chemical analysis of unoxidized portions of several iron-25% chromium-yttrium alloys after 48-hr oxidation at 1000°C in O_2

Alloy	% Fe found	% Cr found	% Y found
Fe-25% Cr-0.5% Y[a]		24.7	0.50
Fe-25% Cr-0.5% Y[b]	75.0	24.7	0.35
Fe-25% Cr-0.5% Y[c]	75.2	24.5	0.34
Fe-25% Cr-1% Y[a]		24.9	0.83
Fe-25% Cr-1% Y[b]	74.3	25.0	0.79
Fe-25% Cr-1% Y[c]	74.7	24.7	0.63
Fe-25% Cr-1.5% Y[a]		24.8	1.32
Fe-25% Cr-1.5% Y[b]	74.0	24.7	1.30
Fe-25% Cr-1.5% Y[c]	77.1	21.9	0.95

[a] Original analysis of as-rolled material.
[b] Analysis of as-rolled material dissolved in bromine-methanol solution.
[c] Analysis of bromine-methanol solution of material oxidized 48 hr at 1000°C in flowing oxygen.

Solubility of Y_2O_3 in Cr_2O_3.—X-ray diffraction and microscopic results indicate that Y_2O_3 is only slightly soluble in Cr_2O_3; see Table VIII. In fact, it is somewhat surprising that the x-ray method was able to detect $CrYO_3$ in a compact containing only 1 mole % (1.5 wt %) of Y_2O_3. The microscopic results indicate that a two-phase region exists at yttrium oxide concentrations as low as one-tenth mole % Y_2O_3.

Microscopic examination.—The oxide formed between 800° and 1000° on the Fe-25% Cr and Fe-37.5% Cr alloys appear to consist of a single phase, fairly uniform in thickness, as seen in Fig. 6. The color of the oxide is emerald green under polarized light, characteristic of Cr_2O_3. There is no evidence of any internal oxide. In tests conducted between 1000° and 1300°C, Seybolt (12) found 13% chromium to be the upper limit at which internal oxide forms, at least for short exposures.

The alloys containing yttrium, in addition to forming a single phase external oxide, also oxidize internally, above 1000°C. Where an internal oxide is formed, for example in an Fe-37.5% Cr-1% Y alloy oxidized at 1000°C (Fig. 7) the thickness of the external scale is markedly less than for the binary alloy (Fig. 6.).

The internal oxide is present as filamentary growths, which appear to be concentrated at the grain boundaries. As the oxidation temperature is raised to 1300°C the amount of internal oxide formed increased for identical heating times.

Discussion

Fe-25% Cr, Fe-37.5% Cr and these alloys with 1% yttrium.—Observations of the oxidation kinetics

Table VIII. Results of microscopic examination and x-ray diffraction of some Cr_2O_3-Y_2O_3 mixtures fired 2 hr at 1800°C in wet hydrogen

Experiment No.	Mole % Y_2O_3	Microscopic examination	X-ray diffraction
174A	0	Single phase	Cr_2O_3
140	0.1	Single phase	Cr_2O_3
175	0.1	Smallest amount second phase	Cr_2O_3
176	0.5	Two phases	Cr_2O_3
50	1	Two phases	Cr_2O_3 plus $CrYO_3$
51	5	Two phases	Cr_2O_3 plus $CrYO_3$

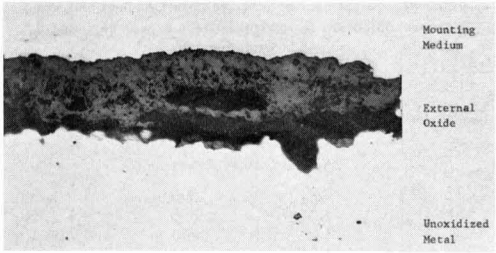

Fig. 6. Fe-37.5% Cr oxidized 90 hours at 1000°C in oxygen. Magnification 750X before reduction for publication.

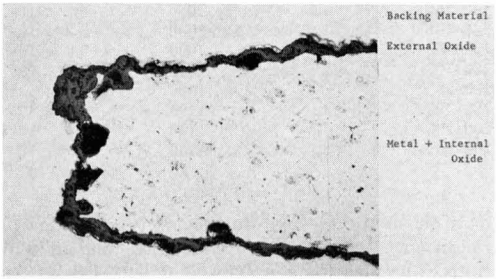

Fig. 7. Fe-37.5% Cr-1% Y oxidized 90 hr at 1000°C in oxygen. Magnification 750X before reduction for publication.

for Fe-25% Cr and Fe-37.5% Cr and these alloys containing 1% Y show agreement with the parabolic rate law, indicating a diffusion controlled mechanism for the times and temperatures investigated. Below 1000°C the results show that alloys containing 25% Cr oxidize more slowly than those containing 37.5% Cr as previously observed by Baldwin, *et al.* (1). The addition of 1% Y improves the oxidation resistance of both alloys. Combined results of the rate studies and oxide structures indicate the same oxidation mechanism for all four alloys between 700° and 1000°C.

At temperatures above 1000°C a different oxidation mechanism is observed for alloys containing yttrium. For these alloys oxidation takes place internally as well as externally, while for the binary alloys only an external oxide scale is formed at these temperatures. For exposure times of 2-4 hr at 1100° or 1200°C there is little difference in the oxidation rates of the two types of alloys. The anomalously low oxidation rates observed in the service tests (see Table III) are probably due to the flowing oxygen atmosphere removing some of the outer scale as volatile CrO_3. However, since both types of alloys were heated under the same conditions, the effectiveness of the additives is demonstrated.

The external oxide formed on all alloys is found to be Cr_2O_3 containing small amounts of iron and sometimes yttrium in solid solution. Seybolt (12) has shown by platinum marker experiments with Fe-20% Cr and Fe-30% Cr alloys that the external oxide is formed by migration of chromium through the oxide to the oxide-gas interface at temperatures between 1000° and 1300°C.

The internal oxide formed in alloys containing yttrium is either Y_2O_3 at 1000° or $YCrO_3$ at 1200°C.

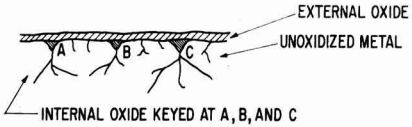

Fig. 8a. Oxide formation expected if keying mechanism were important.

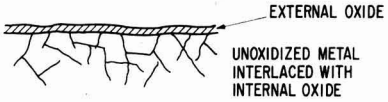

Fig. 8b. Oxide formation found in alloys containing yttrium

The amount of internal oxide formed for equal heating times increases as the temperature is increased. The internal oxide formation is a consequence of the immobility of yttrium combined with its high free energy of oxidation ($\Delta F_{298} = -450$ kcal/mole) (13). Where the mixed oxide is formed it is presumed to be the reaction product of the Y_2O_3 originally formed and chromium, since chromium appears to be the major diffusing species in the metal.

Lustman (14) attributed increased oxidation resistance imparted by rare earth metal additions to internal oxide formation which, he claims, tends to key the external oxide to the metal. Specimens in which such a mechanism were important might be expected to appear in cross section like Fig. 8a. Instead only thin fibrous networks of oxide are found, as shown in Fig. 8b. These formations do not appear capable of supporting, to any great extent, the external scale. However, the appearance of some oxide scales collected after dissolution of the metal (see Fig. 5) gives some support to the views of Lustman. The nature of this scale leads to the conclusion that the fibrous internal oxides are in intimate contact with the external oxide. The large number of minute contacts made between two oxides appears to be related to the scale retention properties of this type of alloy.

Fe-Cr alloys containing other rare earth metal additives.—The iron-chromium alloys with rare earth metal additives of equal atomic concentrations to that of 1% yttrium exhibited similar resistance to oxidation in service tests above 1000°C. Their mode of oxidation at these temperatures appears to be the same as for yttrium-containing alloys.

Summary and Conclusion

The mode and rate of oxidation have been studied for a number of iron-chromium alloys containing either 25 or 37.5% chromium and these alloys to which small additions of yttrium or other rare earth metals have been made. For all alloys, agreement with the parabolic rate law is generally observed. No large differences have been observed in the oxidation rate between the binary and the various ternary alloys. However, the presence of yttrium or the other rare earths leads to a substantial increase in scale retention at temperatures above 1000°C.

The external oxide formed on all alloys is primarily Cr_2O_3. Above 1000°C the alloys containing yttrium or the other rare earth elements also oxidize internally. The quantity and composition of the internal oxide is dependent on the temperature of oxidation. At 1000°C the principle oxide is of the R_2O_3-type (R = Y or other rare-earth) while at 1200°C it is $RCrO_3$. This oxide is found at the grain boundaries as shown by microstructures.

Acknowledgments

The author wishes to thank A. U. Seybolt for many helpful discussions and suggestions during the course of this investigation. Thanks are also extended to R. DeSorbo, D. DeCarlo, and E. Alessandrini who performed the various x-ray and electron diffraction experiments.

Manuscript received June 28, 1960; revised manuscript received Dec. 19, 1960.

Any discussion of this paper will appear in a Discussion Section to be published in the December 1961 JOURNAL.

REFERENCES

1. C. A. Barrett, E. B. Evans, and W. M. Baldwin, Jr., "High Temperature Scaling of Ni-Cr, Fe-Cr, Cu-Cr, and Cu-Mn Alloys," work performed for Office of Ordnance Research at Case Institute of Technology, Cleveland, Ohio, Contract No. DA 33-019-ORD-1077.
2. H. J. Yearian, E. C. Randell, and T. A. Longo, *Corrosion*, **12**, [10], 515t (1956).
3. D. Caplan and M. Cohen, *Trans. AIME*, **160**, 1057 (1952).
4. S. L. Case and K. R. Van Horn, "Aluminum in Iron and Steel," John Wiley & Sons, Inc., New York (1953).
5. H. A. Saller, J. T. Stacy, and N. S. Eddy, "Investigation of Wrought Iron-Chromium-Aluminum Alloys for Service at 2200°F," Battelle Memorial Institute Report No. 922, June 28, 1954.
6. W. Chubb, S. Alfant, A. A. Bauer, E. J. Jablonowski, F. R. Shober, and R. F. Dickerson, "Constitution, Metallurgy, and Oxidation Resistance of Iron-Chromium-Aluminum Alloys," Battelle Memorial Institute Report No. 1298, October 16, 1958.
7. E. A. Gulbransen and K. F. Andrew, *This Journal*, **106**, 941 (1959).
8. J. F. Collins, V. P. Calkins, and J. A. McGurty, "Applications of Rare Earths to Ferrous and Non-Ferrous Alloys" presented at American Society for Metals—Atomic Energy Commission Symposium on the Rare Earths and Related Metals, Chicago, Illinois, November 2, 1959.
9. E. A. Gulbransen, *Advances in Catalysis*, **5**, 39 (1953).
10. S. Geller and E. A. Wood, *Acta Cryst.*, **9**, 563 (1956).
11. S. Geller, *ibid.*, **10**, 243 (1957).
12. A. U. Seybolt, *This Journal*, **107**, 147 (1960).
13. L. Brewer, *Chem. Rev.*, **52**, 1 (1953).
14. B. Lustman, *Trans. AIME*, **188**, 995 (1950).

Kinetics of the Oxidation of Platinum

George C. Fryburg and Helen M. Petrus

Lewis Research Center, National Aeronautics and Space Administration, Cleveland, Ohio

ABSTRACT

The oxidation of platinum has been investigated employing electrically heated ribbons at temperatures from 900° to 1500°C and at pressures from 15 μ to 1 atm. An energy of activation of 42.5 kcal mole^{-1} has been obtained from the temperature-dependence of the rate. An unusual pressure-dependence has been observed which was found to result from the back-reflection of the volatile PtO_2 by the surrounding gas molecules: At 1 atm pressure only a fraction of a per cent of the PtO_2 formed escapes from the platinum.

In connection with our work (1) on the enhanced oxidation of metals in "activated oxygen" some accurate values for the rate of oxidation of platinum in normal oxygen in the temperature region around 1100°C were required. In addition, we were interested in the effects of oxygen pressure on the rate. Several studies (2-4) have been reported in this temperature region, but all were conducted at atmospheric pressure and all employed furnaces to heat the platinum. The use of furnaces for measuring the rates of oxidation of metals that form volatile oxides yields misleading results, as pointed out in a recent communication (5) by us.

To obtain more realistic values for the rate of oxidation of platinum in normal oxygen, we have employed a method similar to the one we used to study the oxidation of platinum in "activated oxygen" (1). The oxidation specimens are long ribbons which are heated electrically in a cooled tube. The gaseous oxide is condensed on the tube. The oxidation process is followed by dissolving the oxide formed and determining the amount of platinum colorimetrically. As the reaction follows a linear rate law in time, the rate constant of the oxidation can be obtained from each experiment. We have determined the rates of oxidation of platinum over a temperature range from 900° to 1500°C under pressures from 15μ to 1 atm.

Experimental

Materials.—The platinum used in these investigations was Sigmund Cohn Corporation's "reference grade" with a purity of 99.999+ %. It was supplied by the manufacturer in the form of fine ribbon with uniform width and thickness. Two different ribbon widths were used: 0.0287 cm (0.0113 in.) and 0.119 cm (0.047 in.). Both widths had a thickness of 0.0014 cm (0.00055 in.).

Ordinary tank oxygen was used for most of the runs, and the rest were performed with air. In either case the gas was water-scrubbed and then freed of all condensable impurities by passage through a trap cooled in liquid nitrogen or liquid oxygen, depending on the pressure of oxygen.

Description of apparatus.—The oxidations were performed in a Pyrex glass apparatus, a part of which is sketched in Fig. 1. The apparatus was vacuum tight so that experiments could be performed at

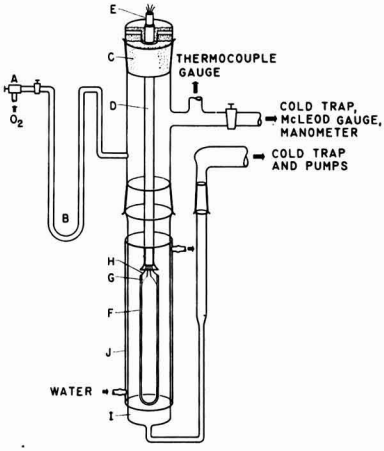

Fig. 1. Apparatus for oxidation of platinum: A, Hoke vacuum needle valve; B, cold trap; C, tapered brass plug with O-ring slip-seal; D, soda-glass tube, 10 mm OD; E, four-holed ceramic insulator; F, U-shaped platinum ribbon, 32 cm long; G, tap wires, 0.00127 cm diameter (0.0005 in.), 1 cm long; H, heavy platinum lead wires sealed through end of soda-glass tube; I, glass bulb, 32 mm OD, 25 cm long; J, removable water jacket.

any pressure from 0.1μ to 750 mm of Hg. Also, by use of a vacuum needle valve, A, constant pressures could be maintained under flowing conditions just as well as under static conditions.

The oxidation specimens, F, used for most of the low-pressure experiments, were U-shaped ribbons about 32 cm long. The ends of the ribbon were spot-welded to heavy platinum lead-ins, H, that served as current leads. Two very fine platinum wires, G, were resistance-welded to the ribbon 1 cm from each end, and these in turn were spot-welded to another pair of heavy platinum lead-ins that served as potential leads. At pressures above 100 mm a U-shaped specimen could no longer be used, as convection effects caused temperature variations along the ribbon. To overcome this difficulty, the part of the apparatus shown in Fig. 1 was mounted horizontally so that the specimen could be fixed in a horizontal position; one of the current and one of the potential leads were extended so that a straight ribbon about 15 cm long

could be mounted on the end of the soda glass tube, D.

The ribbon was heated by direct current supplied from a bank of lead storage cells. The current was determined from the voltage drop across a standard resistor. The current could be set to 1 part in 1000 and could be maintained constant by a servomechanism. The resistance of the ribbon between the potential leads was obtained from its potential drop with an over-all accuracy of ±0.1%.

The oxidation runs were performed with the specimen situated in the bulb, I. In most runs the bulb was fitted with a water jacket, J, through which flowed water thermostated at 25°C. The oxide formed during a run volatilized from the ribbon and was condensed on the inside of the bulb.

Pressures up to 1.5 mm were measured with a calibrated McLeod gauge. Pressures above this were determined with a wide-tube mercury manometer. A cathetometer reading to 0.1 mm was used to measure the heights of the mercury columns in both cases.

Procedure.—After fabrication the oxidation specimens were placed in hot concentrated HNO_3 for 1 hr to remove any copper that might have been deposited from the spot-welding. They were rinsed with distilled water and mounted in the apparatus. Most of the specimens were annealed at 1250°C for ½ hr in flowing oxygen at about 50 to 100μ pressure to stabilize the resistance. With the later specimens, experiments were performed at 1300°, 1395°, and 1480°C, and these specimens were annealed at 1480°C for ¼ hr. After the annealing process the bulb, I, and the specimen were cleaned with hot 12N HCl.

Before each run the resistance of the specimen was measured under atmospheric pressure and with the thermostated water flowing through the water jacket. From this resistance, the resistance of the specimen characteristic of the temperature of the oxidation run could then be calculated. The equation used (6, 7) for the calculations was

$$R_T = R_o(1 + 3.98 \times 10^{-3} T - 5.88 \times 10^{-6} T^2) \quad [1]$$

The desired pressure conditions were then set. The run was begun by bringing the specimen up to temperature as quickly as possible, as indicated by the characteristic resistance. The resistance change during a run, caused by thinning of the ribbon as oxidation proceeded, was small for most of the runs. The runs extended from 15 min to 6 hr depending on the temperature and pressure. The same specimen was used for many experiments.

After the run, the bulb, I, containing the condensed oxide, was removed and filled with 12N HCl. The specimen was also placed in the acid. The acid was boiled gently for 15 min to dissolve the oxide. A blank for analysis was obtained by repeating this procedure. The amount of platinum that had oxidized was determined by a sensitive colorimetric method described previously (1).

The accuracy of the results depends to a large extent on the accuracy of the temperature measurements. Therefore, the temperatures were checked throughout each run with an optical pyrometer of the disappearing filament type that was calibrated for the optical system employed in these experiments. Values for the emissivity of platinum were taken from Smithells (8). The resistance and optical temperature scales were identical up to 1300°C. Above this temperature the platinum resistance scale indicated higher values than the pyrometer scale. The pyrometer scale was shown to be correct by checking the melting point of the platinum ribbon. Therefore, the platinum resistance scale was corrected at 1400° to 1395°C and at 1500° to 1480°C. It is believed that the temperatures are accurate to ±5°C.

Measurements of the temperature distribution along the ribbons with the pyrometer showed that the temperature was uniform except at the ends which were cooled by the leads. The temperature profile at the ends was measured under the various conditions of our experiments. The rate-of-oxidation profile was calculated from this and the "effective area" of the ribbons obtained by graphical integration. The "effective area" is that area at the temperature of the middle of the ribbon that would give the same rate as the total ribbon with the experimental temperature distribution. For the 0.0287-cm width ribbon this was obtained by subtracting 2 cm of length from the total length before calculating the area; and the 0.120-cm width ribbon, 1 cm from the total length. This correction varied slightly with temperature. However, this variation was neglected, since the precision of the results was only ±5%.

Results

In preliminary experiments using pressures below 0.5 mm in a static system, pressure drops were observed that were much too large to be accounted for on the basis of a reaction with platinum. It was suspected that a reaction between the Apiezon N grease vapors and the oxygen was taking place on the platinum. This was shown to be the case by conducting experiments in which the reaction bulb was cooled in liquid nitrogen. The oxidation specimen was pushed to the bottom of the bulb, and any grease vapors entering from the top were condensed on the cold walls before contact with the platinum. Under these conditions the pressure drop corresponded with the value expected for oxidation of the platinum. Surprisingly, the same value for the rate of oxidation was obtained after correction for the change at the lower temperature in the rate of impact of the oxygen on the platinum. Thus, even though reaction between the grease vapor and oxygen was proceeding on the platinum, the rate of oxidation of the platinum was not affected. Therefore, no attempt was made to remove grease vapors from the reaction bulb. Instead, all experiments run at pressures below 1 mm were conducted in flowing gas so that a constant pressure could be maintained through a run.

Experiments were made to determine whether or not the flow rate of gas had any effect on the rate of oxidation. No effect of flow was observed over a pressure range from 150μ up to 10 mm and with flow velocities of gas from 0 to 220 cm/sec.

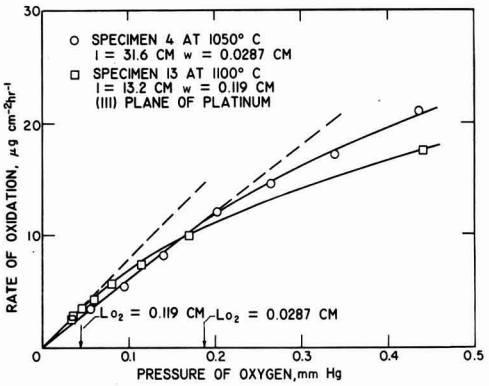

Fig. 2. Rate of oxidation of two specimens under various low pressures of oxygen.

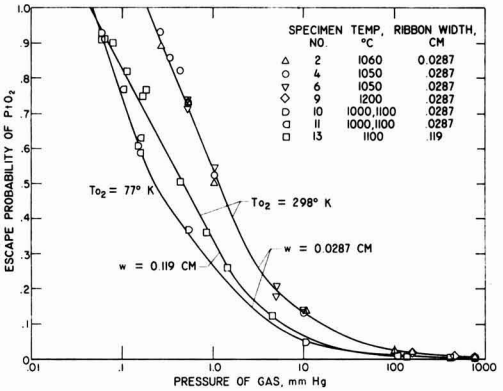

Fig. 3. Variation of escape probability of PtO_2 with pressure of surrounding gas.

Effect of Pressure

The rate of oxidation of platinum was studied from pressures of 15μ to 1 atm. Typical results for two ribbons of different width are shown in Fig. 2 for pressures up to 0.5 mm. At the lowest pressures the rate is directly proportional to the pressure, *i.e.*, the rate is proportional to the rate of collision of the oxygen molecules with the metal surface. At a pressure where the mean free path of the O_2 molecules, L, is about equal to the width of the ribbon, the rate begins to fall below the linear pressure relation. At higher pressures the rate continues to increase with pressure but falls off from the linear relation more and more.

This peculiar pressure-dependence can be explained by assuming that the actual rate of oxidation is directly proportional to the pressure of oxygen at all pressures, and that the fall-off of the measured rate with increasing pressure is caused by a back-reflection of the volatilizing oxide molecules by the surrounding gas; the oxide molecules striking the hot platinum are dissociated on impact, and the platinum is redeposited on the ribbon. At low pressures, where the mean free path of the oxide molecule in the surrounding gas is large compared to the width of the ribbon, all the oxide escapes from the region of the ribbon and is measured. At higher pressures, the mean free path decreases and the oxide molecules suffer collisions with the surrounding gas at distances closed to the ribbon. As a result the probability of being reflected back to the ribbon is increased. This explanation was verified by running experiments in air. With air, the nitrogen acts as an inert gas with the same scattering cross section as the oxygen. The whole behavior is very similar to that of a metal evaporating in an inert gas (9).

One can obtain for any given pressure the ratio of the measured oxidation rate to the actual rate obtained by extrapolating from the straight-line region to the given pressure. This ratio may be considered the fraction of the oxide forming that escapes, or the probability of escape of any oxide molecule formed. A plot of this "escape probability," P_e, against the pressure is shown in Fig. 3 for seven of our specimens. It can be seen that P_e, which is equal to 1 at the lowest pressures, starts dropping off from 1 at the pressure where the mean path of the O_2 molecules is equal to the width of the ribbon. It decreases rapidly throughout a region in which it is proportional to the logarithm of the pressure. At higher pressures it decreases less rapidly but reaches a rather small value at atmospheric pressure; for the 0.0287-cm wide ribbon it is 0.006, and for the 0.119-cm wide ribbon, 0.002. Recent experiments with a ribbon 0.225 cm wide also gave a value of 0.002. The value of 0.002 is in good agreement with the value of 0.0018 predicted by Fonda (10) for the evaporation of tungsten vapor from a large-diameter rod under 1 atm of inert gas. Hence, 0.002 appears to be a minimum value of P_e at atmospheric pressure regardless of how wide the ribbon is.

The data in Fig. 3 also indicate that P_e is dependent on the temperature of the gas. This is to be expected, since the temperature of the gas affects the density and hence the mean free path. On the other hand, from the data presented in Fig. 3, P_e appears to be little affected by the temperature of the platinum for a temperature range from 1000° to 1200°C. Other data not presented indicate that P_e is independent of platinum temperature from 900° to 1500°C for values of P_e around 0.7. One would expect the gas temperature in the immediate vicinity of the platinum to be dependent on platinum temperature at high pressures where the mean free path of the oxygen is small, and this might affect P_e. However, our results indicate the effect must be of secondary importance in this high-temperature region compared to the effect of pressure.

Effect of Temperature

The oxidation was studied over a temperature range from 900° to 1480°C, at pressures low enough that negligible back-reflection of oxide occurred. It was noticed that specimens made from the narrower ribbon suffered permanent decreases in rate every time they were heated to 1300°C or above. The magnitude of the decrease depended on the temperature and the time of exposure. Also, results obtained with specimens made from the wider ribbon were always lower than those obtained from the narrower ribbon.

The explanation for these facts was found in the texture of the surface of the ribbons.

Reflection x-ray diffraction patterns of the ribbons were taken with a Norelco diffractometer and the following facts were determined:

1. For both width ribbons in the hard, as-drawn condition, the platinum crystals were oriented primarily with a (110) plane parallel to the rolling plane, that is, parallel with the surface of the ribbon.

2. The narrow ribbon after annealing at 1250°C for ½ hr (the procedure used to stabilize the resistance of several of the oxidation specimens) showed no single preferred orientation parallel to the surface over most of the surface. However, quite often some individual grains were so oriented, and the following planes were detected: (100), (210), (211), (311), and (331).

3. When the narrow ribbons were heated above 1300°C, the grains became oriented with the (311) and (111) planes parallel with the surface. The longer the heating continued, the greater became the fraction of grains with a (111) plane parallel to the surface. Heating for 6 hr at 1480°C was sufficient to produce a ribbon almost completely oriented with (111) planes parallel to the surface.

4. Annealing of the wide ribbons at 1250°C for ½ hr was sufficient to orient the surface completely with the (111) planes parallel to the surface. The greater ease of orientation of the wider ribbon was possibly due to a greater amount of cold work introduced into it during the fabrication process.

A more detailed description of the morphology of the surface of the specimens is given in the appendix.

Experiments were conducted with some 15 different specimens. Table 1 shows a typical set of results obtained with specimen number 4. The rates of oxidation are given in column 4 in $\mu g\ cm^{-2}\ hr^{-1}$. The values have been corrected for oxide originating from evaporation of platinum. Platinum vapor is known to react rapidly with oxygen molecules (11). This correction is significant only above 1300°C. The rates of evaporation of platinum were calculated using Dushman's equation (12) and were checked experimentally by extrapolating some of our rate data at different pressures back to zero pressure.

Table I. Rate of oxidation of specimen number 4[a] at different temperatures

Experiment No.	Temperature of platinum, °C	Pressure of oxygen, μ	Rate of oxidation, $\mu g\ cm^{-2}\ hr^{-1}$	Collision efficiency, ($\times 10^8$)
1	1100	150	18.1	28.7
2	1100	↓	17.2	27.4
3	1000	↓	4.9	7.8
4	950	↓	2.4	3.8
5	1050	↓	8.6	13.7
6	1150	↓	26.8	42.5
7	1200	↓	44.0	70.0
8	900	↓	1.15	1.8
9	1050	↓	8.6	13.7
10	1050	56	3.45	14.3
11	1050	95	5.5	13.2
24	1200	150	43.2	69.0

[a] Annealed at 1250°C for 30 min, l = 31.6 cm; w = 0.0287 cm; A_c = 1.78 cm²; Temp. of O_2 = 25°C.

Table II. Collision efficiency results obtained at 1100°C with different specimens

No. of specimen and experiment	Pressure of O_2, μ	Temperature of O_2, °K	Collision efficiency, ($\times 10^8$)	% deviation from avg.
3-14	150	298	28.8	3.5
4-1	↓	↓	28.8	3.5
4-2	↓	↓	27.4	−1.5
6-2	↓	↓	27.4	−1.5
6-3	↓	↓	27.2	−2
11-1	42.6	77	27.4	−1.5
11-3	43.5	77	27.6	−0.5

The rates of evaporation found by the two methods were in good agreement.

The rate of oxidation is a function not only of the temperature of the platinum, but also of the temperature and pressure of the gas. For the purpose of correlation, it is convenient to express the rates in terms of a collision efficiency, and this has been done in column 5. The collision efficiency, ϵ, is defined as the fraction of the total number of molecules of oxygen striking the platinum that react. This has been calculated with the aid of the ideal gas laws assuming that the gas is at the temperature of the bulb. This assumption is very nearly true at these low pressures, especially with this experimental arrangement, since a given gas molecule will suffer many collisions with the bulb for every collision with the ribbon. It has also been assumed that the oxide formed is PtO_2, as shown by Rideal and Wansbrough-Jones (13) and by Alcock and Hooper (14).

As can be seen from Table I, the experiments were conducted at the different temperatures in a random manner. The precision of the results can be seen to be about ±5% by comparing the four collision efficiencies obtained at 1050°C and the two obtained at 1200°C.

In Table II we show the results obtained with four different specimens at 1100°C. Here also the precision of the results is better than ±5%, even though two of the experiments were performed with the bulb cooled to liquid-nitrogen temperature.

The collision efficiencies as a function of temperature of the platinum are presented as an Arrhenius plot in Fig. 4. The points at each temperature are

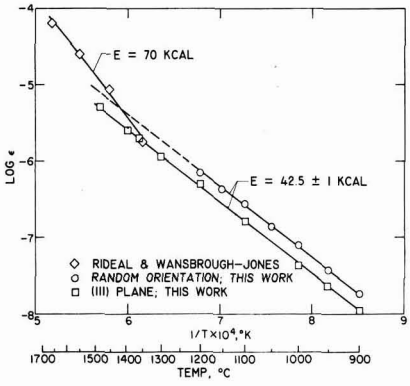

Fig. 4. Arrhenius plot of the collision efficiency, ϵ, for the oxidation reaction.

averages of all the reliable values obtained. The circular points were obtained with specimens made from the narrow ribbon that had not been heated above 1250°C. They should be characteristic of polycrystalline, randomly oriented platinum. The points fall on a straight line from 900° to 1200°C, and the activation energy corresponds to 42.5 kcal mole^{-1}. The square points were obtained with specimens made from the wide ribbon, or with specimens made from the narrow ribbon that had been heated to 1480°C for at least 6 hr. They should be characteristic of the (111) plane of platinum. The points fall nicely on a straight line from 900° to 1480°C, and the activation energy corresponds to 42.5 kcal mole^{-1} also. However, the actual collision efficiencies are only 62% of those of the randomly oriented platinum.

The diamond points are those of Rideal and Wansbrough-Jones (13) obtained at higher temperatures than ours by using a somewhat different technique. The values presented here were taken from their smoothed curve of ϵ against T. The temperature scale was corrected by the use of a newer value for the emissivity of tungsten. Their values, while in the region of our data, have a markedly different slope: energy of activation of 70 kcal mole^{-1}. We have no sound explanation for the discrepancy between the two sets of results, although one might expect that their greased stopcock had more effect on the decrease in pressure than they suspected.

Some support can be given to our results from a comparison with the equilibrium constants that have been measured for the reaction $Pt(s) + O_2(g) \leftrightarrows PtO_2(g)$. The low-pressure oxidation of platinum is a case in which equilibrium conditions may be calculated from kinetic data and is quite similar to Langmuir's method of calculating the vapor pressures of metals from the rates of evaporation in a high vacuum. The assumptions are similar, namely, that the emanation of oxide from the surface of the platinum and the striking of the platinum by oxide from the gas are independent processes, and that none of the oxide molecules that strike the platinum are reflected. This last assumption is true as the oxide molecules are dissociated on striking the hot ribbon. Also, we assume that the rate of emanation of oxide from the surface of the platinum is a direct function of pressure of oxygen.

The rate of emanation of oxide molecules from the platinum surface, z, is equal to the rate at which oxygen molecules are reacting, and is equal to

$$z = \epsilon[3.535 \times 10^{22}\, p_{O_2}\, (32T)^{-1/2}] \qquad [2]$$

where the quantity in brackets is simply the kinetic-theory expression for the rate of collision of oxygen molecules with the surface. A similar expression gives the rate at which oxide molecules are striking the platinum surface, ν:

$$\nu = 3.535 \times 10^{22}\, p_{oxide}\, (227T)^{-1/2} \qquad [3]$$

At equilibrium, z and ν are equal. If Eq. [2] is equated to Eq. [3] and we solve for the equilibrium constant for this reaction, we get

$$K = 2.66\, \epsilon \qquad [4]$$

We have tacitly assumed that the oxide molecules striking the platinum have the same temperature as the surrounding gas. The values of the equilibrium constants calculated from our measured collision efficiencies for randomly oriented platinum are given in Table III for temperatures of 1200° and 1500°C. For comparison we have presented in Table III the equilibrium constant measured by Schneider and Esch (15) at 1200°C and that measured by Brewer and Elliott (16) at 1500°C. Just recently Alcock and Hooper (14) have measured equilibrium constants over the temperature range 1100°-1500°C; the values at 1200° and 1500°C calculated from their free-energy equation are also presented in Table III. It can be seen from the table that the agreement between our calculated values and the measured equilibrium constants is satisfactory considering the wide disparity in experimental techniques.

Discussion

The effect of pressure on the rate of oxidation at any given platinum temperature can be expressed by a simple equation

$$R = k p_{O_2} P_e \qquad [5]$$

where R is the rate of oxidation in μg cm^{-2} hr^{-1}, p_{O_2} is the partial pressure of oxygen in mm of Hg, P_e is the escape probability characteristic of the total pressure and temperature of the surrounding gas, and k is simply the slope of the straight-line portion of the curves of Fig. 2, that is, the hypothetical reaction rate for unit pressure with $P_e = 1$.

The effect of the temperature of the platinum can be expressed by an Arrhenius type equation

$$k = A \exp(-E/RT) \qquad [6]$$

where A is a collision frequency, E is an activation energy, and T is the temperature of the platinum in degrees Kelvin. However, as stated previously, the rate depends also on the temperature of the oxygen, since this affects the rate of collision of the oxygen molecules with the platinum surface. As can be seen from the kinetic-theory expression, the collision frequency is inversely proportional to the square root of the temperature of the oxygen. Consequently,

$$A = A_o T_{O_2}^{-1/2} \qquad [7]$$

where A_o is a proportionality constant. If Eq. [7] is substituted into Eq. [6], and the resulting expression is substituted in Eq. [5], we obtain a general equa-

Table III. Comparison of equilibrium constants calculated from our collision efficiencies and those obtained from equilibrium measurements

Equilibrium constants		
1473°K	1773°K	Investigators
2.0×10^{-6}	[a]2.3×10^{-5}	Fryburg and Petrus
1.7×10^{-6}		Schneider and Esch
	3×10^{-5}	Brewer and Elliott
2.4×10^{-6}	2.3×10^{-5}	Alcock and Hooper

[a] Value of collision efficiency used in this calculation was obtained by extrapolating data since it was not possible to obtain an unoriented platinum ribbon at this temperature.

tion for calculating the rate of oxidation of platinum under any conditions of temperature or pressure:

$$R = A_e T_{O_2}^{-1/2} p_{O_2} P_e \exp(-E/RT) \quad [8]$$

If our results for polycrystalline, randomly oriented platinum are substituted into Eq. [8], we get

$$R = 1.09 \times 10^{10} T_{O_2}^{-1/2} p_{O_2} P_e \exp(-42{,}500/RT) \quad [9]$$

Similarly, for oxidation from the (111) plane of platinum,

$$R = 6.75 \times 10^{9} T_{O_2}^{-1/2} p_{O_2} P_e \exp(-42{,}500/RT) \quad [10]$$

With the aid of Eq. [9] it would be possible to calculate the rate of oxidation of platinum for any experimental conditions if the escape probability, P_e, were known. Unfortunately, we have found that P_e, is a complicated function of the relative dimensions of the specimen and the mean free path of the oxide molecules in the surrounding gas; the latter, in turn, is a function of the temperature of the gas. Even at a pressure of 1 atm where P_e seems to reach a limiting value with increasing width, it is not possible to determine how P_e changes with the temperature of the gas. This is primarily because P_e must also be a function of the flow conditions around the specimen at these high pressures. This can be seen by considering the small value of P_e found in these experiments at a pressure of 1 atm, namely, 0.002. This means that only 0.2% of the oxide formed was able to escape from the vicinity of the specimen; the rest, 99.8%, was reflected back to the platinum. Obviously, chemical equilibrium must be attained in the immediate vicinity of the wire, within a region probably equal to a few mean free path lengths. Consequently, the rate of oxidation at 1 atm is limited by the rate of diffusion of the oxide molecules through the boundary layer. The escape probability, therefore, is determined largely by the boundary-layer conditions. Its value is quite small for the conditions of these experiments where there is only convective flow. However, under conditions of high Mach flow, the value of P_e may be expected to increase markedly with a concomitant increase in the rate of oxidation. Similar conditions can be expected to exist for the other platinum-group metals. Consequently, the application of Eq. [9] is limited to low pressures where $P_e = 1$ until a detailed analysis of the diffusion of oxide through the boundary layer can be derived.

We have pointed out previously that the equilibrium constant for the oxidation reaction can be calculated at any temperature from the collision efficiency simply by multiplying by 2.66. Consequently, it is possible to calculate the free energy of formation of $PtO_2(g)$ at any temperature, and also to obtain the heat of formation for the temperature region. The heat of formation is obviously numerically equal to the activation energy, that is, 42.5 kcal mole^{-1}. It is also a simple matter to calculate the entropy change for the reaction. These calculations have been performed for the platinum oriented with the (111) plane parallel to the surface as this configuration represents the true equilibrium configuration. The results may best be expressed as a free-energy equation:

$$\Delta F^{\circ}_{T} = 42{,}500 \pm 1000 - T\,(1.8 \pm 1) \text{ cal mole}^{-1} \quad [11]$$

The accuracy has been estimated from a general consideration of all the sources of error. This equation is valid for the temperature region 900°-1500°C, over which both ΔH° and ΔS° appear to be constant. The value for the entropy change, +1.8 eu, is somewhat smaller than the 5 to 9 eu predicted by Brewer (16). On the other hand, it agrees within experimental error with the value of 0.93 recently obtained by Alcock and Hooper (14).

Entropies calculated from the temperature-dependence of the free energy at elevated temperatures are often inconsistent. These experiments indicate one possible reason: a change in activity of the metal caused by surface orientation. In our experiments it was observed that the activity of a platinum surface oriented with a (111) plane parallel to the surface is only 0.62 that of a randomly oriented surface. As these orientation changes occur more or less slowly, depending on the temperature, it is often difficult to detect their effect.

Concluding Remarks

It is rather difficult to develop a detailed mechanism for this reaction because of our fragmentary knowledge of the nature of the adsorption of a gas on a metal surface at elevated temperature. While the chemisorption of gases on metals has been under investigation for a considerable period, the experimental difficulties involved are so great that we still possess only a qualitative picture of the process; this is particularly true at elevated temperature. Recent development by Becker and his associates (17) of the "flash-filament technique," complemented by studies with the field emission microscope of Mueller, have added markedly to our knowledge of the chemisorption on tungsten of oxygen and nitrogen. It is possible to reason by analogy from this information and arrive at a qualitative mechanism for the oxidation of platinum.

Any mechanism for the oxidation of platinum must explain the following experimentally observed facts:

1. The rate of oxidation at any temperature is proportional to the pressure, that is, the rate is first-order with respect to oxygen, depending on the number of collisions per second that oxygen molecules make with the surface.

2. The collision efficiency of the oxygen molecules is independent of the temperature of the oxygen and depends only on the temperature of the platinum. This means that the energy for activation is derived solely from some condition of the surface of the platinum.

3. The rate of oxidation is smaller from a (111) surface than from a randomly oriented surface; however, the energy for activation is the same.

The fact that the reaction is first-order with respect to oxygen indicates that reaction takes place between a Pt atom and an O_2 molecule. Such a collision could take place on a bare platinum surface, the number depending directly on number of collisions of the oxygen molecules with the surface, that is, on the pressure. However, it is unlikely that any of the surface is bare at these high pressures; even

our lowest pressure of 10μ is high when considering chemisorption of oxygen. In addition, the fraction of the surface that is bare would decrease with increasing pressure, so that the reaction would be less than first order with respect to oxygen.

It seems more likely that the surface is covered with a tightly bound layer of O atoms and that on top of this is adsorbed a more weakly bound layer of O_2 molecules whose concentration varies with pressure. Morrison and Roberts (18) have advanced evidence for such a picture to explain their results on the chemisorption of oxygen on tungsten. Morrison and Grummit (19) have found the isosteric heat of the admolecules to be 3 kcal. Likewise, Becker and Hartman (20), in a study of the chemisorption of nitrogen on tungsten, found evidence of a "third layer,"[1] which is most probably chemisorbed N_2 molecules, whose rate of adsorption is linear with pressure even at high pressures.

The platinum atoms must collide with these admolecules for reaction to take place. It seems plausible that the same general mechanism by which a metal evaporates (21) should operate here. That is, a Pt atom dissociates from a monatomic ledge and diffuses over the surface; in this case among the O adatoms. Reaction with O_2 admolecules is most probable when the diffusing Pt atom is at the "saddle point" between two adsorption sites. In this position the Pt atom is held to the substrate by only two bonds (to adjacent atoms in the close packed rows) and is relatively close to the O_2 admolecules in the layer above. If conditions are right, an activated complex can form which can desorb as PtO_2 before dissociation can take place. The energy for activation will depend only on the temperature of the platinum.

The mechanism of the reaction is similar regardless of the type of crystal plane, since the reaction site described previously occurs on all the planes. Hence, the energy for activation should be similar on any type plane. However, either the concentration of platinum atoms diffusing over the surface or the concentration of admolecules may vary with crystal plane, and this could give rise to a difference in rate on different planes.

While the mechanism proposed here is largely conjecture, it seems advisable to suggest some plausible hypothesis because of the importance of this type of reaction. This type of reaction is probably the first step in the oxidation of many metals that form oxide films, and it is desirable to stimulate a better understanding of the atomistics involved.

Acknowledgment

The authors are indebted to Dr. C. E. May for many helpful discussions in the course of this work.

Manuscript received Dec. 13, 1960; revised manuscript received Feb. 20, 1961. This paper was prepared in part for delivery before the Ottawa Meeting, Sept. 28-Oct. 2, 1958.

Any discussion of this paper will appear in a Discussion Section to be published in the December 1961 JOURNAL.

[1] Becker's definition of a layer is somewhat different from that usually employed. In this case there is a N atom layer adsorbed on two types of sites which are referred to as the "first" and "second" layers. The "third layer" is probably adsorbed on top of these.

REFERENCES

1. G. C. Fryburg and H. M. Murphy, *J. Chem. Phys.*, **24**, 175 (1956).
2. G. K. Burgess and R. G. Waltenberg, *Bull. Bur. Standards*, **13**, No. 280, 365 (1916-17).
3. F. E. Carter and Lincoln, cited "Corrosion Handbook," H. H. Uhlig, Editor, p. 703, John Wiley & Sons, Inc., New York, N. Y. (1948).
4. O. Kubaschewski, *Z. Elektrochem.*, **49**, 446 (1943).
5. G. C. Fryburg and H. M. Murphy, *Trans. AIME*, **212**, No. 5, 660 (1958).
6. H. F. Stimson, *J. Research Natl. Bur. Standards*, **42**, 209 (1949).
7. M. Gilbert and J. H. Lobdell, Fourth Combustion Symposium, p. 285, Williams and Wilkins Co., Baltimore (1953).
8. C. J. Smithells, Metals Reference Book, p. 463, Interscience Publishers, Inc., New York (1949).
9. S. Dushman, "Scientific Foundations of Vacuum Technique," p. 78, John Wiley & Sons, Inc., New York (1949).
10. See H. A. Jones, I. Langmuir, and G. M. J. Mackay, *Phys. Rev.*, **30**, 214 (1927).
11. I. Langmuir, *J. Am. Chem. Soc.*, **37**, 1161 (1915).
12. S. Dushman, "Scientific Foundations of Vacuum Technique," p. 745, John Wiley & Sons, Inc., New York (1949).
13. E. K. Rideal and O. H. Wansbrough-Jones, *Proc. Roy. Soc. (London)*, **A123**, 202 (1929).
14. C. B. Alcock and G. W. Hooper, *Proc. Roy. Soc.*, **A254**, 551 (1960).
15. A. Schneider and U. Esch, *Z. Elektrochem.*, **B24**, 59 (1934).
16. L. Brewer and G. R. B. Elliott, UCRL-1831, June 1952; see L. Brewer, *Chem. Revs.*, **52**, 1 (1953).
17. J. A. Becker, "Solids State Physics," vol. 7, p. 379, Academic Press, Inc., New York (1958).
18. J. L. Morrison and J. K. Roberts, *Proc. Roy. Soc.*, **A173**, 1 (1939).
19. J. L. Morrison and W. E. Grummit, *J. Chem. Phys.*, **21**, 654 (1953).
20. J. A. Becker and C. D. Hartman, *J. Phys. Chem.*, **57**, 157 (1953).
21. O. Knacke and I. N. Stranski, "Progress in Metal Physics," p. 181, Pergamon Press, Ltd., London and New York (1956); J. P. Hirth and G. M. Pound, *J. Chem. Phys.*, **26**, 1216 (1957).
22. R. Lacroix, *Rev. mét.*, **53**, No. 11, 809 (1956).
23. R. Bakish, *Acta Met.*, **6**, 120 (1958).

APPENDIX

Surface Morphology

A microscopic examination was made of the surfaces of the specimens that had been used to study the effects of temperature on the rate of oxidation. The specimens made from the narrow ribbon that had not been heated above 1250°C appeared similar to the thermally etched surfaces recently depicted by Lacroix (22). They were composed of many grains of the order of tenths of a millimeter in diameter. A large fraction of the grains exhibited the typical striations commonly found with thermally etched metals.

Specimens made from the narrow ribbon that had been heated to 1400° and 1500°C exhibited much larger grain size. The grains usually extended across the entire width of the ribbon and were several millimeters long. Visual examination showed large, very shiny areas, interrupted by smaller, etched-like areas. X-ray back-reflection measurements indicated that the smooth areas had a (111) plane parallel with the surface, while the etched-like areas had a (311) plane parallel with the surface. Microscopic examination showed that the (111) areas were smooth except for some small pips dotting the surface. Occasionally, a smaller striated grain was found in the (111) areas indicating that the (111) plane was not lying exactly in the plane of the surface in this grain. The (311) areas appeared to be

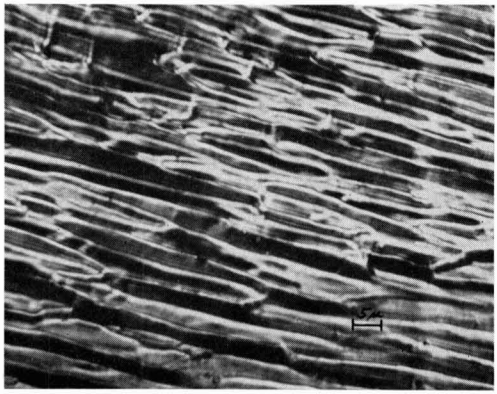

Fig. 5. Typical (311) surface

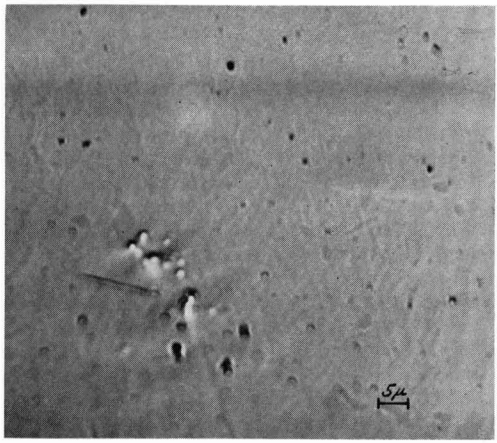

Fig. 6. Surface of wide ribbon after much oxidation

composed of steps; a typical micrograph is shown in Fig. 5.

Specimens made from the wide ribbon and annealed at 1250°C appeared more and more shiny as oxidation proceeded. X-ray back-reflection measurements indicated the entire surface was oriented with a (111) plane parallel to the surface. Microscopic examination revealed that the specimens were fairly large-grained of the order of millimeters in diameter. No striated grains were observed nor were any grains with the typical (311) appearance (Fig. 5) observed. The surfaces were marked with die scratches from drawing and dimpled from rolling. As oxidation proceeded these markings were smoothed out. Figure 6 shows a heavily oxidized ribbon depicting the typical smooth surface dotted with small pips. It was not determined whether these pips were the result of dislocations as found on tantalum by Bakish (23), or whether they resulted from specks of dirt on the surface inhibiting the normal oxidation at that spot. It was noted, however, that the concentration of pips was much greater near places where the ribbons had been bent appreciably.

The Oxide Films Formed on Copper Single Crystal Surfaces in Water

II. Rate of Growth at Room Temperature

Jerome Kruger

National Bureau of Standards, Washington, D. C.

ABSTRACT

Measurements utilizing polarized light were made of the increase in film thickness with time on {100}, {110}, {111}, and {311} surfaces of a copper single crystal immersed in water in equilibrium with atmospheres containing either oxygen or oxygen-helium mixtures containing 1, 10, or 20% oxygen. With the oxygen atmosphere a Cu_2O film rapidly reached a limiting thickness that remained constant for 1.5 to 2 hr after which time the formation of CuO was observed. Stirring increased the time required to observe the formation of CuO. Similar behavior was observed for 10% and 20% oxygen atmospheres; the limiting film thickness of Cu_2O and the time required to observe the formation of CuO increased with decreasing oxygen content in the atmosphere. When a 1% oxygen atmosphere was used, parabolic film growth was observed. In all cases the {111} plane exhibited the lowest growth rate.

The first paper in this series (1) described qualitative studies of the films formed on copper single crystal surfaces immersed in water containing oxygen. It was concerned with the chemical composition of the film, structural relationships between metal and oxide, and the morphology of the oxides. The work described here deals with experiments designed to learn something about the rate of film formation by measuring change in film thickness with time. The polarizing spectrometer or, as it will be called throughout this paper, the ellipsometer was used to measure the thickness of the films formed on copper. With this instrument the thickness of oxide film growing on a metal surface is determined by reflecting polarized light from a polished metal surface and then measuring the change in ellipticity that this polarized light suffers as a result of its being reflected by the film-bearing metal surface. This

change is dependent on, among other things, the thickness of the film.[1]

One of the important advantages in using the ellipsometer to study film formation on metal surfaces immersed in a liquid is that it is possible to study the rate of formation while the process is actually going on without disturbing it. Further, the growth of films on selected areas of a specimen can be studied. This is especially valuable in this study which uses single crystal surfaces in that a number of crystallographic planes on a given specimen can be studied during a single experiment.

With the possible exception of the classic work of Tronstad and co-workers (3, 4) on iron and aluminum, the ellipsometer has not been employed in the study of film formation on immersed metal surfaces. Nothing appears to be available in the literature on the use of the ellipsometer to study the rate of film formation on copper immersed in high-purity water containing oxygen. A few electrometric measurements were made on this system by Davenport, Nole, and Robertson (5), but the thin films formed precluded any detailed analysis because of their method of measurement. Hence very little has been done for this system in spite of the fact that such a study would appear to be of utmost importance in serving as a starting point toward gaining a more fundamental understanding of the corrosion of copper in more complicated systems.

Experimental Method

Ellipsometry.—A detailed description of the type of ellipsometer used and the method and theory employed to interpret the results obtained with it are given elsewhere (6). However, in order that certain points in what follows be clear, it is necessary to outline briefly the manner in which ellipsometric measurements were made.

It should be pointed out first that it is necessary to know the index of refraction of the material making up a film in order to determine its thickness with the ellipsometer. This quantity is a complex number for the oxides of copper and may vary depending on the manner in which the film was formed. In order to determine the refractive index, one has to calculate for the system under study values for the relative phase retardation, Δ, and relative amplitude reduction, $\tan \psi$, for a number of film thicknesses using an assumed refractive index. Since this calculation is a long and tedious one, it has been programmed for an IBM 704 Digital Computer. One then compares the calculated curve with an experimental curve obtained by measuring Δ and $\tan \psi$ for different film thicknesses for the system under study where film growth is taking place. When a theoretical curve for a given refractive index corresponds to the experimental curve, the refractive index of the film material is taken as that of the matching theoretical curve. In order that an accurate determination of the refractive index of the oxide film be made, it is necessary to measure films whose thicknesses range as high as about 1000Å. However, most of the films studied had thicknesses less than 150Å; therefore, the refractive index could not be determined accurately. For films below 100Å, however, thickness values are rather insensitive to changes in the refractive index, and an accurate knowledge of it is not necessary to measure thickness to ±3Å or better (7). Another condition that must be met in order to measure film thickness, with the calculation as presently programmed for the computer, is that the film be composed of a single isotropic component. It is possible to consider two component films but this increases the complexity greatly.

As a check of the ellipsometric method of measuring film thickness, a few crude electrometric reduction measurements were made. These agreed within ±10Å in the 0-100Å range. This agreement is satisfactory when account is taken of the fact that the crystal had to be removed from the reaction apparatus in order to make the electrometric reduction measurements. During this time changes in film thickness could occur.

Reaction apparatus and procedure.—The apparatus used to carry out the film formation studies under controlled conditions is shown in Fig. 1. The copper single crystals used were machined as cylinders with their axes in the <110> direction. Using a crystal of this orientation, it was then possible to cut flat surfaces parallel to the {111}, {110}, {100}, and {311} crystallographic planes, these planes being parallel also to the cylinder's axis as shown in Fig. 1. The {311} plane was studied in addition to the low index planes because it has been found to be the slowest oxidizing plane in gaseous oxidation (8). With such a crystal sealed into this apparatus, the various crystallographic planes could be rotated into position by means of a magnet so that measurements could be made on them with the ellipsometer at various times during the oxidation process.

The analysis of the copper used in the crystal (99.99+% copper), the method of preparation used to render the crystal surface smooth and strain-free, and the manner in which high-purity water was introduced into the lubricated joint-free apparatus are described in the first paper of this series (1). Lubricated stopcocks were used to introduce purified

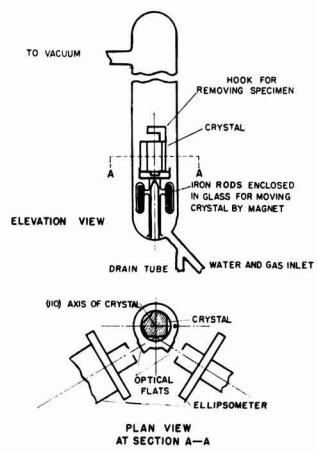

Fig. 1. Apparatus for studying the formation of films on a copper single crystal immersed in water.

[1] The thickness measured by the ellipsometer is that thickness one would observe if one redistributed the material making up the film so as to form a uniform layer (2).

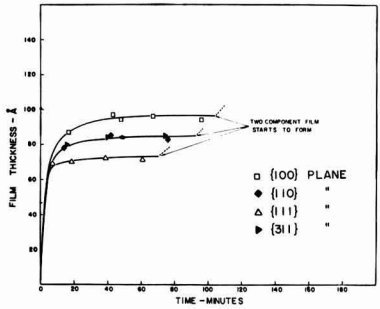

Fig. 2. Growth of oxide film on copper in unstirred water in equilibrium with 1 atm of O_2.

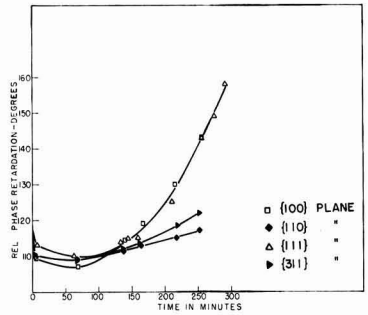

Fig. 3. Change in relative phase retardation for film growing on copper in unstirred water in equilibrium with 1 atm of O_2.

gases, but these were separated from the system by traps containing copper turnings. Satisfactory reproducibility was obtained only after distilling in water a number of times to wash the crystal and apparatus. After each washing the apparatus was baked out over night, and annealed in purified hydrogen at 500°C. The rate of oxidation was checked each time while the crystal was immersed during a wash, the water being drained out before the oxide got thicker than 50Å. When the values obtained matched those obtained previously, a complete run was made. The optical parameters of the unfilmed copper surface in water, on which all of the data on the film surface were based, were determined by measurements on the copper surface in vacuum immediately after annealing in hydrogen. Thus values for the unfilmed copper surface in water then could be calculated from these vacuum values.

Results

The results obtained when a copper crystal was immersed in unstirred water in equilibrium with 1 atm of oxygen are shown in Fig. 2. Very rapid oxidation took place initially, followed by a leveling off at 65-95Å. This leveling off indicated that some type of logarithmic law governed the process. Further it was found that the {111} face exhibited a smaller limiting film thickness than the other three faces studied. This oxidation behavior was similar to that observed by Rhodin (9) for copper single crystal surfaces oxidized at room temperature in gaseous oxygen except that the limiting thickness was greater for oxidation in water.

Another very important feature noted for oxidation under these conditions was that Δ reaches a minimum after from 90 to 120 min and then begins to increase. This is shown in Fig. 3, where instead of film thickness, Δ is plotted *vs.* time because the thickness cannot be determined after Δ reaches the minimum shown in Fig. 3. It can be seen that the greatest change in Δ occurs for the {100} and the {111} faces. This change in optical parameters was probably associated with the formation of a new component or layer in the oxide film. Evidence from the x-ray results described in the first paper of this series (1) would indicate that this is most probably CuO. The reasonableness of this assumption, *i.e.*, that a new component starts to form, is made clear by Fig. 4. In this figure are plotted the two optical

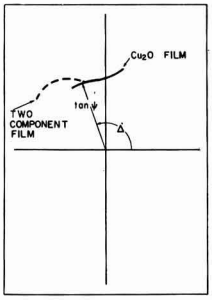

Fig. 4. A comparison between the polar plot of relative phase retardation, Δ, and relative amplitude reduction, tan ψ, calculated for a Cu_2O film growing on copper and obtained experimentally for a film starting out as Cu_2O and then starting to form a second component.

parameters, Δ and tan ψ, determined by the ellipsometer for films of different thicknesses both for the all-Cu_2O film, and for the two-layer film found experimentally. If the Cu_2O film had continued to thicken, the optical parameters would have moved to the right on the solid curve. Instead, after a film of 65-95Å had formed on the copper surface after 90 to 120 min, the parameters suddenly followed the dashed curve. It is also known from previous work on the system that the introduction of CO_2 will convert the CuO to Cu_2O. When this was done, after the parameters measured were those found on the two component curve, subsequent measurements of Δ and tan ψ always lay on the solid curve, that calculated for a film made up of Cu_2O only. If the sudden change in optical parameters was associated with changes in structure or the introduction of strain, as is sometimes the case, it is highly unlikely that introduction of CO_2 would have brought the values of the optical parameters back to the curve calculated for Cu_2O. Hence it seems reasonable to say that the sudden change in the optical parameters was associated with formation of CuO. Since the CuO was formed as a second component, the method described for studying the rate of its formation could not be used because calculations have not been made for films containing two components.

One observation made when a crystal was removed after being immersed for 18 hr should be mentioned. The CuO formed was loosely held and could be par-

tially wiped off. Beneath it a film was observed showing interference colors, presumably Cu_2O. These interference colors indicated thicknesses greater than the limiting thickness of the Cu_2O, 65-95Å, observed before the formation of CuO. Thus it appeared that, as the CuO formed, the Cu_2O layer underneath was also increasing in thickness. Therefore, since both CuO and Cu_2O were growing simultaneously and at different rates, the values of Δ plotted in Fig. 3 were related in a complicated manner to the thickness of the combined film. Hence one cannot say from looking at this plot that the {100} and {111} planes have thicker films on them than the {311} and {110}.

As a valuable aid in understanding the process just described wherein CuO starts to form after 1.5 to 2 hr, spectrochemical analyses of the water in which the copper crystal was immersed were made after given times of exposure. It was found that the concentration of copper was extremely low, no concentration higher than 0.05 mg/l being observed. Further it was found for the case where oxidation was carried out with the water in equilibrium with 1 atm of pure oxygen that before the formation of CuO the concentration of copper was found to be less than 0.02 mg/l. After CuO began to form the concentration was 0.04 mg/l. This concentration of copper agrees quite well with the concentration that one would calculate from the solubility product of CuO. Hence it would appear that the CuO precipitates out on the Cu_2O-copper surface when the concentration of cupric ions reaches the proper level.

Going from these experiments where stagnant water was in equilibrium with 1 atm of oxygen to the case where the water was stirred by bubbling in oxygen at different rates, the same behavior was observed except for one significant difference. The time necessary for the first traces of CuO to appear increased with an increase in stirring rate. Table I illustrates this. The stirring rates were not sufficiently accurately maintained to allow one to draw any quantitative conclusions, and the manner of stirring was not conducive to reproducibility. Qualitatively, however, there was a definite relationship between stirring rate and time required for the formation of CuO to commence.

Oxygen-helium mixtures in equilibrium with pure water.—The next series of experiments was carried out with the copper crystal immersed in water in equilibrium with oxygen at partial pressures less than 1 atm. In all of these experiments the total pressure was brought up to 1 atm by the addition of helium. Figure 5 shows the progress of oxidation under stagnant conditions in an atmosphere containing 1% oxygen. The curves are not plotted for longer times than those shown in Fig. 5 because a gradual change in refractive index took place. Thus, after a film of about 160Å or more was formed, thickness measurements became uncertain. Quite thick films, 1000Å or more, were formed after a period of 18 hr. Electron micrographs of replicas of the four crystal surfaces studied are shown in Fig. 6, 7, 8, and 9. They show that the films formed were not uniform in thickness and that the oxide morphology depended on the crystallographic orientation of the metal surface on which they were growing. This nonuniformity may not be the case, however, for very thin films.

Table I. Effect of stirring on time required for the start of CuO formation

Oxygen flow rate, ml/min	Time, min
0.0	120
0.17	237
0.47	292

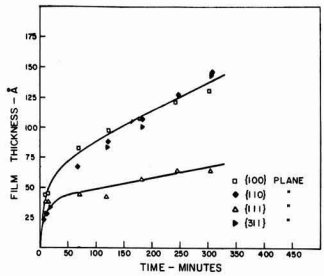

Fig. 5. Growth of an oxide film on copper in unstirred water in equilibrium with 1 atm of a helium-1% oxygen mixture.

Fig. 6. Electron micrograph of {100} surface of copper oxidized in water in equilibrium with a helium-1% oxygen atmosphere for 18 hr. Direct carbon replica, preshadowed with palladium. 40,000X (All magnifications are before reduction for publication.)

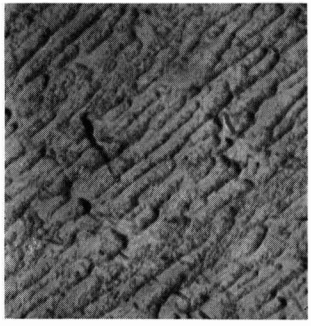

Fig. 7. Electron micrograph of {110} surface of copper oxidized in water in equilibrium with a helium-1% oxygen atmosphere for 18 hr. Direct carbon replica, preshadowed with palladium. 40,000X

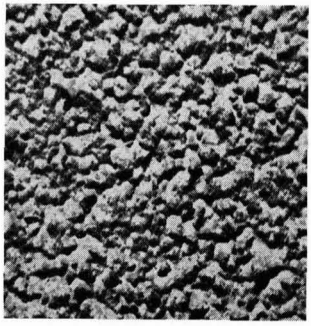

Fig. 8. Electron micrograph of {111} surface of copper oxidized in water in equilibrium with a helium-1% oxygen atmosphere for 18 hr. Direct carbon replica, preshadowed with palladium. 40,000X

Fig. 9. Electron micrograph of {311} surface of copper oxidized in water in equilibrium with a helium-1% oxygen atmosphere for 18 hr. Direct carbon replica, preshadowed with palladium. 40,000X

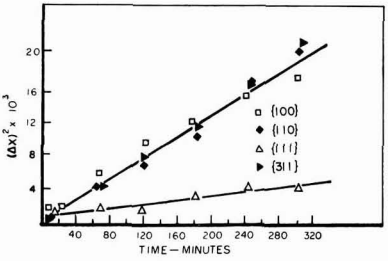

Fig. 10. Parabolic plot for growth of an oxide film on copper in unstirred water in equilibrium with 1 atm of a helium-1% oxygen mixture.

It can be seen from Fig. 5 that the results obtained here differed markedly from the pure oxygen atmosphere case. First, the film thicknesses exhibited were greater than in the pure oxygen case, and second, as Fig. 10 shows, the rate appeared to obey a parabolic law.

The fact that a parabolic rate law appears to be observed poses the question as to whether, at these low concentrations of oxygen, diffusion of oxygen in the solution was the rate-controlling step or whether diffusion in the film was important. It is difficult, however, to explain such a marked difference in the rate between the {111}, which had a parabolic rate constant of 0.13Å²/min, and the other

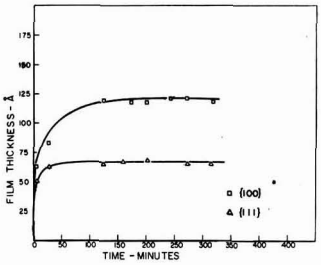

Fig. 11. Growth of an oxide film on copper in unstirred water in equilibrium with 1 atm of a helium-10% oxygen mixture.

orientations, which had essentially equivalent rate constants whose average was 0.63Å²/min, if diffusion of oxygen in solution were rate controlling. Further, stirring did not appear to affect appreciably the rate but tended to make the behavior less parabolic, indicating that greater accessibility of oxygen made the process tend to approach a logarithmic behavior. Figure 11 would indicate that this is so. Here the oxidation occurred in water in equilibrium with an atmosphere of 10% O_2. Only the results for the {111} and {100} planes are plotted since the {110} and {311} gave results similar to that for the {100}. For the 10% oxygen atmosphere the rate of Cu_2O formation was greater than that for the stagnant 100% O_2 case; thicker films of Cu_2O were formed, but less than in the 1% case. Moreover the behavior was logarithmic in nature rather than parabolic as was the case for a 1% oxygen atmosphere. The film thickness for this 10% case lay intermediate between the 100% oxygen and the 1% oxygen. The rate, however, of cupric ion formation was also important. It was increased and hence the rate of Cu_2O formation was still further inhibited. By allowing the crystal to stand in contact with the water and the 10% oxygen atmosphere for two days, CuO was observed to form in the same fashion as in the 100% oxygen case. After the thickness had leveled off to a constant value, the formation of CuO could be brought about immediately by replacing the 10% oxygen atmosphere with pure oxygen.

When the water was in equilibrium with a 20% oxygen atmosphere, the behavior approached that of a 100% oxygen atmosphere in an even more pronounced fashion than for the 10% case, and CuO appearance was observed after about 4 hr.

Discussion

The oxidation of copper in oxygenated water produces two oxides, and the factors that control which of these oxides is the thermodynamically stable phase have a major influence on the rate observed and the type of rate law followed. Those factors as pointed out in the first paper of this series are the partial pressure of oxygen and the *p*H. Cu_2O is always formed next to the copper surface, but whether or not this thin film continues to grow as Cu_2O depends on the oxygen concentration and on the *p*H of the solution. (The *p*H was altered by the introduction of CO_2.) Considering first the situation when the oxygen concentration was high, it was

found that the Cu_2O film after a rapid initial logarithmic buildup ceased to grow appreciably and reached a limiting thickness. It appears that the limiting thickness of the initial Cu_2O film resulted from the competing reactions

$$Cu + Cu^{++} \rightarrow 2Cu^{+}$$

and

$$Cu^{+} \rightarrow Cu^{++} + e^{-}$$

The value of the limiting thickness probably depended on the ability of electrons and ions to get through the oxide film and react at the surface. At thicknesses below the limiting thickness enough electrons were available to reduce Cu^{++} to Cu^{+}, and the film increased in thickness. At greater thicknesses, the cuprous ions were oxidized to cupric, and these went into solution until the solubility product constant for CuO was exceeded. Once this happened, CuO precipitated out onto the surface. This then limited the oxygen available to the surface, and conditions became favorable for cuprous oxide to continue to grow underneath this CuO film. This is just what was observed. When the solution was stirred, the time for CuO to form was increased. This appears to be due to the fact that the cupric ions were simply carried away from the surface by stirring, and precipitation could occur in the body of the liquid, thus increasing the time required before enough CuO was precipitated at the surface to affect the oxidation process.

The fact that the initial buildup of Cu_2O was logarithmic is not too informative because almost any process which tends to come to a standstill would conform approximately to a logarithmic "law" (10). Because of the subsequent formation of CuO, it appears that such a relationship is not necessarily the result of a single uniform process. Consequently no rate constant has been derived. The theories of either Cabrera and Mott (11) or Uhlig (12), both of which predict logarithmic behavior for very thin films at low temperatures, may be applicable if a single process is operative. Studies on the effect of temperature would perhaps decide between the two theories since the Cabrera and Mott theory predicts that the rate constant is temperature independent while Uhlig's does not. Or perhaps, more likely, an entirely new theory is necessary for film growth in contact with a liquid where the dielectric constant of the liquid, electrochemical potentials between various crystal faces, adsorption of ions from solution, and other factors must all influence the oxidation process.

When the oxygen concentration was low, it was found that Cu_2O was the stable phase. Its films grew to greater thicknesses than those formed when the oxygen concentration was high because there was less tendency for the cuprous ions formed to oxidize to the more soluble cupric. Stirring did not increase this rate of Cu_2O formation in the 1% oxygen atmosphere experiment because oxygen accessibility was increased and the equilibrium shifted toward CuO. This is further emphasized when the oxygen concentration was increased by using a 10% oxygen atmosphere because the rate of Cu_2O formation became logarithmic again and CuO was eventually formed. Here, however, the limiting thickness of Cu_2O was higher than in the case where 100% oxygen atmosphere was in equilibrium with the solution.

For both high and low oxygen concentrations, the {111} crystallographic plane exhibited the smallest rate of oxidation. This fact may be related to Tragert and Robertson's observation (13) that the {111} plane of copper exhibited the most noble electrochemical potential of all of the low index planes studied.

This points out that electrochemical considerations may be of great importance in determining the order of increasing rate of oxidation for the various crystal planes. While the {111} is the slowest for oxidation in water, it is, next to the {100}, the fastest in gaseous oxidation at temperatures from 70° to 178°C (8). The fact that {111} exhibits both the slowest oxidizing rate and the most noble potential may be due to the fact that of all the planes in the F.C.C. system it has the highest work function, *i.e.*, it gives up its electrons least easily. Another important factor, however, in determining order of rate of oxidation among crystallographic planes is the physical nature of the oxide formed (degree of preferred orientation, imperfections, morphology, etc.). As the earlier study of this system (1) showed, the {100} has the most poorly oriented oxide film and would tend to oxidize faster. However, a great deal more has to be learned before any really definite reasons for the order in rate of oxidation between the various orientations can be given.

Besides the differences of rate of oxide formation between the different planes, work by a number of investigators (14-16) points to differences observed on the same crystal face where impurities, dislocations, and other imperfection may play a great role. Figures 6, 7, 8, and 9 illustrate the noncontinuous nature of the oxides formed and their dependence on crystallographic orientation. A study of these considerations will be the next step in the investigation.

Acknowledgment

The author is indebted to R. H. Duff, who carried out the electron microscopy and to Mrs. Martha M. Darr, who performed the spectrochemical analyses. He is also very grateful to the Corrosion Research Council, who supported this work in part.

Manuscript received Oct. 21, 1960; revised manuscript received Feb. 20, 1961. This paper was prepared for delivery before the Ottawa Meeting, Sept. 28-Oct. 2, 1958.

Any discussion of this paper will appear in a Discussion Section to be published in the December 1961 JOURNAL.

REFERENCES

1. J. Kruger, *This Journal*, **106**, 847 (1959).
2. A. B. Winterbottom, "Optical Studies of Metal Surfaces," p. 47, Det Kgl Norske Videnskabers Selskabs Skrifter 1955, *1*, F. Bruns Bokhandel, Trondheim (1955).
3. L. Tronstad, *Trans. Faraday Soc.*, **29**, 502 (1933).
4. L. Tronstad and T. Hoverstäd, *ibid.*, **30**, 362 (1934).
5. W. H. Davenport, V. F. Nole, and W. D. Robertson, *This Journal*, **106**, 1005 (1959).
6. J. Kruger and W. J. Ambs, *J. Opt. Soc. Amer.*, **49**, 1195 (1959).

7. L. Tronstad, *Trans. Faraday Soc.*, **31**, 1151 (1935).
8. F. W. Young, Jr., J. V. Cathcart, and A. T. Gwathmey, *Acta Met.*, **4**, 145 (1956).
9. T. N. Rhodin, Jr., *J. Am. Chem. Soc.*, **73**, 3143 (1951).
10. O. Kubaschewski and B. E. Hopkins, "Oxidation of Metals and Alloys," p. 45, Academic Press, New York (1953).
11. N. Cabrera and N. F. Mott, *Repts. Prog. Phys.*, **12**, 163 (1948-49).
12. H. H. Uhlig, *Acta Met.*, **4**, 541 (1956).
13. W. E. Tragert and W. D. Robertson, *This Journal*, **102**, 87 (1955).
14. W. W. Harris, F. L. Ball, and A. T. Gwathmey, *Acta Met.*, **5**, 574 (1957).
15. J. Bardolle and J. Benard, *Rev. Metall.*, **49**, 613 (1952).
16. G. T. Miller, Jr. and K. R. Lawless, *This Journal*, **106**, 854 (1959).

Use of Polarization Methods in the Determination of the Rate of Corrosion of Aluminum Alloys in Anaerobic Media

S. Evans and E. L. Koehler

Central Research and Engineering Division, Continental Can Company, Inc., Chicago, Illinois

ABSTRACT

Tafel-type cathodic polarization curves were obtained for aluminum alloys corroding in anaerobic acid and food media. The overvoltage-intercept method was found to give corrosion currents equivalent to the measured rates of hydrogen evolution. Tafel-type anodic polarization curves could not be obtained. Anodic polarization curves calculated from cathodic polarization data in the vicinity of the corrosion potential gave Tafel slopes which were identical to the cathodic Tafel slope, within 20%, in each individual case. On using suitable values for the Tafel slopes in the Stern and Geary equation, the polarization resistance method likewise gave corrosion currents in good agreement with measured rates of hydrogen evolution.

This investigation arose from the need for a sensitive method of determining the instantaneous corrosion rate of aluminum in anaerobic media under conditions where it is not possible to measure such quantities as weight loss and hydrogen evolution. The use of polarization methods in determining the corrosion rate of iron and steel has been demonstrated (1-3). The purpose of this investigation was to determine the applicability of such methods to the corrosion of aluminum.

In a study of the corrosion of iron in a variety of deaerated acid media it has been found that there exists a *p*H range for each acid studied wherein the corrosion potential varies by approximately 0.059 v for each unit *p*H range (1, 4-6). In effect the corrosion potential of an iron electrode behaves in a manner analogous to the reversible hydrogen electrode.

Stern (1) has reported that the cathodic polarization curve for iron in deaerated acid media exhibits Tafel-type behavior and has derived a relationship between corrosion rate, corrosion potential and hydrogen overvoltage. Utilizing these principles, Kaesche and Hackerman (2) graphically determined corrosion rates for iron in 1*N* HCl from cathodic polarization measurements. This graphical method is referred to in this paper as the overvoltage-intercept method.

Polarization data obtained in the region of the corrosion potential have also been used to determine corrosion rates. Skold and Larson (7) have demonstrated that for iron and steel in media of varying corrosiveness the polarization potential is a straight line function of the applied anodic or cathodic currents at low current density. Since the slope, $\Delta E/\Delta I$, has units of resistance, this term has been conveniently called the polarization resistance (8). A plot of corrosion rates *vs.* polarization resistances on logarithmic scales yields a straight line with a slope of minus one.

Stern and Geary (9), in a discussion of the shape of polarization curves for corroding systems controlled by activation polarization, showed that a linear relationship is expected in the region where the polarized potential is close to the corrosion potential. The following equation was derived:

$$\frac{\Delta E}{\Delta I} = \frac{\beta_a \beta_c}{2.3\,(I_{corr})\,(\beta_a + \beta_c)} \qquad [1]$$

where $\Delta E/\Delta I$ is the polarization resistance, β_c and β_a are the slopes of the logarithmic local cathodic and anodic polarization curves, and I_{corr} is the corrosion current, equivalent to the rate of corrosion by Faraday's law. Stern has described the polarization resistance method in detail, discussing its advantages and limitations (8).

Each of these two methods has its advantages and limitations, and both will find their areas of application. The polarization resistance method has the advantages of greater general applicability and greater ease of use. Successful use of the polarization resistance method depends on proper evaluation of the beta constants in the Stern and Geary equation,

but fortunately this is not usually much of a problem. Stern and Weisert discuss possible errors in the method (10). In most cases the corrosion rate can be estimated with useful accuracy even with no advance knowledge of the value of these constants. Consideration as to their proper value for the individual cases is given here, however, because maximum accuracy is desired and because some of the unusual corrosive media employed may result in unusual beta values.

The polarization methods are particularly desirable in the determination of the corrosion of aluminum in food media since they represent a practical approach to the determination of corrosion rates where such rates are too low to measure accurately by direct means. In addition, however, this represents an application of sound electrochemical principles, generally believed valid only for highly purified systems, to corroding systems which are "electrochemically impure."

Experimental

The test cell assembly and the polarization equipment used in this study have been described (11). The test cell was designed so that hydrogen evolution could be measured, and so that a saturated calomel electrode could be exposed to the test solution by means of a stopcock. The area of specimen exposed to the solution was 5.31 cm^2. A potentiostatic device provided a selected linear rate of change of potential *vs.* saturated calomel with respect to time. Polarization curves were plotted directly on a current recorder chart.

The specimens used in this study were degreased in carbon tetrachloride solution. The acid media were made from reagent grade chemicals. Water used in tests was first passed through a deionizing column and then distilled from an alkaline permanganate solution. Solutions were flushed with oxygen-free hydrogen for 2 hr prior to filling the cells. Cells were flushed with air-free nitrogen and filled in such a manner as to exclude all air.

The food media selected for this study included a commercial brand of each of the following: apple juice, beef gravy, beer, cream style corn, frozen green beans, prune juice and tomato juice. With corn, green beans, and beef gravy it was necessary to use a blender to put these media in such a form that they could be transferred to test cells. Prune juice was saturated with hydrogen and then transferred to cells as above. The pressure above the other media was reduced to about 20 mm to eliminate air and held at this level prior to filling the cells. Food media were pasteurized at 170°F for 20 min by placing the filled cells in an oven prior to placing them in the constant temperature room. There was no indication of spoilage in any of the food media.

Test cells were placed on shelves in a constant temperature room maintained at 37.8°C (100°F). All desired electrical readings were made off panel boards on the outside of the room. Polarization data ordinarily were not obtained until after one week at temperature. It is to be anticipated that any oxygen remaining in the medium after filling the cell would be reduced during the pasteurization treatment and subsequent storage at 37.8°C. The polarization data indicated this to be the case.

To enable the easy handling of more than a thousand tests in this program it was judged to be more expedient to use the simplest possible test cell and to correct for *IR* drop in the test medium rather than to use a Luggin capillary. A cell consisted essentially of a horizontal cylinder with specimens sealed on opposite ends. It was geometrically symmetrical about the plane through the center parallel to the specimens, which plane contained the reference electrode. With the overvoltage-intercept method potentials were corrected where the *IR* drop was significant ($\geqq$1 mv). The resistance of each test medium was determined at 37.8°C with standard conductance equipment, and the correction was one half the *IR* drop through the cell. It was found that any significant resistance error would result in a nonlinearity of the Tafel plot at high current densities. For the data reported here, current densities were well below such a point. In the polarization resistance method, ½*R* was subtracted directly from the polarization resistance.

Beta values.—The value of β_c in the Stern and Geary equation could in all cases be determined directly from the slope of the Tafel plot. In only one case, that of the very lowest corrosion rate, was a Tafel-type anodic polarization curve found. As a matter of practical necessity, therefore, use could be made only of the cathodic polarization curve plus a small segment of the anodic polarization curve near the corrosion potential.

The overvoltage-intercept method actually requires no precise definition of an anodic reaction curve in the vicinity of the corrosion potential. The only assumption required is that the Tafel equation for the hydrogen evolution reaction holds down to the corrosion potential.

The derivation of the Stern and Geary equation is based upon the following two relationships:

$$\epsilon = \beta_c \log \frac{i_c}{i_{corr}} \qquad [2]$$

$$i_{applied} = i_{cathodic} - i_{anodic} \qquad [3]$$

The first of these, [2], is merely a convenient form of the Tafel equation. This is an expression for the determination of i_{corr} by the overvoltage-intercept method. It follows that the i_{corr} in the Stern and Geary equation should be mathematically identical to the i_{corr} determined by the overvoltage-intercept method.

The second expression [3] is the basis for the determination of the "calculated anodic polarization curve" (9) in the vicinity of the corrosion potential. Introduction of β_a in the Stern and Geary equation through Eq. [3] mathematically defines β_a as the slope of the calculated anodic polarization curve. The validity of the method is not dependent on the existence of an experimentally determinable anodic polarization curve nor is it necessarily dependent on the agreement of any experimentally determined anodic reaction curve with the calcu-

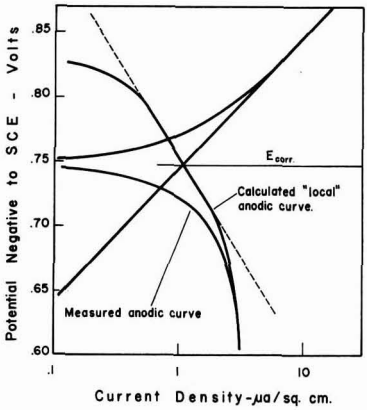

Fig. 1. Typical relationship between calculated "local" anodic curve and experimentally determined anodic curve.

lated. However, any such agreement is in confirmation of the validity of the treatment.

Figure 1, showing the polarization behavior of 3003 aluminum in pH 3.5 citrate buffer, is typical. The measured anodic polarization curve was not of Tafel form. The calculated anodic polarization curve, which is determined at each potential from the applied current and the cathodic current represented by the extrapolated Tafel line according to Eq. [3], has a straight line section, the slope of which gives β_a. The values of the betas were so determined for each system studied in the program and in all cases it was found that $\beta_a = \beta_c$ within 20%. Since a 20% variation is negligible, corrosion rates were calculated on the basis that $\beta_a = \beta_c$. It is not meant to infer that this simplification will be valid for metals other than aluminum.

The work reported here is for confirmatory purposes. From a practical standpoint it would make no sense to determine even β_c for each case in which the polarization resistance method is used, since once the Tafel plot is made it is simpler to determine directly the corrosion rate by overvoltage-intercept. All that is needed is an approximate knowledge of the beta values for the system (*10*).

Corrosion in air-free acid media.—Hydrogen evolution and weight loss measurements for 3003-0 aluminum in hydrogen-saturated acetate buffer (pH 4.6) are shown in Fig. 2. The acetate buffer was at its maximum buffer capacity. The pH of these solutions was measured after each time interval and was found to remain constant throughout the test. Similar experiments were conducted with citrate buffer. The results indicate that the measured rate of hydrogen evolution is essentially equal to the hydrogen equivalent of the aluminum weight loss rate.

The variation of corrosion potential of 3003-0 aluminum with pH, dE/dpH, in citrate buffer solutions[1] was determined by the method of least squares and is shown in Fig. 3. The corrosion potentials recorded were measured after the test had run for three days, when potential values became fairly constant. The range of the measured potentials is shown by the vertical lines. The potential of a platinized platinum (hydrogen) electrode in these solutions is also presented in Fig. 3, and it can be seen that the line representing corrosion potential as a function of pH is of like slope but above that for a reversible hydrogen electrode. Over the pH range investigated, aluminum was approximately 300 mv more active than a reversible hydrogen electrode in the same solution.

The corrosion rates of 3003-0 aluminum in citrate buffer solutions of varying pH are presented in Fig. 4. The slope of the straight line obtained from a plot of milliliters of hydrogen evolved *vs.* time was used

[1] The citrate buffer solutions used in these tests were made so that the molar sum of citric acid and sodium citrate was 0

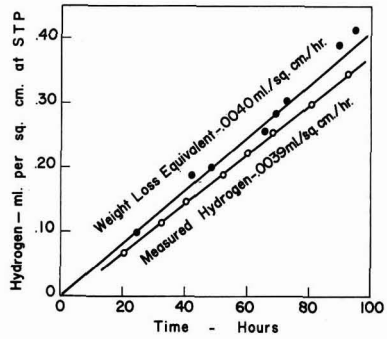

Fig. 2. Rate of hydrogen evolution from 3003 aluminum in acetate buffer together with the hydrogen equivalent of the aluminum weight loss (37.8°C).

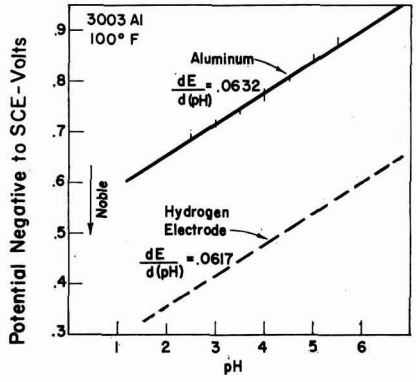

Fig. 3. Effect of pH on the corrosion potential of 3003 aluminum in hydrogen-flushed citrate buffer solutions (37.8°C).

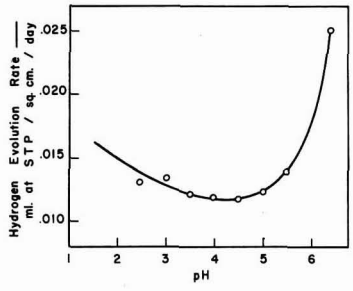

Fig. 4. Dissolution rate of 3003 aluminum at 37.8°C as a function of pH.

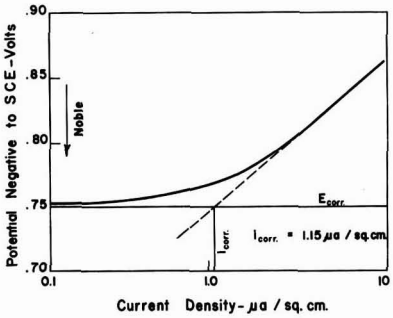

Fig. 5. Typical cathodic polarization curve obtained on 3003 aluminum in hydrogen-flushed pH 3.5 citrate buffer solution (37.8°C).

to determine corrosion rate from hydrogen evolution. Each value is an average of six replicate experiments. The average deviation from the mean was in the range 0.0003 ml/day/cm² at STP.

Cathodic polarization curves obtained on aluminum in hydrogen-flushed citrate buffer solutions exhibit Tafel-type behavior (Fig. 5). (It is to be emphasized that Fig. 5 and all other polarization curves shown are not schematic; they represent actual data. These curves were determined continuously and not as a series of distinct experimental points.) The portion of the overvoltage curve in the vicinity of the corrosion potential is obtained by extrapolating the Tafel line to the corrosion potential. The current density at which the straight line intersects the corrosion potential is equivalent by Faraday's law to the corrosion rate. This is the overvoltage-intercept method.

Corrosion rates determined by this method for a series of citrate buffer solutions are listed in Table I. Cathodic polarization did not affect the corrosion potential of a specimen appreciably. The value of the Tafel slope (β_c) was essentially constant between pH 2.5 and 5 and was 0.12.

The polarization rate used to obtain these data was 5 mv/min. It was found that polarization rates of 10 mv/min and 50 mv/min yielded almost identical results.

Corrosion rates were also determined by the polarization resistance method according to the Stern

Table I. Corrosion rates of 3003-0 aluminum in citrate buffer solutions (37.8°C)

pH	Hydrogen evolution rate (ml/day/cm²) STP	Corrosion current, μa/cm² Overvoltage intercept method*	Corrosion current, μa/cm² Polarization resistance method*
2.5	0.0132	1.2	1.2
3.0	0.0135	1.2	1.2
3.5	0.0121	1.1	1.1
4.0	0.0119	1.2	1.1
4.5	0.0119	1.2	1.2
5.0	0.0123	1.1	1.1
5.5	0.0140	1.4	1.3
6.4	0.0251	2.3	2.0

* Multiplication of these values by 0.010 gives equivalent hydrogen evolution rate in ml at STP/cm²/day.

Table II. Corrosion rates of 3003-0 aluminum in hydrogen-flushed acid media (37.8°C)

Test solution	Hydrogen evolution rate, (ml/day/cm²) STP	Corrosion current, μa/cm² Over-voltage intercept method*	Corrosion current, μa/cm² Polarization resistance method*	
Acetate buffer pH = 4.6	0.0915	8.2	8.1	0.15
Citrate buffer pH = 4.3	0.0076	0.68	0.71	0.12
H_2SO_4 (0.1% by wt)	0.352	29	27	0.15
H_2SO_4 (1% by wt)	0.744	67	68	0.15
H_2SO_4 (5% by wt)	1.23		101	
H_3PO_4 (0.01M)	0.233	26	23	0.22
Malate buffer pH=4	0.0112	1.1	1.0	0.1

* Multiplication of these values by 0.010 gives equivalent hydrogen evolution rate in ml at STP/cm²/day.

and Geary equation, considering $\beta_a = \beta_c = 0.12$. These are also recorded in Table I. In general no significant linear portion was found at low current densities. $\Delta E/\Delta I$ was determined by plotting the tangent to the polarization curve at zero applied current.

The corrosion rates of 3003-0 aluminum in a variety of anaerobic acid media reported in Table II represent average values for six replicate determinations. Individual polarization resistance values are indicated in Fig. 6. While in the citrate buffer solutions it was found that the values of the corrosion current were unaffected by a change in the rate of polarization above 5 mv/min, it was necessary to use higher polarization rates to obtain valid polarization curves in the stronger acid media. These data were therefore obtained at a rate of 50 mv/min, the maximum rate obtainable with our instruments. This rate is generally satisfactory for corrosion currents up to approximately 75 μa/cm². For 5% H_2SO_4 (123 μa/cm²) the polarization resistance method could be used, but not overvoltage-intercept. Tests in buffered media could extend for periods of at least twenty days with no appreciable change in corrosion rate or pH, whereas the results for the stronger acid media had to be accumulated over a period of about six hours. The corrosion rate reported for citrate

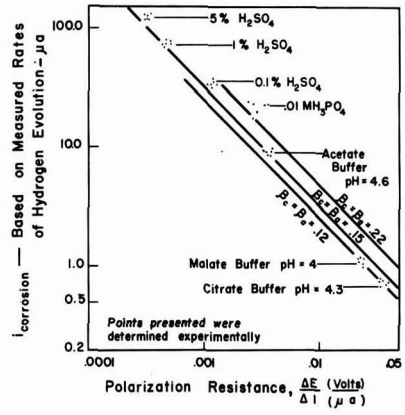

Fig. 6. Relationships between corrosion rate and polarization resistance for hydrogen-flushed acid media.

Table III. Corrosion rate of aluminum in de-aerated food media (37.8°C)

Medium	Alloy	Hydrogen evolution rate, (ml/day/cm²) STP	Corrosion current, μa/cm² Over-voltage intercept method*	Polarization resistance method*	β_c
Prune juice	3003	0.0147	1.4	1.4	0.1
Tomato juice	3003		0.16	0.19	0.1
Apple juice	3003	0.0217	1.6	1.6	0.09
	5052	0.0233	2.3	2.6	0.14
Beef gravy	3003		0.20	0.20	0.4
	5052		0.20	0.26	0.4
Beer	3003		0.65	0.62	0.14
	5052		0.71	0.68	0.14
Corn	3003		0.078	0.062	0.15
	5052		0.078	0.065	0.15
Green Beans	3003		0.22	0.19	0.15
	5052		0.17	0.16	0.20

* Multiplication of these values by 0.010 gives equivalent hydrogen evolution rate in ml at STP/cm²/day.

buffer solution in Table II is not in agreement with those in Table I, since the buffer used here was based on different concentrations of acid and salt. Here the molar sum of citric acid and sodium citrate was 0.1.

Corrosion in food media.—The corrosion rates of aluminum in a variety of deaerated food media are reported in Table III. The hydrogen evolution rate was too low to be measured directly in most of the systems. In each system studied the cathodic polarization curve exhibited Tafel-type behavior. In no case was rate of diffusion of hydrogen ion a controlling factor over the range included. Corrosion currents were determined by both the overvoltage-intercept and the polarization resistance methods. Each value presented is an average of six replicate experiments. Alloys studied here were: 3003-0, 3003-H18, and 5052-H18. For each medium the results obtained with 3003-H18 aluminum were identical to those obtained with 3003-0 aluminum. Polarization resistance values remained constant during the period of testing for each system except beer. The duration of the test was thirty days. The given corrosion current for beer (Table III) is the value which was found reproducible for the first twenty days of the test. For the period of 20-30 days the current decreased in all cases to 0.26 μa/cm². Polarization resistance values plotted against the current determined by the overvoltage-intercept method on logarithmic scales are represented by points in Fig. 7. The plot of polarization resistance *vs.* corrosion current according to Eq. [1] is represented by the straight lines.

Anodic polarization curves obtained with 3003 aluminum in de-aerated corn exhibit Tafel-type behavior (Fig. 8). This is the only case in which this type of curve was found. The corrosion rate of aluminum in this medium was the lowest of any tested. Comparison of the anodic and cathodic curves of Fig. 8 reveals that β_c is essentially equal to β_a and the extension of both Tafel lines intersects the corrosion potential at approximately the same current density.

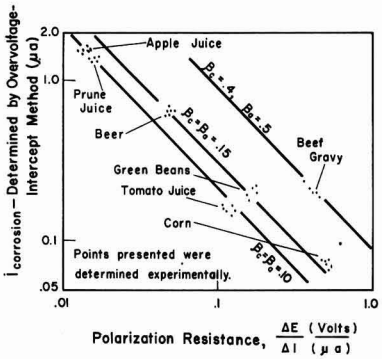

Fig. 7. Relationships between corrosion rate and polarization resistance for food media.

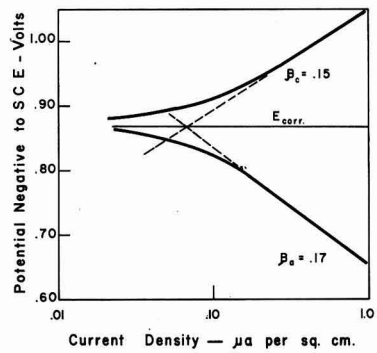

Fig. 8. Experimental cathodic and anodic polarization curves for cream style corn.

Discussion

Over the *p*H range 2.5-5 the corrosion potential of aluminum varies in much the same manner as does the potential of a reversible hydrogen electrode. Cathodic polarization curves for aluminum in de-aerated acid media exhibit Tafel-type behavior, and the corrosion current obtained with the overvoltage-intercept method is equivalent to the rate of hydrogen evolution.

Factors such as *IR* drop in solution and concentration polarization cause deviations from the Tafel relationship. Corrections for resistance effects have been applied. The onset of concentration polarization is delayed in buffered solutions (3). Furthermore, concentration polarization can be easily detected as a deviation from Tafel-type behavior. In the systems studied concentration polarization was no problem whatever.

Except in one case, Tafel-type anodic polarization curves were not obtained. Values of β_a were determined in each system investigated by calculation of the anodic reaction curve from cathodic polarization data. In every case β_a was found to be equal to β_c for the system, within 20%. It was found that, by using the proper value of β_c for the system and by considering $\beta_a = \beta_c$, the polarization resistance method also gave corrosion currents which were equivalent to the rate of hydrogen evolution. Only in the case

where cream style corn was used as the corrosive medium (the lowest corrosion rate of any) was a Tafel-type anodic polarization curve encountered. The extrapolation of the Tafel portion of the experimental curve was identical to the calculated anodic curve for the system.

The use of polarization data to predict corrosion rates is particularly valuable in food systems since: (*a*) hydrogen evolution is generally too low to accurately measure, (*b*) weight loss measurements would have to be accrued over a long time period, (*c*) the polarization methods are straightforward, rapid and accurate. In addition, the use of polarization methods has been extended to systems which are far removed from ideality, and represent a realistic approach based on electrochemical theory.

Direct confirmation of these methods by comparison to hydrogen evolution or weight loss data could be made only for the more rapidly corroding food systems. While it might be argued that for an ideal case a comparison of results obtained by polarization resistance with results obtained by cathodic overvoltage-intercept is essentially an experimental confirmation of a mathematical identity, the indicated nondeparture from ideal, Tafel-type behavior together with the correspondence to directly measured corrosion rates at the high end of the range and the result obtained by anodic overvoltage-intercept at the low end of the range gives full confidence in the general application of these methods to the corrosion of aluminum in such electrochemically impure media as natural foods.

While the overvoltage-intercept method possesses definite advantages in specific instances, the polarization resistance method generally will be the more convenient to use. For aluminum it may be assumed that $\beta_a = \beta_c$. Use of a chart of the type suggested by Skold and Larson and by Stern, as indicated in Fig. 7, together with the assumption $\beta_a = \beta_c = 0.12$ to 0.15 gives useful corrosion rates for all the systems included except for that in which beef gravy was the corrosive medium.

There is a widespread belief that polarization curves should be determined slowly and that each point on the curve should represent a more or less steady-state condition. This is definitely not the case, unless the purpose is to determine how the test specimen would react as one element of a galvanic couple. In the present case we are interested in activation parameters for the corroding system in such condition as exists at its corrosion potential. This requirement is satisfied with a more or less rapidly determined polarization curve; a slow rate only produces interactions which disturb the system from the condition in which it existed at the corrosion potential. A rate which is too slow may produce any of the following effects: (*a*) a value for β_c which is too high, (*b*) a curve which is not of Tafel form, and (*c*) instability.

Among other things these undesirable interaction disturbances appear to be a function of the total number of coulombs passed to the specimen. Since higher currents are necessary for determining polarization curves of rapidly corroding specimens, this means that while a wide range of polarization rates may be satisfactory for slowly corroding systems, rapid polarization rates are required for rapidly corroding systems. This is in agreement with the findings of Okamoto, Nagayama, and Sato (12), who used very high polarization rates in studying the use of the overvoltage-intercept method in the corrosion of iron in sulfuric acid solution.

While slow polarization rates are not suitable for rapidly corroding systems there is, of course, a limit somewhere at the other end of the scale. At some point a very rapid polarization rate will not be satisfactory for a very slowly corroding system because of the current required to charge the double layer. There is no reason to believe that we are near such a point in this work. A 50 mv/min polarization rate has been found satisfactory for all systems in this study except for the 5% H_2SO_4, as noted.

Manuscript received Oct. 3, 1960; revised manuscript received Jan. 16, 1961. This paper was prepared for delivery before the Houston Meeting, Oct. 9-13, 1961.

Any discussion of this paper will appear in a Discussion Section to be published in the December 1961 JOURNAL.

REFERENCES

1. M. Stern, *This Journal*, **102**, 609 (1955).
2. H. Kaesche and N. Hackerman, *ibid.*, **105**, 191 (1958).
3. R. A. Legault and N. Hackerman, *Corrosion*, **15**, 517 (1959).
4. J. D'Âns and W. Breckheimer, *Z. Elektrochem.*, **56**, 585 (1952).
5. K. Bonhoeffer and W. Jena, *ibid.*, **55**, 151 (1951).
6. S. Bodforss, *Z. physik. Chem.*, **160**, 141 (1932).
7. R. V. Skold and T. E. Larson, *Corrosion*, **13**, 139 (1956).
8. M. Stern, *ibid.*, **14**, 440 (1958).
9. M. Stern and A. L. Geary, *This Journal*, **104**, 56 (1957).
10. M. Stern and E. D. Weisert, *Proc. Am. Soc. Testing Materials*, **59**, 1280 (1959).
11. E. L. Koehler, *Corrosion*, **17**, 93t (1961).
12. G. Okamoto, M. Nagayama, and N. Sato, *Denki Kagaku*, **25**, 166 (1957).

Anodic Polarization and Passivity of Ni and Ni-Cu Alloys in Sulfuric Acid

J. Osterwald and H. H. Uhlig

Corrosion Laboratory, Department of Metallurgy, Massachusetts Institute of Technology, Cambridge, Massachusetts

ABSTRACT

Potentiostatic data are reported for anodic polarization of Ni at 25° and 40°C and for Ni-Cu alloys at 25°C in deaerated 1*N* H_2SO_4. The critical potential for passivity of Ni follows the relation: E_H (25°C) = −0.125 + 0.059 *p*H and the critical current density (ma/cm²) follows: log *i* (25°) = − 0.76 *p*H + log 27. At 40° the critical potential in 1*N* H_2SO_4 is the same as at 25° within experimental error; the critical current density for passivity or for maintaining the passive state is higher. A Tafel relation holds in the transpassive region with slope of 0.140 v (25°) independent of *p*H. The critical current density for passivity and the minimum current density to maintain passivity move to higher values as Cu is alloyed with Ni. Above about 70% Cu, vestiges of passivity are lost and the alloy behaves as does Cu. This critical alloy composition is related to a filled d band electronic structure corresponding to relatively short life of the adsorbed passive film above 70% Cu. Thermodynamic properties of the passive film are discussed.

The potential behavior of a metal capable of becoming passive, plotted with respect to anodic current density using potentiostatic techniques, has proved useful to the further understanding of passivity particularly in the case of iron (1). Data of this kind have been reported for Fe (1, 2), Ni (3-5), Ti (6), stainless steels (3, 7-9), and Cr (3, 9).

It is observed generally, starting from the active and progressing to the more noble region of potential, that anodic current density increases to a value called the critical current density for passivity. Beyond the corresponding potential, the current density decreases and the metal becomes passive. Further change of potential usually results in a small or no further change of current density, and anodic dissolution rate of the electrode is orders of magnitude lower than in the active region. Still further shift of potential to more noble values leads into the transpassive region, and the current density again increases accompanied by a higher dissolution rate of the electrode. Should the potential reach a sufficiently noble value, evolution of oxygen also occurs.

It was considered of interest to examine a similar potential-current density curve for a nontransition metal, *e.g.*, Cu, which does not become passive at high anodic current densities in comparison with a transition metal, *e.g.*, Ni, and also to examine solid solution alloys of these two metals. Data along these lines are presented herewith.

Experimental Procedure

For polarization measurements, an electronic potentiostat was used employing a circuit diagram originated by H. Wenking and supplied to us by courtesy of Professor U. F. Franck. Continuous potential change was effected by means of an electric clock motor operating through a changeable gear box. Corresponding current flow was recorded automatically. Electrode materials were commercial grade or spectroscopically pure Ni, and commercially pure Cu. Laboratory melts of Ni-Cu alloys were made available through courtesy of F. L. LaQue of International Nickel Company. Electrodes measured approximately 1-3 cm² in area. The reference electrode was Ag-AgCl in 0.1*N* KCl which was checked periodically against 0.1*N* calomel electrode. No corrections were made for liquid junction potentials. The electrolyte was sulfuric acid through which purified nitrogen could be bubbled in order to remove dissolved oxygen. For measurements in electrolyte of *p*H < 2, sulfuric acid alone was used, but for *p*H > 2, the solution was 0.5*M* K_2SO_4 plus sulfuric acid in order to increase conductivity. The cell was located in an air thermostat maintained at 25° ± 0.1°C.

Results

Figure 1 shows a typical potentiostatic polarization curve for spectroscopic Ni in deaerated 1*N* H_2SO_4 for which the potential change was automatically set at 400 mv/hr. The run was begun short of the O_2 evolution region, with continuous adjustment of potential to more active values, as shown by arrows on the curve. When the run was begun instead in the active region of potential moving toward the passive region, a curve similar to that of Fig. 1 was obtained in the active region up to about point a of the curve and again in the transpassive region beyond point b, but not between a-b. In the a-b region, current densities were higher before reaching a low value at b. The potential at P_1 was reproducible for either direction of polarization. Because direction of potential change was significant, runs were uniformly started beginning from passive to active states. This choice resulted in better reproducibility, perhaps because a disturbing high corrosion rate of the electrode in the active region was avoided at the beginning of the run. A high corrosion rate con-

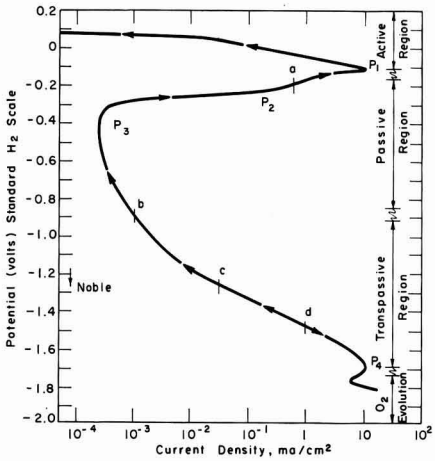

Fig. 1. Potentiostatic polarization curve for spectroscopic nickel in deaerated 1N H_2SO_4, 25°C, 0.4 v/hr.

taminated the electrolyte and produced deep pitting of the electrode.

The shape of the curve also was affected by rate of potential change. Again, more change occurred in the passive region than elsewhere, slower rates tending to increase the minimum current density at P_3. The slowest speed chosen was 130 mv/hr, but this was still far from providing steady-state conditions, hours being required to obtain constant current at any given potential. The potentials corresponding to P_1, however, were found to be insensitive to rate of potential change within the rates studied, and hence this particular region of the curve was considered to describe a fundamental property of the metal-electrolyte system. Whether P_1 approximates the Flade potential for Ni is discussed later. Potentials at P_1 obtained from potentiostatic curves in H_2SO_4 were linear with *p*H as shown in Fig. 2. Data approximately follow the relation:

$$E\ (\text{volt, H}_2\text{ scale}) = -0.125 + 0.059\,pH \qquad [1]$$

Critical current densities at P_1 increase with decrease of *p*H in accord with the relation Log i(crit) = $-\lambda pH + \log K$ where $\lambda = 0.76$ and $K = 27$ ma/cm^2.

The potentiostatic polarization curve for spectroscopic Ni at 40°C in 1*N* H_2SO_4 (400 mv/hr) is shown

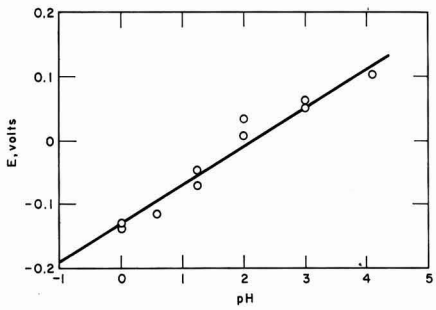

Fig. 2. Dependence of critical passivating potential P_1 on pH, deaerated H_2SO_4, 25°C.

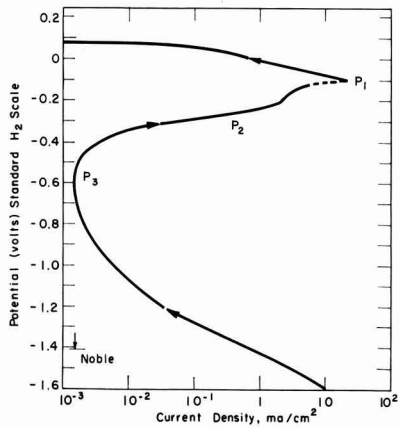

Fig. 3. Potentiostatic polarization curve for spectroscopic nickel in 1N H_2SO_4, 40°C, 0.4 v/hr.

in Fig. 3. The critical potential for passivity at P_1 comes at −0.11 v which is almost the same value as that at 25° equal to −0.12 v (Fig. 1). The difference is well within the experimental error of measurement.

Comparison of Fig. 1 with data for nickel by other investigators shows good agreement in some regions of potential, but particular lack of agreement in the passive region. The transpassive region is reasonably well established in that all reported data are in close accord. Between points c and d, the average Tafel slope is 0.140 v which is independent of *p*H. This confirms data by Vetter and Arnold (5) who also reported a Tafel slope of 0.140 v independent of *p*H.

In the passive region, comparable data show that the current density decreases to minimum values in the order of μa/cm^2. For our data in 1*N* H_2SO_4, the minimum comes at about 0.45 v in agreement with Vetter's data, both curves being obtained for polarization proceeding from passive to active states. Polarization in the opposite direction produces a minimum at potentials more noble by several tenths volt. The shape of the polarization curve in Fig. 1 is similar to that obtained by Vetter. On the other hand, Kolotyrkin reports a linear dependence of *E vs.* log *i* between −0.4 and −1.20 v. Similarly Okamoto and Sato (10) show a restricted linear region between about −0.7 and −0.9 v.

The potential at P_1 equal to −0.12 v, 1*N* H_2SO_4 agrees with the corresponding potential reported by Kolotyrkin. Vetter reports a more noble value of −0.34 v which he finds to be the same for either direction of polarization at a rate of potential change equal to 340 to 780 mv/hr. However, at higher speeds of potential change, 12,000-48,000 mv/hr with rotation of electrode for the first named speed, he reports two major current density maxima. The first of these comes at about −0.15 v which is close to our value, and the second comes at the more noble value of about −0.38 v, to which he ascribes the Flade potential. Further measurements by one of us (J. O.) indicate that occurrence of 1 or 2 maxima in this region is a function of the source of nickel used for

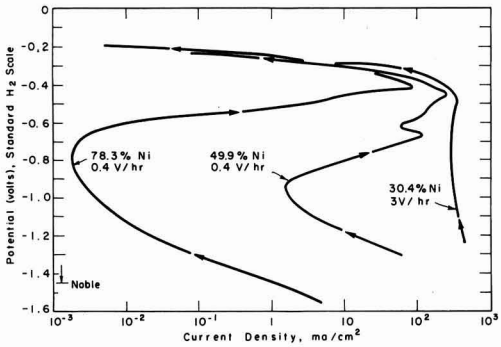

Fig. 4. Potentiostatic polarization curves for Cu-Ni alloys in 1N H_2SO_4, 25°C, rates of potential change as shown.

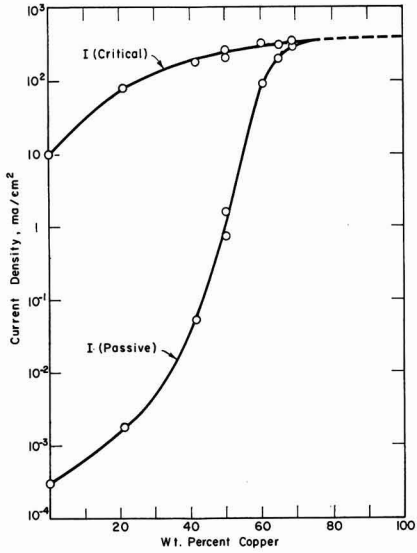

Fig. 5. Critical current densities for passivity and passive current densities as obtained in 1N H_2SO_4 for Cu-Ni alloys, 25°C.

the electrodes, different nickels presumably varying in structure and impurity content.

The small change in slope shown in Fig. 1 at P_2 was found also by Vetter and Arnold for curves obtained at low rates of potential change.

As copper is alloyed with nickel, the value of the passive current density at P_3 increases markedly and the critical current density at P_1 also increases, but to a lesser extent. Potentials at P_1 are more noble than for Ni. This is shown by curves of Fig. 4. Copper itself shows no critical current at P_1 or minimum current at P_3; instead the current density merely increases continuously with potential along a curve similar to that of the active region in Fig. 1, with appreciable bending over at current densities in the order of 150 ma/cm². The polarization curve is similar to those of Ni-Cu alloys containing 30% Ni or less. Speed of potential change was higher for low-Ni alloys in order to avoid effects of a high electrode dissolution rate, but steady state was reached so quickly that the polarization data are expected to be independent of this factor. When two maxima in current density occurred as for 49.9% Ni-Cu, the larger of the two was considered to be the critical value. Values of critical current density at P_1 and passive current density at P_3 are plotted for several Ni-Cu alloys in Fig. 5. It is apparent that vestiges of passivity are lost above 70% Cu, and that characteristics of passivity become more pronounced as Ni content increases above 30%.

Discussion

A critical composition for passivity in Ni-Cu alloys at about 30% Ni is consistent with data obtained by P. Bond of the M.I.T. Corrosion Laboratory on critical current densities for passivity employing a direct galvanostatic method (11). He found that below about 35% Ni, the critical current density for passivity in 3% Na_2SO_4 became very large or infinite, whereas the critical current densities for alloys containing more than 35% Ni were small and decreased with increase in nickel content. The corrosion rates of Ni-Cu alloys in 3% NaCl at 80°C also reach low values beginning at about 30% Ni (11). As have been pointed out previously by Mott and Jones (12) and discussed by one of us (11, 13), 40% Ni corresponds to a critical electronic configuration, alloys of more Ni containing d-electron vacancies typical of transition metals exhibiting passivity, whereas those with less Ni in common with Cu correspond to an essentially filled d-band of energy levels and are active.

Referring to Eq. [1], potentials corresponding to critical current densities for Ni at P_1 are linear with *p*H with a slope of 0.059 v. This linearity parallels similar behavior for Flade potentials of iron plotted with *p*H the slope of which is also 0.059 v (14-16). But whether potentials at P_1 coincide with Flade potentials for nickel is a question of definition. In an attempt to resolve this matter, potential-time curves were observed for decay of passivity (self-activation) of Ni in acids of known *p*H. Flade (17) originally proposed that the potential for passive iron just before rapid decay to the active state is the critical potential, now called the Flade potential, and showed that this critical potential is more active the lower the concentration of acid in which passivity decays. Preliminary self-activation data in H_2SO_4 of various *p*H values showed that a precipitate decay of passivity does not occur for Ni as for Fe; instead, more than one discontinuity in slope of the potential-time curve is observed which is less pronounced than for Fe. Potentials corresponding to such discontinuities most active in the potential scale, or those nearest the active state of Ni, are only about 0.05 v more noble than the values at P_1. They are linear with *p*H, the slope of which is similarly 0.059 v. Such critical potentials are consistent, therefore, with values at P_1 and are consistent with Flade's original definition.

It is reasonable to expect that observed discontinuities in the potential-time decay curves at more noble values than P_1 correspond to surface reactions of another kind. This is also the conclusion of Okamoto (10) from measurements of self-activation

potential-time data. His equation for the potential in volts for the most active discontinuity in slope is $-0.13 + 0.06$ pH which coincides with Eq. [1] for pH dependence of potentials at P_1 and is in reasonable agreement with our self-activation data. However, contrary to our conclusions, he defines the potential in volts at the next most noble discontinuity, corresponding to $-0.48 + 0.06$ pH, as the Flade potential, and that the corresponding reaction is $3NiO + H_2O \rightarrow Ni_3O_4 + 2H^+ + 2e$.

Vetter (5) reports discontinuities in the self-activation potential-time curve in 1*N* H_2SO_4 at -16 and -0.54 v with poor reproducibility of the latter value. For reasons that are not clear, he did not find a discontinuity at more active values of potential, as reported by Okamoto and as found in the present work.

If one assumes NiO formation during passivation of Ni at P_1, the reaction is as follows:

$$Ni + H_2O\ (l) \rightarrow NiO + 2H^+ + 2e;\ E^\circ = -0.13\ v \quad [2]$$

From standard free energy values for formation of NiO (-51.7 kcal) and H_2O (-56.69 kcal) (18), the calculated value $E^\circ = -0.108$ v is in fair agreement with the above value. Okamoto (10) pointed out similar agreement.

On the other hand, assuming that an adsorbed oxygen film on Ni composes the passive film, the reaction is:

$$2H_2O + Ni \rightarrow O_2\ (\text{adsbd. on Ni}) + 4H^+ + 4e;\ E^\circ = -0.13\ V \quad [3]$$

From the heat of adsorption of O_2 on Ni ($\Delta H = -130{,}000$ cal/mole) (19) and assuming an entropy change approximated by that for N_2 chemisorbed on Fe (-46.2 e.u./mole°C) (20), ΔG° (O_2 adsbd. on Ni) $= -116{,}250$ cal/mole. This leads to a calculated value of $E^\circ = +0.031$ v.

Offhand, therefore, the above calculations appear to favor formation of NiO as the substance making up the initial passive film. However, the distinction between NiO and adsorbed O_2 formation is not so easily made. The actual reaction resulting in passive film formation involves displacement of adsorbed water from the metal surface; for this reason, a more realistic equation than Eq. [2] for passivation is the following:

$$nH_2O{\cdot}Ni\ (\text{adsbd.}) + H_2O \rightarrow nH_2O{\cdot}NiO\ (\text{adsbd.}) + 2H^+ + 2e;\ E^\circ = -0.13\ v \quad [4]$$

An equation corresponding to Eq. [3] can be written similarly for $nH_2O{\cdot}O_2$ (adsbd. on Ni). An expected larger negative free energy for adsorption of H_2O on Ni than on NiO or on O_2 (adsbd. on Ni) would tend to make the calculated value of E° for reactions [2] and [3] more noble (larger negative value). Experimental values are not available, but it was estimated in the case of iron that a free energy difference of 3000 ($n = 2$) to 6000 cal/mole H_2O, ($n = 1$) would account for the difference between the calculated and observed values for the Flade potential of Fe based on O_2 (adsbd. on Fe) for the passive film (21). It would require a corresponding 7450 to 14,900 cal/mole H_2O in the case of nickel to account for the discrepancy between the observed (-0.13 v) and the calculated ($+0.031$ v) value based on the adsorbed film model. These are reasonable values for adsorption of H_2O and a correction in this amount probably is justified. A similar correction in the same amount applied to the NiO model would make the calculated value more noble than the observed value by 0.3 v.

From the relation $(dE^\circ/dt)_p = (\Delta S/nF)$ and molal entropies for Ni (7.1 e.u.), H_2O (l) (16.716 e.u.), and NiO (9.22 e.u.), ΔS for reaction [2] equals -14.60 e.u. and $(dE/dt)_p = -0.32$ mv/°C. Similarly for reaction [3] from entropy of adsorption of O_2 on Ni approximated by the value for N_2 on Fe (-46.2 e.u.), $(dE/dt)_p = -0.94$ mv/°C. Since the maximum experimental scatter of potentials at P_1 (Fig. 2) equals about 30 mv, the lack of observed change of potential within this scatter for a 15°C temperature rise is consistent with either calculated temperature coefficient of potential. More precise data for potentials at P_1 at several temperatures are needed for a more fruitful correlation.

It is apparent, therefore, that presently reported data cannot be employed alone to support one viewpoint of passive film structure over the other. In this connection it may be significant that Vetter found only 0.004 coulomb/cm² necessary to passivate Ni in 1*N* H_2SO_4 to a potential of -0.62 v corresponding at most, as he points out, to formation of a monomolecular film. A film of this kind which is still thinner at P_1, fits the description of a chemisorbed structure better than a metal oxide whose unit cell dimensions impose a lower limit to passive film thickness. The present data otherwise confirm that the potential behavior of the initial passive film on Ni with respect to pH is similar to that on iron, and that the temperature coefficient of Flade potential at P_1 for Ni is small, as is also the Flade potential for Fe (17). The more active standard Flade potential for the passive film on Ni (-0.12 v) than on Fe (-0.6 v) is in line with greater stability of passivity in Ni. Rocha and Lennartz (22) showed for example that increased stability of passivity in Cr-Fe alloys accompanies their more active Flade potentials. The same conclusion was reached by Feller and Uhlig (23) based on their data for decay of passivity in the Cr-Ni-Fe ternary alloy system. Looked at another way, the free energy increase for reaction [3] is less in the case of Ni than for Fe, and hence the tendency is less in the case of Ni for the reverse reaction to proceed accompanying breakdown of passivity.

For Ni-Cu alloys, a passive film probably similar in structure to that on pure nickel continues to exist on alloys containing more than about 30% Ni. Alloys with less than this amount of nickel behave as does copper, and the Flade potential at P_1 disappears. The more noble potentials at P_1 for the alloys compared to Ni may be associated with decreasing affinity for OH (or oxygen) as copper is added to the alloy similar to the situation proposed for Cr-Fe alloys as Fe content increases (21). Hence, higher current densities are required for the Ni-Cu alloys than for Ni to reach the potential at which OH^- discharges with subsequent formation of the passive film. The increase of passive current density at P_3 with Cu content probably corresponds to a higher

conversion rate of adsorbed oxygen to metal oxide, or in other words, the adsorbed oxygen film has shorter life as Cu content increases. When Cu reaches about 70%, the life of the adsorbed film is so short that, for practical considerations, the metal ions enter into solution directly.

Acknowledgment

This research was supported by the International Nickel Company, to whom the authors express their appreciation.

Manuscript received Dec. 13, 1960. This paper was prepared for delivery before the Houston Meeting, Oct. 9-13, 1960.

Any discussion of this paper will appear in a Discussion Section to be published in the December 1961 JOURNAL.

REFERENCES

1. U. F. Franck, Quoted by K. F. Bonhoeffer, *Z. Metallkunde*, **44**, 77 (1953).
2. J. Bartlett and L. Stephenson, *This Journal*, **99**, 504 (1952).
3. Y. Kolotyrkin, *Z. Elektrochem.*, **62**, 664 (1958).
4. G. Okamoto, H. Kobayashi, M. Nagayama, and N. Sato, *ibid.*, **62**, 775 (1958).
5. K. Vetter and K. Arnold, *ibid.*, **64**, 244, 407 (1960).
6. M. Stern and H. Wissenberg, *This Journal*, **106**, 755 (1959).
7. C. Edeleanu, *Nature*, **173**, 739 (1954); *J. Iron and Steel Inst.*, **185**, 482 (1957).
8. M. Prazak, V. Prazak, and V. Cihal, *Z. Elektrochem.*, **62**, 739 (1958).
9. R. Olivier, Dissertation, Univ. Leiden (1955).
10. G. Okamoto and N. Sato, *J. Inst. Metals (Japan)*, **23**, No. 11, 662 (1959).
11. H. H. Uhlig, *Z. Elektrochem.*, **62**, 700 (1958).
12. N. Mott and H. Jones, "Theory of Properties of Metals and Alloys," p. 196, Oxford Press (1936).
13. H. H. Uhlig, *Trans. Electrochem. Soc.*, **85**, 307 (1944).
14. U. F. Franck, *Z. Naturforschung*, **4A**, 378 (1949).
15. H. H. Uhlig and P. King, *This Journal*, **106**, 1 (1959).
16. G. Cartledge and R. Sympson, *J. Phys. Chem.*, **61**, 973 (1957).
17. F. Flade, *Z. phys. Chem.*, **76**, 513 (1911).
18. W. Latimer, "Oxidation Potentials," Prentice-Hall, New York (1952).
19. B. Trapnell, "Chemisorption," p. 150, Academic Press, New York (1955).
20. B. Trapnell, *ibid.*, p. 212.
21. P. King and H. H. Uhlig, *J. Phys. Chem.*, **63**, 2026 (1959).
22. H. Rocha and G. Lennartz, Archiv. Eisenhüttenw., **26**, 117 (1955).
23. H. Feller and H. H. Uhlig, *This Journal*, **107**, 864 (1960).

The Conductivity of Undehydrated Insulating Liquids

R. Guizonnier

Faculty of Sciences, Bordeaux, France

ABSTRACT

The study of the conductivity of undehydrated liquids allows us to redetermine the variations in conductivity of water in relation to its temperature

$$i_0 = Ae^{-W/kT}$$

where $W = 0.41$ ev, and shows (*a*) the point of solidification of water, (*b*) the change in the properties of water, between 30° and 40°C, and (*c*) a residual difference of potential, as well as the water, between 0.9-1.7 v.

The studies reported here involve determining the electrical conductivity of undehydrated insulating liquids over a range of temperatures, and from the results demonstrating that the water which is present retains its integrity under such conditions.

The liquids were used as they were obtained from the manufacturers; however, when necessary, they were hydrated or dried out partially by putting them either in a saturated or in a very dry atmosphere for a few hours. In a separate series of experiments some waxes were used.

Currents were measured by a method described in an earlier paper (1), using the sensitivity of thermoelectronic lamps, when the first grid receives an electric charge, allowing 10^{-12} amp to be measured easily. This paper deals with the initial current i_0, measured as rapidly as possible, after the application of the difference of potential. All the experimental apparatus was carefully screened and the screen rigorously grounded. The electrodes were either of nickel-plated copper or platinum; the gap between the electrodes was between 5 and 10 mm.

Conductivity of Insulating Liquids

For a first series of insulating liquids (pure analytical grade benzene, pure carbon analytical grade tetrachloride, transformer oil A), the temperature was varied from the room temperature to 80°. Plotting log i_0 as ordinate and $1/T$ as abscissa, (Fig. 1) a straight line is obtained:

$$\log i_0 = a - - b/T$$

where a and b are constants. This may be transformed into:

$$i_0 = Ae^{-W/kT} \qquad [1]$$

The constant A depends on the insulating liquid: if we make k equal to the Boltzmann constant, we find, whatever the nature of the insulator be, that $W = 0.41$ ev.

A second category of insulating liquids (paraffin oil, silicone oil, 200 centistokes, transformer oil B) only obeys Eq. [1] from 30° or 40° to 80°, the temperature to which we limited ourselves: the value W still equals 0.41 ev (Fig. 2).

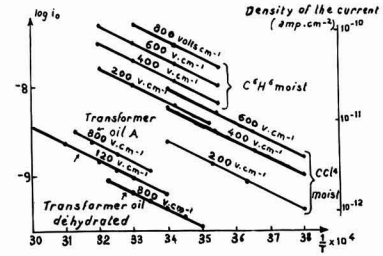

Fig. 1. Verification of the relation $i_0 = Ae^{-W/kT}$ in the case of CCl^4, C^6H^6 and of certain oils. On the right the density of the current is indicated which corresponds to the logarithms indicated on the left (electrodes of nickel plated copper).

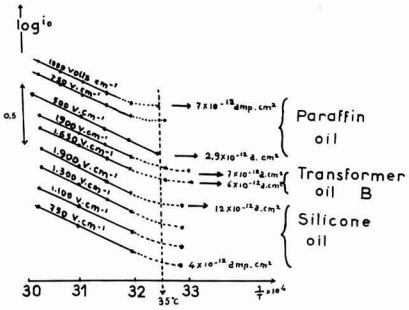

Fig. 2. Verification of the relation $i_0 = Ae^{-W/kT}$ starting from 30°-40°C, in the case of paraffin oil or silicones, transformer oil B. On the right, the density of the current, in each case when the temperature is at its lowest point; on the left, the logarithms scale (electrodes of nickel-plated copper).

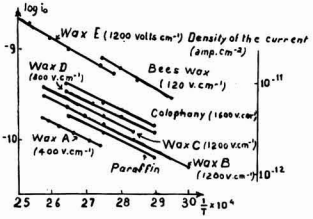

Fig. 3. Verification of the relation $i_0 = A_e^{-W//kT}$ in the case of melted solids (electrodes of nickel plated copper).

Some insulating waxes of various kinds, in a temperature range from their melting point (60°-70°) to 90° (the temperature which was not exceeded for fear of spoiling the products which were used) give results which conform with Eq. [1] with the numerical value of W which was previously determined (Fig. 3).

Equation [1] giving a value of W common to all the insulating materials in a liquid state leads us to conclude that their conductivity has a common cause which we have already attributed (2) to the moisture contained in these insulating materials.

Conductivity of Purified Water

If we study the variation in conductivity with temperature of samples of distilled water or redistilled water, we obtain practically straight lines for log $i_0 = f\ (1/T)$ whose slopes correspond to various values of W, all of which are lower than 0.41 ev.

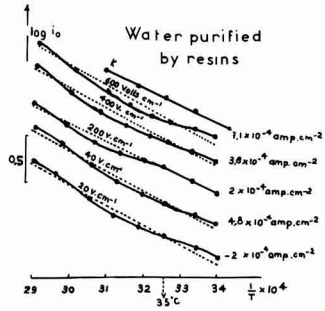

Fig. 4. Verification of the relation $i_0 = Ae^{-W/kT}$ in the case of deionized water (electrodes of platinum) (same remarks as for Fig. 2). The curve k is obtained with the experimental values found by Kolhrausch.

We experimented on deionized water, of which the resistance was in the order of 1 megohm-cm. For a series of experiments, we were able to obtain numerous points. The straight lines which pass, at the best, through these points have a slope corresponding to the value of $W = 0.41$ ev, already found for insulating liquids (Fig. 4). In Fig. 4 curve K, which is below the others, has been traced with the aid of the findings of Kohlrausch (3) concerning very pure water.

It is perhaps interesting to note that 0.41 ev is a value near the work which is required to extract one molecule of water from the molecules which surrounds it, in conformity with the model of Bernal and Fowler (4). Magat (5) has calculated this work in theory: he found 0.46 ev.

Determination of the Point of Solidification of Water

If, for fields under 2 kv/cm, water is really the cause of the conductivity of insulating liquids, when the temperature is lowered sufficiently significant changes in the slope of the curves should be found.

Measurements were made with nickel-plated copper electrodes. The change in the slope which was expected occurred often when cooling took place, but on reheating, we noticed a high maximum as soon as the temperature rose above 0°. On using platinum electrodes treated with an oxidizing mixture ($H_2SO_4 + KMnO_4$) the curves then took a regular form.

The study took place on nine liquids, including those which we have already mentioned, pure carbon disulfide and commercial grade hexane and toluene. Between the electrodes, 10 mm apart, a difference of potential equal, in general, to 200 v was applied and in the case of liquids with a lower level of conductivity (paraffin oil, silicone oil) rising to 1000 v.

The curves of cooling which have already been published (6) and not reproduced here all show toward 0°C the expected change in slope; most of them also have a tendency to remain constant near this temperature. Toward (−20°C) the conductivity seems to have attained a value with a very low limit, in the case of oils and benzene; in the other cases we can assume that conductivity still existing at (−20°C) is due, above all, to impurities in prod-

ucts of commercial grade and products which are of analytical purity, but which are prone to decomposition in time (carbon sulfide, carbon tetrachloride). On reheating, a change in slope is found. This is less distinct in the case of toluene, towards 0°C.

Changes in Properties of Water around 30°-40°C

The curves of variations $i_0 = f(T)$ of the liquids producing homocharges, which do not obey Eq. [1] except above 30°-40°C, have a minimum toward this interval of temperature. If the product is very moist, the minimum is almost flat: if it is dry it tends to disappear. Figure 5 concerns a liquid of average moisture content. The study of the distribution of potentials shows that above 30°-40°C it has become liquid, producing heterocharges. It is for that reason that it follows the law [1].

Stannet (7) has explained the minimum in conductivity around 30°-40°C of transformer oil as due to the presence of water. Before the temperature reaches 30°-40°C the water is in particles spread about in the liquid, which by the electrostatic attraction of the electrodes take a charge from them. But Stannet thinks that about 30°-40°C the water dissolved, and thus it no longer contributes to the conductivity, which is then due to the impurities contained in the insulating liquids and which, when the temperature rises, grows because the coefficient of viscosity diminishes.

The results obtained in our work lead us to think that after the minimum this should not be so, since after 30°-40°C we find the same law for all these liquids, which applies to liquids producing heterocharges, with a common numerical value $W = 0.41$ ev which we attributed to water. Thus, in the case of the relatively weak fields which we use (lower than 2 kv/cm) above as well as below 30°-40°C, it is seemingly the water which is always the cause of the conductivity. The type of conductivity has changed.

This change in the type of conductivity seems to be confirmed by the fact that water around 30°-40°C changes form. In fact, Magat (5), in studying the variations of the Raman spectrum of liquid water in relation to the temperature, found that the intermolecular bands situated in the interval 500-700 cm^{-1} disappear quite suddenly around 40°C. He thought that this change in the property of water at this temperature is connected with the transformation of oscillations of molecules around the direction of the minimum energy, in rotation, which brings about a considerable change of the forces of molecular interaction. In a second article (8) Magat has grouped together the phenomena which show a change in the properties of water around 40°C. We think that the minimum at 30°-40°C in our curves of conductivity should be considered as a new confirmation of the change in the properties of water in this interval of temperature.

Perhaps it is useful to mention that the liquids producing homocharges which show the minimum of conductivity toward 30°-40°C are, at ordinary temperature, much more viscous than liquids producing heterocharges, which do not show this minimum, and that they are composed of bodies having weak chemical affinities (paraffins, silicones).

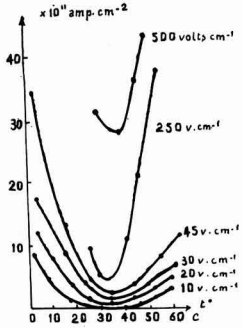

Fig. 5. Existence of the minimum of conductivity between 35° and 40°C for transformer oil B, moist, on the ordinate, the current density (electrodes of nickel-plated copper).

Residual Difference of Potential

In the case of platinum electrodes, if distilled water is subjected to fields in the range of 10 v/cm or purified water, to fields in the range of 100 v/cm, we observe on the electrometer a difference of residual potential of which the value comes in the interval of 0.9-1.70 v. The same result is obtained from palladium electrodes, but everything being the same, the necessary average field is much weaker.

If an insulating liquid such as benzene or transformer oil A is subjected, in the case of electrodes of platinum or palladium, to an average field in the range of a few ten or a few hundred v/cm we obtain on the electrometer a residual difference of potential, v. We can, by using the same field, construct the curve of the evolution of v in relation to the time of the application of the field, this curve tends toward the value V as its limit. If we work with increasing average fields, without going too high, the limiting value V tends to reach a value comparable to the interval already found in the case of water: if the field is too high, the limiting value V becomes even greater: the phenomenon is thus comparable to that which we obtain in the case of solid insulators or of insulating liquids with electrodes coated with varnish (9). Figure 6 shows a number of curves obtained in these conditions.

Conclusion

The conductivity of insulating liquids, when the field is less than 2 kv/cm arises from the water con-

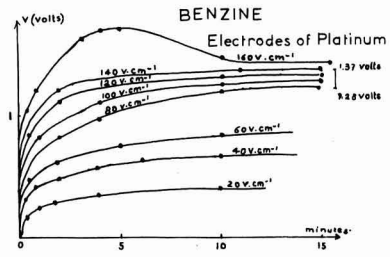

Fig. 6. Residual tension in the case of benzene (electrodes of platinum). When the field applied is sufficient without being too intense (80-160 v/cm) there is a tendency to approach the individual tension obtained in the case of water.

tained in those liquids. The energy of activation 0.41 ev is due to the structure of the water.

Acknowledgment

The author is pleased to acknowledge the collaboration of M. Besnard in determining the conductivity of purified water, C. Thomas in determining the changes at 30°-40°C, and M. Besnard and J. Tillous in determining the residual differences of potential.

Manuscript received Feb. 19, 1960; revised manuscript received Dec. 10, 1960. This paper was prepared for delivery before the Philadelphia Meeting, May 3-7, 1959.

Any discussion of this paper will appear in a Discussion Section to be published in the December 1961 JOURNAL.

REFERENCES

1. R. Guizonnier, *Rev. Gen. Elec.*, **62**, 247 (1953).
2. R. Guizonnier, *ibid.*, **65**, 373 (1956).
3. F. Kolrausch and A. Hendweitter, *Wied. Ann.*, **53**, 209 (1894).
4. J. D. Bernal and R. H. Fowler, *Chem. Phys.*, **1**, 515 (1933).
5. M. Magat, Researches into the Raman spectrum and the constitution of liquid water. (Thesis, Paris) p. 79 (1936).
6. R. Guizonnier, A. Bouygard, and C. Besson, *Compt. rend.*, **246**, 1937 (1958).
7. A. W. Stannet. Brit. J. Appl.. Phys., **t.2**, 110 (1951).
8. M. Magat, *J. phys., Radium*, **36**, 179 (1935).
9. R. Guizonnier, *ibid.*, **t.17**, 121A (1956).

The Effects of Hydrostatic Pressure, Temperature, and Voltage Duration on the Electric Strengths of Hydrocarbon Liquids

K. C. Kao[1] and J. B. Higham[2]

Electrical Engineering Department of the University of Birmingham, England

ABSTRACT

The electric strengths of simple hydrocarbons and of transformer oil have been found to be dependent on applied hydrostatic pressure under all conditions investigated, including conditions of extreme cleanliness and for voltage pulses lasting only 1 μsec. A special feature of the investigation is that most of the results are for fresh liquids and electrodes, with which there had been no previous breakdown. It is suggested that electric breakdown is partly governed by dielectric layers on the cathode, which change with successive breakdowns, and that breakdown first takes place in a bubble of gas or vapor.

The present investigation is a continuation of earlier investigations (1, 2) in the same laboratory and the authors make acknowledgment of some equipment and techniques which they inherited. Electric strengths have been measured in transformer oil and in several simple hydrocarbon liquids with wide ranges of purities, applied hydrostatic pressures, temperatures, voltage durations, and gap lengths, and with uniform and nonuniform fields. Most of the results being reported refer to the first breakdown in a new sample of carefully treated liquid using freshly polished and cleaned electrodes.

Experimental Apparatus and Techniques

High-voltage supplies and test-gap protection.—The basic circuit for producing high-voltage rectangular pulses of duration ranging from 0.5 μsec to 1 msec and up to 75 kv is shown in Fig. 1; details of parts of the circuit have already been published (3). As drawn, the high-voltage source is a three-stage Marx-Goodlet generator, arranged to isolate the test gap from the charging voltage, but the generator is readily modified to apply one third of the ultimate output voltage to the test gap for pre-

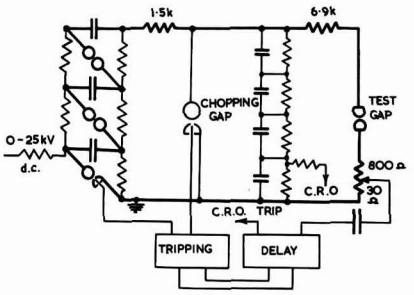

Fig. 1. High-voltage circuit

stressing. The pulse voltage rises to a peak on the low-capacitance test-gap in 0.2 μsec, and the time constant of the generator is high so that the output voltage decays by less than 1% in times up to the order of 1 msec. The delay unit and the thyratron tripping-unit are arranged to trip the high-speed oscillograph time-sweep, the high-voltage generator, and the chopping gap in turn, and after predetermined variable delays. The chopping gap comes into earlier operation if the test gap fails, thus limiting the duration of breakdown current in a test sample to about 1 μsec. The protection circuit operates on

[1] Present address: Brush Electrical Engineering Co. Ltd., Loughborough, England.

[2] Present address: Pilkington Brothers Ltd., St. Helens, Lancashire, England.

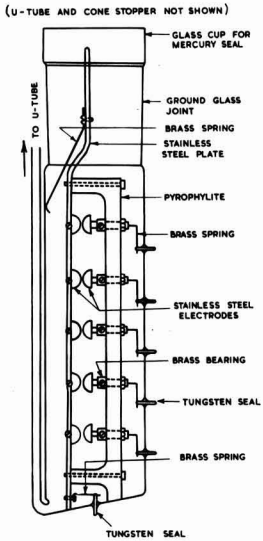

Fig. 2. Test cell and multiple-electrode assembly

either polarity of pulse voltages or on positive or negative half-cycles of alternating voltages.

Electrode system.—In order to have both fresh liquid and electrodes available without the need for frequent laborious filling of the test cell, a multiple electrode system was designed as shown in Fig. 2. All the electrodes on the stainless steel bar are connected to the earth end of the test circuit, and the electrodes supported on the pyrophylite may be connected separately to the high-voltage end. The hemispherical electrodes are ground from ¼ in. diameter stainless-steel balls, and mounted on their shanks by electric welding in a jig (4). A few results are also being reported for modified electrode systems using pointed steel and phosphor-bronze spherical electrodes.

The gap length between each pair of electrodes is adjusted and measured with the aid of a microscope and collimated back-illumination, a sharply defined interference band appearing on each electrode being adopted as the focusing criterion. The measurements are based on feeler-gauge calibrations, and they are estimated to have an error of not more than ±2% for gap lengths of about 200μ. The few results being reported for gap lengths of about 40μ are subject to a possible error of ± 3%.

Details of the techniques developed for preparing and cleaning the electrodes are given in Appendix I.

Sample preparation.—Each sample of liquid for test, except transformer oil, is stored for several weeks in contact with self-indicating silica gel in order to remove moisture, and then it is taken at least six times through a circulatory vacuum-distillation and filtration system in which the minimum pressure is about 1 mm Hg. There are two sintered-glass filters in series in the system, each of pore size less than 1μ. The 150 ml glass test cell is part of this system, coupled to it by hemispherical joints which are sealed by surrounding cups of mercury. There are no glass taps carrying liquid, so contamination by tap grease is avoided, and the air admitted to the system is dried and filtered. It was found that the use of an electrostatic cleaner intended for removing ionic impurities, with 22 kv d.c. across the 1.5 cm gap between the 7.5 x 2.5 cm plates, had no significant effect on the subsequent results. When the test cell is finally filled, air is admitted to the system and, unless tests are to be made on a partially degassed liquid, the sample is left in contact with the air for at least an hour. Then the sample is sealed in the cell by admitting purified mercury from reservoirs to U-tubes which are connected one to the bottom of the cell and the other to the top, and the cell is uncoupled from the system ready for mounting in the pressure chamber [already described (1)] or in a thermostatically controlled tank (5). There is no air cushion in the test cell.

The procedure for cleaning the glass system is described in Appendix II.

For continuity with earlier work, a few typical results for transformer oil also are being reported. Transformer oil (conforming to British Standard 148: 1951) is dried with silica gel and treated at 70°C by pulling through a sintered-glass filter of 10-15 μ pore size into a vacuum at about 1 mm Hg. After treatment the oil is re-gassed by standing in contact with dried air for an hour.

Measurements

Most of the breakdown field strengths being reported are those for only the first breakdown with any liquid sample and pair of electrodes, although, as a partial check on each first measurement, the second and third breakdowns have been made after first using all five gaps in the multiple-electrode assembly.

Table I shows some typical results with two random series of pressure changes, performed in this way to ensure that the position of the gap in the test cell is of no significance. They show the consistent reduction in electric strength always found after a first breakdown in a gap using highly purified liquid and the consistent change in electric strength with pressure.

Except where stated otherwise, the results have been obtained using a "multiple pulse" technique in

Table I. Electric strengths of degassed n-hexane with 4.5 μsec pulses and ¼ in. diameter stainless-steel electrodes

	First measurement with each gap					Second measurement with each gap				
Breakdown No.	1	2	3	4	5	6	7	8	9	10
Gap No.	1	2	3	4	5	1	2	3	4	5
Gap length, μ	188	188	184	174	185	188	188	184	174	185
Gauge pressure, lb/in.^{2}	350	100	0	200	50	100	0	200	50	350
Electric strength, Mv/cm	1.94	1.64	1.35	1.80	1.51	1.53	1.28	1.52	1.32	1.71

which a rectangular pulse of pre-set duration is first applied of about two-thirds the expected breakdown voltage. Successive pulses are then increased in magnitude by about 0.4 kv (corresponding to about 20 kv/cm on a 200 μ gap) until breakdown occurs.

Dependence of electric strength on applied hydrostatic pressure.—It is well known that the measured electric strength of a liquid dielectric may rise on the average with successive breakdowns until, after perhaps fifty breakdowns, the strength may remain practically constant. Many previous investigators have carried out this "conditioning process" before determining the effects of variables such as applied hydrostatic pressure. There remained the possibility, however, that the conditioning might affect the subsequent results, and even be responsible for the observed effect of hydrostatic pressure (6). This doubt was removed in the early stages of the present work by changing the applied hydrostatic pressure during the first few measurements on a given sample of liquid with initially new electrodes. Typical results are shown in Fig. 3. Undoubtedly, an increase in pressure causes an increase in the electric strength of transformer oil, which has been found to be true for filtered and unfiltered oil, with and without dissolved air, for spherical electrodes and pointed ones, and for voltages ranging between 1 μsec pulses and direct and alternating. Pre-stressing for 15 min with a direct voltage producing about 200 kv/cm causes a lowering in electric strength, probably owing to thermal effects and to the presence of particles smaller than 10 μ, but no pre-stressing effect has been observed with carefully purified liquids.

A repetitive breakdown technique has also been used with pointed electrodes owing to the difficulty of making a large number of points near enough alike. Some of the results are shown in Fig. 4, for which the pointed electrode was a 5/64 in. diameter stainless-steel rod tapering uniformly to a 25 μ radius point over a length of ¼ in. and the plane was a stainless steel strip, ⅜ in. wide by 3/32 in. thick with rounded corners, similar to the one used for holding the fixed electrodes in the multiple electrode assembly. The breakdown voltage at atmospheric pressure is always slightly higher with the point negative than when it is positive, and the difference becomes

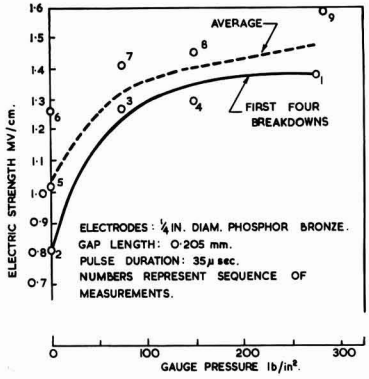

Fig. 3. Electric strength as a function of pressure for transformer oil.

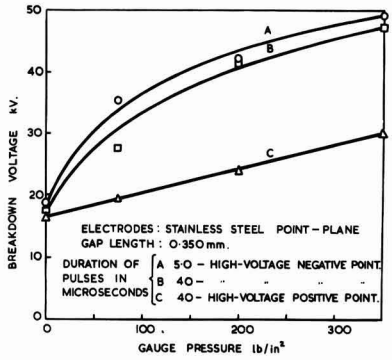

Fig. 4. Electric strength as a function of pressure for point-plane electrodes in n-hexane.

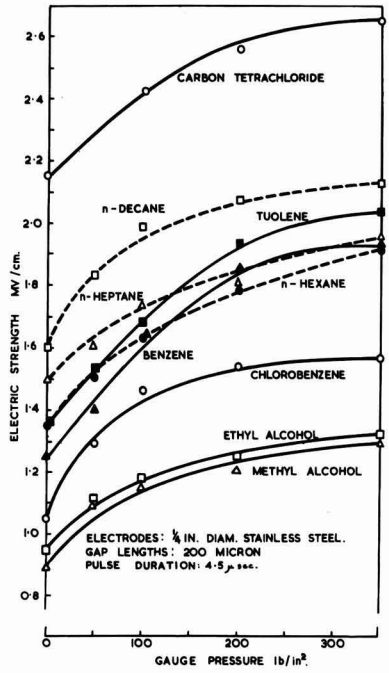

Fig. 5. Electric strength as a function of pressure for several degassed liquids.

more marked at higher pressures. The differences are accentuated when the gap is made double the length.

All the remaining results being reported are those for the first breakdown with freshly prepared electrodes and liquid. Figure 5 shows that the measured electric strengths of several liquids, polar and nonpolar, increase with an increase in applied hydrostatic pressure. This finding is true for voltage pulse-durations between 1 μsec and 1 msec as illustrated for n-hexane in Fig. 6.

A few measurements have been made on n-hexane with 5 μsec pulses at pressures down to 5 mm Hg with the test-cell left coupled to the distillation system. A distinct minimum in the electric strength is found at an absolute pressure of about 45 mm Hg,

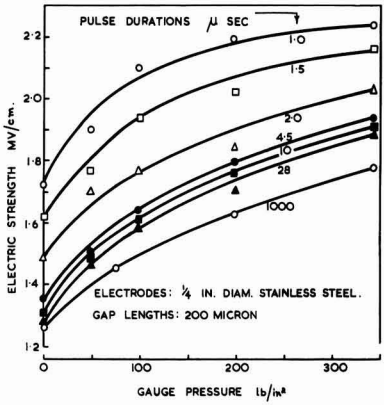

Fig. 6. Electric strength as a function of pressure for degassed n-hexane with a range of pulse durations.

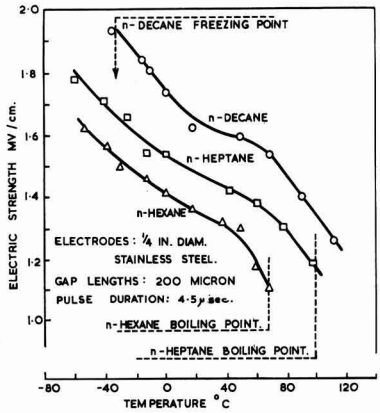

Fig. 7. Electric strength as a function of temperature for three liquids.

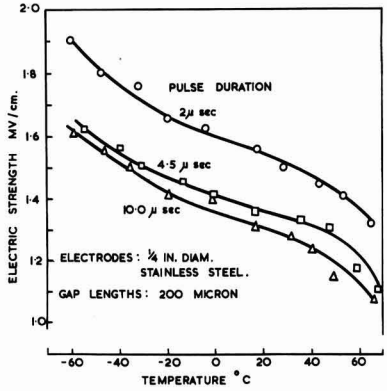

Fig. 8. Electric strength as a function of temperature for n-hexane with three different pulse durations.

qualitatively similar to that reported for alternating voltages and transformer oil (1, 7).

Dependence of electric strength on temperature.—In determining the effect of temperature on electric strength, allowance is made for the small change in

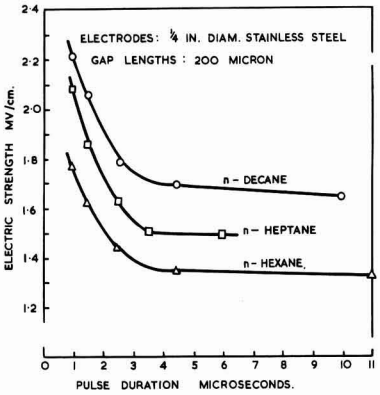

Fig. 9. Electric strength as a function of pulse duration for three liquids.

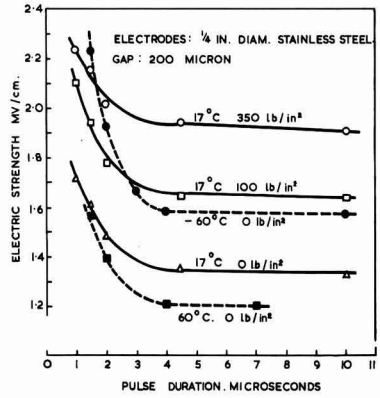

Fig. 10. Electric strength as a function of pulse duration for n-hexane with three gauge pressures and three temperatures.

gap length as the temperature is varied, and adequate time is given for temperature stabilization throughout the test cell. Some results for three nonpolar liquids are shown in Fig. 7 and 8. Results for the polar liquids, ethyl alcohol, and chlorobenzene, have similar characteristics.

Dependence of electric strength on voltage pulse-duration and the time-lag of breakdown.—Figure 9 shows the measured electric strengths of three different liquids as a function of voltage pulse-duration, and Fig. 10 shows results for n-hexane at various gauge-pressures and temperatures. Using the multiple-pulse technique, and gaps of the order of 200 μ, it has been found that the time-to-breakdown on the final pulse is closely the same as the pulse durations if these are less than about 3.5 μsec, but it is variable and usually considerably less if these are about 10 μsec or more. Further, for pulse durations less than 3.5 μsec, the electric strength is critically dependent on pulse duration, but it shows little dependence for longer duration pulses. The time of 3.5 μsec is thus what is termed the critical time-lag for gaps of about 200 μ in the various liquids tested. The critical time-lag is dependent on gap length, being about 1 μsec for a gap length of 33 μ, but it

is independent of pressure, temperature, and chain length in the paraffin series, in the ranges investigated.

An investigation has been made replacing the usual succession of pulses of increasing magnitude by a single pulse of magnitude sufficient to ensure breakdown, using fresh liquid and electrodes for each breakdown. Whatever the prospective duration of this single pulse, breakdown always occurs in less than about 1.5 μsec in n-hexane for gaps of about 200 μ, as shown in Fig. 11. The same is true with pressures up to 350 lb/in.^{2} and for point-point gaps. The scatter in these results has made it impracticable to conduct full investigations with single pulses, but the electric strengths measured in this way are clearly dependent on pressure and temperature.

Dependence of electric strength on gap length.—Sphere-sphere gaps ranging between 20 and 220 μ have been used in n-hexane, and it is found that the breakdown voltage is a linear function of gap length, as shown in Fig. 12. This graph illustrates the reason for having chosen a gap length of about 200 μ for most of the measurements reported in the rest of the paper; small variations in gap length have little effect on the measured breakdown field.

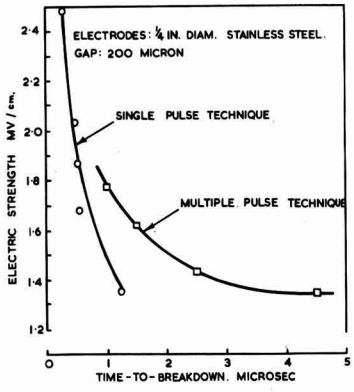

Fig. 11. Electric strength as a function of time-to-breakdown for n-hexane measured by single-pulse technique and by normal multiple-pulse technique.

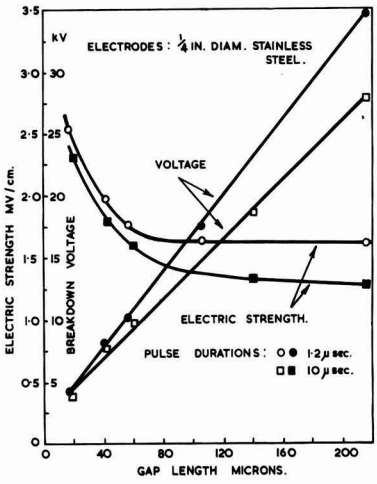

Fig. 12. Electric strength and breakdown voltage as functions of gap length for n-hexane.

Electric strengths of mixed liquids.—A few experiments have been performed with mixed liquids. The electric strength of treated n-hexane is significantly increased by the addition of a small percentage of certain other untreated liquids, reaching a peak with an addition of about 5% and falling from there as the percentage is increased. The addition of 5% of carbon tetrachloride gives an increase in electric strength of about 35%, and the corresponding increases for chlorobenzene, chloroform, and ethyl alcohol are 28%, 13%, and 7%, respectively, despite the fact that these last three liquids have a lower electric strength than n-hexane. It may be significant that these additives have oxygen or halogen groups in their molecules.

Discussion of Results

It has been found that the measured electric strength of a liquid, however pure, using electrodes that are not carefully prepared, increases during the course of a few tens of breakdowns. On the other hand, if the electrodes are carefully polished and cleaned, the electric strength may fall during the first few breakdowns. These are known as conditioning processes. The ultimate measured strength for a given liquid reaches about the same value in both series of measurements. Further, if precautions are taken to minimize damage to a given liquid sample and fresh electrode surfaces are provided for each breakdown (using a rotatable electrode system), a constant measured electric strength results for a dozen breakdowns and, if the electrodes are changed only after a conditioning process has been carried out, the conditioning is repeatable with the new electrodes. It has also been found that the conditioning process is not repeatable with the same electrodes even if there is a pause in testing for several days or if the liquid alone is changed.

All this evidence, which is confirmed in part or whole by other investigators (1, 8, 9), leads to the obvious deduction that the conditioning effect is a function of the electrodes rather than of the liquid. Other experiments, in which the anode and cathode have been treated in various ways and also changed separately, show that it is the cathode and not the anode which controls the conditioning effect.

The authors have suggested (10) that the conditioning effect is primarily governed by dielectric layers on the cathode. Such a layer is inevitably present as an oxide film on the newly prepared metal surface, and further layers can be produced by polymerization of the liquid induced by breakdowns and probably as a result of the application of a high electric stress without breakdown. Thus, during the course of breakdown measurements, the dielectric layer on the cathode will be modified. This layer plays a part in the breakdown process by acting as a barrier to positive ions which have been formed in the gap by electron bombardment of molecules. The positive ions, which are prevented from reaching the cathode itself, enhance the electric field at the cathode, thus increasing the field emission of electrons (11-13).

The effect of the dielectric layer on electric strength at any stage in the measurements will be influenced by the geometry and microgeometry of the cathode. The authors and others (14) have found that there is practically no conditioning effect for the extreme case of a sharply pointed cathode. The increase in electric strength with a succession of breakdowns is associated with an initially rough or scratched cathode, from which there will be high electron-emission at protrusions and at the edges of scratches. The subsequent deposition of polymerized material, coupled with the destruction of the sharpest points, could make electron emission more difficult, and so increase the breakdown voltage. On the other hand, a highly polished and cleaned cathode, with its almost uniform surface and dielectric layer, will cause a high electric strength in a well purified liquid, and subsequent breakdowns will be at lower voltages owing to the changes in the microgeometry of the surface and in the dielectric layers. Incidentally, the new layer, after the first breakdown, is easily seen with the aid of a microscope, and the color and thickness of the layer differ with different liquids.

This theory not only explains the conditioning process and part of the mechanism of breakdown, but it accounts for other observations. For example, the statistical variations in breakdown voltages will result from variations in the dielectric layer from place to place on the cathode and from time to time as testing proceeds. Also, the movement of the breakdown site on an initially unblemished spherical cathode with successive breakdowns may be caused by the destruction of the original film at the first site and the building of a new layer of polymerized material. Finally, the normal multiple-pulse measuring technique may modify the distribution of layers on the cathode by polymerizing some liquid before a breakdown is initiated, thus making the electron emission characteristics of the cathode more uniform and accounting for the consistency and repeatability of the measured electric strengths found throughout the investigation. Using the single-pulse technique, there is no time for this to occur, and breakdown may be initiated rapidly from a site on the cathode having by chance a high emission characteristic (Fig. 11).

The dependences of electric strength and critical time-lag on gap length are well-known effects, and it is generally agreed that they arise from a collision ionization process.

The increase in electric strength with increasing pressure, always obtained with the whole ranges of liquid purities, electrode conditions and geometry, and voltage durations, indicates that bubbles play a part in the breakdown process. The authors postulate that a small bubble, either existing in the liquid (15) (in the pores and cracks of solid impurities, or in pits in the cathode surface) or produced by molecular dissociation of the liquid by electron bombardment, is caused to elongate in the direction of the electric field while decreasing in volume, and that breakdown commences in this bubble when its length and the voltage along it are suitable. The conditions for bubble elongation in a sphere-sphere gap are most propitious near the cathode, where the electric field is highest owing to positive ion space-charge enhancement. The details of the theory, which has been worked out quantitatively (16), take into account the permittivity, vapor pressure, and surface tension of the liquid.

The authors' results do not conform to the theories that the bubbles are formed from gases present in solution in the liquid (7, 17) nor that they are formed by gases adsorbed on the cathode surface (18-20). It is found that the dependence of electric strength on pressure is not significantly different for liquids saturated with air at atmospheric pressure and for liquids containing about a hundredth of this amount of dissolved air, and the pressure dependence is similar before and after a long run of breakdowns. Further, the pressure dependence is strong and persistent even with a sharply pointed cathode.

The diminution in the rate of increase in electric strength as a function of pressure at high pressures is accounted for by the fact that the ratio of the field near the cathode to the applied field increases steeply as the applied field becomes higher owing to a nonlinear increase in ionization by collision (21). Thus the electrostatic forces causing the elongation of a bubble increase in a manner to counteract the increased electric strength of the gas or vapor in the bubble.

The polarity effect at atmospheric pressure shown in Fig. 4 is similar to that reported for transformer oil using impulse voltages (22), but contrary to that reported for n-hexane using direct voltages (23). The reason for the discrepancy is not clear, but the authors' results are explained by the fact that ionization predominates near the point, whatever its polarity, and with the point positive, the positive ion space-charge helps to increase the field strength toward the plane cathode while with the point negative, the space charge tends to be confined to a small volume near the point and it opposes the applied field. Thus there is a higher breakdown voltage for a negative point than for a positive point. At high pressures, which require a higher effective field for bubble elongation and breakdown, a part of the increased applied field will be needed to counteract the effect of the space charge when the point is negative, thus the polarity effect is increased.

The temperature dependence of electric strength can be explained on the basis of bubble formation and elongation. When the temperature increases, the surface tension decreases and the vapor pressure increases, thus the electric field needed to elongate a bubble for breakdown is less. It seems probable that this effect will predominate over others, such as changes in the ionization coefficient of the liquid and in the electron emission characteristic of the cathode. Similarly, the longer the chain length in the paraffin series, and thus the higher the surface tension and the lower the vapor pressure, the higher the electric strength (Fig. 7 and 9).

The present results show that the critical time-lag is dependent on gap length, but independent of temperature, hydrostatic pressure, and of the chain length in the paraffin series (Fig. 9 and 10); the last

is in agreement with that reported earlier by Edwards (24) and Crowe (25), but in disagreement with that by Goodwin and Macfadyen (21). According to the authors' hypothesis the critical time-lag is a formative lag which is mainly associated with the time to accumulate a space charge in order to enhance the field to a value high enough to cause the elongation of a bubble. The dependence of the time-lag on the cathode surface condition has been reported by several investigators (8, 26), and the discrepancy between the authors' result and that of Goodwin and Macfadyen may be partly owing to different cathode surface conditions. Using pulse durations greater than the critical time-lag, the electric strength is practically a constant, probably owing to the fact that a minimum field strength is required for effective ionization as a prelude to the remaining parts of the breakdown mechanism.

Conclusion

All the experimental results fit the hypothesis that electric breakdown in liquid dielectrics is basically dependent on three processes: (*a*) electron emission from the cathode governed by dielectric layers on it, (*b*) impact ionization and space-charge formation in the liquid, and (*c*) bubble formation and elongation which triggers the breakdown. Impurities, electrode condition, applied voltage duration, applied hydrostatic pressure, temperature, and the physical and chemical characteristics of the liquid, affect the electric strength through their influence on one or more of these processes.

Acknowledgments

The authors are grateful for constant encouragement from Professors A. Tustin and D. G. Tucker, Mr. C. G. Garton of the Electrical Research Association, and the E/B Sub-Committee of the Electrical Research Association, and for numerous instances of help from their colleagues at Birmingham University. The skill of the technical staff, particularly of Mr. A. Powell, was invaluable. The authors make grateful acknowledgment of financial support from the Electrical Research Association.

Manuscript received March 1, 1960; revised manuscript received Feb. 27, 1961. This paper was prepared for delivery before the Philadelphia Meeting, May 3-7, 1959.

Any discussion of this paper will appear in a Discussion Section to be published in the December 1961 JOURNAL.

REFERENCES

1. P. K. Watson and J. B. Higham, *Proc. Inst. Elec. Engrs.*, **100**, Pt. IIA, 163 (1953).
2. K. H. Stark, Unpublished.
3. K. H. Stark and J. B. Higham, *Elec. Res. Assoc. (British)* Techn. Rep. No. E/T70 (1958).
4. A. Powell and K. H. Stark, *J. Sci. Instr.*, **33**, 163 (1956).
5. K. C. Kao, Ph.D. thesis, University of Birmingham (1957).
6. J. B. Higham, *Proc. Inst. Elect. Engrs.*, **100**, Pt. IIA, 183 (1953).
7. F. M. Clark, *J. Franklin Inst.*, **216**, 429 (1933).
8. T. A. Holbeche, Ph.D. thesis, University of Birmingham (1956).
9. W. Ferrant, *Z. Physik*, **89**, 317 (1934).
10. K. C. Kao and J. B. Higham, *Elect. Res. Assoc. (British)*, Techn. Rep. No. E/T67 (1956).
11. W. B. Green, *J. Appl. Phys.*, **26**, 1257 (1955).
12. F. Llewellyn Jones and C. G. Morgan, *Proc. Roy. Soc.*, **A218**, 88 (1953).
13. A. von Hippel, "Dielectric Materials and Applications," John Wiley & Sons, Inc., New York (1954).
14. M. E. Zein El-Dine and H. Tropper, *Proc. Inst. Elect. Engrs.*, **103C**, 35 (1956).
15. L. Liebermann, *J. Appl. Phys.*, **28**, 205 (1957).
16. K. C. Kao, Conference Paper No. CP.60-84, Amer. Inst. Elect. Engrs. (1960).
17. F. Koppelmann, *Z. tech. Physik*, **16**, 125 (1935).
18. A. Gemant, *ibid.*, **9**, 398 (1928).
19. S. Hirano, *J. Inst. Elect. Engrs. Japan*, **63**, 359, 463 (1943).
20. H. Tropper, *Proc. Inst. Elect. Engrs.*, **100**, Pt. IIA, 176 (1953).
21. D. W. Goodwin and K. A. Macfadyen, *Proc. Phys. Soc.*, **66B**, 85 (1953).
22. T. W. Liao and J. G. Anderson, *Trans. Am. Inst. Elect. Engrs.*, **72**, Pt. 1, 641 (1953).
23. T. J. Lewis, *Proc. Inst. Elect. Engrs.*, **100**, Pt. IIA, 141 (1953).
24. W. D. Edwards, *Can. J. Phys.*, **29**, 310 (1951).
25. R. W. Crowe, *J. Appl. Phys.*, **27**, 156 (1956).
26. R. F. Saxe and T. J. Lewis, *British J. Appl. Phys.*, **6**, 211 (1955).

APPENDIX I

Electrode preparation and cleaning technique.—The stainless-steel electrodes are polished with a succession of mops at a surface speed of 7600 ft/min, using a succession of polishing compounds ending with "superfine green rouge," until there are no pits and only a few very slight scratches visible at a magnification of 500 diameters. After the polishing process is complete, the electrodes are immersed in boiling n-hexane for 30 min and then assembled in the electrode system. The whole unit is finally cleaned for 1 hr in dustless condensed n-hexane vapor.

APPENDIX II

Cleaning the glass system.—Before assembling the distillation system, all glass parts are cleaned with hot detergent solution, rinsed with distilled water, and dried. The sintered-glass filters are cleaned by immersing them for 12 hr or more in a solution containing sulfuric acid, and a little potassium nitrate and sodium chlorate.

Each time after assembling the electrode unit and test cell into the system, and before starting the distillation of a liquid sample, the whole enclosed system is evacuated for about 1 hr, cleaned with n-hexane, and then left under vacuum (0.5 to 1.0 mm Hg) for 3-4 hr. Only air passing through calcium chloride, phosphorus pentoxide, and then glass wool, is then allowed to enter the system.

Each time after a test during which the test cell has been immersed in oil (for example, in the pressure chamber), the cell is cleaned in trichlorethylene and then in boiling chromic acid with potassium dichromate and concentrated sulfuric acid. After thorough rinsing with distilled water, it is scrubbed with boiling distilled water and then dried.

The Wien Effect and Ionic Association

Andrew Patterson, Jr.

Sterling Chemistry Laboratory, Yale University, New Haven, Connecticut

and Harlow Freitag

International Business Machines Corporation, Poughkeepsie, New York

ABSTRACT

High field conductance is sensitively dependent on ion association, so that if one has available theoretical means to compute high field conductances, experimental measurements can be used to determine association constants. The authors have programmed for machine computation the Onsager-Kim strong electrolyte theory of the Wien effect, combined with the Onsager weak electrolyte theory in such a way as to account for the high field conductances of associated electrolytes. The computation is a considerable improvement over previous ones, being both more precise and much faster. Graphs are presented of a number of computed results, compared with experimental measurements, illustrating the way in which theory and measurement can be combined to obtain information about ion association. The majority of these calculations have not been attempted previously.

Experimental measurements of the high field conductance quotient (Wien effect) have been found useful for studying ionic association in solutions ranging from those which one would characterize as involving strong electrolytes, through the middle ground where ionic association significantly alters the behavior of what would otherwise be regarded as strong electrolytes, to those of electrolytes which are sufficiently associated to be classified as weak. It is convenient to compare the experimental Wien effect measurements with computed theoretical results and to use the theory to derive estimates of ionic association in the solutions. Until recently, application of this approach has been hindered by the lack of a theory of the Wien effect for nonsymmetrical valence-type strong electrolytes and by the complexity and tediousness of the calculations required. The first of these impediments has been removed by the appearance of the Onsager-Kim theory (1) for the high field conductance of nonsymmetrical strong electrolytes. The authors have now programmed this theory for machine computation on the IBM 650 computer, have included in this program a correction for association utilizing the Onsager theory for weak electrolytes, and have also incorporated into the program a computation of the mean activity coefficient of the electrolyte under examination, at zero field, by the method developed by Poirier (2) based on the Mayer cluster theory of imperfect gases. The present authors have used this program to refine considerably an earlier calculation of Bailey and Patterson (3) and to show a number of possible ways to study ionic association, the results of these computations being presented in the sections which follow.[1] Harned and Owen review in their monograph (4) the high field conductance theories of Onsager, Onsager and Wilson, and Onsager and Kim, and the experimental measurements of Patterson and co-workers. All symbols used below are those of Harned and Owen, to whose work (4) reference should be made for definition of their meaning.

[1] This material is taken in part from a dissertation submitted by Harlow Freitag to the Graduate School, Yale University, in partial fulfillment of the requirements for the degree of Doctor of Philosophy, May, 1959. For those who are interested, a limited number of copies of this dissertation is available and one can be provided on request. Punch-card decks for the computation program can also be made available.

Theoretical

While details of high field conductance calculations and the computer program can be obtained elsewhere (4) it is pertinent to describe here where the calculations differ from those described in the most readily available reference, Harned and Owen (5).

For symmetrical electrolytes, the Onsager-Kim theory reduces essentially to that of Onsager and Wilson. In ref. (4) values of the functions of Wilson, $f(x)$ and $g(x)$, are tabulated and must be used to perform the calculation of the high field conductance quotient. We have arranged to perform the equivalent Onsager-Kim calculation with a choice of the increments of the field variable a. This allows the convenient calculation of theoretical points as closely spaced as need be.

For nonsymmetrical electrolytes, the Onsager-Kim theory (1) is presented in two forms, one for low values of the field where a has a range of zero to about 2.5, another for values of a above 2.5. The first is in the form of double integrals which can be simplified for manual calculation through numerical quadrature by the trapezoidal rule. The second is in the form of polynomials the first seven terms of which are tabulated by Harned and Owen (4) for certain arbitrary valence types. We have preferred to perform the numerical integration directly for the low field case ($a < 2.5$), although it is convenient to do the high field calculation ($a > 2.5$) first to leave more drum locations for the integration available to

the computing machine. The program calculates eight terms of the series expansion, rather than the seven given in the tabulation of Kim's values in ref. (4). In both ranges of field, the field parameter a can be incremented in as reasonably small increments as may be desired. The entire calculation is thus more precise, and may, if desired, have data points much more closely spaced than would be practical with manual calculation. In any case the saving of time is enormous.

The calculation of the high field conductance quotient when association is present is accomplished by calculating the conductance of the solution at zero field and at field X using the proper value of the degree of dissociation, α. One solves for $\alpha(0)$ using the mass action law in the form

$$\alpha(0) = (-K(0) + \{K(0)^2 + 4K(0)cf_\pm^2\}^{1/2})/2cf_\pm^2 \quad [1]$$

The quantity $f_\pm$, the mean molar activity coefficient, is calculated in the program as described below. In order to calculate the degree of association at field X the relation

$$K(X) = c\alpha^2/(1-\alpha) \quad [2]$$

is used. The approximation is made that the mean activity coefficient is unity at any nonzero field. The effect of this approximation and the significance of an activity coefficient at nonzero field will be discussed later. The quantity $K(X)$ is calculated from the theory of Onsager (6) for the displacement of the dissociation constant on the application of a field as described in ref. (3), this calculation having been incorporated in the program at the appropriate point. A value of the low field equilibrium constant for a particular electrolyte is chosen from the literature values, and with the Onsager theory (6) $K(X)$ and then a value of α are calculated. Since the Onsager-Kim field parameter a is dependent on the ionic strength, the value of a would have to be corrected as a result of the association. This correction would produce a slightly different value of the field, so the entire calculation would be repeated until a consistent value of the field was obtained. One does not wish to adjust the value of a, however, since the Onsager-Kim variable $\theta(a)$ is calculated for a specific value of a. As noted, if there is ionic association in the solution, the ionic strength will assume a different value. The field associated with a will change, hence Onsager's b, $K(X)/K(0)$, and α will be changed in turn. A new value of α will yield a new ionic strength, but since the quantity (FIELD/$\Gamma^{1/2}$) must be kept constant, the quantity FIELD will change along with α until, using $\alpha(0)$ as a first approximation to $\alpha(X)$ and iterating on α, a final consistent value of α and of Γ will result. Bailey and Patterson (3) did not perform this iteration; it is quite convenient to do so on a data processing machine, and the program is so constructed.

As noted in the preceding paragraph, the mean molar activity coefficient at zero field, $f_\pm$, is required. Although this quantity can be calculated with the precision required for this computation using Eq. 3-5-7 of ref. (4) for low values of the concentration of electrolyte, at higher concentrations the theory of Poirier (2) is more appropriate. Because we had been asked to program the Poirier calculation for another purpose, this routine was incorporated into the high field conductance program to calculate $f_\pm$ for the association correction, thus making the program more general and useful to higher concentrations of electrolyte than would otherwise be possible. In performing the Poirier calculation, where Poirier has used c, the solute concentration, we have used αc, the ionic concentration. The power series expansions converge more rapidly when αc is used than when c alone is used as the starting point, although the end result is the same in either case and either approach is in principle correct.

Because our experimental measurements are almost always performed relative to some reference electrolyte, usually potassium chloride, the program has been arranged to calculate the reference electrolyte Wien effect, using the concentration and limiting ionic conductances for the reference which are read in on a separate data card. This reference Wien effect is then subtracted from the absolute Wien effect of the electrolyte being studied to yield the relative Wien effect for comparison with experiment. The reference electrolyte must be symmetric.

The program described here for the Onsager-Kim theory is in some ways more general than that outlined in ref (4), since it can be used to perform calculations for any valence-type electrolyte, including fractional valence types, rather than the restricted set represented by the table on pp. 188-193 of ref. (4). The ionic association correction cannot be extended in this fashion, however.

Results

The results of employing the computer program described above are given in Fig. 1-10. A description of the system under study is given in the legend of each figure. In each case, the high field conductance quotient, $\Delta\lambda/\lambda(0)$, in per cent, is plotted *vs.* field. The temperature in every case is 25.00° ±0.05° or less, and the solutions are in conductance water.

Discussion

Figure 1 shows results calculated for potassium chloride at concentrations ranging from 10^{-3} to 10^{-5}M. In Fig. 2 is shown an expanded rendition of the low-

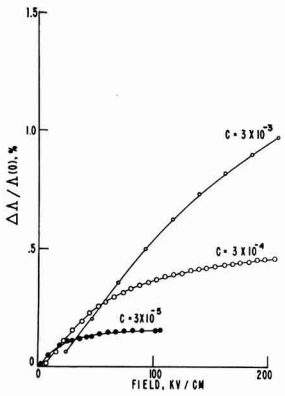

Fig. 1. Computed high field conductance quotients for potassium chloride solutions at three concentrations.

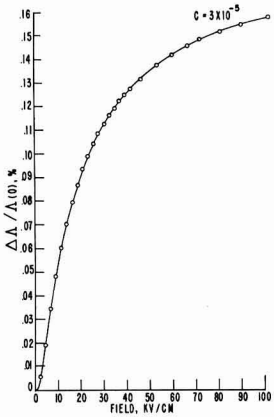

Fig. 2. Computed high field conductance quotient for potassium chloride at low concentration showing on expanded scale the smooth approach of the curve to the origin.

field portion of the curve for $c = 10^{-5}$M. Figure 2 shows a very smooth and uniform variation of the conductance quotient as a function of field, but Fig. 1 shows some unusual features.

In the low field region below 20 kv/cm, the Wien effect decreases with increasing concentration, quite the opposite of the trend at higher fields such as 100 kv/cm. Since atmosphere effects become more pronounced at higher concentrations, one would predict an increase in Wien effect with increase in concentration as is noted at the higher fields. However, close study of the calculation shows that the screening effect of the ionic atmosphere decreases the effective field to which an ion is exposed, yielding, as one would expect, a field smaller than that applied externally; since it is at the lower fields where the conductance quotient *vs.* field curve has its greatest slope, a small change in effective field has a comparatively large effect on the change of conductance, causing the cross-over of curves shown on the figure. At higher fields in the same solutions, the atmosphere-disrupting effect of the field is sufficiently great to give the expected result. The curve for $c = 3 \times 10^{-3}$ terminates at the low-field end because a becomes too small to allow precise calculation in this region. At smaller concentrations, when a is sufficiently large, the curves come smoothly into the origin as shown on expanded scale in Fig. 2. Because of difficulties associated with making precise measurements at low fields, these effects have not been demonstrated experimentally.

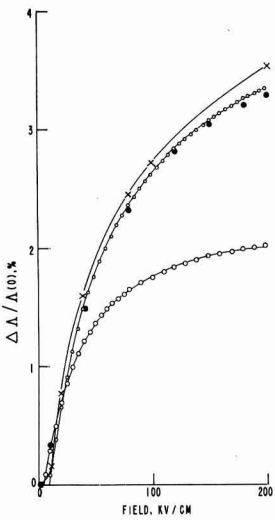

Fig. 3. Computed and experimental high field conductance quotients for magnesium sulfate solution, 1.39×10^{-4} molar; $K(0) = 6.3 \times 10^{-3}$. Reference electrolyte KCl, 2.335×10^{-4} molar. Reading from bottom up, large open circles, Onsager-Kim calculation without association correction; black circles, experimental results, Ref. 3; small open circles, calculation described in this paper; crosses, calculation with association correction, Ref. 3.

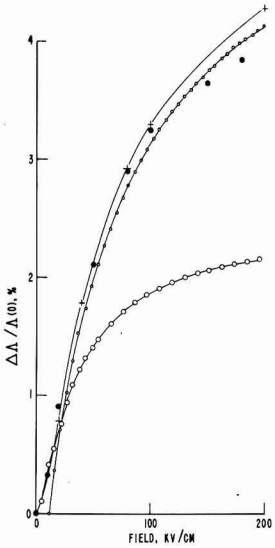

Fig. 4. Computed and experimental high field conductance quotients for zinc sulfate solution, 1.64×10^{-4} molar; $K(0) = 4.9 \times 10^{-3}$. Reference electrolyte KCl, 2.880×10^{-4} molar. Reading from bottom up, large open circles, Onsager-Kim calculation without association correction; black circles, experimental results, Ref. 3; small open circles, calculation described in this paper; crosses, calculation with association correction, Ref. 3.

In Fig. 3, 4, and 5 are shown results calculated with the improved theory described in this paper, compared with calculations of Bailey and Patterson (3) for magnesium and zinc sulfate and of Berg and Patterson (7) for copper sulfate, and with the experimental results reported in refs. (3) and (7). In each, there is considerable improvement in the match between experiment and theory at the high fields, but an actual deterioration in the agreement at the low fields, near the origin. Here, the theoretical curves plunge below the experimental and actually become negative, a result not to be expected in these systems, although experimental negative Wien effects have been observed with some uranyl ion solutions (8). This is the result of the approximation made in order to use Eq. [2], namely, that the activity coefficient is unity at any nonzero field. The concept of a high field activity coefficient is a contradictory one. Activity

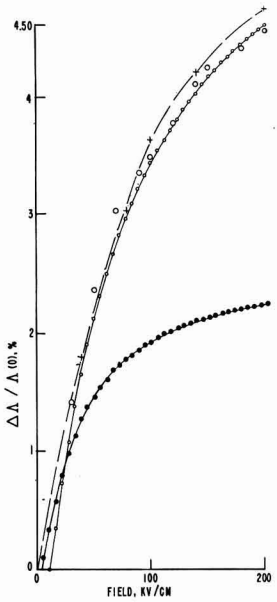

Fig. 5.—Computed and experimental high field conductance quotients for copper sulfate solution, 1.77 x 10^{-4} molar; K(0) = 4.3 x 10^{-8}. Reference electrolyte KCl, 3.180 x 10^{-4} molar. Reading from bottom up, black circles, Onsager-Kim calculation without association correction; large open circles, experimental results, Ref. 7; small open circles, calculation described in this paper; crosses, calculation with association correction, Ref. 7.

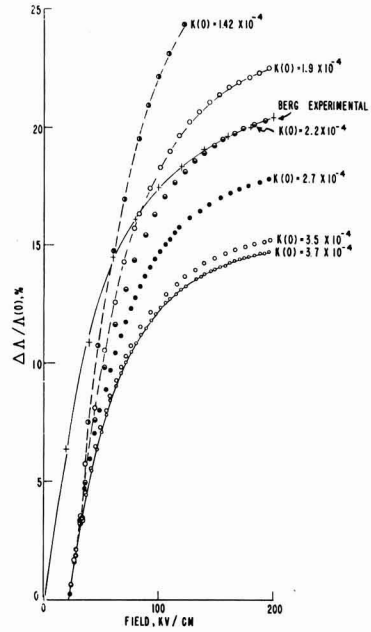

Fig. 6.—Computed and experimental high field conductance quotients for lanthanum ferricyanide solution, 1.025 x 10^{-4} molar; reference electrolyte KCl, 3.0 x 10^{-4} molar. Crosses are the experimental results of Ref. 10. The other curves are calculated for various values of K(0) as shown.

coefficients refer to true equilibrium thermodynamic states, and are measured under equilibrium conditions. Application of high electrical fields during Wien effect measurements displaces the system from equilibrium, so that the term "activity coefficient" does not seem appropriate. At the same time, however, the interionic forces described quantitatively by the activity coefficient at equilibrium are gradually and smoothly overcome by the increasing field. We suggest that the phrase "un-screening coefficient" be substituted for "nonzero-field activity coefficient" as a representation of what is happening in the solution under the influence of the field, in order to avoid confusion with a well-defined equilibrium concept. A precise analytical interpretation of the screening phenomenon and of the unscreening coefficient is mathematically feasible and is currently under study (9).

On the graph for zinc sulfate, Fig. 4, it will be noted that the theory predicts a Wien effect approximately 0.1 unit higher than that observed experimentally. There is good reason to believe that the value of $K(0)$, obtained by extrapolation to zero concentration of conductance data at low fields, may be uncertain to the extent of 5% because of the difficulty of making correction for hydrolysis of such salts as those under study here. Increasing the value of $K(0) = 4.9 \times 10^{-8}$ by 6% of its value to $K(0) = 5.2 \times 10^{-8}$ will bring the theory into good agreement with experiment at the high field end of the curve.

It is interesting to note that at zero field, these electrolytes, all at concentrations in the range of 10^{-4}M, dissociate to an extent less than 3% of the total solute present. At 200 kv/cm, however, less than 1% of the solute is undissociated. This corresponds to a fivefold increase in the dissociation constant. One may observe from tabulated results that the unscreening coefficient of magnesium sulfate approaches unity more rapidly than is the case with zinc and copper sulfates as field is increased, so that the calculated Wien effect approaches the experimental results more rapidly. This theoretical anomaly should disappear when an analytical solution for the screening effect at low fields becomes available. The influence of screening has already been shown in Fig. 1. With the higher valence-type electrolytes, the phenomenon becomes important and the effect of neglecting it experimentally demonstrable, as Fig. 3, 4, and 5 illustrate.

In Fig. 6 similar results are shown for lanthanum ferrocyanide, compared to the experimental results of Berg and Patterson (10). Here the error at low fields is even more pronounced. Shown also is a group of curves computed for different values of the association constant, ranging from 1.42×10^{-4} to 3.70×10^{-4}. The best fit is found with a value 2.20×10^{-4}. Low field conductance data analyzed by Davies (11) led to a value of 1.82×10^{-4}. It is apparent from Fig. 6 just how sensitive the high field conductance results are to a variation in the value of $K(0)$.

In Fig. 7 is shown what happens when one goes to the extreme of simulating a true weak electrolyte by artificially reducing the dissociation constant. Here the same data have been used as for Fig. 3, but the

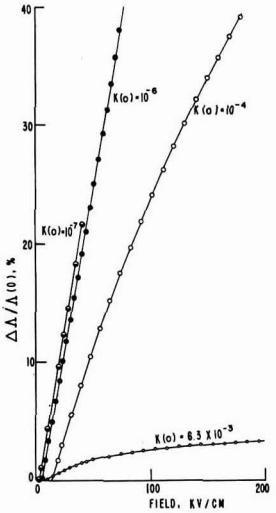

Fig. 7.—Computed results for magnesium sulfate solution. Data are the same as in Fig. 3, but the scale has been changed to accommodate the high values of $\Delta\lambda/\lambda(0)$ resulting from arbitrary assignment of the K(0) values shown.

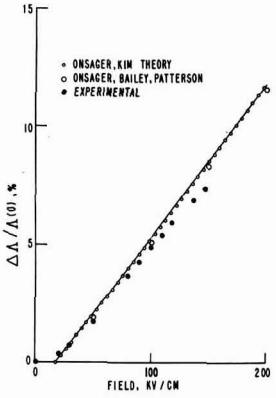

Fig. 8.—Computed and experimental high field conductance quotients for acetic acid solution, 7.405 x 10^{-4} molar; K(0) = 1.754 x 10^{-5}. Reference electrolyte KCl, 1.01 x 10^{-4} molar. Reading from bottom up, black circles are the experimental results of Ref. 12; large open circles are the calculated results using the Onsager weak electrolyte theory; small open circles are calculated with the theory described in this paper.

dissociation constant has been set arbitrarily at smaller and smaller values. We note that as the dissociation constant is decreased the curve approaches a straight line, matching the results obtained experimentally with a weak electrolyte. Another interesting result is that the curves do not cross, although the plot otherwise resembles one for potassium chloride in which the solute concentration has been varied over the wide range. This confirms the belief that in the case of potassium chloride the curve crossing was due to electrostatic shielding. In the present case, although the Wien effect of the "weaker" solution, that is, the one to which a smaller dissociation constant has been arbitrarily given, has a much higher value than does the "stronger" solution, the curves do not cross because the ionic strength of the weaker solution is lower than in the cases with potassium chloride at higher concentration, and the electrostatic shielding effects are therefore absent.

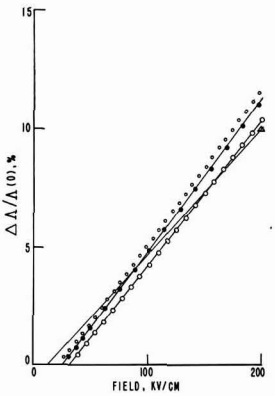

Fig. 9.—Computed and experimental high field conductance quotients for ammonia solution, 1.585 x 10^{-8} molar; reference electrolyte KCl, 2.335 x 10^{-4} molar. Curve marked Δ is experimental data taken from Ref. 13 for which only the slope is shown. Large open circles are for K(0) = 8.0 x 10^{-6}; black circles are for K(0) = 3.34 x 10^{-6} from Ref. 13; small open circles are for K(0) = 1.774 x 10^{-6} from Ref. 14.

Pursuing further the results of the calculation shown in Fig. 7, we have applied the combined Onsager-Kim theories to two weak electrolytes for which experimental data are available, acetic acid and ammonia (12, 13). Both calculations result in straight lines with negative intercepts. In the case of acetic acid, the calculation made with the Onsager theory for weak electrolytes (6) agrees closely with the calculation made with the combined theory, while the experimental results gradually fall below these curves at higher fields. This experimental result has been explained as due to high field produced polarization in the vicinity of the electrodes, which modifies the distribution of field to which the bulk of the ions and molecules are exposed. For ammonia, two dissociation constants have been used: one is that of Bates and Pinching (14) and the other is that obtained by Berg and Patterson (13) from high field conductance results assuming the existence of dissolved but unhydrated ammonia in solution. Neither calculation reproduces the experimental data exactly.

In Fig. 10 is shown an attempt to deal with the equilibria in cadmium chloride solution, using data of Bailey and Patterson (15) and Harned and Fitzgerald (16). The two reactions assumed are the complete dissociation of cadmium chloride into Cd^{++} and Cl^- ions, in contradiction to the conclusions of Harned and Fitzgerald, and the equilibrium

$$CdCl^+ \rightleftharpoons Cd^{++} + Cl^-$$

to which the value of $K(0) = 1.1 \times 10^{-2}$ was assigned by these authors (16). This is a difficult case for electrochemical theory, since high field calculations for a mixture of ions lead to mathematical complexities

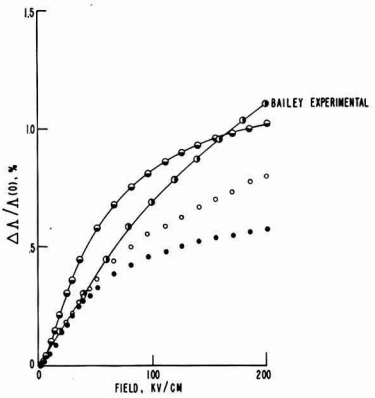

Fig. 10.—Computed and experimental high field conductance quotients for cadmium chloride solution, 1.697×10^{-4} molar. Reference electrolyte KCl, 2.889×10^{-4} molar. Black circles, Onsager-Kim calculation for unsymmetrical strong electrolyte; open circles, Onsager-Kim calculation with conductance quotient for assumption of symmetrical charge type weak electrolyte, $K(0) = 1.1 \times 10^{-2}$, added; large half-black circles close to curve marked "Bailey experimental" are for the Onsager-Kim calculation without reference electrolyte correction. The experimental data are from Ref. 15. The topmost two curves may be contrasted, since one is for a strong electrolyte, the other for the partly-associated cadmium chloride.

currently unsolved, although a solution for the low field case has been presented by Onsager and Kim (4). Because the Cd^{++} ion has one greater unit charge than does the $CdCl^{+}$ ion, we have arbitrarily assigned it unit charge and CdCl zero charge in order to perform an association calculation. Then a second calculation has been made on the assumption that cadmium chloride is a strong unassociated electrolyte, and the high field conductance quotients added. The computed curve for the equilibrium reaction was a straight line, as it should be for a normal weak electrolyte. None of these calculations satisfactorily match the experimental results, which for the present must be regarded as beyond the reach of our mathematical apparatus.

The authors have used the computation program to compute the high field conductance quotients for a number of other unsymmetrical valence-type electrolytes. These calculations have been compared with experimental results in a further test of the Onsager-Kim theory, in a paper submitted to another journal.

Acknowledgment

The financial support of a contract with the Office of Naval Research is gratefully noted. Professors Raymond Southworth and B. B. Owen made a number of valuable suggestions while this work was in progress.

Manuscript received May 3, 1960; revised manuscript received March 4, 1961. This paper was prepared for delivery before the Philadelphia Meeting, May 3-7, 1959.

Any discussion of this paper will appear in a Discussion Section to be published in the December 1961 JOURNAL.

REFERENCES

1. L. Onsager and S. K. Kim, *J. Phys. Chem.*, **61**, 198 (1957).
2. J. C. Poirier, *J. Chem. Phys.*, **21**, 956, 972 (1953).
3. F. E. Bailey and A. Patterson, *J. Am. Chem. Soc.*, **74**, 4426 (1952).
4. H. S. Harned and B. B. Owen, "The Physical Chemistry of Electrolytic Solutions," 3rd ed., pp. 127-153, 183-193, 327-330, Reinhold Publishing Co., New York (1958).
5. *Ibid.*, pp. 146-153, 183-193; also ref. (3).
6. L. Onsager, *J. Chem. Phys.*, **2**, 599 (1934).
7. D. Berg and A. Patterson, *J. Am. Chem. Soc.*, **74**, 4704 (1952).
8. F. E. Bailey, J. F. Spinnler, and A. Patterson, *ibid.*, in press.
9. L. Onsager, Private communication.
10. D. Berg and A. Patterson, *J. Am. Chem. Soc.*, **75**, 1484 (1953).
11. C. W. Davies and J. C. James, *Proc. Roy. Soc. (London)*, **A195**, 116 (1948).
12. F. E. Bailey and A. Patterson, *J. Am. Chem. Soc.*, **74**, 4756 (1952).
13. D. Berg and A. Patterson, *ibid.*, **75**, 5731 (1953).
14. R. G. Bates and G. D. Pinching, *ibid.*, **72**, 1393 (1950).
15. F. E. Bailey and A. Patterson, *ibid.*, **75**, 1471 (1953).
16. H. S. Harned and M. E. Fitzgerald, *ibid.*, **58**, 2624 (1936).

ZnS:Cu,Si Phosphors

A. Wachtel

Research Department, Westinghouse Electric Corporation, Bloomfield, New Jersey

ABSTRACT

Firing of ZnS + $(CH_3COO)_2Cu$ + SiS_2 causes incorporation of copper and promotes orange fluorescence under firing conditions whereby the "self-coactivated copper" emission is normally not obtained. This is accomplished by simultaneous incorporation of Si. It is proposed that silicon can replace vacancies or interstitial Zn atoms in proposed models for the orange-emitting copper center. With high concentrations of Cu and Si, a ternary (Zn,Cu,Si)S forms which may show a deep-red fluorescence peaked at 840 mμ.

An attempt to use tetravalent coactivators in ZnS phosphors has been described by Kröger and Dikhoff (1). Unfortunately, their results do not show an effect in the case of copper activation. Since SiO_2 was used as the source of Si and since SiO_2 vessels are normally employed for the preparation of ZnS phosphors without interference due to Si, it is assumed that SiO_2 is not a sufficiently reactive source material for introduction of Si into the ZnS lattice. In the present investigation, the Si was introduced as SiS_2 which in turn was formed from reaction of elemental Si with the atmosphere during the firing process.

Preparation of Phosphors

ZnS(RCA33Z19), prefired in H_2S at 700°C, was slurried with the required amount of Cu as $(CH_3COO)_2Cu \cdot H_2O$, dried at 110°C, and ground with 5 wt % purified S (General Chemical Company, Research Laboratory) and the required amount of elemental Si (Mallinckrodt Grade I Transistor AR). Although the Si as received showed a high degree of purity, ball milling to pass 200 mesh as necessary to achieve homogeneity in the subsequent firing introduced between 0.01 to 0.1% Al. Consequently, phosphors prepared without Cu or with small additions of Cu (0.01 mole %) and with 1-10 mole % additions of Si always showed blue or green photoluminescence characteristic of self-activated or of Cu + Al activated ZnS.

Most firings were conducted at atmospheric pressure in small, loosely capped transparent silica tubes in an atmosphere of purified N_2 or H_2S, or in open tubes or boats in H_2S at temperatures of 950° or 1100°C. The H_2S was purified by passage through dibutyl phthalate, $Ba(OH)_2$ solution, $CrSO_4$ solution, "Drierite," and P_2O_5. Some problems were encountered concerning incorporation of the Si. Firing with S in N_2 did not allow a sufficient amount of S to remain in contact with the sample to effect complete conversion of the Si to SiS_2. Firing in H_2S permitted sufficient access of the gas to the sample (open tubes or boats), but at 950°C the reaction between Si and H_2S is slow. At 1100°C, the reaction proceeds satisfactorily, but there is also appreciable sublimation of SiS_2. Maximum Si incorporation could be achieved by using large additions (up to 20 mole %) of Si and conducting two firings at 1100°C with brief grinding between firings. Results for phosphors prepared at 950°C are also reported here. An alternate method consisted of prefiring ZnS + $(CH_3COO)_2Cu \cdot H_2O$ + S in N_2 at atmospheric pressure, mixing with Si and S in the proportion of 1 Si:2S, and refiring overnight in sealed evacuated silica tubes at 1020°C. This method has the advantage of avoiding losses of SiS_2, but was subject to the danger of explosions due to high S pressure.

The fired phosphors were usually covered with needles of SiS_2 which, in contact with air, rapidly hydrolyze to $SiO_2 + H_2S$. In order to avoid excessive contamination of the phosphors with inactive SiO_2 they were rapidly plunged into 10% NaOH solution, which decomposes SiS_2 to form $Na_2SiO_3 + Na_2S$. Where there was evidence of excess Cu_2S on the phosphors (discernible by gray body color) they were subsequently washed in NaCN solution.

Analytical Determinations

Silicon was determined gravimetrically by dissolving a weighed sample of phosphor in aqua regia and collecting the silica by filtration. Copper was determined in the filtrate by adding enough NH_4OH solution to complex all Cu and Zn, and measuring the absorbance of the solution against a known standard at 630 mμ. In cases of a high ratio of Zn/Cu, the final volume of solution was kept small by H_2S precipitation of the Cu from the acid filtrate, centrifuging, dissolving the CuS in a few drops of aqua regia, and then adding the NH_4OH solution.

The values obtained for Si represent not only the amount in the ZnS lattice, but also any SiO_2 which formed on the surface of the fired sample immediately on exposure to the atmosphere. Although the exposure to air, prior to contact with the NaOH solution, was kept to a minimum (a few seconds) the hydrolysis of SiS_2 is extremely rapid. Moreover, even a more elaborate technique, which might have avoided such exposure, would not have eliminated all errors, since the reaction of SiS_2 on contact with the NaOH solution is sufficiently exothermic to produce local development of steam with consequent formation of hydrated SiO_2. Values of Si in ZnS fired without Cu ranged from 0.13 to 0.28 mole % and, without evidence to the contrary, they should be regarded as representing surface contamination.

Physical Measurements

Emission spectra were determined by exciting the phosphors with a 100-w high-pressure mercury-vapor lamp equipped with a Corning No. 5860 filter and measuring with a Perkin Elmer Universal Spectrometer, Model 13-U, using a 1P22 photomultiplier tube for the visible region and a PbS cell for the infrared region.

Diffuse reflectance spectra were determined with a Beckman Model DU Spectrophotometer with diffuse reflectance attachment. Measurements were taken relative to a $MgCO_3$ block, freshly smoked with MgO, set at 100 at each wave length. Suitable filters were employed to eliminate fluorescence.

The relative orange output (fluorescence) as a function of phosphor composition was determined with a Spectra Brightness Spot Meter set on the "open" position. A Corning No. 2418 filter was used to eliminate blue and green emission.

Crystallographic data were obtained with a Philips x-ray diffractometer operated at 35 kv and 15 ma, using a Cu target and Ni filter.

Experimental Results

Table I shows the results obtained on firing ZnS at 1020°C with different concentrations of Cu and Si in sealed tubes. Higher temperatures and higher concentrations of Si than 3 mole % were not employed because the amount of S necessary to form SiS_2 might have exerted dangerously high pressures within the tubes. The S additions were chosen to be in slight excess over the amounts necessary to combine with the Si present. It should be mentioned that all samples with orange fluorescence and yellow body color did not really require NaCN washing, because inspection of the tubes after firing failed to reveal any gray discoloration. In those cases, the washing procedure was employed merely for the sake of uniformity in phosphor preparation. At high Cu and Si concentrations (3 mole % each) a new phase with green-gray body color and deep red fluorescence appeared. It was slowly attacked by boiling NaCN solution (or by hot NaOH solution with visible formation of black Cu_2S). Green fluorescence noted on some samples with 1 or 3 mole % Si added was probably due to higher concentrations of Al introduced accidentally with the Si. Excitation with 365 mμ ultraviolet and simultaneous irradiation with infrared quenched all

Table I. 365 mμ-excited photoluminescence (upper rows) and body colors after NaCN washing (lower rows) of ZnS:Cu,Si phosphors fired in sealed tubes. Figures represent mole % activator added prior to firing

Si \ Cu	0.01	0.03	0.1	0.3	1.0	3.0
0.01	blue-green	wk. blue	blue	blue	wk. blue	wk. violet
	tan-white	tan	white	lt. gray	lt. gray	lt. gray
0.03	blue-green	wk. blue	blue	blue	wk. blue	pink
	tan-white	tan	lt. gray	lt. gray	lt. gray	lt. gray
0.1	blue-green	wk. blue	blue	blue	wk. blue	wk. pink
	tan-white	tan	lt. gray	lt. gray	lt. gray	lt. gray
0.3	orange	wk. orange	wk. blue + orange	s. blue + orange*	wk. blue	v. wk. pink
	yel.-white	lt. yellow	lt. yellow	lt. gray	lt. gray	green-gray
1.0	orange	wk. orange	wk. blue + orange	wk. green	wk. orange	red
	yel.-white	lt. yellow	lt. yellow	yellow	gray-green	gray green
3.0	orange	wk. orange	wk. green + orange	green	green	wk. green†
	yel.-white	lt. yellow	lt. yellow	yellow	deep yellow	deep yellow

* Strongest orange emission as observed through red filter.
† Red fluorescence and gray-green body color prior to NaCN washing.

blue and green emission, a phenomenon which does not occur in the absence of Si or "killer" elements.

The blue fluorescence of all samples prepared with less than 0.3 mole % Si shows that this particular method of phosphor preparation (S-pressure, 1020°C) did not, in itself, result in the formation of "copper orange" emitting centers (2-4). Consequently, any orange fluorescence which was observed depended on the presence of Si. The yellow body color of these phosphors prior to NaCN washing clearly showed incorporation of more Cu into the ZnS lattice than possible in the absence of a coactivator.

Figure 1 shows room-temperature emission spectra of four phosphors fired at 1100°C in H_2S at atmospheric pressure. As the Si additions are increased it is noted that an emission band peaked at longer wavelengths increases in relative strength. In the case of curve A which represents the fluorescence of a typical orange-emitting ZnS: Cu phosphor, the presence of the long wavelength emission band cannot be explained, unless it is due to a slight contamination with Si. In phosphors B and C, the long wavelength emission band may be due to the gradual formation of a separate phase whose fluorescence, in the absence of "Cu-orange" emission, is represented by Curve D.

X-ray powder diffraction measurements on sample D showed hexagonal ZnS as the major phase. In addition there were lines which could be indexed on the basis of two hexagonal phases, with lattice dimensions a = 7.38Å, c = 9.47Å and a = 7.42Å, c = 9.46Å. Boiling in NaOH solution caused decomposition with formation of Cu_2S, which was subsequently dissolved by addition of NaCN. After water washing and drying, the ZnS residue no longer showed any fluorescence or evidence of the new phase. Its deep yellow body color suggested a high concentration of incorporated Cu (see Table II sample 6).

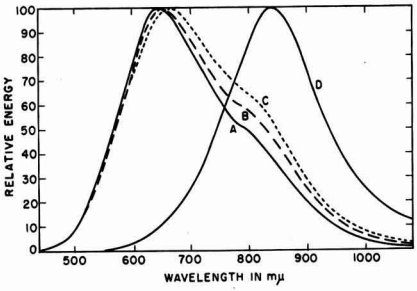

Fig. 1. Emission spectra of ZnS:Cu,Si phosphors. (A) 1.0% Cu, no Si; (B) 0.01% Cu, 0.1% Si; (C) 0.1% Cu, 5% Si; (D) 10% Cu, 20% Si.

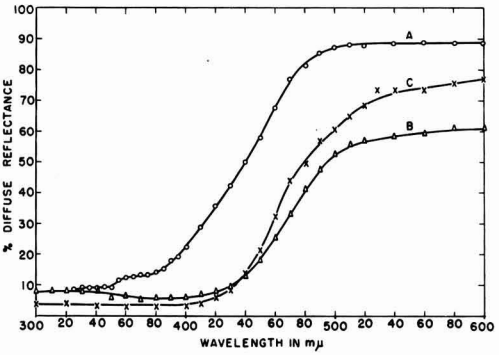

Fig. 2. Diffuse reflectance spectra of three ZnS:Cu,Si phosphors. (A) 0.6% Cu, 5% Si; (B) 10% Cu, 20% Si, unwashed, (C) B boiled in NaOH solution and NaCN washed.

Figure 2 shows the diffuse reflectance spectra of the same sample with high Cu and Si content after cold NaOH washing (B, separate phase intact) and after hot NaOH + NaCN washing (C, separate phase removed). The figure also shows the diffuse reflectance spectrum of a typical orange-emitting ZnS: Cu,Si phosphor (Curve A) prepared with a moderate concentration of Cu.

Figure 3 shows the intensity of orange photoluminescence of phosphors with different Si concentrations as a function of Cu added before firing. The curves are not normalized, but represent total orange emission in arbitrary units. The phosphors were fired at 1100°C in H_2S at atmospheric pressure and washed in NaCN. It can be seen that with no Si or 0.01 mole % Si added before firing, the output increases with

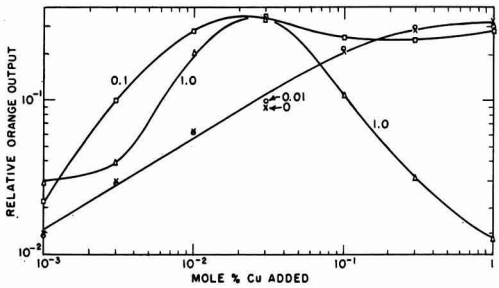

Fig. 3. Intensity of orange emission of ZnS:Cu,Si phosphors as a function of Cu addition. The numbers on the curves denote mole % Si added. Phosphors fired in silica tubes.

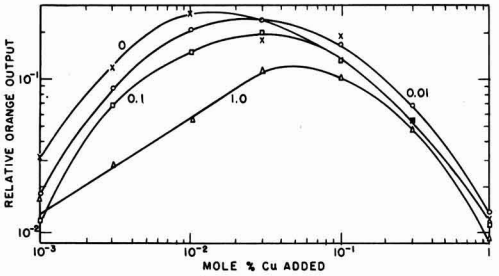

Fig. 4. Intensity of orange emission of ZnS:Cu,Si phosphors as a function of Cu addition. The numbers on the curves denote mole % Si added. Phosphors fired in graphite tubes.

Cu addition and appears to level off in the neighborhood of 1 mole % Cu added. With larger amounts of Si added, approximately the same maximum output is achieved, but at lower Cu additions. At 1% Si, the decrease of fluorescence at higher Cu additions was accompanied by increasingly yellow body color. This suggests that more Cu is incorporated in the presence of Si; this may result in concentration quenching.

Figure 4 shows the results of a similar experiment, except that the phosphors were fired in high-purity graphite, instead of silica tubes. Note that in this case, high Cu additions lead to decreased fluorescence in all cases, and it was observed that even without Si, high Cu additions resulted in yellowish body color.

Table II shows some analytical data on a number of phosphors. The column headed "cold NaOH washed" represents the samples from which only excess SiS_2 has been removed. The amount of Cu in these samples is essentially equal to the amount added before firing. The column headed "hot NaOH + NaCN washed" represents phosphors from which any extraneous phase (as mentioned earlier) has also been removed. In the case of ZnS:Cu,Cl electroluminescent phosphors, the amount of Cu found at this point would represent not only Cu dissolved in the lattice, but also any excess Cu_2S segregations (5) which may form in the interior of the particles, particularly along dislocations and similar faults. On the other hand, the phosphors represented in Table II were not electroluminescent, which means that, in the presence of the large excess of Si used in the firing, no free Cu_2S was formed. ZnS fired with Cu and enough Si to result in the disappearance of gray discoloration never formed an electroluminescent phosphor, while firing with less Si and more Cu led to blue photo- and electroluminescence only. Orange to lavender emitting electroluminescent phosphors could, however, be prepared by refiring orange photoluminescent ZnS:Cu,Si with more Cu, although their brightness was lower than that of orange electroluminescent ZnS:Cu phosphors.

Table II. Cu and Si content of ZnS fired with 20 mole % Si, 2 x 90 min in H_2S

Sample No.	Firing temp, °C	Amount added, mole %		Amount found, mole %		
				Cold NaOH washed	Hot NaOH + NaCN washed	
		Cu	Cl	Si	Cu	Si
1	950	0.01	0	0.44	—	—
2	950	0.01	0.3	0.42	—	—
3	950	5.0	0	3.0	1.0	1.4
4	950	5.0	0.3	1.5	1.2	0.6
5	1100	5.0	0	—	2.55	1.36
6	1100	10.0	0	5.7	2.4	1.44

The data in Table II indicate a maximum solubility of about 2.5 mole % Cu and 1.1 to 1.3 mole % Si in ZnS. Sample 6, cold NaOH washed, represents the phosphor indicated by Curve D in Fig. 1 and by Curve C in Fig. 2. The effect of Cl in decreasing the incorporation of Si into ZnS has not been checked on a sufficient number of samples to be considered real at present. Its effect of increasing the incorporation of Cu is, of course, well known.

The decreased concentrations of Si found after hot NaOH + NaCN washing indicate that a portion of the Si was not incorporated in the ZnS lattice, and that it was not present in the form of free SiS_2. Samples No. 5 and 6 which were fired at 1100°C showed little gray discoloration, yet the Cu concentration was similarly decreased by the washing process. These observations, as well as the x-ray diffraction patterns of sample 6 indicated that Cu and Si were somehow associated. At this point, attempts were made to prepare the separate phase in the absence of excess ZnS.

Table III shows the results of firing a number of mixtures of ZnS, CuS, and Si in varying proportions. Additional compositions were tried and red fluorescence was also obtained for a starting molar ratio of 2ZnS + 1CuS + 1Si; however, x-ray diffraction measurements were not taken in all cases. It will be noted that, for all except three samples, the diffraction pattern indicated the presence of two phases with hexagonal structure and very similar lattice dimensions. These are arbitrarily designated as "A" and "B." The lattice spacings and relative intensities of lines obtained on sample 7 (compound "A") and sample 9 (compound "B") are shown in Table IV. The lattice spacings of these two phases differ by only 0.02Å for the 200 reflection. The justification for calling them separate phases lies in the fact that the relative intensities of the two sets of lines vary with the composition of the starting mixture, as shown in the last column of Table III. The failure of the products to show a definite relation to the starting composition is believed to be related to

Table III. Some properties of ZnS + CuS + Si + S mixtures, fired at 1100°C in H_2S at atmospheric pressure. "A" = hex. phase a = 7.38Å, c = 9.47Å; "B" = hex. phase a = 7.42Å, c = 9.46Å

Sample No.	Molar composition*			Body color after washing	Fluorescence, 365μ exc. 'n	X-ray diffraction data		
	ZnS	CuS	Si			ZnS detected	Rel. intensity of strongest line "A"	"B"
1	5	1	2	deep yellow	none	cubic + hex.	20	15
2	4	1	2	yel.-brown	none	cubic + hex.	34	25
3	3	1	2	brown	none	cubic + hex.	31	36
4	2	1	2	brown	none	cubic	75	38
5	1	1	2	brown-gray	deep red	cubic + hex.	34	9
6	1	1	3	yellow-brown	deep red	cubic + hex.	36	44
7	1	3	4	blue-black	none	none	118	0
8	4	3	2	green-black	none	cubic	0	60
9	4	3	1	green-black	none	cubic	0	62

* Starting composition prior to firing. All other data refer to materials from which SiS_2 and any free Cu_2S was removed by careful washing with cold NaOH + NaCN solution.

Table IV. Relative intensities of lines obtained by x-ray powder diffraction on samples of (Zn,Cu,Si)S

(hkl)	Compound "A" d in Å	Compound "A" I	Compound "B" d in Å	Compound "B" I
110	3.69	9	—	—
200	3.19	100	3.21	100
201	3.06	8	3.07	37
112	2.92	4	2.92	11
103	2.83	30	2.84	53
120	2.42	3	2.42	5
104	2.21	5	2.21	20
300	2.12	3	—	—
220	1.85	81	1.85	40
222	1.72	16	1.72	34
400	1.60	9	1.61	13
223	1.59	14	—	—
304	1.58	16	1.59	11
413	1.55	10	—	—

volatilization of SiS_2 during firing and to partial hydrolysis of that compound during intermediate grindings.

Compound "B" could not be prepared free of excess ZnS, whose diffraction pattern made measurements of some of the lines of phase "B" unreliable. Moreover, the diffraction lines which were obtained on compound "B" consisted of very closely spaced doublets, and the lattice spacings reported in Table IV are average values.

Chemical analysis of sample 7 (Table III) showed the composition: Zn = 23.8 mole %, Cu = 50.5 mole %, Si = 25.7 mole %. This is the only sample which was obtained free of excess ZnS and which showed no trace of the other complex phase. When one considers that the value for Si is probably high because of the presence of a certain amount of free SiO_2, the data indicate a composition close to $ZnCu_2SiS_4$, or a 1:1:1 ratio of ZnS, Cu_2S, and SiS_2. Attempts were made to duplicate this composition by firing the required proportion of ZnS, CuS, Si, and S in sealed tubes at 1000°C. This, however, resulted in much of the ZnS remaining unreacted, probably because of the lower firing temperature and lack of excess SiS_2. It should also be mentioned that the preparation of (Zn,Cu,Si)S compounds by firing either at atmospheric pressure or in sealed tubes was generally not reproducible with respect to appearance, fluorescence or chemical composition of the samples. X-ray diffraction measurements always indicated the presence of both phases described in Table IV, but with varying relative intensities of the lines, as well as varying concentrations of unreacted ZnS. More detailed investigations would be required before definite statements as to the nature of the (Zn,Cu,Si)S compounds could be made.

Table V shows the results obtained by firing ZnS + Cu with tetravalent additives other than Si. It can be seen that Ti, Zr, and Th led to increased incorporation of Cu. In the case of Zr and Th, this also resulted in yellow body color and fluorescence. The results with Ti are inconclusive because discoloration of the fired sample with excess Ti suggests that the remainder of this element may well have been present in the trivalent state. Here again, it should be noted that the firing atmosphere employed (N_2) did not allow for the development of "self-coactivated

Table V. Some properties of ZnS fired with 0.1 mole % Cu and 1 mole % tetravalent element at 1100°C in N_2

Additive	Body color: Before NaCN washing	Body color: After NaCN washing	Fluorescence	Mole % Cu found in NaCN-washed phosphors
None	light brown	off-white	blue	0.023
GeS_2	light brown	off-white	weak blue	0.012
Ti + S	dark gray	dark gray*	none	0.077
Zr + S	brown	yellow-white	yellow†	0.0435
$Th(NO_3)_4 \cdot 4H_2O$	light yellow	light yellow	weak orange	0.081

* Contamination by excess Ti.
† Orange phosphorescence and infrared stimulation.

Cu" (orange) fluorescence in the absence of additions other than Cu.

Discussion

The results obtained in this investigation indicate that addition of Si promotes incorporation of Cu in the ZnS lattice, but does not result in orange fluorescence of greater intensity than obtainable with "self-coactivated" ZnS:Cu phosphors. On the other hand, maximum orange fluorescence of ZnS:Cu,Si phosphors occurs with additions of Cu which are of the order of magnitude of the probable concentration of self-coactivated Cu centers in ZnS:Cu phosphors (3). It is therefore suggested that the probable configuration of Cu in the lattice of ZnS:Cu,Si phosphors resembles that of the self-coactivated Cu center. A survey of models proposed for this center has been presented by Aven and Potter (3). All of the models involve two Cu atoms. The authors also specifically propose model V ($Cu_s^- \cdot Cu_s^+$) as derived from model II ($Cu_s^- \cdot V_A^{2+} \cdot Cu_s^-$), due to Kröger (6), by oxidation with elementary sulfur, but admit that the stability of the self-coactivated Cu center to reducing conditions is an argument against such oxidation.

The approximate ratio of 2 Cu/1 Si found analytically on some ZnS:Cu,Si phosphors and on the (Zn,Cu,Si)S compound suggests that, if the orange fluorescence observed here is due to the same type of center as that of self-coactivated ZnS:Cu, one of the models involving the association of two Cu atoms with a divalent vacancy is probably correct. Since it is possible that Si may substitute either for Zn or for S, the results of this investigation cannot be used to distinguish between Kröger's model of $Cu_s^- \cdot V_A^{2+} \cdot Cu_s^-$ and the model of $Cu_{i+} \cdot V_c^{2-} \cdot Cu_{i+}$ as proposed by Bowers and Melamed (7).

From the standpoint of simplicity, it appears most attractive to regard the center $Cu_s^- \cdot Si^{2+} \cdot Cu_s^-$ as emitting, and then to assume that an increase in the number of such centers simply leads to concentration quenching as previously mentioned. Because of the isolation of the hypothetical compound $ZnCu_2SiS_4$, this model also bears a qualitative resemblance to the ZnS:$CuGaS_2$ system described by Apple (8). Unfortunately, the preliminary nature and limited scope of the present investigation allow for no conclusions as to the physical nature of the orange-emitting Cu center, other than what may be inferred from chemical data with respect to its formation in the presence of Si.

The behavior of a number of tetravalent elements other than Si appears to be similar, although no attempts were made to prepare definite compounds of the type $ZnCu_2M^{4+}S_4$. The results with carbon (Fig. 4) are difficult to evaluate. The homogeneity of the phosphors on the one hand, and the low vapor pressure of C on the other, suggests that interaction of carbon with the firing atmosphere may have caused the formation of C-bearing gases such as CS_2, CO, etc. The suggestion that C may be incorporated into the ZnS lattice appears to be far fetched, and it has been noted that the purified graphite tubes used in this study contain about 10-30 ppm. Although this figure is much smaller than the amount of Si intentionally added, it cannot be neglected. Furthermore, the appreciable dissociation of H_2S at elevated temperatures may result in combination of S with C as well as with Si. The excess H_2 thus formed may have a profound influence on the phosphor (4).

The reducing conditions which prevail on firing ZnS with Si or C in H_2S suggest the possibility that these elements may merely act as scavengers for traces of O_2 or halides which may be present in the firing atmosphere and consequently promote the formation of self-coactivated Cu centers. There are, however, some arguments against this:

1. Orange emission could be obtained under firing conditions which normally do not lead to self-coactivated Cu emission. Froelich (2) has shown that the mere absence of O_2 or halides under such conditions is not sufficient to produce the orange emission. A typical case is firing in sealed evacuated tubes under slight S-pressure (Table I). Orange fluorescent ZnS:Cu,Si has also been prepared in S vapor at atmospheric pressure at temperatures as low as 1000°C, although with considerable difficulty.

2. Firing in $N_2 + S$ at atmospheric pressure at 950°C usually resulted in bright blue or green fluorescence. At this temperature, Al in the Si used is not likely to enter the ZnS lattice, unless converted to Al_2S_3 by reaction with SiS_2. On the other hand, evidence of some SiS_2 in such samples indicates that any scavenger action with respect to oxygen or halides should have taken place. The same can be said about samples with less than 0.3 mole % Si in Table I. Generally, the formation of orange fluorescent phosphors required the complete incorporation of all added Cu during the firing process (large Si excess), although in other samples orange fluorescence could usually be observed by simultaneously irradiation with ultraviolet and infrared radiation.

3. The development of orange fluorescence in ZnS:Cu, Th fired in N_2. Thorium was added as the nitrate and therefore was not likely to act as a scavenger under the firing conditions used. Although most of the experiments described in this paper deal with Si, it appears that the greater ease with which additions of Th [as $Th(NO_3)_4$] can be regulated makes further investigation with Th as tetravalent addition particularly attractive.

It should finally be admitted that it may not be justified to assume that the same orange emission in ZnS is merely caused by a pair of associated Cu atoms, although two such models have been listed by Aven and Potter (3). The influence of different coactivators such as Zn_i^{2+}, V_A^{2+} or M_s^{IV2+}, all of which may stabilize a pair of substitutional Cu atoms, may be reflected by differences in the emission spectrum and other physical properties of the phosphor. Further investigations of this type are necessary before definite conclusions can be drawn.

Acknowledgments

The writer wishes to thank Miss I. Walinski for phosphor preparations and measurements, as well as Mr. I. Meister and Dr. C. K. Lui-Wei for emission spectra and x-ray diffraction measurements, respec-

tively. He is also indebted to Professor E. Banks and Dr. H. F. Ivey for reading and suggesting improvements of the original manuscript.

Manuscript received Oct. 17, 1960; revised manuscript received Jan 19, 1960. This paper was prepared for delivery before the Indianapolis Meeting, April 30-May 3, 1961.

Any discussion of this paper will appear in a Discussion Section to be published in the December 1961 JOURNAL.

REFERENCES

1. F. A. Kröger and J. Dikhoff, *Physica*, **16**, 297 (1950).
2. H. C. Froelich, *This Journal*, **100**, 280 (1953).
3. M. H. Aven and R. M. Potter, *ibid.*, **105**, 134 (1958).
4. W. Van Gool and A.P.D.M. Cleiren, *ibid.*, **106**, 672 (1959).
5. W. Lehmann, *ibid.*, **104**, 45 (1957).
6. F. A. Kröger, *Brit. J. Appl. Phys.*, Suppl. #4, S58 (1954).
7. R. Bowers and N. T. Melamed, *Phys. Rev.*, **99**, 1781 (1955).
8. E. F. Apple, *This Journal*, **105**, 251 (1958).

Activation by Anions in the Oxy-Acid Phosphors

Yoshihide Kotera, Michiko Yonemura, and Tadao Sekine

Government Chemical Industrial Research Institute, Tokyo Hatagaya-Honmachi, Shibuya-ku, Tokyo, Japan

ABSTRACT

The luminescence of alkaline earth sulfates and silicates activated by anions, has been observed. The activating anions were WO_4^{2-}, MoO_4^{2-}, $V_2O_7^{4-}$, PO_4^{3-}, AsO_4^{3-}, $Sb_2O_7^{4-}$, GeO_4^{2-}, SiO_4^{2-}, CO_3^{2-}, BO_3^{3-}, AlO_2^{-}, S^{2-}, and SO_3^{2-}. The products showed fluorescent emissions varying in color from blue to red and in visible intensity from very faint to strong. The samples showing the strongest emission are: $CaSO_4(WO_4^{2-})$ and $MgSO_4(WO_4^{2-})$, both emitting in the blue. Evidence is presented to show that these phosphors are truly activated by the $WO_4^{=}$ ion, and not simply dilute samples of the tungstates. It is proposed that activation by anions can be divided into two classes: intraionic, where the emission occurs within the impurity anion; and interionic, where more complex interactions occur. The latter class shows strong shifts in emission color as the host crystal is changed; the intraionic group, including tungstate and vanadate, generally show stronger emission than the others.

In the case of sulfide phosphors, it has been said that an anion, (for example, halogen, oxygen, phosphorus, or arsenic ion) may act as an activator. Kroeger and Hellingman (1, 2) explained for the first time the action of halogen compounds on zinc sulfide, while Kroeger and Dikhoff (3) investigated activation by oxygen ion in zinc sulfide matrix. Several other researchers also studied the action of halogen or oxygen ion in zinc sulfide (4). Subsequently McKeag and Ranby (5) and Prener (6) reported phosphorus- or arsenic-activated zinc sulfide, both of which were proposed for use as a single white screen for television and also to prepare transparent luminescent screens.

It was established by Gobrecht and Hahn (7) that activation by polysulfide ions occurs in alkali and alkaline earth sulfide and sulfate. Meanwhile Thomson (8) assumed that the emission of pure zinc oxide required the presence of sulfide ions, but Kroeger and Dikhoff (3) denied this assumption on the basis of their investigations.

It has not yet been reported that such activation occurs in oxy-acid phosphors. We thought that anions might be able to give localized levels between filled and conduction bands in those matrices and act as activators when they have a smaller electron affinity than that of the oxy-anions which compose the host crystal. We have prepared various oxy-acid phosphors activated by anions and found some remarkable results.

Experimental Results

Preliminary experiments.—First, it is necessary to determine what kind of matrices and activators should be selected. Two types of matrices were used, the sulfates of alkali earth metals and magnesium, and the silicates of alkali earth metals, magnesium and zinc. It was thought that these anions might have greater electron affinity, and they were not expected to decompose during firing at relatively high temperature. For the electron affinity of oxy-anions there are few data, but we presume that, if two salts were prepared from two anions with a common metal ion and the fundamental absorption of one salt has an edge at shorter wavelength than a second, then the former would have a greater electron affinity than the latter. As to decomposition, the fact that some sulfate compounds decompose partially above 1000°C would be overcome by lowering their firing temperatures. The activators, silicate, phosphate, borate, carbonate, or sulfide were used, because they surely exist in the matrix as anions. Also tungstate, molybdate, vanadate, or germanate ion were tried, since they would probably exist in the matrix as the anions, and further arsenate, antimonate (9), or aluminate ion (9), because they are anionic components of phosphor matrix.

Sulfates of alkali earth metals were precipitated by mixing of purified ammonium sulfate with the purified metal solution. In the purification the precaution was taken that the residue of sulfide used for

Table I. Emissions of sulfates activated by anions

Matrix \ Activator	WO_4^{2-}		MoO_4^{2-}		$V_2O_7^{4-}$		PO_4^{3-}		AsO_4^{3-}		$Sb_2O_7^{4-}$	
$CaSO_4$	blue	s	yellowish green	m	none		white	f	yellow	f	red	m
$SrSO_4$	bluish white	m	yellow	m	none		white	ff	white	ff	pink	ff
$BaSO_4$	none		none		none		yellow	f	blue	ff	blue	ff
$MgSO_4$	bluish white	s			yellow	m	red	f	red	f		

Matrix \ Activator	GeO_4^{2-}		SiO_4^{2-}		CO_3^{2-}		BO_3^{3-}		AlO_2^{-}	
$CaSO_4$	greenish white	f	greenish white	f	blue	ff	white	ff	blue	ff
$SrSO_4$	white	ff	white	ff	yellow	ff	white	ff	white	ff
$BaSO_4$	red	m	blue	f	none		white	f	white	f
$MgSO_4$	red	f	yellow	f			none		blue	f

Matrix \ Activator	S^{2-}		SO_3^{2-}	
$CaSO_4$	blue	m	bluish white	f
$SrSO_4$	bluish white	f	yellow	f
$BaSO_4$	orange	m	orange	f
$MgSO_4$				

s, strong; m, medium; f, faint; ff, very faint.

Table II. Emissions of silicates activated by anions

Matrix \ Activator	$V_2O_7^{4-}$		PO_4^{3-}		AsO_4^{3-}		$Sb_2O_7^{4-}$		GeO_4^{4-}		BO_3^{3-}	
$CaSiO_3$	yellow	ff	none		none		none		none		yellow	ff
Ca_2SiO_4	none		red	m	red	m	red	ff	red	m	red	m
$BaSi_2O_5$	yellow	f	yellow	f	yellow	f	bluish white	f	yellow	f	bluish white	f
$Ba_2Si_3O_8$	yellow	m	yellow	f	yellow	f	yellow	f	yellow	f	yellow	f
$MgSiO_3$	yellow	m	yellow	ff	red	f	yellow	ff	yellow	ff	none	
Zn_2SiO_4	yellow	f	yellow	f	yellow	f	yellow	f	yellowish white	ff	yellow	f

ff, very faint; f, faint; m, medium.

the purification was thoroughly decomposed by the addition of distilled hydrogen chloride. Magnesium sulfate was prepared by the solid-state reaction between purified magnesium oxide and ammonium sulfate crystals. The silicate matrices were prepared by well-known processes.

The following salts were used as the activators: $SiO_2 \cdot nH_2O$, $(NH_4)_2HPO_4H_3BO_3$, metallic carbonate, metallic sulfide, $WO_3 \cdot nH_2O$ or metallic tungstate, MoO_3, NH_4VO_3, GeO_2, As_2O_3, Sb_2O_3, and $Al(OH)_3$. They were purified by the process previously described (9), and metallic sulfides were prepared by the reaction between the metallic sulfate and a reducing agent, for example, cane sugar.

In general the amount of activators was optimum at 0.01-0.1 mole per 1 mole of sulfate and 0.001-0.05 mole for silicate. Flux was seldom used, and it was found that flux has little effect. Firing was done in air, except for a special case, for 2 to 4 hr at 1100°C. For the activation of calcium sulfate by vanadate or carbonate ion firing was done at 500°C and for barium sulfate activated by carbonate at 900°C, while the firing for preparation of magnesium sulfate phosphors was carried out at 1000°C.

The results are shown in Tables I and II for two kinds of matrices. These emissions are excited both by 2537Å and 3650Å in most cases, whereas magnesium silicate activated by antimonate ion has emission only for the excitation by 3650Å.

Activation by tungstate ion.—It was seen from Table I that calcium or magnesium sulfate, activated by tungstate ion, has rather strong luminescence. Because of the similarity between calcium or magnesium sulfate and tungstate, it might be presumed that sulfate salt would be activated effectively by tungstate ion. The relation between the brightness of calcium sulfate activated by tungstate ion and the mixing ratio of batch components ($CaSO_4$, $CaCO_3$, $WO_3 \cdot nH_2O$, and $CaWO_4$) was studied. This relation is shown in Fig. 1, the excitation being done by 2537Å, and the brightness being determined by means of a photocell. In Fig. 2 and 3 the brightness and the decay characteristic under x-ray excitation are plotted as functions of the mixing ratio of the components.

In Fig. 1 the value of 100 corresponds to the brightness of a commercial calcium tungstate phosphor, while the brightness and decay characteristics under x-ray excitation (Fig. 2 and 3) were determined by the blackening of a photographic plate. The commercial product shows a brightness value of 1.40 for those prepared by the precipitation and firing of

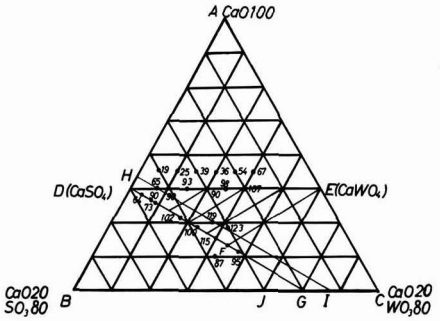

Fig. 1. Relation between the brightness of calcium sulfate activated by tungstate ion and the mixing ratio of batch components: A, CaO; B, CaO 20, SO_3 80; C, CaO 20, WO_3 80; D, $CaSO_4$; E, $CaWO_4$.

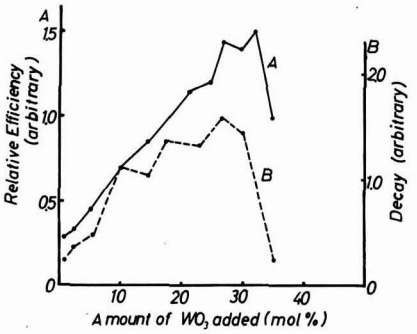

Fig. 2. Brightness and decay characteristics as the function of amount of WO_3 added to calcium sulfate (x-ray excitation): A, brightness; B, decay.

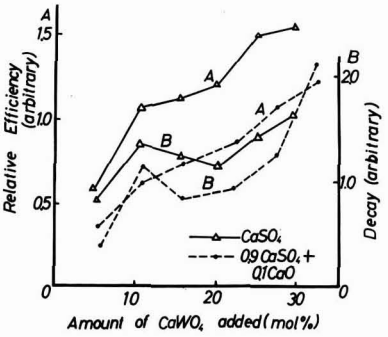

Fig. 3. Brightness and decay characteristics as the function of amount of $CaWO_4$ added to calcium sulfate and (0.9 $CaSO_4$ + 0.1 CaO) (x-ray excitation): A, brightness; B, decay.

calcium tungstate or 1.80 for those prepared by the solid-state reaction between calcium compound and tungsten trioxide, and 1.20 for decay.

In these preparations it is probable that the reaction

$$CaSO_4 + H_2WO_4 \rightarrow CaWO_4 + H_2SO_4$$

proceeds. Accordingly, it has to be assumed that, for mixtures of compositions below the line DE (Fig. 1), the composition changes during firing, along lines parallel to line EF, the reaction ending when the

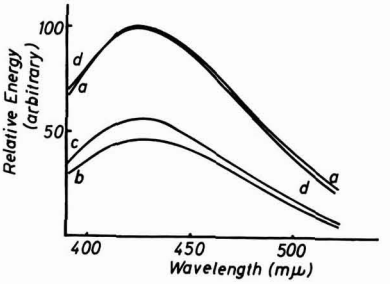

Fig. 4. Spectral distributions of calcium tungstate and calcium sulfate activated by tungstate ion: a, $CaWO_4$; b, c, d, $CaSO_4$ activated by tungstate ion. [$CaSO_4$:H_2WO_4 (mole ratio) = 99:1(b), 9:1(c), 7:3(d)].

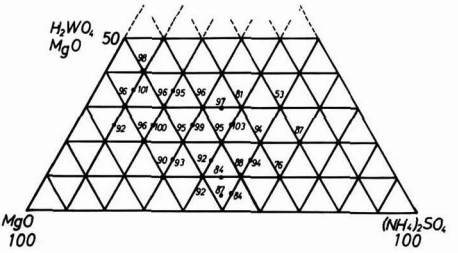

Fig. 5 Relation between the brightness of magnesium sulfate activated by tungstate ion and the mixing ratio of batch components.

composition reaches line DE. Spectral distributions are shown in Fig. 4.

Similar experiments were carried out for magnesium sulfate activated by tungstate ions. Figure 5 shows the relation between the brightness of phosphors and the mixing ratio of magnesium oxide, ammonium sulfate, and tungsten trioxide.

Activation by vanadate ion.—It is shown in Table I that tungstate, molybdate, or vanadate ion is able to activate the oxy-acid phosphors to cause relatively strong luminescence, and we hoped to learn how vanadate ions activate the oxy-acid phosphors. Magnesium sulfate, silicate, or pyrophosphate were prepared by the reaction between magnesium oxide and oxy-acidic compound. Other phosphates proved to be worse than pyrophosphate. Their spectral distributions are almost the same as that of magnesium vanadate and their brightnesses are shown in Table III.

The system $MgWO_4$-$Mg_2V_2O_7$ was examined by firing mixtures of magnesium oxide, tungstic acid, and ammonium vanadate at 1050°C for 2 hr. The spectral distributions of these phosphors are shown in Fig. 6, in which the numbers attached to the curves represent the relative height at their peaks.

Activation by sulfide and sulfite ion.—Alkaline earth sulfides were prepared by the reaction between purified alkaline earth sulfate and reducing agent, for example, cane sugar, while alkaline earth sulfites were precipitated by the addition of purified sulfite solution to purified alkaline earth salt solution. Optimum conditions for preparing the phosphors are shown in Table IV; it was necessary to maintain the

Table III. Optimum conditions for preparation of magnesium compounds activated by vanadate ion and their brightness

Matrix	Optimum mixing ratio, mole		Firing temp, °C	Relative brightness
Mg silicate	MgO 1.5 SiO_2 0,7	NH_4VO_3 0.3	1050	70
Mg phosphate	MgO 2.0 $(NH_4)_2HPO_4$	0.5NH_4VO_3 0.2	1050	85
Mg sulfate	MgO 1.0 $(NH_4)_2SO_4$	0.8NH_4VO_3 0.2	1000	160

Table IV. Optimum conditions for preparation of sulfate compounds activated by sulfide and sulfite ion

	Mixing ratio, mole	Flux	Firing conditions
$CaSO_4$: S	$CaSO_4$ 1 CaS 0.01	Na salt	
$SrSO_4$: S	$SrSO_4$ 1 SrS 0.01	—	
$BaSO_4$: S	$BaSO_4$ 1 BaS 0.035	NaCl 10 mole %	1100°C, 4 hr in N_2
$CaSO_4$: SO_3	$CaSO_4$ 1 $CaSO_3$ 0.01	—	
$SrSO_4$: SO_3	$SrSO_4$ 1 $SrSO_3$ 0.01	—	
$BaSO_4$: SO_3	$BaSO_4$ 1 $BaSO_3$ 0.1	NaF 10 mole %	

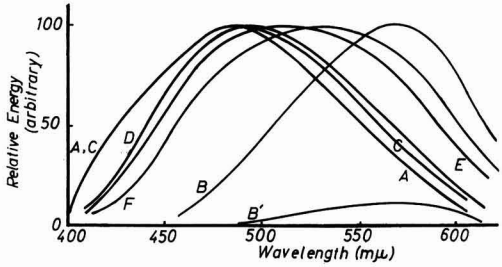

Fig. 6. Spectral distributions of the system of $MgWO_4$ — $Mg_2V_2O_7$: A, $MgWO_4$; B, $Mg_2V_2O_7$; C, calculated from A and B for the mixture of A and B with equivalent molar ratio; D, $MgWO_4$ 0.95 + $Mg_2V_2O_7$ 0.05 (mole); E, $MgWO_4$ 0.7 + $Mg_2V_2O_7$ 0.3 (mole); F, $MgWO_4$ 0.5 + $Mg_2V_2O_7$ 0.5 (mole); B': relative value of B to A.

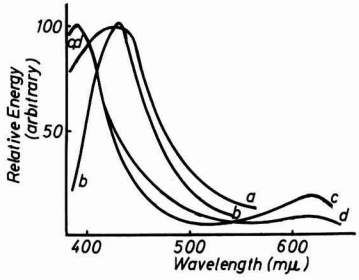

Fig. 7. Spectral distributions of alkali earth sulfate activated by sulfide.
a,b: calcium sulfate activated by sulfide
a: 0.01 g $CaS/CaSO_4$ 1 g
b: 0.1 g $CaS/CaSO_4$ 1 g
c,d: barium sulfate activated by sulfide
c: 0.035 g $BaS/BaSO_4$ 1 gr
d: c + NaCl flux

firing atmosphere in a neutral condition because oxidizing or reducing atmospheres cause a variation of the characteristics of the products. Spectral distributions are shown in Fig. 7, and in those cases it was difficult to obtain accurate ones of calcium and barium sulfate activated by sulfite ion because of their weak emission.

Discussion

It was confirmed that in oxy-acid phosphors anionic centers are present, although their luminescence is weak in most cases. From the results obtained we suggest that anionic activators are divided into two groups, as follows:

1. The first group might be called "intraionic activators." They have emissions almost the same as those found in the matrices whose anion is identical with the activating one. In this group, the luminescence originates from electronic transitions in the anions. Activations by tungstate and molybdate ions are typical examples of this group and that by vanadate might belong to it too.

2. The other group might be described as "interionic activators." Their emissions have various colors, depending on the matrices even for the same activator. This activation occurs when the electronic affinity of activating anions is smaller than that of the host crystal anions. Some ions of this group show a tendency for the emission color to shift to longer wavelength in the order of calcium, strontium, and barium. Phosphate, germanate, aluminate, sulfide, and sulfite ions show this tendency.

Phosphors with intraionic activation have rather strong emission, and it might be found that such activation occurs in phosphors which were studied by other researchers, who assumed them to be activated by other sources (10).

There is disagreement in the literature (10, 11) as to the nature of the activator center in phosphors with low tungsten concentration. Roberts (12) found that the brightness of calcium tungstate increases when sulfuric acid, in amounts corresponding to the excess calcium oxide in the tungstate, is added on firing. This addition of sulfuric acid might cause the formation of calcium sulfate, reducing the amount of calcium oxide, which seems to poison the luminescence of calcium tungstate.

It is found that calcium sulfate is activated by tungstate ion and the brightness of this phosphor under 2537Å excitation is high. The spectral distribution of this emission is almost the same as calcium tungstate, although a small shift was found in

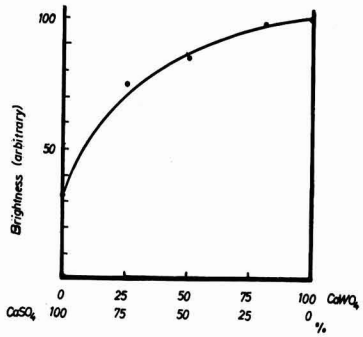

Fig. 8. Relation between the brightness under 2537Å excitation and the mixing ratio of mechanical mixture of calcium sulfate and calcium tungstate.

some cases. But, as already stated, the reaction between calcium sulfate and tungstic acid might occur during the firing, and also we found (13) that the addition of ammonium persulfate to calcium tungstate causes its brightness to increase. It is proposed that, at low contents to tungstic acid, calcium sulfate is being activated by tungstate ion because the brightness is much higher than that obtained from a mixture of calcium sulfate and calcium tungstate, whose brightness is increased by the addition of sulfate. However, when the content of tungstic acid is high, the reaction with calcium sulfate occurs to produce calcium tungstate, while the activation by tungstate occurs simultaneously to increase the brightness of the product. In Fig. 8 the brightness of mechanical mixtures of calcium sulfate and calcium tungstate under 2537Å excitation is shown, which clarifies the activation by tungstate ion compared with Fig. 1.

Some qualitative results which might clarify this assumption were obtained from crystallographic analysis by means of a recording x-ray diffractometer. In the phosphor, which was prepared by the firing of mixture of 1 mole calcium sulfate and 0.2 mole tungstic acid, patterns of both calcium sulfate and tungstate were found, while the pattern of the phosphor from the mixture of 1 mole calcium sulfate and 0.05 mole tungstate was almost the same as that of calcium sulfate. Because of the crystallographic similarity it is quite difficult to determine the content of the constituent. On the other hand, absorption measurements were carried out to compare the spectra of pure calcium sulfate and one activated by tungstate ion, but the special peak was not found till 2800Å, and the measurements at shorter wavelengths were disturbed by the emission, which is excited by the light in this region. The final decision as to the occurrence of tungstate activation in the case of calcium sulfate phosphors could be based on measurements of excitation spectra.

Magnesium sulfate, when activated by tungstate, shows the same characteristics as in the case of calcium sulfate. In this case it is necessary to lower the firing temperature because of the relatively lower decomposition temperature of magnesium sulfate (14). It was possible to obtain a phosphor which has higher brightness than that prepared by the ordinary process.

It was found that some magnesium compounds could have higher brightness than that of pure magnesium metavanadate (9) when a large amount of vanadate compound was added to them. It might be concluded from the consideration in the case of calcium sulfate, to which a large amount of tungstic acid was added, that a part of the product is activated by vanadate ion. The formation of magnesium metavanadate could be proved crystallographically, in contrast to the system of calcium sulfate-calcium tungstate, whose components are much alike in the structure.

The system of $MgWO_4$-$Mg_2V_2O_7$ shows almost the same characteristics as the results obtained in the case in which zinc or cadmium oxide is added to calcium sulfate activated by tungstate ion (15). Those results might be explained by the formation of solid solutions.

The spectral distribution of emission of calcium, strontium, or barium sulfate activated by sulfide ion may differ from that of polysulfide, which was reported by Gobrecht, *et al.* (7), but it is impossible to compare our results with theirs, because they concluded that the preparation by the reduction of sulfate salts is unsuitable for the preparation of their phosphors. Barium sulfate activated by sulfide ion has an emission like that of barium polysulfide, and it is possible that the activation by sulfur ion might be the intermediate case between intraionic and interionic activation. The emission of sulfate salts activated by sulfite ion is weak, but it was recognized that the emission differs from that of sulfate activated by sulfide ion. Such comparisons are made difficult by the fact that the control of atmosphere is important during the firing of phosphors.

Acknowledgment

The authors wish to express their thanks to Professor S. Makishima for general discussions on the subject and some of their experimental work.

Manuscript received Sept. 9, 1960.

Any discussion of this paper will appear in a Discussion Section to be published in the December 1961 JOURNAL.

REFERENCES

1. F. A. Kroeger and J. E. Hellingman, *J. (and Trans.) Electrochem. Soc.*, **93**, 156 (1948).
2. F. A. Kroeger and J. E. Hellingman, *ibid.*, **95**, 68 (1949).
3. F. A. Kroeger and J. A. M. Dikhoff, *This Journal*, **99**, 144 (1952).
4. F. A. Kroeger, *Physica*, **16**, 297 (1950); H. A. Klasens, *This Journal*, **100**, 72 (1953); N. Riehl and H. Ortman, *J. phys. Radium*, **17**, 620 (1956); N. T. Melamed, *J. Phys. Chem. Solids*, **7**, 146 (1958).
5. A. H. McKeag and P. W. Ranby, *J. (and Trans.) Electrochem. Soc.*, **96**, 85 (1949).
6. J. S. Prener, *This Journal*, **98**, 406 (1951).
7. H. Gobrecht and D. Hahn, *Z. Physik*, **132**, 111 (1952); **135**, 523 (1953).
8. S. M. Thomson, *J. Chem. Phys.*, **18**, 770 (1950).
9. Y. Kotera, *et al.*, *Bull. Chem. Soc. Japan*, **27**, 13 (1954); **28**, 129 (1955); **29**, 742 (1956).

10. Y. Uehara, *et al.*, *Shomei Gakukaishi*, **43**, 13 (1959); Japan Pat. 215362 (1955); N. Otani and T. Toriu, XIth Annual Meeting Chem. Soc. Japan, April 1956.
11. F. A. Kroeger, "Some Aspects of the Luminescence of Solids," p. 107, Elsevier Publishing Co., Inc., New York (1948).
12. W. A. Roberts, U. S. Pat. 2312267 (1943).
13. Y. Kotera and T. Sekine, *J. Chem. Soc. Japan* (*Ind. Sect.*), **54**, 625 (1951).
14. H. J. Knopf and H. Staude, *Z. physik. Chem.*, **A204**, 265 (1955).
15. Y. Kotera, *et al.*, *Bull Chem. Soc. Japan* (in press).

A Comparative Study of Infrared Luminescence and Some Other Optical and Electrical Properties of ZnS:Cu Single Crystals

I. Broser and H.-J. Schulz

Institut für Elektronenmikroskopie am Fritz-Haber-Institut der Max-Planck-Gesellschaft, Berlin-Dahlem

ABSTRACT

An attempt has been made to fix the position of the optical transitions leading to infrared luminescence of ZnS:Cu within the general picture of electronic states of crystal phosphors. For this purpose, many optical and electrical properties, such as emission spectra of the infrared and visible luminescence, excitation and quenching spectra of luminescence and photoconductivity as well as optical absorption spectra, have been investigated on the same single crystal within a temperature range between 4° and 300°K. Most of the experimental results could be explained in terms of a relatively simple energy band scheme, which differs in some respects from those published during the last years.

It has been shown by several authors (1-5) that the simple one-level activator model for the interpretation of luminescence processes in ZnS-type phosphors is not sufficient to explain the infrared effects such as quenching and stimulation of photoconductivity and of visible luminescence and the occurrence of infrared luminescence. The luminescent center created by the incorporation of copper into the crystal has to be represented by at least two energy levels within the forbidden zone of the energy band scheme. These levels can be occupied by two electrons, or by one electron in two different positions; or they can be vacant. Considering the Franck-Condon principle this leads to a two-level activator model as shown in Fig. 1. As pointed out below, a study of infrared effects and some other optical and electrical properties of ZnS-Cu single crystals shows that the discussion of all possible transitions within the model leads to a satisfactory understanding of the absorption and emission mechanisms in this sort of photoconducting phosphor.

Emission Spectra

It is well known that four emission bands can be obtained by activating ZnS with copper (6). The crystal investigated[1] shows all these bands situated in the blue, green, red, and infrared region, the latter one being split into three sub-bands (3) (Fig. 2). If luminescent transitions into the valence band are excluded, our model has four possibilities to include the four emission bands as indicated by the arrows E_1 to E_6.

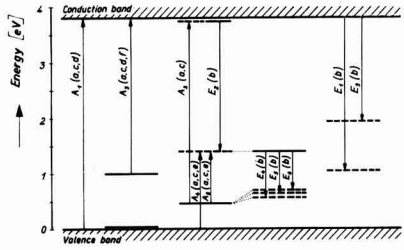

Fig. 1. Two-level-activator energy model (dashed lines represent unoccupied levels). (a) Absorption; (b) emission; (c) excitation of luminescence; (d) excitation of photoconductivity; (e) quenching; (f) sensibilization.

Table of Transitions

Transition	(a) Absorption	(b) Emission	(c) Excitation of Luminescence	(d) Excitation of Photoconductivity	(e) Quenching	(f) Sensibilization	Energy difference ev
A_1	335	—	328	326	—	—	3.80
A_2	365	—	375	—	—	—	3.35
A_3	430	—	435	440	—	452	2.82
A_4	850	—	865	—	900*	—	1.43
A_5	1280	—	1350	—	1330*	—	0.94
E_1	—	451	—	—	—	—	2.75
E_2	—	528	—	—	—	—	2.35
E_3	—	670**	—	—	—	—	1.85
E_4	—	1490	—	—	—	—	0.83
E_5	—	1650	—	—	—	—	0.75
E_6	—	1800	—	—	—	—	0.69

In columns a-f the wavelengths corresponding to the essential points in the respective plots are given in nm (= 10^{-9} m), whereas the last column gives the mean energy differences. The numbers are valid for 80°K, unless denoted otherwise.
* T = 295°K.
** See Ref. (7).

[1]All figures in this paper show measurements taken with the same crystal. It was grown within 3-4 hr from the vapor phase, from white, luminescent grade ZnS powder evaporated at 1450°C. The crystal has a size of 21 × 3 × 2 mm³ and exhibits a green color in daylight. It was not doped intentionally, but a qualitative spectral analysis has demonstrated that copper is the only activating impurity which is present in the crystal in larger quantities. Other elements, found by this method, are Cd, Ga, and in smaller amounts Mg, Al, and Si.

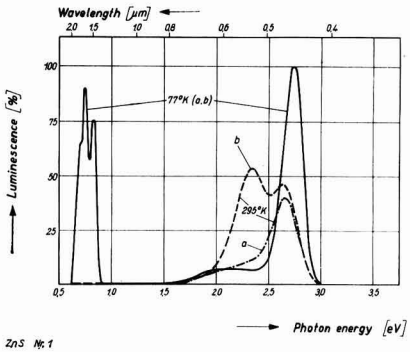

Fig. 2. Emission spectrum under irradiation with uv-radiation ($\lambda = 0.365$ μm). Chopping of (a) exciting, (b) emitted light.

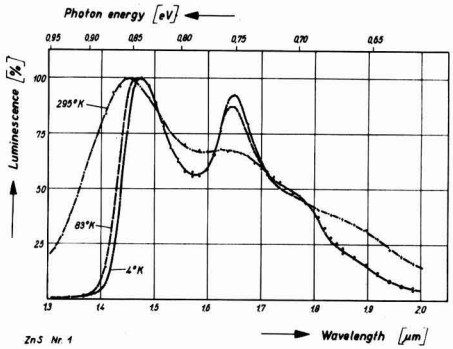

Fig. 3. IR emission at three different temperatures (excitation: 0.33 μm . . . . . 0.85 μm).

The emission emitted by a given phosphor specimen is determined mainly by the distribution of electrons over the different luminescence centers. The distribution is determined by the position of the Fermi level, which depends on the donor impurities (*e.g.*, coactivators) as well as on the activator concentrations and, of course, on the crystal temperature. In the case considered here, the ratio of the blue and green emission intensities is given by the ratio of the numbers of singly and doubly occupied centers in the nonirradiated crystal. At low temperatures a considerable part of the excited electrons will be captured at deep traps. Thus, the number of singly occupied centers is enlarged, and so, consequently, is the intensity of the blue emission (E_1). A second cause of this enhancement is the prevention of electron transitions from the valence band to the lower level of an entirely emptied center in the cooled phosphor. At higher temperatures, however, a singly occupied center may also exhibit a green luminescence (E_2) after excitation of its electron, since the above mentioned process becomes more probable. For the green band we assume that the recombination process begins from a localized state near the conduction band, but not from a state within it, since no temperature shift of the the emission peak is observed (2).

The red emission might be included tentatively in this picture (E_3). Several observations support this possibility, for example the simultaneous appearance with blue luminescence in many crystals (7), and the similar structure of excitation spectra of red and blue emission bands as indicated by some of our unpublished measurements. However, a more detailed investigation should be carried out.

We cannot offer here a satisfactory explanation of the splitting of the infrared emission (E_4-E_6) into sub-bands, but it is obvious from the measurements (Fig. 3) that the three sub-levels lie very close together, for the bands do not change their intensity ratio significantly when the temperature is varied between 4° and 295°K.

By chopping the emitted radiation one obtains the "real" emission spectra (curves b, Fig. 2) by means of a selective amplification method, while the chopping of exciting light (130 cps) implies that the green band apparently diminishes (curves a, Fig. 2) because of its longer rise and decay times, causing a weaker modulation of this emission band. The very fast response of infrared luminescence enabled us to use the chopping of excitation to distinguish the effects caused by this beam from those caused by the absorption of a second one which was not modulated.

Absorption Spectra

For the investigation of the absorption spectrum of the ZnS-Cu crystals, measurements have been made in the region of wavelengths from 0.3 to 2.5 μm[2] (Fig. 4A, 4B). The curves have exactly the shape

[2] Following standard German practice, the unit of length used in this paper and in the figures is 1μm = 10^{-6}m (= 1μ).

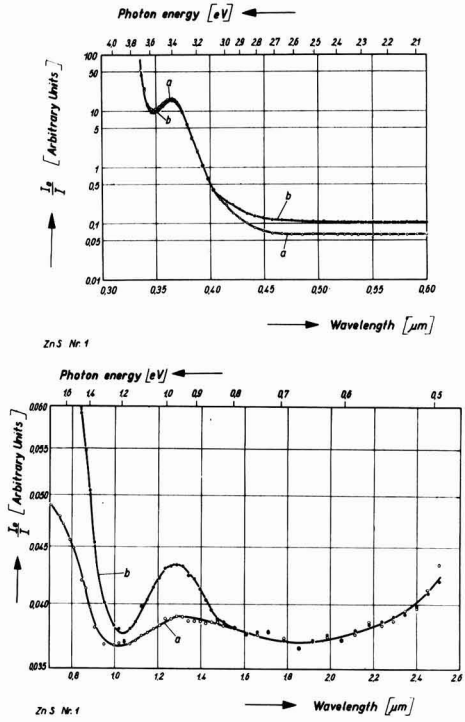

Fig. 4A and Fig. 4B. Absorption spectrum at 78°K, (a) without and (b) with additional blue exciting radiation (0.33 μm ≤ λ ≤ 0.49 μm).

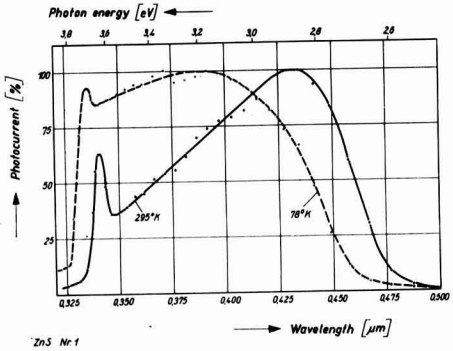

Fig. 5. Excitation spectrum of the photoconductivity

which one expects from consideration of the possible absorption processes in the model of Fig. 1. The absorption edge (A_1) at about 0.33 μm and the absorption caused by a transition from the lower term of the doubly occupied center apparently coincide. Consequently, this level cannot be detected by absorption measurements. At 0.365 μm the well-known absorption peak (8) of copper-activated ZnS appears. This peak is not shifted by temperature and is obviously caused by a transition within a localized center instead of a transition into a state of a band. The most probable process (A_2) is the absorption within the singly occupied center (2). In the region between 0.4 and 0.45 μm photoconductivity (and also green luminescence) can still be excited (Fig. 5). Here, an important part of the absorption is due to transitions from the upper term of the doubly occupied center to states in the conduction band (A_3). A relatively sharp absorption edge appears at about 0.9 μm; it is due to transitions of electrons from the valence band to the upper level of the singly occupied center (A_4), requiring a minimum energy of about 1.4 ev. Simultaneously free holes should be created in the valence band. However, we could not establish the expected appearance of the recently reported (9, 10) p-type photoconductivity with our crystals. The absorption peak at about 1.3 μm is caused by transitions between the two levels of the singly occupied center (A_5). In agreement with our model we obtain very exactly $A_5 = A_2 - E_2$. In connection with the vacant center no absorption effects are observed, probably because the number of these unoccupied centers is small compared with the number of occupied ones.

If one excites the crystal with blue or ultraviolet light during the absorption measurement, an increase of the absorption coefficient in the region between 0.4 and 1.5 μm occurs. This can be explained by the assumption that light of a short wavelength raises electrons from the doubly occupied centers over the conductivity band to traps, thus changing a considerable part of the centers into singly occupied ones which are responsible for the additional absorption in this part of the spectrum.

Excitation of Infrared Luminescence

In good agreement with the absorption spectra is the behavior of the infrared luminescence of the

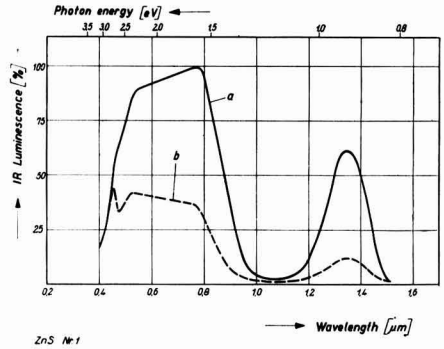

Fig. 6. Excitation spectrum of infrared luminescence at 77°K (a) with and (b) without simultaneous blue irradiation (0.436 μm).

crystal under irradiation with different wavelengths. Figure 6 shows a typical excitation spectrum in the region of 0.4-1.5 μm. The maximum in the long wavelength region is distinctly connected with the absorption peak of Fig. 4B and corresponds therefore with transition A_5 in Fig. 1. At about 0.9 μm where the energy of the exciting radiation becomes high enough to raise electrons from the valence band to the upper level of the singly occupied center, a sharp increase of the light yield appears. The curve remains nearly constant in the wavelength range from 0.8 to 0.5 μm. Without additional blue irradiation it goes through a small maximum at the point where excitation of electrons into the conductivity band starts (0.45 μm). This maximum is built up slowly since the weak measuring beam needs a time of some minutes to change a considerable number of doubly occupied centers into singly occupied ones. Beyond this peak the luminescence decreases very rapidly with wavelength. This latter effect is not explained by the absorption spectrum and is still open for discussion. As can be seen from Fig. 7, no marked change of the emission spectrum occurs under different wavelengths of irradiation. This is especially important for the case of excitation in the 1.3 μm absorption band. All other models for the *IR* luminescence except that of Fig. 1 are thus contradicted.

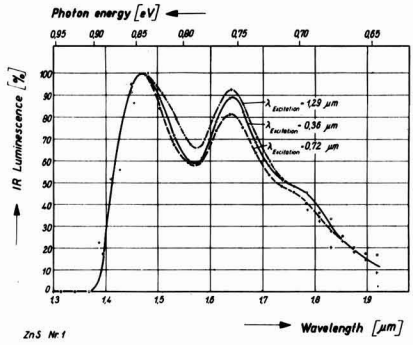

Fig. 7. IR emission spectrum at 77°K under different excitations with additional blue irradiation (0.34 μm ≦ λ ≦ 0.48 μm).

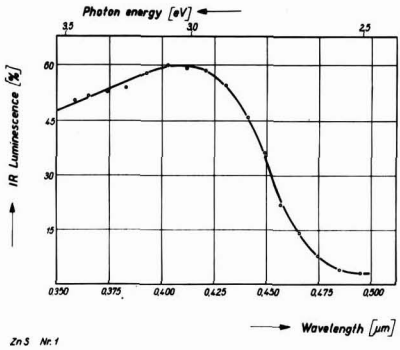

Fig. 8. Efficiency of different wavelengths for the increase of infrared luminescence at 80°K (primary excitation: 0.56 $\mu m \leq \lambda \leq 0.95$ μm).

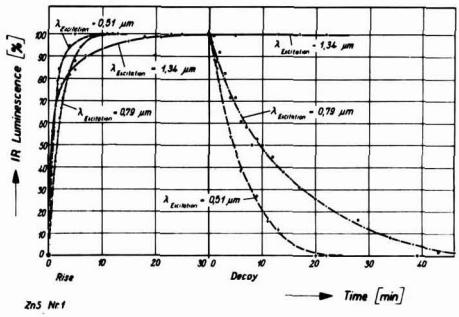

Fig. 9. Time dependence of the additional infrared luminescence caused by additional blue irradiation (λ = 0.436 μm) at 77°K for three different primary excitation wavelengths.

The increase of the light yield of the infrared luminescence by short wavelength irradiation has also been investigated. Figure 8 shows the efficiency of different wavelengths of the additional radiation for the increase of infrared luminescence after an illumination period of 3 min. This curve is very similar to the photoconductivity response of Fig. 5, demonstrating that transition A_3 (Fig. 1) causes the change of doubly occupied into singly occupied centers.

Another interesting effect is the time dependence of the change of the infrared light yield by the action of additional blue radiation and of the primary green, red, and infrared excitation (Fig. 9). The most important result of these measurements is the fact that light, which creates free holes in the valence band by transition A_4, "bleaches" the absorption centers by reducing the number of trapped electrons (quenching), whereas light in the 1.3 μm band (transition A_5) gives no decrease.

It may be pointed out that several further experimental results, such as quenching spectra of photoconductivity and of visible luminescence (2), temperature dependences of all luminescence bands, and excitation spectra of the visible luminescence, have been obtained with the same crystals, giving no difficulties of interpretation. The only problem which is not yet solved is the interpretation of the well-known 1.2 μm peak of the stimulation spectra in our model. We believe that the stimulation is also connected with the double-level activator model and that further experiments will lead to a still better understanding of the excitation and emission mechanism of ZnS-type-phosphors.

Manuscript received Sept. 1, 1960; revised manuscript received March 7, 1961. This paper was prepared for delivery before the Chicago Meeting, May 1-5, 1960.

Any discussion of this paper will appear in a Discussion Section to be published in the December 1961 JOURNAL.

REFERENCES

1. R. Bube, *Proc. IRE*, **43**, 1836 (1955).
2. I. Broser and R. Broser-Warminsky, *J. Phys. Radium*, **17**, 791 (1956).
3. P. F. Browne, *J. Electronics*, **2**, 1 (1956).
4. G. Meijer, *J. Phys. Chem. Solids*, **7**, 153 (1958).
5. E. F. Apple and J. S. Prener, *ibid.*, **13**, 81 (1960).
6. G. F. J. Garlick, Hdb.d.Physik, edited by S. Flügge, Springer-Verlag Berlin (1958).
7. R. Bowers and N. T. Melamed, *Phys. Rev.*, **99**, 1781 (1955).
8. J. H. Gisolf, W. De Groot, and F. A. Kröger, *Physica*, **8**, 805 (1941).
9. F. G. Ullman and J. J. Dropkin, *This Journal*, **105**, 46C (1958); *ibid.*, **108**, 154 (1961).
10. R. M. Potter and M. H. Aven, *Bull. Am. Phys. Soc. II*, **4**, 227 (1959).

Vapor Phase Preparation of Gallium Phosphide Crystals

M. Gershenzon and R. M. Mikulyak

Bell Telephone Laboratories, Incorporated, Murray Hill, New Jersey

ABSTRACT

A method is described for the preparation of single crystals of GaP by the vapor phase reaction of gallium suboxide with phosphorus. Several crystal habits are distinguished including that of a filamentary form which appears to be a precursor of the other types. The crystals are strong and relatively free of strains. Electrical measurements indicate carrier densities and total donor and acceptor concentrations that are significantly less than those corresponding to crystals prepared by other methods. Low resistivity crystals of either n- or p-type may be prepared by doping during growth.

Gallium phosphide is difficult to grow from a stoichiometric melt because of its high melting point, ~1500°, and the large decomposition pressure at this temperature, somewhat greater than 20 atm (1). Moreover, the containment of such a melt presents two additional serious problems. First, impurities introduced into the melt by the container are readily incorporated in the growing crystals (2). Second, the

grown crystals generally exhibit considerable strain because the density of solid gallium phosphide is less than that of the melt from which it is produced (3). Both the impurity concentrations and the degree of strain are somewhat reduced if the crystals are grown from gallium-rich solutions at lower temperatures and pressures (4). However, both the growth rate and the total yield are reduced considerably in this method. Furthermore, it is apparently possible to incorporate defects when the growing crystals are not in equilibrium with a stoichiometric melt (5). These deviations may exist in the form of concentration gradients if the crystals are grown from solutions whose compositions are not held stationary in time.

The preparation of gallium phosphide from the vapor phase may be accomplished at relatively low temperatures and pressures. At the same time the introduction of both impurities and strain is alleviated because the container has been eliminated. Deviations from stoichiometry, however, may still occur. The preparation of a number of Group III-V zinc-blende structure compounds including gallium phosphide by the vapor phase reaction of the Group III halide with the Group V element has been reported recently (6).

An apparent sublimation of gallium phosphide between 800° and 1100° giving rise to small whisker-like crystals was concluded to be due to vapor phase transport induced by the presence of small amounts of oxygen in the system (3). Conclusive evidence for the existence of the vapor species gallium suboxide (Ga_2O) has since appeared (7) and is here identified as the active species in the vapor phase transport of gallium in the temperature range investigated. Accordingly, this report describes the preparation of gallium phosphide from gallium suboxide and phosphorus vapors, the resulting crystal habits, the growth process, and some of the properties of the crystals.

Experimental

Gallium suboxide may be prepared by the partial oxidation of gallium, the partial reduction of gallium oxide, or the direct reaction of gallium with gallium oxide. Because the first two methods require the control of an additional gaseous constituent which may react simultaneously with the phosphorus, the latter technique was adopted. The equilibrium vapor pressure of gallium suboxide over a 4-1M mixture of gallium to gallium oxide has been determined by Frosch and Thurmond in a limited temperature range (7). From 0.2 mm Hg at 800° it rises smoothly to 10 mm at 1000°.

The whiskers were prepared by raising the phosphorus pressure in a chamber in which a steady-state flow of gallium suboxide vapor had been established. The reaction vessel shown in Fig. 1 was a sealed, evacuated, fused silica tube containing the 4 to 1 gallium to gallium oxide mixture well macerated in a quartz cup at one end and a red phosphorus reservoir at the other end. The gallium was Alcoa 99.999%. The gallium oxide was either McKay C. P. or was prepared from Alcoa 99.999% gallium by dissolving in hydrochloric acid, precipitating with

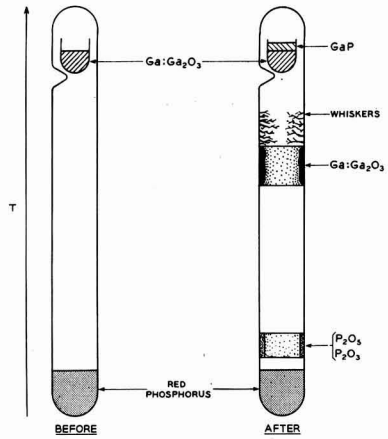

Fig. 1. Reaction vessel

sodium hydroxide, washing, and igniting. The red phosphorus was Fisher micrograde, washed and dried, used directly or sublimed as white phosphorus and reconverted to the red allotrope. A monotonically increasing temperature distribution was established between the phosphorus end and the gallium-gallium oxide end. The minimum temperature determined the vapor pressure of phosphorus, and the maximum temperature governed the volatilization of the suboxide. In practice, the maximum temperature, 975°-1060°, was established first to initiate the flow of gallium suboxide down the thermal gradient. The temperature of the phosphorus reservoir was then raised to yield a vapor pressure of 0.1-1 atm of phosphorus. After the reaction period the tube was cooled, maintaining the thermal gradient direction to prevent condensation of phosphorus in the crystallization region. In this method no precautions were taken to prevent the contact of phosphorus vapor with the gallium-gallium oxide mixture. This resulted in a direct reaction on the surface of the mixture producing a layer of gallium phosphide which effectively isolated the gallium suboxide source from the reaction chamber, thereby terminating the reaction. For this reason the estimated period of growth of the whiskers was of the order of only several minutes. Attempts to sustain the reaction by better isolation of the cup from the phosphorus vapor using different tube geometries or throttling capillaries yielded a larger number of crystals without increasing the average crystallite size.

After the tubes had been cooled, several distinct zones, indicated in Fig. 1, were apparent. In the region of highest temperatures the gallium-gallium oxide mixture was coated with gallium phosphide as already noted. Farther down the tube, at temperatures 25°-100° below the maximum temperature, the whiskers formed, nucleating on the quartz envelope or on other whiskers. Contiguous with this zone was a region where the gallium suboxide had condensed and disproportionated on the walls of the tube. Next was the band of the reaction by-product, an oxide of phosphorus. Finally, the unreacted, excess phosphorus remained at the coolest end of the tube.

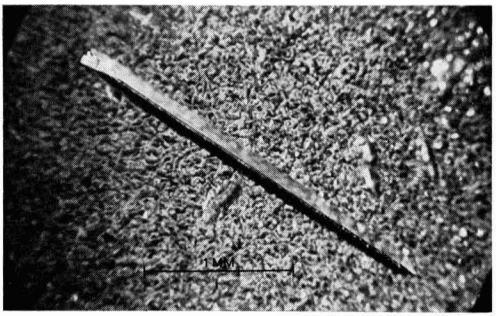

Fig. 2. Typical whisker habit

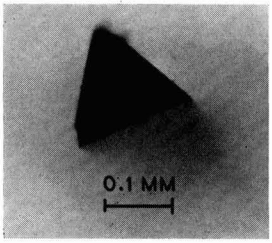

Fig. 3. Cleaved whisker viewed normal to its long axis

Fig. 4. Typical needle habit

Crystals doped with sulfur or zinc were produced by introducing the desired element into the vapor phase. Sulfur was incorporated by adding sufficient sulfur to establish a pressure of 1 mm of the dimer. A 0.07-0.30 mm pressure of zinc was maintained by adding elemental zinc or zinc phosphide and controlling the minimum temperature in the tube which also governs the phosphorus pressure.

Discussion

Five distinct crystal habits have been observed:

1. The predominant whiskers (Fig. 2) are pale orange in color, highly transparent and from 1 to 20 mm long. In cross section they are perfect equilateral triangles (Fig. 3) having edges of between 100 and 200 μ. The long whisker axes are the <111> crystallographic directions of the gallium phosphide lattice and the developed faces are either the $\{\bar{2}11\}$ or the $\{2\bar{1}\bar{1}\}$ set as determined by x-ray crystallography. Sometimes both sets are simultaneously present and observed as slightly developed flats at the apices of the triangle. The crystals generally terminate in {311} faces.

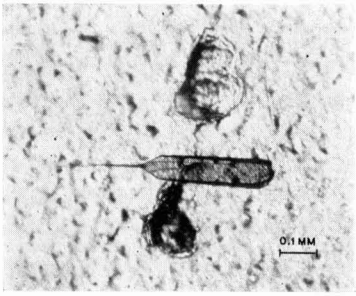

Fig. 5. Sulfur-doped ribbon with filamentary precursor

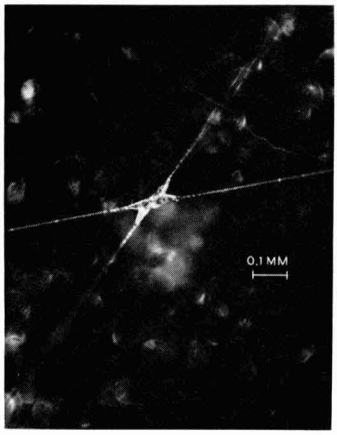

Fig. 6. A pair of filaments epitaxially connected

2. Needles of the type indicated in Fig. 4 were sometimes observed both in the doping experiments and during rapid growth conditions without the intentional introduction of an impurity. They were identical to the normal whiskers except for a taper of about 1°.

3. The presence of sulfur completely altered the growth mechanism, predominantly producing ribbons 0.1-2 mm long, 30-80 μ wide and only 1-2 μ thick as seen in Fig. 5. The major faces were {111} planes.

4. Some fairly imperfect, small platelets exhibiting {111} facets resulted from rapid growth conditions.

5. Hairlike filaments 0.1-5 mm long and only 1-2 μ thick were found under all growth conditions investigated (see Fig. 6).

True epitaxial growth was frequently encountered joining crystallites of both similar and dissimilar habits. Figure 7 shows two normal whiskers which were joined producing the tetrahedral angle between the long axes, which is the angle appropriate to a pair of <111> directions in a single crystal. The whisker whose long axis extends out of the plane of the photograph was cleaved near its intersection with the second crystal. Note the depleted region of the parent crystal near the junction of the crystals. The developed faces in this area are {320} planes. The intersection of a ribbon and a filament is shown in Fig. 5.

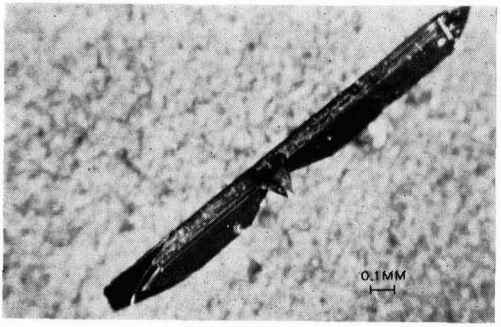

Fig. 7. A pair of whiskers epitaxially connected. The second crystal, which has been cleaved close to its junction with the first crystal, extended out from the plane of the photograph by the tetrahedral angle.

The filaments are believed to constitute the first stage in the growth of the other crystals. They have been observed under all conditions of growth and are found epitaxially attached to all other crystal types. They were found most profusely in regions of crystallization where the reactant densities were the least. It is noted that while filaments are generally as long as normal whiskers, their widths, 1-2 μ, are considerably less than that of the whiskers, 100-200 μ. Since crystals of thickness intermediate between filaments and whiskers were extremely rare it is concluded that the filaments are the precursors of the whiskers and that the rate of growth necessary to convert a filament to a full grown whisker is extremely rapid.

A large portion of the crystals are attached to a small number of sites on the quartz substrate indicating favorable nucleation sites. The bulk of the growth occurs on filaments directly attached to these sites, implying that such substrate sites act as a sink for the reactive molecules or provide a low surface nucleation energy path for growth even after the filaments are already present. The filaments may have been grown from single screw dislocations along [111] axes, although careful observations of cleaved whiskers produced no confirmatory evidence. However, a straight line bisecting the ribbons lengthwise was usually evident. Whenever a filament was found attached to a ribbon such as is shown in Fig. 5, this line joined the filament at the edge of the ribbon although the filament was never coplanar with the ribbon. The bisected parts of the ribbon were crystallographically coherent, *i.e.*, they were not twins. This line could then be indicative of a dislocation line lying within the ribbon and coinciding with the filament from which the ribbon grew.

The vapor grown crystals were fairly strong mechanically, tolerating flexures equivalent to an elastic strain of more than 1%. They exhibited little strain birefringence compared to crystals grown from gallium-phosphorus solutions.

Since the vapor growth occurs at a much lower temperature than that generally used for the preparation of massive gallium phosphide ingots, and since the usual contact between molten phase and container does not occur, the risk of chemical contamination is less severe. Dislocation densities may also be much lower because the strain introduced by the expansion of the melt on freezing in a confining vessel is not present. If only few electrically active centers are introduced due to any deviations from stoichiometry, then the whiskers produced from the vapor phase should exhibit low carrier concentrations, high mobilities, and long minority carrier lifetimes.

From resistivity measurements on a number of n-type whiskers, and using the highest electron mobility observed at room temperature on an ingot recrystallized by the floating zone technique [110 cm^2/v-sec (3)], free carrier concentrations of 10^{14} to 10^{11} cm^{-3} are indicated. These values are up to 6 orders of magnitude below the best values hitherto reported for gallium phosphide. Photoconductivity has recently been observed in the whiskers, implying that the lifetimes are much longer than those in the other modifications of gallium phosphide in which photoconductivity has never been detected, even in samples of comparable free carrier concentrations (8).

The introduction of sulfur introduced about 10^{15} donor at./cc as deduced from resistivity, and doping with zinc converted the crystals to p-type with 4 x 10^{17} acceptors/cc, using $\mu_h = 70$ cm^2/v-sec (9, 10). An alloyed diode prepared on a high resistivity whisker by techniques described elsewhere (10) was characterized by a breakdown potential of 135 v. This is considerably greater than the maximum breakdown potential of 40 v observed in diodes fabricated from crystals grown from the melt.

Although the gallium phosphide crystals produced from gallium suboxide and phosphorus in the vapor phase are small in size they are single and have been purer, free of strain, and easier and quicker to prepare than crystals grown from the melt.

Acknowledgments

The authors are grateful to E. A. Wood and W. L. Bond for the x-ray crystallography.

Manuscript received Dec. 6, 1960; revised manuscript received Feb. 20, 1961. Much of this material was presented at the Spring Meeting of the American Chemical Society, Cleveland, 1960.

Any discussion of this paper will appear in a Discussion Section to be published in the December 1961 JOURNAL.

REFERENCES

1. C. J. Frosch and L. Derick, *This Journal*, **108**, 251 (1961).
2. C. J. Frosch, M. Gershenzon, and D. F. Gibbs, Paper presented at Electrochemical Society Meeting, Chicago (1960).
3. C. J. Frosch, M. Gershenzon, and D. F. Gibbs, Symposium on Preparation of Single Crystals of the III-V Compounds, Battelle Memorial Institute, Columbus (1959).
4. G. Wolff, P. H. Keck, and J. D. Broder, *Phys. Rev.*, **94**, 753 (1954).
5. H. G. Grimmeiss and H. Koelmans, *Philips Research Rpts.*, **15**, 290 (1960).
6. G. R. Antell and D. Effer, *This Journal*, **106**, 509 (1959).
7. C. J. Frosch and C. D. Thurmond, to be published.
8. L. F. Johnson, D. F. Nelson, and M. Gershenzon, to be published.
9. G. F. Alfrey and C. S. Wiggins, *Z. Naturforschg.*, **15a**, 267 (1960).
10. M. Gershenzon and R. M. Mikulyak, *J. Appl. Phys.*, July 1961 (In press).

Gaseous Diffusion of Arsenic and Phosphorus into Germanium

Kurt Lehovec and Carl Pihl

Sprague Electric Company, North Adams, Massachusetts

ABSTRACT

The diffusion of arsenic and phosphorus from a gaseous ambient into germanium is investigated using capacitance and breakdown measurements of diodes produced by plating indium into indentations of various depths. The diffusion constants found for arsenic in germanium agree well with those published by Bosenberg. On the other hand, the diffusion constant of phosphorus in germanium at 780°C was found to be 5.5 x 10^{-13} cm^2/sec which differs considerably from data by Dunlop. The surface concentration of arsenic in germanium appears to increase in proportion to the fourth root of the arsenic vapor pressure at 725°, 750°, and 800°C, with no significant differences among these temperatures. In the case of phosphorus a fourth root dependence was found also at 780°C, the only temperature investigated.

Presence of germanium arsenide was found at the germanium surface, particularly at arsenic surface concentrations exceeding 10^{19} at./cc, using electron diffraction techniques. Thermal conversion of the interior of the germanium wafers (which were 15 ohm-cm N-type) to P-type could be suppressed by arsenic surface concentrations exceeding 5.10^{18} at./cc. This elimination of thermal conversion depends on the surface to volume ratio of the wafer. It is proposed that the thermal conversion level in the bulk of the indiffused material depends on the electric field which arises during diffusion if the impurity concentration exceeds the intrinsic carrier concentration.

Diffusion of electrically active impurities into germanium from a gaseous ambient has received much attention in conjunction with the preparation of semiconducting devices (1). The early work of Fuller (2), Dunlop (3), and Saby and Dunlop (4) was concerned with the diffusion constants of most of the elements of groups 3 and 5 of the periodic table in germanium as a function of temperature. The objective of this paper is to establish the surface concentration of phosphorus and of arsenic in germanium as a function of the vapor pressure of these group 5 elements in the ambient surrounding the germanium, as well as to check the diffusion constants mentioned in the literature. During the course of this work we have observed an interesting relation between the diffusion of impurities into the germanium and the thermal conversion level in the bulk of the germanium.

Experimental Conditions

The germanium surface was exposed to a hydrogen stream passed at a controlled temperature over the impurities which were in powder form. This temperature will be referred to subsequently as the "impurity temperature." The temperature along the tube containing the hydrogen increased gradually from the position of the solid impurities to the position of the germanium. Therefore, the impurity temperature is considered characteristic for the partial vapor pressure of the impurities adjacent to the surface of the germanium. The hydrogen flow rate was typically 160 ccm/min. Deliberate variation in flow rate by a factor 2 did not seem to affect the diffusion results significantly.

Furthermore, a few runs made in a closed evacuated system provided concentrations of arsenic in the germanium surface in substantial agreement with those obtained in the gas stream. This indicates that the germanium surface was in quasi-equilibrium with the vapor pressure of impurities as determined from the impurity temperature.

The doping elements used were in the form of red phosphorus powder supplied by the Central Scientific Company or spectrographic grade arsenic powder supplied by Johnson Mathey, Ltd. The phosphorus experiments were done before a source of specially high-purity phosphorus became available recently. The powder was contained between quartz wool plugs placed across the entire cross section of the tube carrying the hydrogen to assure an intimate contact of the gas stream with the doping elements. The germanium was single crystal, N-type, containing approximately 5.10^{13} at./cc antimony atoms. The germanium was cut in slices of (110) orientation, lapped, diced, and etched by an HF, HNO_3, and acetic acid mixture. The dice were approximately 0.01 cm thick. The germanium dice were placed in a quartz crucible which was inserted into the diffusion tube. No significant difference was found between the diffusion with dice piled in the crucible and that with dice placed upright at regular intervals into grooves cut in the crucible. This suggests that surface diffusion is substantially more rapid than bulk diffusion, providing the entire surface with the same concentration of impurities, regardless of direct exposure to the ambient or partial shielding by adjacent dice.

A "single cycle" diffusion was used which is characterized by an "impurity temperature," a "germanium temperature," and a diffusion time. The germanium was heated to a stationary temperature before the gas stream carrying the impurities was introduced. After the gas stream was stopped, the germanium was cooled in a time short compared to the diffusion time. Initial cooling rates were of the order of 12°C/min. Considering the temperature dependence of the diffusion constant for arsenic, the effective diffusion time will be prolonged by this cooling rate by approximately 3 min (see Appendix I).

Evaluation of the Impurity Distribution

After the indiffusion, the dice were attached to a metal tab with tin antimony solder and diodes were fabricated in the following manner. Part of the dice surface was etched off by an anodic jet etch (5) in a dilute fluoride solution under conditions providing a substantially flat indentation. The depth of the indentation was controlled by the etching current, usually 5 ma at 0.04 cm jet diameter, and the duration of the etch, which was varied between 0.25 and 5 sec. The current density and the resistivity of the solution are important factors in providing a flat-bottomed etch indentation.

The shape of the indentation was monitored by placing an optically flat glass slide over the indentation and illuminating with parallel monochromatic light to produce an interference fringe system between the light waves reflected from the germanium surface and those reflected from the bottom of the glass slide. The depth of the etch indentation was calibrated accurately using polished germanium wafers and varying the duration of etching. This calibration curve was then used for the indiffused wafers, which were not polished, and where roughness interfered with accurate evaluation of the reference wafer surface for determination of etch depth. No significant difference could be detected between jet etch depth into lapped indiffused wafers and polished homogeneous wafers under the conditions used in our investigation.

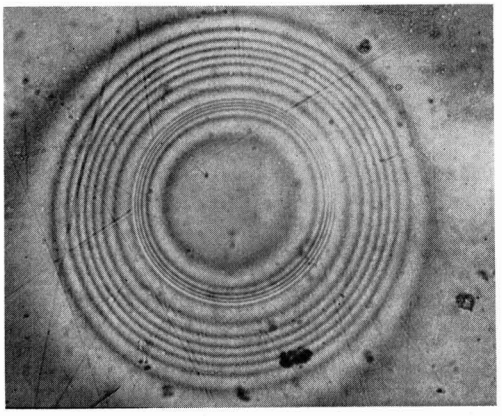

Fig. 1. Interference fringe photograph of a jet etched indentation showing a flat bottom on which the indium plated diode will be placed.

Figure 1 is an example of such an interference fringe pattern indicating the flatness of the bottom of the indentation. Two adjacent fringes differ in depth from the germanium surface by 2.94×10^{-5} cm when yellow sodium light is used. A rectifying contact was made to the flat center of the indentation by jet plating indium as described by Bradley (5). A typical plated contact had a diameter of 0.015 cm. Deviations from perfect flatness within the plated region can be inspected easily by the interference fringe method and should be avoided in order to assure that the impurity concentration adjacent to the contact is constant.

The impurity distribution of the indiffused layer was evaluated by: (*a*) capacitance measurements, and (*b*) breakdown measurements of the diodes.

The capacitance of a diode was measured as a function of the applied bias voltage in the blocking direction. The evaluation of the capacitance measurements is based on the theory by Schottky (6) for a rectifying contact between a metal and a semiconductor. From the variation of capacitance, C, with applied bias voltage, E, the impurity concentration, N, over a certain range of distance, d, from the contact can be derived by the equations:

$$N = \frac{2}{e\,\epsilon\epsilon_0 A^2} \cdot \frac{\partial E}{\partial (1/C^2)} \qquad [1]$$

and

$$d = A\,\epsilon\epsilon_0 / C \qquad [2]$$

where $\epsilon = 16$ is the dielectric constant of germanium, A is the area of the contact, $\epsilon_0 = 8.86 \times 10^{-14}$ amp-sec/volt-cm, and e is the electron charge.

The impurity concentration of Eq. [1] is present at the boundary of the space charge layer, that is, at the distance, d, from the contact.

The capacitance was measured in a Wayne-Kerr bridge using the circuit shown in Fig. 2. The principal error sources of this evaluation method are: (*A*) The deviation from the flatness of the bottom of the indentation over the contact area. This error can be suppressed by proceeding to smaller contacts. (*B*) The stray capacitance resulting from holding jigs and wiring of the test circuit. In our arrangement, the stray capacitance was typically 0.6 $\mu\mu$f. The stray capacitance becomes the more troublesome the smaller the junction capacitance, that is, with increasing bias voltage, lower impurity concentration, and smaller contact area.

To obtain maximum accuracy it is advisable to change the size of the plated area, depending on the

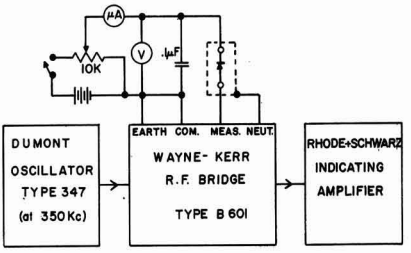

Fig. 2. Circuit for measuring the capacitance

position of the indentation from the surface: if the indentation is close to the surface where there is a high impurity concentration in a wafer with indiffused impurities, the diode capacitance is fairly high, and the stray capacitance unimportant. In this case, a small contact is preferred in order to suppress variations in flatness of the contact. On the other hand, for deep indentations which reach to low impurity concentrations, the effect of the stray capacitance becomes quite important, and we found it advisable to increase the contact area, even though this may cause some deviation from the flatness across the contact.

The available range of bias voltages for capacitance evaluation of the impurity distribution is restricted upward by the breakdown voltage and downward by minority carrier diffusion effects. Capacitance measurements are particularly suitable for the evaluation of the impurity distribution in the range from 3×10^{14} to 3×10^{16} at./cc.

A serious error source arises from surface conversion layers having a lateral extension which depends on the bias voltage. Such samples may exhibit an abnormal dependence of capacitance on bias voltage which can even provide apparent impurity concentrations increasing with distance from the surface if evaluated indiscriminantly by Eq. [1] and [2].

Bias voltages, much less than a tenth of a volt, cannot be used in conjunction with Eq. [1] and [2], since there is already a substantial effect of the hole storage capacitance of minority carriers (Appendix II) and, furthermore, time lag effects arising from slow surface states become noticeable.

As the range of useable bias voltages is quite limited at low breakdown voltages, i.e., high impurity concentrations, one may attempt to evaluate the impurity concentration in the space charge layer from measurements at one bias voltage only. The evaluation is based on the equation:

$$N = \frac{2}{e\,\epsilon\epsilon_0 A^2}(E + V_b)C^2 \qquad [3]$$

and requires an estimate of the built-in potential, V_b. For highly doped germanium, $N \geqq 10^{17}$ at./cc, and a plated indium contact, $V_b \approx 0.7$ v provided an impurity concentration by Eq. [3] in agreement with those derived from Eq. [1] and [2] and with the known impurity concentration of homogeneously doped calibration samples. An example of an impurity distribution determined by the capacitance method is shown in Fig. 3.

Also shown in Fig. 3 are breakdown voltages measured on diodes placed at various positions from the surface. The breakdown voltage, E_z, was defined as the voltage in the blocking direction at which a current of 1 ma flows. From these data an empirical relation between breakdown voltage and impurity concentration at the contact was established. This empirical relation is

$$N \approx \text{const}/E_z \qquad [4]$$

with the constant between 2 and 5×10^{17} at./cc v.

Eq. [4] was found valid for breakdown voltages in the range from 0.1 to 10 v and for impurity distributions which are sufficiently gradual that the impurity

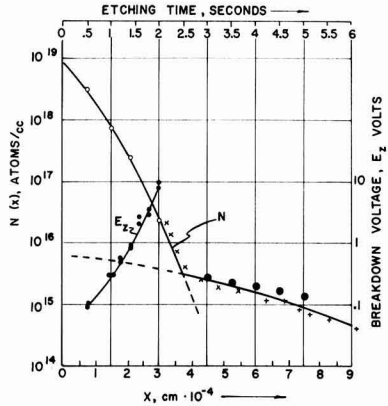

Fig. 3. Impurity distribution determined from capacitance measurements as follows: ×, o, and + from the bias variation of capacitance of three diodes evaluated by Eq. [1] and [2]; o from the capacitances of four diodes using Eq. [3]. The figure also shows the dependence of breakdown voltage on the positions of diodes and by comparison with the impurity distribution the relation [4] of the text was obtained.

concentration is substantially constant across the space charge layer. This is usually the case for high impurity concentrations where the breakdown voltage is low and the width of the space charge layer quite small. A correction factor for the determination of the impurity concentration at the rectifying metal contact in the case of an exponentially varying impurity concentration in the space charge layer is derived in Appendix III, assuming that the maximum field in the space charge layer determines breakdown.

Breakdown measurements are much less time consuming than capacitance measurements; however, their evaluation depends on the empirical relation [4] and, furthermore, each diode provides only one point for the impurity distribution in the wafer. Of course, breakdown voltages lower than those corresponding to Eq. [4] can be obtained by improper surface etching of the diodes, and such samples were spotted and eliminated by comparing the breakdown voltages of several diodes made under identical conditions.

In spite of these possible error sources, the evaluation method based on diodes was chosen because of the availability of, and familiarity with, jet etching and jet plating in our laboratory. Furthermore, these methods enable a point by point determination of an impurity distribution and do not depend on the assumption that the impurity distribution is a complementary error function.

The evaluation methods described cease to be applicable at impurity concentrations above 5.10^{18} at./cc. Surface concentrations higher than this value have been estimated by extrapolation. After determining the impurity concentration at various distances from the surface using breakdown or capacitance measurements it was attempted to fit these points by a complementary error function curve assigning suitable values to surface concentration and diffusion constant.

In the case of arsenic diffusion, the diffusion constant was found in good agreement with published values (7) and the curves were then merely fitted by using the published diffusion constants and selecting the surface concentration. In the case of phosphorus diffusion, it was found that the diffusion constant published by Dunlop (3) would not provide a good fit to our data. Furthermore, in the case of phosphorus indiffusion it was found that the experimental data could not be described by a single error function curve. A fairly good fit could be obtained, however, by using the super position of two error function curves of different diffusion constants and different surface concentrations, as shown in Fig. 3.

If the concentration of diffusing impurities exceeds the intrinsic carrier concentration at the diffusion temperature, a correction must be applied to the extrapolated surface concentration to allow for the electric field arising from the diffusion impurities. This electric field may cause a drift current of impurities of a magnitude equal to or smaller than the diffusion current (8). In the absence of the results of more extensive calculations, now in progress, we have obtained the correction by integration of Fick's law using the ordinary diffusion constant D at concentrations less than the intrinsic carrier concentration, $C < n_i$ and the diffusion constant $2D$ at concentrations $C > n_i$ (see Appendix IV). Figure 4 shows C_s/n_i *vs.* C_o/n_i where C_s is the true surface concentration and C_o the apparent surface concentration as extrapolated from the tail of the impurity distribution by using a complementary error function curve of diffusion constant D. The intrinsic carrier concentration in germanium was taken from data given by Conwell (9).

In our experiments using phosphorus no correction of the surface concentration for the drift field was required. However, in some of the experiments using arsenic diffusion substantial corrections were required.

Results

Arsenic diffusion in germanium.—Germanium temperatures of 700°, 725°, 750°, and 800°C and arsenic temperatures between 60° and 350°C were used at diffusion times ranging between 10 and 160 min. Diffusion conditions and surface concentrations are summarized in Table I. Runs were listed in sequence of decreasing arsenic temperature and within each group of same arsenic temperature in sequence of decreasing germanium temperature. The accuracy of the evaluation method as well as the scatter of the results from run to run suggested the listing of surface concentrations only to two digits.

Runs marked by an asterisk exhibited thermal conversion of the bulk of the wafer to P-type, although a substantial part of the indiffused layer remained N-type. The accuracy of evaluation of the surface concentration was seriously impaired in such cases and the values listed can be considered only estimates. Note that thermal conversion occurred only at surface concentrations under 5.10^{18} at./cc. This suggested that thermal conversion could be eliminated by a second high arsenic temperature cycle which would not modify, substantially, the long main cycle except at positions very close to the surface. This procedure was successful as can be seen from runs 100, 102, and 125. The conditions for the second short cycle are listed in parentheses in Table I.

No significant dependence of surface concentration on time of diffusion and on germanium temperature was observed. Therefore, average surface concentrations, regardless of the diffusion time and germanium temperature, were calculated and these are plotted as a function of arsenic temperature in Fig. 5. The number of diffusion runs from which the average

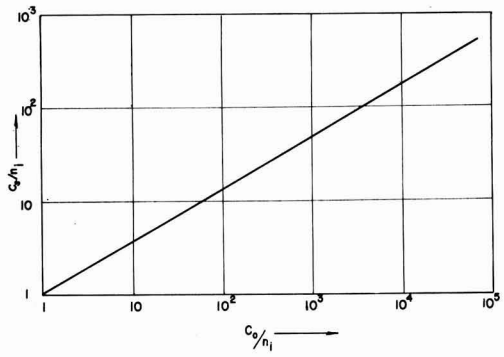

Fig. 4. True surface concentration, C_s vs. surface concentration, C_o, extrapolated from the impurity distribution at large distances from the surface; according to Eq. [IV.10] and [IV.11] of Appendix 4. n_i is the intrinsic carrier concentration at the diffusion temperature.

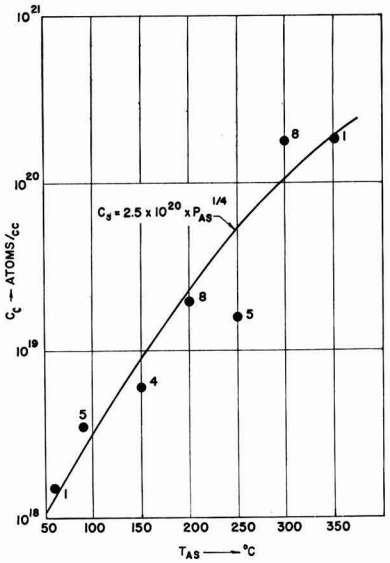

Fig. 5. Surface concentration of arsenic in germanium as function of the arsenic temperature. The points are averages of the number of experiments listed in the figure at the points. Data are taken from Table I excluding runs exhibiting thermal conversion. The point at 90°C was obtained from experiments in a closed system, not listed in Table I. The dotted line represents the fourth root of the arsenic vapor pressure multiplied by a constant chosen to fit the arsenic surface concentration.

Table I. Gaseous diffusion of arsenic in germanium

The bulk of the wafers converted to the P-type in the runs marked by asterisks. Values in parentheses pertain to a second brief diffusion cycle.

Run No.	T_{Ge}, °C	T_{As}, °C	t, min	C_s, 10^{18} at./cc
82	800	350	10	180
81	800	300	40	130
67	800	300	10	360
43	750	300	10	140
44	750	300	40	140
175	750	300	40	260
65	725	300	40	300
62	725	300	10	18
45	700	300	40	61
68	800	250	10	22
59	750	250	160	10
48	750	250	40	15
47	750	250	10	7
66	725	250	40	24
56*	700	250	10	4
57*	700	250	40	4
69	800	200	10	20
75	800	200	40	16
170	750	200	40	37
50	750	200	10	6.9
51	750	200	40	6.9
88	750	200	40	39
193	750	200	40	26
100	725	200 (250)	40 (5)	5
58*	700	200	10	0.4
71	800	150	10	8
89	750	150	10	2
53*	750	150	40	5
54*	750	150	10	1
93A	750	150	40	7.3
102	725	150 (300)	40 (5)	6.8
125	750	60 (200)	40 (3)	1.5

was formed are listed in the figure. Runs exhibiting thermal conversion were omitted. The point at 90°C is not taken from Table I, but comes from five runs made in an evacuated closed system. The solid line is the relation:

$$C_s(\text{in at./cc}) = 2.5 \times 10^{20}\, p_{As_4}^{1/4}\ (\text{in mm Hg}) \quad [5]$$

The arsenic pressure, p_{As}, was taken from data by Honig (10). A fourth root relation may be expected for a reaction involving the dissociation of four-atomic arsenic molecules into monoatomic arsenic at the germanium surface.

Electron diffraction patterns were made on dice of selected diffusion runs. Germanium arsenide lines were observed as already reported by Waring, *et al.* (11). The intensity of the pattern is related to the surface concentration of arsenic dissolved in germanium: at concentrations $C_s \geqq 10^{19}$ at./cc only the strongest germanium spots are still visible. On the other hand, at surface concentrations substantially less than 10^{19} at./cc only traces of germanium arsenide lines were found.

Phosphorus diffusion in germanium.—The germanium temperature was kept at 780°C and the phosphorus temperature was varied between 150° and 325°C. Table II lists diffusion conditions, surface concentrations, and diffusion constants. The surface concentrations are plotted in Fig. 6 against the phosphorus temperature. In the same figure, the fourth root of the vapor pressure of red phosphorus is plotted. It is seen that the relation

Table II. Gaseous diffusion of phosphorus in germanium at 780°C

All runs at 4 hr diffusion time, except 1-74, which was made at 2 hr. The bulk of the wafers converted to the P-type in the runs marked by asterisks.

Run No.	Phosphorus temp, °C	Surface concentration in 10^{18} at./cc	Diffusion constant in 10^{-13} cm²/sec
1-74	325	2.4	4.3
1-66	300	2.2	3.3
1-109	300	3.0	6.1
2-101*	250	1.2	7.3
1-107*	250	1.0	7.2
1-108*	200	1.0	7.2
1-117*	150	0.52	3.3
			avg 5.5

$$C_s(\text{at./cc}) = 2 \cdot 10^{18} p^{1/4}(\text{mm Hg}) \quad [6]$$

provides a fair fit of the surface concentrations.

The runs marked by an asterisk in Table II have shown thermal conversion to P-type in the bulk of the germanium dice. Note that this thermal conversion occurs only at phosphorus temperatures below 300°C, corresponding to surface concentrations below 2.10^{18} at./cc.

All phosphorus indiffusion runs exhibited a "tail" as shown in Fig. 3, corresponding to a high diffusion constant and low surface concentration. The diffusion constants corresponding to the tail varied in the range $1.2 \times 10^{-11} \pm 0.4 \times 10^{-11}$ cm²/second.

Discussion of the diffusion data.—The phase diagram of germanium and arsenic (12) (Fig. 7) shows the existence of two compounds, GeAs and $GeAs_2$, and the possibility of liquid phases above 723°C. Since we approach the equilibrium condition from the germanium-rich side of the phase diagram during indiffusion, we would expect the germanium to accept up to a few atomic per cent of arsenic in solid solution until the concentration corresponding to the dotted solidus line at the left of Fig. 7 is reached. More recent measurements (13) place the solidus line at an arsenic concentration of 1.8×10^{20} at./cc.

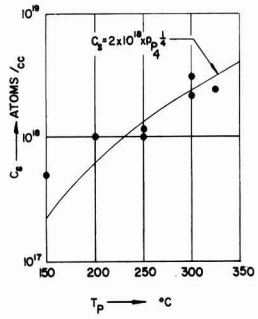

Fig. 6. Phosphorus surface concentration in germanium at 780°C as function of phosphorus temperature; data taken from Table II. The dotted line is proportional to the fourth root of the vapor pressure of four atomic phosphorus.

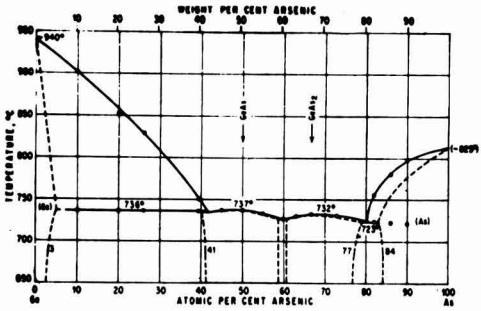

Fig. 7. Phase diagram germanium-arsenic according to Hansen (12). The solid solubility line of arsenic in germanium has been determined by Thurmond, et al. (13) to be 1.8 x 10^{20} at./cm^3, much less than indicated in the figure.

At this point, a GeAs phase, somewhat deficient in arsenic, should form if the temperature is below 736°C, and a liquid germanium-arsenic phase should form if the temperature is above 736°C. Diffusion of arsenic from the vapor phase into GeAs could cause the formation of $GeAs_2$, and possibly of a liquid germanium-arsenic phase above 723°C.

It is obvious from the phase diagram that drastically different conditions for indiffusion could exist in the temperature ranges below and above 723°C, respectively:

The existence of liquid and solid germanium-arsenic phases, the growth rate of these phases in relation to the diffusion rate of arsenic in solid germanium, the equilibrium between atomic arsenic distributed in germanium and germanium arsenides, deviations from stochiometric composition in the germanium arsenides as functions of arsenic vapor pressure could all conceivably influence the gaseous diffusion of arsenic in solid germanium.

In view of these possibilities, it is rather surprising that the surface concentration of arsenic in germanium increases approximately with the fourth root of the arsenic vapor pressure, regardless of the germanium temperature in the temperature range, 725°-800°C, where significant changes occur in the phase diagram.

Since we have only one run No. 45, at 700°C which is not affected by thermal conversion the dependence of surface concentration on arsenic vapor pressure at 700°C has not been established. However, the fact that the surface concentration at 700°C, where only solid phases occur, is in the same range as those at 725°, 750°, and 800°C suggests strongly that the surface concentration of arsenic in solid germanium was not affected by the presence of germanium arsenide phases under the conditions used in our experiments.

The presence of germanium arsenide phases was established by electron diffraction. It was not established, however, whether these phases were a continuous film covering the entire surface or merely patches of crystallites. Electron microscope replica studies may shed more light on this question. It was noted that the arsenide diffraction lines were continuous in some cases and contained single crystal spots in others.

The fourth root relationship between vapor pressure of arsenic, and also of phosphorus, and surface concentrations in germanium suggests a quasi-equilibrium between four atomic vapor molecules and atomically dispersed impurities in the germanium. The highest surface concentration of arsenic in germanium listed in Table I are a few times 10^{20} at./cc which should be compared with the solid solubility of 1.8 x 10^{20} at./cc[13]. The comparatively wide scatter of surface concentrations between runs made under equivalent conditions may be partially related to the complex mechanism of evaporation of arsenic and phosphorus. The main species in the vapor of these two elements are 4-atomic molecules, while the solid substances have stable modifications with atomic lattices. Evaporation from the stable modifications and recondensation leads to unstable molecular modifications of substantially higher evaporation rates (14). Evaporation of arsenic and phosphorus from solutions in other metals, such as lead and thalium, may provide more reproducible conditions (15).

In the case of phosphorus, the diffusion constant was not in agreement with data published by Dunlop (3). Actually, Dunlop's value is only an estimate based on an assumed surface concentration. The tail in the "phosphorus" distribution observed by us is tentatively attributed to arsenic traces in the phosphorus supply since the observed diffusion constant comes close to the value published by Bösenberg (7) for arsenic.

Thermal Conversion in Indiffused Samples

Of great interest is the discovery of a relation between thermal conversion of the bulk of the wafer to the P-type and the arsenic indiffusion conditions. It should be emphasized that the removal of thermal conversion from the bulk cannot be attributed to diffusion of arsenic into the bulk in view of the known diffusion constant of arsenic and the times and distances involved. Rather, the thermal conversion centers must have migrated to the surface of the crystal. Copper, which is usually associated with thermal conversion, diffuses sufficiently rapidly so that migration rate should not be a limiting factor for removal of thermal conversion. It is very interesting to note that thermal conversion occurred in our samples quite frequently at surface concentrations under 5.10^{18} at./cc arsenic, but never at higher surface concentration. This suggests that excessive arsenic acts somehow as a getter for thermal conversion centers. If so, the possibility exists that the getter may become saturated if the surface to volume ratio is too small. Indeed, a thin slice (0.01 cm) and a thick slice (0.6 cm) of the same crystal were subjected simultaneously to gaseous diffusion of arsenic, and it was found that the bulk of the thick slice was converted while that of the thin slice was not. The original N-type doping level was 5 x 10^{18} at./cc. The P-type level of the thick converted slice was 7 x 10^{14} at./cc. Thus, at least 3 x 10^{12} potential conversion cen-

ters have been removed per 1 cm^2 of the surface of the not converted thin slice.

Surface concentrations of runs showing thermal conversion lie sometime below the curve of Fig. 5 for runs without thermal conversion. In such cases one could assume that most of the indiffused impurities have been compensated by thermal conversion centers. Thermal conversion up to levels of several 10^{16} at./cc has been observed occasionally, and the total number of centers available in a 10^{-2} cm thick slice is then of the order of 10^{14} cm^{-2}, which could be sufficient for some compensation of the indiffused impurities, depending on surface concentration and diffusion length.

It is unlikely that a liquid phase is involved in the gettering action since thermal conversion was prevented at 700°C in sample No. 45 where no liquid phase exists. While it is conceivable that a germanium arsenide phase is responsible for the getter action, removal of thermal conversion by high phosphorus surface concentrations has been observed also. Presence of a germanium phosphide on the surface of the phosphorus diffused samples is unlikely, since the only germanium phosphide, GeP, has a boiling point of 580°C (16).

We would like to propose the following tentative explanation for the removal of thermal conversion by indiffusion of N-type impurities into germanium. It is known (17-19) that substitutional copper causes "thermal conversion" and that these thermal conversion centers are quite mobile at elevated temperatures due to dissociation into fast moving interstitial copper and vacancies. It is also known that the vacancies represent P-type centers, while the charge of the interstitial copper has not yet been established definitely. If there is an electric potential present between the surface and the bulk of the germanium during the indiffusion of impurities, the mobile vacancies should arrange in a Boltzman distribution of a surface concentration determined by the free energy of a vacancy in germanium and by the diffusion temperature, and of a bulk concentration which differs from the surface concentration of vacancies by the Boltzman factor

$$\exp\ (-e\,V_s/kT) = n_i/C_s \qquad [7]$$

where n_i is the intrinsic carrier concentration at the diffusion temperature and C_s is the surface concentration of indiffusing impurities. Equation [7] applies to the case $C_s >> n_i$ and the upper sign refers to indiffusion of N-type impurities, which suppresses the bulk vacancy concentration with respect to the surface, while the lower sign refers to indiffusion of P-type impurities which enhances the bulk concentration of vacancies with respect to the surface.

The distribution of substitutional copper is determined not only by that of vacancies but also by that of interstitial copper according to the mass action law pertaining to the reaction

$$Cu_{subst.} \rightleftarrows Cu_{interst.} + \text{vacancy}$$

If interstitial copper were electrically neutral, the distribution of substitutional copper would equal that of vacancies except of a space independent factor. On the other hand, if interstitial copper were a donor, as it is suspected, its Boltzman distribution would be the inverse of the Boltzman distribution of vacancies and the distribution of substitutional copper would then become space independent being proportional to the product of the concentrations of vacancies and of interstitial copper. The high surface concentration of donor type interstitial copper, with respect to bulk concentration, in the case of indiffused N-type impurities, should lead to a fairly rapid rate of loss of copper by evaporation from the surface, while the low surface concentration of interstitial copper, in the case of indiffused P-type impurities, should lead to a fairly slow rate of loss of copper by evaporation from the surface.

Thus, regardless of the effective charge of interstitial copper we may expect a suppression of bulk thermal conversion by indiffusion of N-type impurities: in the case of neutral interstitial copper, due to the space distribution of substitutional copper, and in the case of donor-type interstitial copper due to enhanced loss of copper from the sample.

The situation may become more complicated if the solubility limits for interstitial or substitutional copper are reached and if these solubility limits were affected by presence of the indiffused impurities.

Investigations of Busen and Meeks (21) of this laboratory suggest that thermal conversion decreases from the bulk toward the surface in the case of indium diffusion into germanium.

More quantitative investigations on thermal conversion in relation to arsenic and phosphorus indiffusion would be desirable; however, such investigations are quite difficult in view of the sensitivity of thermal conversion to many factors related to crystal growth, handling, contamination in the diffusion apparatus, etc.

Appreciation

The authors would like to express their gratitude to their co-workers Messrs. Charles Wrigley, John Schimmel, and Seymour Saposnik for carrying out the capacitance measurements; Messrs. Karl Busen and Earl Meeks for contributing their data on closed system diffusion of arsenic and helpful discussions; and to our consultants, Messrs. Ernest Fulham and Douglas Halgren, Schenectady, N. Y., for the electron diffraction work.

Manuscript received Nov. 23, 1960; revised manuscript received Feb. 15, 1961. This paper was prepared for delivery in part before the Philadelphia Meeting, May 3-7, 1959 and in part before the Chicago Meeting, May 1-5, 1960.

Any discussion of this paper will appear in a Discussion Section to be published in the December 1961 JOURNAL.

REFERENCES

1. C. A. Lee, M. Tanenbaum, and D. E. Thomas, *Bell System Tech. J.*, **35**, 23 (1956).
2. C. S. Fuller, *Phys. Rev.*, **86**, 136 (1952).
3. H. C. Dunlop, *ibid.*, **94**, 1531 (1954).
4. J. S. Saby and H. C. Dunlop, *ibid.*, **90**, 630 (1953).
5. H. E. Bradley, *Proc. I.R.E.*, **41**, 1702 (1953).
6. W. Schottky, *Z. Physik*, **118**, 539 (1942).
7. W. Bösenberg, *Z. Naturforsch.*, **109**, 285-291 (1955).
8. F. M. Smits, *Proc. I.R.E.*, **46**, 1049 (1958).
9. E. M. Conwell, *ibid.*, **40**, 1327 (1952).
10. R. E. Honig, *RCA Rev.*, **18**, 2 (1957).

11. W. Waring, D. T. Pitman, and S. R. Steele, *J. Appl. Phys.*, **29**, 1002 (1958).
12. M. Hansen, "Constitution of Binary Alloys," 2nd ed., McGraw-Hill Book Co., New York (1958).
13. C. D. Thurmond, T. A. Trumbone, and M. Kowalchik, *J. Chem. Phys.*, **25**, 799 (1956).
14. J. van den Boomgaard and K. Schal, *Philips Research Repts.*, **12**, 127 (1957).
15. L. Brewer and J. S. Kane, *J. Phys. Chem.*, **59**, 105 (1955).
16 M. Zumbush, M. Heimbrecht, and H. Biltz, *Z. anorg. u. algem. Chem.*, **242**, 237 (1939).
17. F. van der Maesen and J. A Brenkman, *This Journal*, **102**, 229 (1955).
18. F. C. Frank and D. Turnbull, *Phys. Rev.*, **104**, 617 (1956).
19. A. G. Tweet, *J. Appl. Phys.*, **30**, 2002 (1959).
20. W. Shockley, "Electrons and Holes in Semiconductors," p. 317, D. Van Nostrand Co., New York (1950).
21. K. M. Busen, E. L. Meeks, and G. A. Shirn, paper presented at Columbus Meeting of this Society, Oct. 18-22, 1959 and by K. M. Busen and E. L. Meeks paper presented at the Chicago Meeting, May 1-5, 1960.

APPENDIX I

Correction for Diffusion during Cooling

The correction added to the diffusion time at the temperature T_o to account for further diffusion during cooling is:

$$t_c = \int_0^\infty D\, dt/D_o \qquad [I.1]$$

where D_o is the diffusion constant at the temperature T_o. It is well known that the diffusion constant decreases rapidly with temperature according to a function:

$$D = ae^{-b/T} \qquad [I.2]$$

where $b/T >> 1$. Therefore, diffusion during cooling will arise only during the initial cooling periods, and the cooling curve, $T(t)$, can be replaced by any analytic expression without appreciable influence on the cooling time, t_c, provided that initial temperature T_o and initial cooling rate, $(dT/dt)_{t=0}$ are fitted.

We shall use a temperature-time function for cooling determined by the radiation law:

$$dT/dt = -qT^4 \qquad [I.3]$$

and shall fit q by the measured initial cooling rate, $(dT/dt)_{t=0}$.

Integration of [I.1] with [I.2] and [I.3] provides:

$$t_c = \frac{1}{q\, b^3}\left[b^2/T_o^2 + 2b/T + 2\right] \qquad [I.4]$$

Since $b/T_o >> 1$, and considering the definition of q, we have

$$t_c \approx -\frac{T_o^2}{b\,(dT/dt)_{t=0}} \qquad [I.5]$$

For arsenic diffusion: $b \approx 2.8 \times 10^4$ °K, $T_o = 1023$°K and with $(dT/dt)_{t=0} = 12.5$°C/min, we obtain $t_c \sim 3$ min.

APPENDIX II

Hole Storage Capacitance

According to Shockley (20), the hole storage capacitance C_{st} is obtained from the complex conductance:

$$G + i\omega C_{st} = (1 + i\omega\tau)^{1/2}\, G_p \exp\,(eE/kT) \qquad [II.1]$$

where τ is the life time of minority carriers (holes in our case), ω is the angular frequency of the applied potential, and G_p is a voltage independent real conductance which is related to the hole current:

$$I_p = G_p(kT/e)\,[\exp(eE/kT) - 1] \qquad [II.2]$$

Eliminating G_p from Eq. [II.1] and [II.2], and considering the cases of low frequencies and high frequencies separately, we obtain

$$C_{st} \approx \frac{I_p}{\exp\,(eE/kT) - 1} \cdot \frac{e}{kT} \cdot \frac{\tau}{2} \exp\,(eE/kT) \qquad [II.3]$$

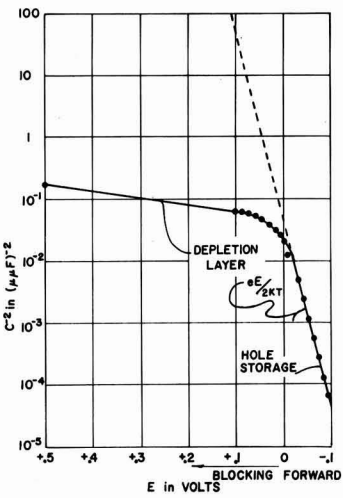

Fig. 8. Measured capacitance as function of small bias voltages separating the contributions of depletion layer and hole storage capacitances.

for $\omega\tau << 1$

and

$$C_{st} \approx \frac{I_p}{\exp\,(eE/kT) - 1}\,\frac{e}{kT}\left(\frac{\tau}{2\omega}\right)^{1/2} \exp\,(eE/kT) \qquad [II.4]$$

for $\omega\tau >> 1$.

Since $I_p/[\exp eE/kT - 1]$ should be independent of the bias voltage in germanium P-N junctions, the hole storage capacitance varies as $\exp eE/kT$.

Figure 8 shows a plot of $1/C^2$ against bias voltage. For bias voltages exceeding 30 mv in the forward direction, a straight line is approached of a slope as predicted by Eq. [II.3] or [II.4]. Extrapolating this hole storage capacitance to bias voltages in the blocking direction, we observe that the hole storage capacitance is 10% of the total capacitance at 60 mv and 3% at 100 mv bias voltage in the blocking direction.

Thus, it appears that the validity of Eq. [1] and [2] of the text is seriously impaired for bias voltages less than 0.1 v, unless corrections for the hole storage capacitance are made. Such corrections could be based on extrapolation of the hole storage capacitance from forward biases, shown in Fig. 8, or else on an investigation of the frequency dependence of the total capacitance at a fixed bias voltage. The space charge layer capacitance should be frequency independent, while the hole storage capacitance should vary with frequency as indicated by Eq. [II.2], [II.3], or [II.4]. However, it should be kept in mind that contributions to a frequency dependence may result also from channel effects associated with surface states.

APPENDIX III

Zener Breakdown for a Metal-Semiconductor Junction with Exponentially Varying Impurity Concentration

It will be assumed that breakdown occurs if the electric field at the contact, F_c, exceeds a critical value F_z.[1]

Considering an impurity concentration decreasing exponentially from the contact toward the semiconductor:

$$N = N_c \exp\,(-x/x_o) \qquad [III.1]$$

one has

$$F_c = (e/\epsilon\epsilon_o)\, N_c\, x_o\,[1 - \exp\,(-d/x_o)] \qquad [III.2]$$

and

$$E + V_b = (e/\epsilon\epsilon_o)\, N_c\, x_o^2\,[1 - (1 + d/x_o)\exp\,(-d/x_o)] \qquad [III.3]$$

[1] This assumption implies that the electric field does not decrease substantially over the distance tunneled by the electron, that is

$$B/(F_z e) << d_z$$

where B is the forbidden band width, and d_z is the width of the space charge layer at breakdown.

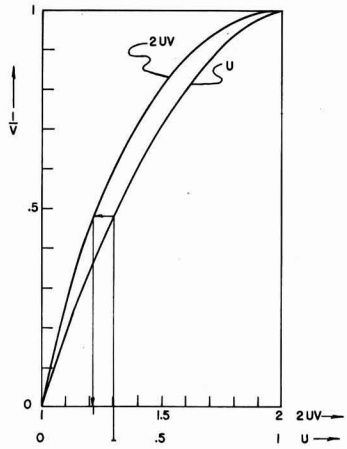

Fig. 9. Correction for determining the impurity concentration at the metal boundary from the breakdown voltage in the case that impurity concentration varies exponentially with position within the space charge layer.

where d is the width of the space charge layer.

Elimination of the width of the space charge layer, d, leads to the relation

$$u = 1 + (v - 1) \ln (1 = 1/v) \qquad \text{[III.4]}$$

where

$$u = \frac{E + V_b}{F_c\, x_o} \qquad \text{[III.5]}$$

and

$$v = \frac{eN_c\, x_o}{\epsilon\epsilon_o\, F_c} \qquad \text{[III.6]}$$

The impurity concentration at the contact becomes:

$$N_c = \frac{\epsilon\epsilon_o\, F_c^2}{2e\,(E + V_b)} \quad (2uv) \qquad \text{[III.7]}$$

In Fig. 9 the functions u and $2uv$

$$2uv = 2v + 2v(v - 1) \ln (1 - 1/v) \qquad \text{[III.8]}$$

are plotted *vs.* $1/v$.

Note that the factor $2uv$ in Eq. [III.8] varies only between the limits 1 and 2 which limits are approached for very gradual and very steep impurity distributions, respectively.

For a complementary error function distribution:

$$N = C_s \operatorname{erfc} (X/L) \qquad \text{[III.9]}$$

one has

$$(dN/dX)_{Nc} = -\frac{2}{\sqrt{\pi}} \frac{C_s}{L} \exp (-X_c^2/L^2) = -\frac{2}{\sqrt{\pi}} \frac{N_c}{L} \cdot \frac{\exp (-X_c^2/L^2)}{\operatorname{erfc} (X_c/L)} \qquad \text{[III.10]}$$

where $L = 2\sqrt{Dt}$ is the diffusion length, and X_c is the position of the contact. Distances X are counted from the original surface of the wafer, while distances x are counted from the contact, *i.e.*, $X = x + X_c$. Approximating the complementary error function curve by an exponential [III.1] in the vicinity of the contact we have from [III.10] with $(dN/dx)_{Nc} = -N_c/x_o$

$$x_o = \frac{\sqrt{\pi}}{2} L \cdot \frac{\operatorname{erfc} (X_c/L)}{\exp (-X_c^2/L^2)} \approx \frac{\sqrt{\pi}}{4} \frac{L^2}{X_c} \qquad \text{[III.11]}$$

where $x_o/L >> 1$ has been assumed.

We have followed the following procedure in correcting the impurity distribution to evaluate the breakdown voltage: u is calculated from the measured breakdown potential, $E = E_s$, using $F_c = 2.2 \times 10^5$ v/cm and x_o. Inserting this u-value in Fig. 9, the corresponding correction factor $2uv$ is obtained. Inserting this correction factor into Eq. [III.7] the impurity concentration at the contact is found.

For the diffusion lengths occurring in our work, the built in potential was negligible against the breakdown voltage in the range where the correction factor deviated significantly from unity. In the range where the built in potential was not small compared to the breakdown voltage, the impurity concentration was quite homogeneous within the space charge layer and the empirical Eq. [4] of the text was used.

APPENDIX IV

Correction for Enhanced Diffusion Due to an Electric Field

The diffusion current has to be multiplied (4) by the factor $1 + f(c)$ where

$$f(c) = \left(\frac{C^2}{C^2 + 4n_i^2} \right)^{1/2} \qquad \text{[IV.1]}$$

in order to obtain the sum of diffusion and field currents of impurities. This corresponds to an effective diffusion constant

$$D^* = D[1 + f(c)] \qquad \text{[IV.2]}$$

The divergence of the impurity current arises mainly from the space variation of the impurity concentration, and the contribution due to the space variation of the diffusion constant is negligible. This leads to the diffusion equation

$$\partial C/\partial t = D^*\, \partial^2 C/\partial x^2 \qquad \text{[IV.3]}$$

By introducing

$$U = x/2\sqrt{Dt} \qquad \text{[IV.4]}$$

and rearranging one obtains

$$d \ln C^2/dU = -2U/(1 + f) \qquad \text{[IV.5]}$$

This equation has been integrated using the approximation

$$f = 1 \text{ for } C > n_i$$
$$f = 0 \text{ for } C < n_i \qquad \text{[IV.6]}$$

and the boundary conditions

$$C = C_s \text{ at } U = 0$$
$$C = n_i \text{ at } U = U^*$$
$$2C^1_{U=0} = C^1_{U=0} \text{ at } U = U^*$$
$$C = 0 \text{ at } U = \infty \qquad \text{[IV.7]}$$

The solution is

$$C = C_s - (C_s - n_i) \frac{\operatorname{erf} (U/\sqrt{2})}{\operatorname{erf} (U^*/\sqrt{2})} \text{ for } U \leq U^* \qquad \text{[IV.8]}$$

$$C = n_i \frac{1 - \operatorname{erf} U}{1 - \operatorname{erf} U^*} \text{ for } U \geq U^* \qquad \text{[IV.9]}$$

where

$$Cs = n_i \left[1 + \frac{1}{\sqrt{2}} \frac{\exp (-U^{*2}/2) \operatorname{erf} (U^*/\sqrt{2})}{1 - \operatorname{erf} U^*} \right] \qquad \text{[IV.10]}$$

Extrapolating [IV.9] to $U = 0$ we obtain

$$C_o/n_i = (1 - \operatorname{erf} U^*)^{-1} \qquad \text{[IV.11]}$$

Eliminating U^* from the Eq. [IV.10] and [IV.11], we obtain the relation between true surface concentration C_s and apparent surface concentration C_o, plotted in Fig. 4.

Saturation Currents at n-Type Silicon and Germanium Electrodes in Chemical Etching Solutions

D. R. Turner

Bell Telephone Laboratories, Incorporated, Murray Hill, New Jersey

ABSTRACT

The anodic saturation current density of an n-type Si or Ge electrode is considerably larger in chemical etching solutions than in nonetching solutions because the chemical etching process produces excess holes at the surface of the semiconductor. The rate at which these excess holes become available to the electrolytic anodic dissolution reaction is proportional to the chemical etching rate, the surface recombination velocity, and the anodic multiplication factor. Three practical applications of the experiment are indicated: (*a*) a monitor for chemically etching semiconductors; (*b*) a tool to study the process of chemical etching; and (*c*) a simple method for fluoride ion analysis.

The saturation or limiting current observed for the anodic dissolution of n-type Ge or Si in a suitable electrolyte has been shown by Brattain and Garrett (1) and others (2, 3) to be due to a depletion of holes at the electrode surface. Since holes are the minority charge carriers in n-type semiconductors, the saturation current represents the point at which holes are used up in the anodic dissolution reaction as fast as they are made available at the electrode surface. In a solution which does not chemically etch the semiconductor and where there is no hole injection by any process, the saturation current density is given by the following relation:

$$i_s = \alpha e p \left[\left(\frac{D}{\tau} \right)^{1/2} + v_s \right] \qquad [1]$$

where α is the current multiplication factor in the anodic dissolution process (1), e is the electron charge, p is the equilibrium bulk hole density, D is the diffusion constant for holes in the semiconductor, τ is the lifetime of holes in the semiconductor bulk, and v_s is the surface recombination (generation) velocity for holes.

Experimental Results

When the electrolyte does chemically etch the semiconductor, then the saturation current may be many orders of magnitude larger than that given by Eq. [1]. This is illustrated in Fig. 1 where anode potential-current density curves for a 3 ohm-cm n-type Si electrode are given at various chemical etch rates. The Si electrode was shielded from all light whenever light had an effect on the saturation current. When the etch rate is effectively zero, as for example in concentrated (70%) nitric acid, the anodic saturation current density is limited to the value given by Eq. [1] which amounts to about 1 μa/cm^2. If 49% HF is added to concentrated HNO_3, the etch rate of Si increases and so does the saturation current density as shown in Fig. 1. The rate of chemical dissolution of Si was increased stepwise by adding 49% HF, 2 ml at a time, to 100 ml of concentrated HNO_3 and the etch rate was determined from the solution composition-etch rate data of Robbins and Schwartz (4). At the highest chemical etch rate, 0.8 μ/sec, the solution contained 14% by weight 49% HF. The rate of Si dissolution as a result of the electrolytic saturation current is negligible as compared to the chemical etch rate. If the saturation current densities of Fig. 1 are plotted against the chemical etch rate at a constant anode potential, a linear relation is obtained. The significance of this result will be discussed later.

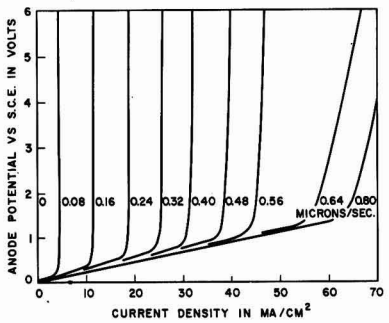

Fig. 1. Anode potential-current density relation for 3 ohm-cm n-type Si at various chemical etch rates, HNO_3-HF solution, unstirred.

Discussion

The results shown in Fig. 1 indicate that, during chemical etching, a large number of holes are produced at the semiconductor surface. In a previous paper (5), it was shown that the chemical etching of silicon or germanium is an electrochemical process, in which cathodic reduction of the oxidizing agent (with hole injection) occurs at cathodic sites while semiconductor dissolution (with hole consumption) takes place at anodic sites. Only a portion of the holes produced by the cathodic reaction is consumed by the anodic dissolution process, and for each Si or Ge atom dissolved, (4-n) excess holes

become available to increase the saturation current, where n is the average number of holes required to dissolve anodically one Ge or Si atom.

The anodic saturation current density of an n-type Si or Ge electrode due to excess holes produced by a chemical etching solution is given by

$$i_s' = \left[\frac{(1-Y)(4-n)}{n} \right] i_{corr.} \qquad [2]$$

where Y is the fraction of the excess holes which are annihilated by recombination and are not used in the electrolytic anodic dissolution process, and $i_{corr.}$ is the corrosion current density which may be calculated from chemical etch rate data with the equation

$$i_{corr.} = 2\,\Delta\,\epsilon\,d \qquad [3]$$

where Δ is the etch rate in cm/sec, ϵ is the electrochemical equivalent in coulombs/g and d is the density in g/cm³. The factor of 2 arises from the assumption that, during uniform chemical etching, the surface is on the average half anode and half cathode.

In most practical chemical etching solutions $i_s' >> i_s$; thus i_s often can be neglected, and the total saturation current may be taken as i_s'. The current multiplication factor, α, during the anodic dissolution of Si and Ge is equivalent to $4/n$. Thus Eq. [2] becomes

$$i_s' = (1-Y)(\alpha-1)\, i_{corr.} \qquad [4]$$

Since α may range (6) from 1 to 2 and Y from 0 to 1, the combined terms $(1-Y)(\alpha-1)$ can vary from 0 to 1. If $(1-Y)(\alpha-1)$ is a constant in a given chemical etching system, then i_s' is directly proportional to the corrosion rate. The anodic saturation current density for n-type Si in HNO_3+HF acid solutions is proportional to the chemical etch rate, as described earlier; therefore, $(1-Y)(\alpha-1)$ is a constant for this etching system. Experimental results such as shown in Fig. 1 give a value of about 0.01 for $(1-Y)(\alpha-1)$ for Si in HNO_3+HF.

When Y and/or α vary with $i_{corr.}$, the relation between $(1-Y)(\alpha-1)$ and $i_{corr.}$ can be determined by measuring i_s' and the chemical etch rate and applying Eq. [3] and [4]. Gerischer and Beck (6, 7) and also Pleskov (8) have shown that α for Ge dissolution decreases rapidly at first with increasing hole injection current density, and then slowly approaches a limiting value of about 1.1 above 50 ma/cm². Gerischer and Beck (7) neglected the recombination effect in the analysis of their results. Pleskov (8), however, states that the recombination of injected holes must be considered when the dissolution current becomes large. Harvey (9) found that the recombination rate of holes injected into n-type Ge by illumination also could be very great. If $(1-Y)(\alpha-1)$ remains relatively constant over the practical range of chemically etching Ge or Si, then i_s' should be directly proportional to $i_{corr.}$ and thus to the etch rate, Δ. This provides a simple method for measuring or monitoring the corrosion rate of Ge or Si in any etching solution. Furthermore, the process is independent of solution composition, temperature, and stirring. When $(1-Y)(\alpha-1)$ is not a constant for a given etching system, the same monitoring technique can be used, but a complete calibration curve is required relating i_s' to Δ. A single electrode can be used to monitor the chemical etch rate of any number of pieces in the same solution provided that the surface area of the monitoring electrode is known and that the conditions of etching are the same for the monitor electrode as they are for the other semiconductor pieces.

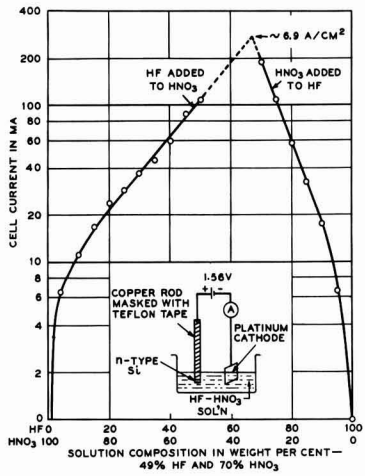

Fig. 2. Etch rate vs. solution composition data for Si in HF-HNO_3 mixtures obtained by monitoring the saturation current on an 0.084 ohm-cm n-type Si electrode (~ 0.04 cm² area) made anode at 1.56 v cell voltage.

Other Applications

When i_s' is proportional to Δ, two other applications are indicated. First, the experiment may be used to study the effect of any variable in chemically etching semiconductors. For example, the relation between i_s' and solution composition has been determined for Si in HNO_3+HF as shown in Fig. 2 where the logarithm of the cell current is plotted against solution composition. A dry cell serves as a power source, as illustrated in the arrangement shown in Fig. 2. On n-type Si, the cell current is determined by the anodic saturation current. The resistance of the Si electrode must be low in such an experiment to avoid an appreciable I^2R heating effect in the electrode. Since the current densities involved at the high etch rates are in the order of amp/cm², it is also desirable that the electrode area be small. The form of the curves shown in Fig. 2 is identical with the results on etching Si in HNO_3+HF obtained by Robbins and Schwartz (4) and also Klein (10).

Another application of the technique may be in fluoride ion analysis. At the present time, there is no simple analytical method for fluoride ion analysis. The idea is to add the sample containing fluoride ion, reduced to a relatively small volume, to a known volume of concentrated (70%) nitric acid. This produces a chemical etching solution for Si. Since the etch rate is directly proportional to the amount of fluoride ion in solution up to about 10% F^- in concen-

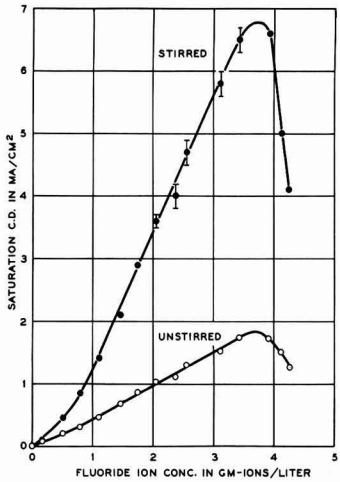

Fig. 3. Effect of adding fluoride ion as KF · $2H_2O$ to conc. HNO_3 on the anodic saturation current density of an n-type Si electrode (0.7 ohm-cm), with and without stirring. Cathode: platinum; cell voltage: 1.56 v, cell in dark.

trated HNO_3 (4, 5), the anodic saturation current density of an n-type Si electrode will be directly proportional to the amount of fluoride in the original sample. The effect of adding fluoride ion as KF · $2H_2O$ to concentrated HNO_3 on the anodic saturation current density of an n-type Si electrode is demonstrated in Fig. 3. Data were obtained with and without stirring and the Si electrode was shielded from all light. A linear relation between i_s' and F^- concentration is observed up to about 3.5 g-ions/liter of fluoride ion with a break at about 0.7 g-ions/liter. When the solution is stirred, the saturation current density oscillates over part of the range, as indicated by the brackets. For this reason, the unstirred condition is preferred. The break in the straight line curve at about 0.7 g-ion/liter F^- is not understood. The decrease in i_s' above 3.5 g-ion/liter F^- is caused by the precipitation of K_2SiF_6 on the silicon electrode and this reduces the effective electrode area. Thus the maximum K^+ ion concentration that can be tolerated in solution is about 3.5 g-ion/liter. Similar results are obtained when sodium or lithium ions are present, but the corresponding fluosilicate precipitate forms at much higher cation concentrations.

Certain anions, such as the acetate ion, in $F^- + HNO_3$ solutions have the effect of reducing the chemical etch rate of Si. Thus these anions will interfere with the method for fluoride in analysis as described. When interfering anions are present in the fluoride sample, their effect on i_s' can probably be determined in the following manner: the sample with the unknown amount of fluoride ion is added to a known amount of HNO_3 and i_s' for n-type Si made anode is determined. Then a known amount of fluoride ion, for example, as KF · $2H_2O$, is added and the new i_s' is measured. The increase in i_s' caused by the known amount of fluoride ion added should serve to calibrate the system regardless of the nature or amount of interfering anions present.

Acknowledgments

The author is grateful to U. B. Thomas and P. C. Milner for their discussion and comments on the manuscript.

Manuscript received Jan. 24, 1961. This paper was prepared for delivery before the Houston Meeting, Oct. 9-13, 1960.

Any discussion of this paper will appear in a Discussion Section to be published in the December 1961 JOURNAL.

REFERENCES

1. W. H. Brattain and C. G. B. Garrett, *Bell System Tech. J.*, **34**, 129 (1955).
2. J. B. Flynn, *This Journal*, **105**, 715 (1958).
3. D. R. Turner, in "Surface Chemistry of Metals and Semiconductors," H. C. Gatos, Editor, John Wiley & Sons Inc., New York (1960).
4. H. Robbins and B. Schwartz, *This Journal*, **106**, 505 (1959).
5. D. R. Turner, *ibid.*, **107**, 810 (1960).
6. F. Beck and H. Gerischer, *Z. Elektrochem.*, **63**, 943 (1959).
7. H. Gerischer and F. Beck, *Z. Physik. Chem. (Frankfurt)*, **24**, 378 (1960).
8. Yu. V. Pleskov, *Doklady Akad. Nauk SSSR*, **132**, 1360 (1960).
9. W. W. Harvev, Private communication.
10. D. L. Klein, Recent News Paper, Electrochem. Soc. Meeting, Chicago 1960.

Growth Steps on Germanium Dendrites

G. R. Booker

Research Laboratories, Westinghouse Electric Corporation, Pittsburgh, Pennsylvania

ABSTRACT

The two main faces of a number of germanium dendrites grown under different conditions have been examined in detail by optical, interference, and electron microscopy. Regular growth steps up to approximately 5000Å in height were observed. The steps were not single, low-index crystallographic planes, nor were they steeply inclined, the gradients h/v ranging from 4 to more than 15. A number of irregular types of growth step were also observed and their formation is discussed. The regions between observable growth steps were shown to contain additional steps too small to be detected individually. The evidence suggests that small steps of this type were also frequently present on well-grown dendrites not possessing observable growth steps.

Curved growth steps on the two main faces of germanium dendrites grown by pulling from a supercooled melt have been observed by several investigators (1-3). Billig (1) reported step heights in the range 500-5000Å, while Bennett and Longini (2) and Longini, Bennett, and Smith (3) gave values from approximately 600Å down to less than 100Å.

Billig (1) using reflection electron microscopy observed on some dendrites small regions between the growth steps which were flat down to the limit of resolution of the method of examination, 50Å. These regions were thought to be true {111} lattice planes on an atomic scale. Longini, Bennett, and Smith (3) employing two-beam interference microscopy concluded that with well-grown dendrites the regions between the growth steps were atomically flat {111} planes.

Longini, Bennett, and Smith (3) proposed the following mechanism for the formation of the steps. Occasional nucleations occur on the two main faces of the dendrite beneath the surface of the melt. Each nucleation is followed by "two-dimensional" growth terminating at the meniscus of the melt, a single atom step thereby being created. As the dendrite is pulled upward through the melt, the meniscus momentarily sticks to the corner of the step, additional atom planes are formed, and the step height is increased. Eventually the meniscus falls back down the side of the dendrite and the procedure is repeated. The sticking of the meniscus was attributed to the high surface free energy associated with the corner of the step.

In order to gain more information concerning growth steps on germanium dendrites, a comprehensive examination has been made of a selected number of normally and highly doped dendrites grown under different conditions and embracing a wide range of step heights. The dendrites were examined by optical microscopy using normal and side illumination and then by two-beam interference microscopy using thallium green and white light. Some of the dendrites were subsequently examined by electron microscopy using normal and shadowed carbon replicas. Both the directly detectable growth steps and the regions between them have been studied in detail.

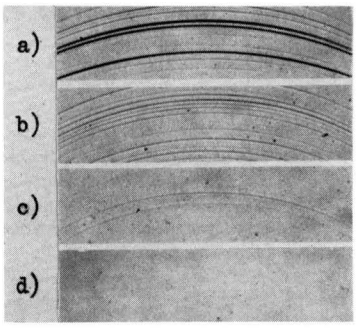

Fig. 1. Portions of the main faces of germanium dendrites. Growth direction is downwards. The dendrite thickening rates are approximately (a) 2.0, (b) 0.40, (c) 0.06, and (d) 0.01 mils/in., respectively. Optical micrographs 100X.

Results

Regular growth steps.—Measurement showed that the dendrites investigated thickened at rates varying from approximately 10 mils/in. to less than 0.01 mils/in. Optical microscope examination (Fig. 1) revealed that the growth steps became less pronounced as the thickening rate of the dendrites decreased, no steps being detected on the dendrites with very small thickening rates. The steps were curved with the convex side toward the pull direction, approximately parallel and at irregular intervals along the length of the dendrite. High-magnification optical micrographs (Fig. 2a) revealed that the steps did not possess sharp edges and varied in width ('h' of Fig. 3) up to approximately 30,000Å.

Examination by interference microscopy using thallium green light revealed growth steps on the dendrites of Fig. 1a, b, and c but not on that of Fig. 1d. With the direction of the fringes set approximately perpendicular to the growth steps, the shift of the fringes on crossing a step (Fig 2b) enabled the step height ('v' in Fig. 3) to be directly deduced. For many of the steps the fringes could be traced

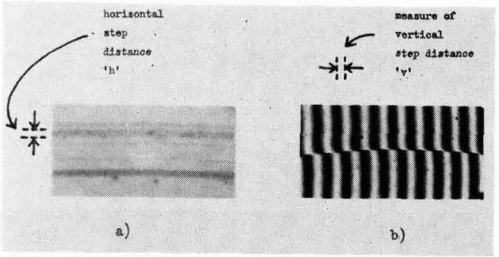

Fig. 2. Regular growth steps similar to those of Fig. 1a. (a) Optical micrograph 1000X, (b) interference micrograph 200X.

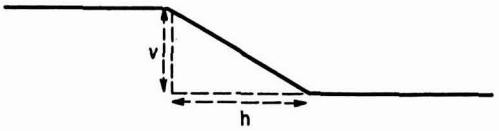

Fig. 3. Diagrammatic cross section through a growth step

across the step and the shift unambiguously determined. Any uncertainties which arose were resolved by using white instead of thallium green light. Step heights up to approximately 5000Å were observed. All the steps were 'forward' steps, *i.e.*, steps tending to increase the thickness of the dendrite. The shape of the interference fringes in transit across a growth step could only be observed clearly when the steps were high. In most of these instances the fringes were approximately straight.

By determining values of 'h' and 'v' for an individual step, the mean slope of the step expressed as h/v could be determined. The values obtained for a number of steps on several different dendrites are plotted against the step height, 'v', in Fig. 4. Although the points do not fall on a single curve, there is a definite trend for the higher steps to be the steeper. The steepest slope recorded was h/v = 4.

By observing growth steps on opposite faces of dendrites containing an even number of twin planes (2), it was possible to ascertain whether the steps were dependent on crystallographic orientation. This is because such dendrites possess faces which are differently oriented crystallographically. Thus, one face has $[\bar{2}11]$ in the growth direction, the so-called "favorable" growth face, and the other has $[2\bar{1}\bar{1}]$ in the growth direction, the so-called "unfavorable" growth face (1,2). Little, if any, difference in the growth steps on opposite faces of such dendrites could be detected.

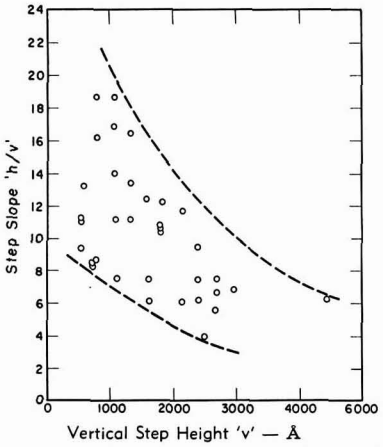

Fig. 4. Variation of the slope 'h/v' of regular growth steps with the height 'v'.

The effect of doping on the growth steps was investigated by examining both normally and highly doped dendrites. No differences in the general form and distribution of the steps on the two types of dendrite were observed. However, the steps on the highly doped dendrites tended in general to be somewhat higher.

The electron microscope studies were performed to reveal any fine detail associated with the growth steps and to detect any smaller steps present. It was disappointing to find, therefore, that when normal carbon replicas from the dendrites were examined, no steps could be detected owing to a complete lack of contrast between the steps and the regions between them. In order to increase the contrast, the replicas were shadowed transverse to the growth steps and at an angle of $\cot^{-1}2$ to the replica surface. Growth steps were then revealed as bands with diffuse edges (Fig. 5) on the dendrites of Fig. 1a and b, but no steps were detected on the dendrites of Fig. 1c and d.

Examination of the replicas in the electron microscope at high magnification showed that the shadowing metal continued over the portions of the replica corresponding to the growth steps, indicating that the steps were less steep than the shadowing angle employed. The contrast in the image arose from slightly thinner layers of shadowing metal on the growth-step areas due to the smaller angles of inclination of these areas to the shadow direction. When similar replicas were shadowed transverse to the steps in the opposite direction, the bands were again revealed but with reversed contrast. When the shadowing angle was reduced to $\cot^{-1}6$, similar results were obtained.

The electron microscope observations confirm the results of the optical and interference microscope studies, namely, that the growth steps do not possess sharp edges and have slopes which are in general less steep than h/v = 6.

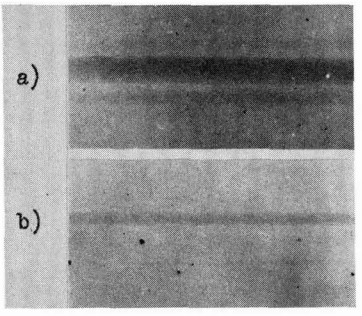

Fig. 5. 'Shadow-cast' carbon replicas from germanium dendrites showing regular growth steps. (a) Dendrite similar to Fig. 1a, (b) dendrite similar to Fig. 1b. Electron micrographs 3000X.

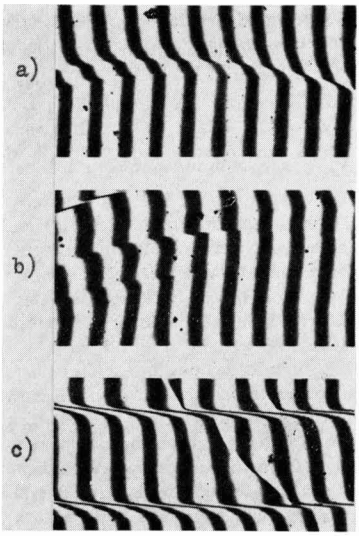

Fig. 6. Irregular growth steps on germanium dendrites, (a) merging, (b) of varying height, and (c) directed along rather than across the dendrite. Interference micrographs 200X.

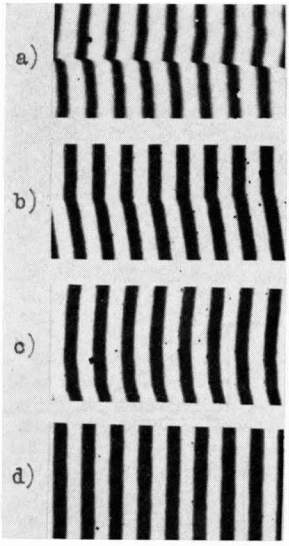

Fig. 7 (a), (b), and (c). Irregular areas on germanium dendrites, (d) regular area on germanium dendrite. Interference micrographs 200X.

Irregular growth steps.—In addition to the regular growth steps, various types of irregular steps were occasionally observed as follows.

(*a*) Curved, slightly nonparallel steps close to one another which merged to give single steps (Fig. 6a). The sum of the heights of the individual steps was usually, but not always, approximately equal to the height of the single steps.

(*b*) Steps which varied in height on traversing the dendrite and occasionally decreased sufficiently to be eliminated part-way across the dendrite (Fig. 6b).

(*c*) Steps which branched from the main step and proceeded in directions more along than across the dendrite (Fig. 6c). These branches either decreased in height until eliminated or joined other main steps crossing the dendrite.

Regions between growth steps.—Examination of the regions of the dendrites between the growth steps by both optical and electron microscopy did not enable any deviation from flatness to be detected. However, examination of interference micrographs from almost all of the dendrites on which growth steps were observed revealed that the fringes between the steps were not always precisely regular. The irregularities comprised fringes which: (*a*) changed direction after having traversed an observable growth step (Fig. 7a), (*b*) changed direction without having traversed an observable growth step (Fig. 7b), (*c*) were slightly curved (Fig. 7c), and (*d*) were of nonuniform spacing across the width of the dendrite.

Dendrites without observable growth steps gave fringes which were often regular (Fig. 7d) over relatively large distances.

Discussion

The investigation has shown that the regular growth steps on the two main faces of germanium dendrites do not possess sharp edges and are far from steep. The step slopes have h/v values which vary from 4 to more than 15, corresponding to inclinations of approximately 15° and less than 4°, respectively, with the surface of the dendrite.

The curved nature of individual steps and the range of slope values show that the faces of the growth steps are not parallel to any single crystallographic plane. In particular, none of the step faces are single {111} planes which would require h/v = 0.36.

The straight interference fringes crossing the more pronounced steps indicate that each of these steps was approximately uniform in slope. However, whether these steps were single steps or consisted of a number of steps too small to be individually detected by the interference microscope, *i.e.*, less than approximately 100Å in height, could not be determined.

If the steps are single steps, then because the shoulders of the steps vary between approximately 165° and 176°, it is unlikely that the sticking of the meniscus can be entirely accounted for by an increase in surface energy at the shoulder, as suggested by Longini, Bennett, and Smith (3). On the other hand, if the steps consist of a number of smaller steps, then not only will the number of shoulders be increased but the shoulder-angles will be decreased, rendering the theory of Longini, Bennett, and Smith (3) more admissible.

An additional factor which may contribute to the sticking and falling back of the meniscus is the effect of the two side-faces of the dendrite, which, although narrow, are extremely irregular and highly

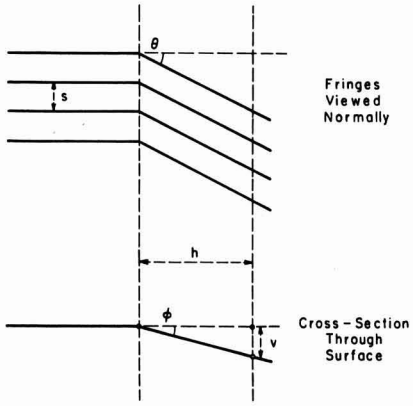

Fig. 8. Diagram showing the change in direction, 'θ', of the interference fringes due to a change in slope, 'φ', of the surface.

faceted. It is almost certain that the meniscus will move in a nonuniform manner over these faces, and this in turn could influence the motion of the meniscus over the two main faces of the dendrite.

The irregular growth steps observed consisted of three main types. The formation of the first type (Fig. 6a) is doubtless associated with a meniscus which has moved down the dendrite in a slightly different manner depending on its position across the width of the dendrite. In other words, these steps resulted from nonuniform sticking of the meniscus.

The second type (Fig. 6b) is thought to have arisen as follows. Nucleation occurred near the left side of the dendrite. This was followed by "two-dimensional" growth, the layer moving to the right across the dendrite, but stopping short of the opposite side. This was repeated, successive layers terminating after having traveled progressively shorter distances. A step at the meniscus of varying height was thus built up. The steps running down the face of the dendrite were, in this instance, too small to be individually detected.

The third type (Fig. 6c) is thought to have occurred in a similar manner except that the successive layers moving across the dendrite terminated at the same places, the result being a relatively large step running down the dendrite. Although the exact conditions for the second and third type of step are not known, it seems probable that both were due to pronounced temperature gradients across the dendrite.

Consideration of the irregular growth steps has revealed that growth steps too small to be individually detected sometimes occur. Further evidence for the presence of such extremely small steps is provided by the irregularities in the interference fringes between observable growth steps. The magnitude of the surface irregularities which give rise to some of these fringe irregularities has been ascertained as follows.

Suppose that the surface of a dendrite changes slope abruptly at a particular point along its length, the new slope making an angle ϕ with the old slope (Fig. 8). The interference fringes will also change direction at this point. If the fringes are initially perpendicular to the line where the change in slope occurs (Fig. 8), the new fringe direction makes an angle θ with the old fringe direction, the initial fringe spacing is 's' microns and the light has wavelength 'λ' microns, then it can readily be shown that

$$h/v = \cot\phi = \frac{2s}{\lambda}\cot\theta$$

For a typical value of $s = 30$ and with $\lambda = 0.55$ for thallium green light, $2s/\lambda = 109$. Substitution then shows that for fringe deviations 'θ' of 3° and 10°, $h/v = 2080$ and 618, respectively, and $\phi = 0.028°$ and 0.093°, respectively. These values correspond to changes in thickening rates of 38 and 127 atom steps/mil length of dendrite, respectively.

The equation can also be used to calculate the slopes of the more pronounced growth steps because the angle through which the fringes are deviated on traversing these steps can be measured readily. For a typical value of $\theta = 85°$, $h/v = 9.5$ and $\phi = 6.0°$.

Clearly, small deviations from atomic flatness could be present between growth steps without being detected by the interference microscope. Thus, a change in fringe direction of $\theta = 1°$, which would be extremely difficult to detect, corresponds to a change in thickening rate of 13 atom steps/mil.

A further limitation is that, although straight, parallel, and equally spaced fringes indicate a uniform slope, they do not enable the inclination of the slope with respect to the (111) plane to be determined. This is because when the interference microscope is used, the direction of the fringes is set by selecting a convenient, but arbitrary, reference plane.

An indication of the amount by which the regions between the observable growth steps deviate from the (111) plane can be obtained, however, by comparing the total height of all the observable growth steps on both sides of the dendrite with the total increase in thickness. When this comparison was made for the highly doped dendrite of Fig. 1a, the observable growth steps only accounted for approximately 40% of the total increase in thickness. The remaining 60% must have occurred along the regions between the observable growth steps without being detected. Clearly, in this instance these regions deviated markedly from the (111) plane.

The examination has shown, therefore, that for dendrites with observable growth steps, the regions between the steps are not usually atomically flat {111} planes. For dendrites without observable growth steps, in many instances it was not possible to detect deviations from atomic flatness. However, it is presumed that steps in the size-range between the limit of detection of the interference microscope and atomic flatness were nevertheless frequently present.

If it is assumed that no reverse steps down to atomic levels occur on the dendrites, the mean deviation from atomic flatness can be calculated directly from the measured thickening rate. Thus, for a well-grown dendrite with a thickening rate of, say, less

than 0.01 mils/in., the calculated deviation is less than 0.79 atom steps/mil for both sides, *i.e.*, less than 16 atom steps/mm/side. However, if reverse steps do occur when extremely small step-heights are involved, then deviations from atomic flatness in excess of the calculated value could be present.

Although the two main faces of well-grown germanium dendrites may not always be precisely atomically flat {111} planes, they are thought to represent by far the closest approach to such surfaces yet obtained.

Summary and Conclusions

1. A number of normally and heavily doped germanium dendrites grown under different conditions have been examined in detail by optical, interference and electron microscopy.
2. The two main faces of the dendrites exhibited a range of growth steps varying from pronounced to not detected.
3. Regular growth steps running across the width of the dendrites possessed heights varying from approximately 5000Å down to less than 100Å, the limit of detection of the interference microscope.
4. The steps were shallow, the gradients, h/v, varying from 4 to more than 15.
5. Irregular growth steps comprising merging steps, steps of varying height, and steps running more along than across the dendrite were also sometimes present.
6. The interference fringes between growth steps were frequently irregular, indicating the presence of additional growth steps too small to be individually detected.
7. For dendrites without observable growth steps, the interference fringes were often regular over relatively large areas. However, it is believed that extremely small growth steps were again often present.

Acknowledgments

The author wishes to thank Dr. R. Stickler for his willing cooperation with the electron microscope studies and Drs. H. F. John and J. W. Faust, Jr., for numerous stimulating discussions. Thanks are also due to several colleagues especially Drs. A. I. Bennett and S. O'Hara, for supplying the dendrites.

Manuscript received Jan. 3, 1961. This paper was prepared for delivery before the Houston Meeting, Oct. 9-13, 1960. This work was performed on Contract No. AF33(600)-39378 BPSN 9-(8-4608)-42019, Wright Air Development Center.

Any discussion of this paper will appear in a Discussion Section to be published in the December 1961 JOURNAL.

REFERENCES

1. E. Billig, *Proc. Roy. Soc.*, **A229**, 346 (1955).
2. A. I. Bennett and R. L. Longini, *Phys. Rev.*, **116**, 53 (1959).
3. R. L. Longini, A. I. Bennett, and W. J. Smith, *J. Appl. Phys.*, **31**, 1204 (1960).

High-Temperature Phase Studies in the Tantalum-Boron System between Ta and TaB

James M. Leitnaker and Melvin G. Bowman

University of California, Los Alamos Scientific Laboratory, Los Alamos, New Mexico

and Paul W. Gilles

Department of Chemistry, University of Kansas, Lawrence, Kansas

ABSTRACT

Phase relationships in the tantalum-boron system between Ta and TaB have been studied. A phase diagram of the solid portion of the system has been determined and is shown. Two three-phase equilibria exist within the system: (*a*) Ta-Ta_2B-Ta_3B_2 at 2040° ±30°C, and (*b*) Ta_2B-Ta_3B_2-TaB at 2180° ±20°C. The chemical composition of the Ta_2B phase is $Ta_{2.4\pm0.2}B$. The composition of the Ta_3B_2 phase is $Ta_{1.60\pm0.05}B$. The melting point of TaB lies above 2800°C. The extreme slowness of reactions within the system has been investigated qualitatively, and the necessity for seeding at temperatures in the neighborhood of 2000°C has been noted. The results disagree markedly with data previously reported in the literature.

During a preliminary investigation of tantalum as a possible crucible material for studies of boride systems, a new phase was discovered in an x-ray pattern of some of the material. Attempts to characterize this new phase and to clarify the unusual behavior of the tantalum-boron system led to the high-temperature phase study reported here.

Kiessling's (1) work characterized five phases in the tantalum-boron system. Of these five phases, three lie within the range of study of this work. The α-phase is a solid solution of boron in cubic tantalum. The β-phase was determined to have tetragonal symmetry with a space group of D_{4h}^{18}-*I*4/mcm and lattice constants of $a_o = 5.778$Å, $c_o = 4.864$Å, $c_o/a_o = 0.842$, and, since it was isomorphous with a number of other borides of the formula Me_2B, he concluded it should have the formula Ta_2B. Kiessling's γ-phase was obtained homogeneous in preparations with a

boron content of 50 at. %. He concluded that the material had orthorhombic symmetry with a space group of D_{2h}^{17}-Cmcm and lattice constants of $a_o = 3.276$Å, $b_o = 8.669$Å, $c_o = 3.157$Å.

Brewer, Sawyer, Templeton, and Dauben (2) were in essential agreement with Kiessling except for the discovery of an additional phase, TaB_m, which has recently been shown to be Ta_3B_2.

Nowotny and Wittmann (3) and, independently, Eick, (4) succeeded in indexing the Ta_3B_2 phase, reporting tetragonal symmetry with a space group of D_{4h}^5-P4/mbm and lattice constants of $a_o = 6.18_4$Å, $c_o = 3.28_6$Å, $c_o/a_o = 0.531$.

At the conclusion of the experimental work reported here, Nowotny, Benesovsky, and Kieffer (5) published a phase diagram of the tantalum-boron system. There are major areas of disagreement between that work and the work reported here.

The present work covers a study of the phase relationships in the tantalum-boron system in the solid portion of the system between Ta and TaB. The intermediate compounds were investigated. Their regions of stability and slowness of reaction were demonstrated. The necessity for seeding in some cases to obtain equilibrium within a reasonable time at 2000°C was shown.

Experimental

The experiments consisted of heating pressed ½ in. diameter cylinders of intimate mixtures of Ta and and TaB or TaB_2. After the samples had cooled, they were subjected to chemical, x-ray diffraction, and metallographic analysis.

Nearly all of the heatings reported here were done in an "eddy current concentrator" or just "concentrator." These concentrators (see Fig. 1 for a typical example) were designed at Los Alamos by Donald E. Hull of Group CMB-7, based on principles described by Northrop (6) and by Babat and Losinsky (7). These concentrators have the very useful property of increasing the efficiency of linking to a crucible by the coils of an induction heater. Various modifications, such as a shutter to protect the sight glass in the present work, have been made by users of these concentrators, but the essential features remain those worked out by Hull.

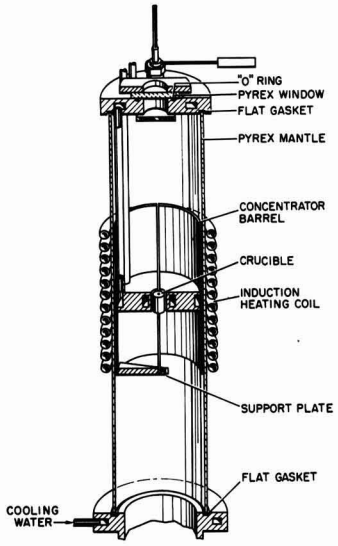

Fig. 1. Typical eddy current concentrator

Temperatures were measured with a L&N optical pyrometer in a sight hole in a crucible or in a hole drilled in a pressed and sintered plug. The pyrometer was calibrated against a standard pyrometer which had been calibrated both at the Bureau of Standards and at Argonne National Laboratories. Corrections were made for the transmissivity of the optical window and the front-surface mirror.

X-ray powder patterns were obtained on both a 114.59 mm Debye-Scherrer camera and a Norelco diffractometer. Nickel-filtered, copper radiation was used in all cases, ($K\alpha_1 = 1.54050$, $K\alpha_2 = 1.54434$). Lattice parameters were calculated on an IBM-704 computer by the method of Hess (8). When diffractometer patterns were obtained on plugs, the surface of the plug was ground on a surface grinder to eliminate a surface layer of tantalum, arising from a preferential evaporation of boron. This method was not satisfactory for all purposes, because it only imperfectly removed the tantalum layer. Hence some samples were ground in a hardened steel mortar to −200 mesh after which diffractometer patterns and film patterns were obtained.

Crucibles used were either of tantalum or, when hydrogen gas was used, of molybdenum. Plugs were supported in the crucible on a many-pronged "crown" to minimize contact with the crucible.

Mixtures of metal and boride were used instead of the elements, as previous investigators had done, to eliminate the uncontrollable, rapid, and large temperature rise associated with the synthesis. The cylinders, or plugs, were pressed in a ½ in. steel die and were ¼ to ⅜ in. in length. The starting borides were made by reaction of −325 mesh tantalum powder and amorphous boron. Analyses (9) of these powders and of five samples of borides are given in Table I. Analysis of the Ta_2B phase was not straightforward and a special technique had to be developed (10). By spectrographic analysis, the major impurities in the tantalum and boron powders were iron (200 ppm), Nb (500 ppm), Si and Ca (0.1-1%). The other impurities were negligible. The balance was presumed to be oxygen.

Unless specifically noted otherwise, all heatings were performed in a partial atmosphere of argon. The argon was purified by passing it over heated uranium powder which had previously been hydrided and then dehydrided.

Table I. Analyses of materials, %

Material	−325 Mesh Ta	Amor. B	TaB-1	TaB-2	TaB-3	TaB-4	TaB-5
Ta	98.3	—	95.1	93.3	94.6	93.64	94.7
B	—[a]	97.3	4.9	5.20	5.35	5.24	5.3
C	—	0.26	—	—	—	—	—
O	0.15	—	—	—	—	—	—
B/Ta	—	—	0.86	1.00	0.95	0.94	0.94

[a] A blank indicates the analysis was not made.

Results and Discussion

Qualitative rates of reactions.—Although amorphous boron and tantalum powder mixed together react rapidly (at about 900°C) with the evolution of a great deal of heat, the reaction of tantalum metal with TaB is extremely slow. Three examples may be given to illustrate the slow reaction rate. Equal proportions of 1-μ tantalum metal and −200 mesh TaB were ball-milled together for 24 hr. The resulting mixture was then pressed into pellets and heated at 1200°C for 1800 hr in sealed quartz containers under vacuum. At the end of this time faint lines arising from Ta_3B_2 could be detected in x-ray patterns of the material; however, the reaction by no means had gone to completion. Some oxide contamination was also evident. Second, a plug of over-all composition Ta_3B_2 was heated for 5 hr at 2000°C with intermediate cooling and pulverizing before equilibrium was established. Third, a plug of over-all composition $Ta_{1.9}B$ was heated for 7 hr at 2150°C before equilibrium was established.

By adding a metallic sintering aid, such as iron or cobalt, to these mixtures equilibrium could be established in a shorter length of time. Reaction in plugs heated for an hour above 1900°C which contained these metals had gone substantially to completion in every case. Hydrogen gas also had a favorable effect on the attainment of equilibrium. A sample of composition $Ta_{2.44}B$ heated at 2180°C in oxygen-free, dried hydrogen reached apparent equilibrium within 1 hr, whereas a second identical sample heated at the same temperature in argon obviously had not.

It is apparent that one must be careful in order to attain equilibrium within this system. The relatively short times of heating of previous investigators [*e.g.*, Kiessling (1) heated for 150 hr at 1100°-1200°C] must have been responsible for their not attaining equilibrium. In all cases of doubt in this study, equilibrium was approached from two directions.

Compositions and lattice parameters of the phases.—The phase heretofore called Ta_2B has been determined by chemical means to have a composition of $Ta_{2.4}B$. In order to determine this composition a series of heatings of Ta + TaB mixtures richer in tantalum than Ta_2B was made at 2190°C for periods of 1-2 hr. Following the heating the samples were powdered and x-rayed. Relative intensity measurements of the strong lines of each phase, although somewhat scattered, indicated the composition could not be $Ta_{2.0}B$ but, more reasonably, $Ta_{2.4}B$. Another experiment tending to confirm this was performed in which a plug of over-all composition $Ta_{1.9}B$ was heated a total of 27 hr at 2150°C with four intermediate grindings. At the end of this time the composition had shifted to $Ta_{2.16}B$ and gave an intensity ratio (Ta_3B_2/Ta_2B) of 0.185.[1] All the data are consistent with a composition of $Ta_{2.4\pm0.2}B$ for the Ta_2B phase.

The composition of the Ta_3B_2 phase was set at $Ta_{1.60\pm0.05}B$. The definitive experiment was the heating of a plug of synthetic composition $Ta_3B_{2.00}$ for a total of 9 hr at 2000°C with three intermediate pulverizings. At the end of this time the powdered material was single phase, within the limits of the diffractometer measurement, and the analysis indicated a composition of $Ta_{1.60}B$. A break in the lattice parameters between the third and fourth heatings, slightly outside the limits of error of the parameters, may indicate the compound crossed a narrow homogeneity range during the final heating (see Table II, No. 1 and 2.)

Lattice parameters determined for pure and impure Ta_2B and Ta_3B_2 are summarized in Table II. Lattice parameters were obtained on both sides of the regions of homogeneity. Judging from these parameters and from the chemical analysis of the samples, both intermediate phases have narrow ranges of homogeneity. The extent of impurities such as carbon, oxygen, and nitrogen in the samples are unknown but must be small, according to the analyses. Ten samples of compositions near Ta_2B analyzed (total of boron plus tantalum) 99.87% with a standard deviation of 0.072%. The parameters for Ta_3B_2 reported here are somewhat lower than those of Nowotny and Wittmann (3) and outside of the limit of error. Values for Ta_2B obtained in this work agree with those of Kiessling (1) but are lower than those of Brewer *et al.* (2). No one has investigated the

[1] All tantalum borides lose boron by preferential vaporization during heating. One could also lose tantalum, however, by fractionation during the grinding operations, since the tantalum is maleable, tends to form flakes during grinding, and hence will not pass quantitatively through the sieve.

Table II. Lattice parameters of Ta_2B and Ta_3B_2

No.	Compound	Lattice parameter a_0, Å	Lattice parameter c_0, Å	Impurity[a]	Remarks
1	Ta_3B_2	6.1760±0.0006[b]	3.28445±0.00004	None	This work; 3rd heat of this material.
2	Ta_3B_2	6.1747±0.0005	3.28404±0.00002	None	This work, reheat of above sample.
3	Ta_3B_2	6.171±0.001	3.2834±0.0005	Fe	This work
4	Ta_3B_2	6.1754±0.0010	3.2845±0.0005	Co	This work
5	Ta_3B_2	6.18_4	3.28_7	?	Nowotny (3)
6	Ta_2B	5.7862±0.0005	4.8656±0.0001	Co[c]	This work
7	Ta_2B	5.7795±0.0005	4.8645±0.0003	None	This work
8	Ta_2B	5.778	4.864	?	Kiessling (1)
9	Ta_2B	5.785±0.003	4.867±0.003	?	Brewer (2)

[a] Refers only to known, substantial impurities as added Co.
[b] In general, statistical errors of the individual lattice parameters were of this order. Larger errors represent a range of lattice parameter calculations on a number of samples. No correction was made for refraction.
[c] No investigation was made of the effect of Fe on the lattice parameter.

Table III. Experiments to establish three-phase line Ta-Ta_2B-Ta_3B_2

No.	Starting phases	Synthetic comp.	Temp, °C	Time,[a] hr	Final phases	Remarks
2	Ta, TaB_2	Ta_5B	2000	1	Ta, Ta_3B_2	b
5	Ta, Ta_3B_2	Ta_5B	2050	1	Ta, Ta_2B	b
6, 7, 8	Ta, Ta_2B	Ta_5B	2000	1	Ta, Ta_2B	b
			1980	1		
			1975	3		
14	Ta, Ta_2B + ~5% of powder containing Ta_3B_2	Ta_5B	2015	1	Ta, Ta_3B_2	b, c
13	Ta, Ta_3B_2	Ta_5B	2030	0.7	Ta, Ta_2B	b, c
16	Ta, TaB_2	$Ta_{1.9}B$	2000	2	Ta, Ta_3B_2	b, d
17	Ta, Ta_3B_2	$Ta_{1.9}B$	2050	1	Ta, Ta_3B_2	b, c
19	Ta, Ta_3B_2	$Ta_{1.9}B$	2140	1	Ta, Ta_3B_2, Ta_2B	b
23	Ta, TaB_2	$Ta_{1.9}B$	2035	0.5	Ta, Ta_2B, (TaB, Ta_3B_2—weak)	c

[a] All heatings were done in argon; the plugs contained ~1% metallic Co.
[b] Examined on diffractometer after surface grinding.
[c] Entire plug powdered in a hardened steel mortar to pass 200 mesh screen and x-ray film taken.
[d] Plug bisected with diamond cut-off wheel and examined metallographically.

effect of oxygen, nitrogen, or carbon on the lattice parameters of these compounds and discrepancies might be attributable to this effect.

Three-phase equilibria: Ta-Ta_2B-Ta_3B_2.—Previous work, (1, 2) as well as that reported here, has shown that when tantalum and boron powders are mixed together in a proportion around Ta_2B and heated to about 900°C a violent reaction takes place with evolution of a large amount of heat. On examination a three phase mixture is found: Ta, Ta_2B, and TaB. On the other hand, when TaB and Ta are mixed together in the same proportions, no such reaction takes place at 900°C; this mixture must be heated to 1700°-1800°C before reaction takes place at a reasonable rate. At equilibrium, the phases found in the latter case are always Ta and Ta_3B_2.

Further evidence indicated that on heating a mixture of Ta + TaB to temperatures around 2100°C the phase Ta_2B was produced. These experiments indicated that Ta_2B is stable only at high temperatures, whereas Ta_3B_2 is stable at low temperatures, contrary to the hypothesis of Brewer, *et al.* (2).

In Table III data are given which were used to establish the invariant line (at constant pressure) of Ta-Ta_2B-Ta_3B_2 at 2040° ± 30°C. These data were selected from a larger group of 27 experiments. Other than the invariant temperature itself, the most interesting facet of the series is the necessity for seeding at these temperatures in order to establish equilibrium. Heating No. 6, 7, and 8 indicated a sample containing Ta + Ta_2B would not transform to the Ta_3B_2 + Ta phase region in some 5 hr of heating well below the stated ternary line. On the other hand, the addition of a small amount of the phase stable at low temperatures (Ta_3B_2) allowed the transformation to take place within something less than an hour. There was some evidence, although not clear-cut, that seeding helped obtain the high-temperature phase at temperatures slightly above the ternary line.

Nowotny and co-workers (5) obtained melting of their samples in this region, quoting temperatures as low as 1800°C. No melting behavior was observed in any of the experiments reported here performed below 2200°C. Neither was a three-phase line reported by them. They appeared to find peritectic melting of Ta_2B at about 1920°C, but this work indicates Ta_2B is not stable at this temperature. Brewer's hypothesis (2) that Ta_3B_2 is stable at high temperatures while Ta_2B is stable at low temperatures seems also to be refuted. At one place Nowotny and coworkers stated a melt was contaminated with ThO_2. It seems possible that thoria was used as a stand or container and eutectic or ternary melting was observed between the thoria and boride phase or phases. It is not at all clear how they "confirmed" the Ta_2B phase.

The formation of the high-temperature stable phase Ta_2B from a reaction of tantalum and boron powders beginning at 900°C is extremely interesting. This reaction is clearly a nonequilibrium one. One may speculate that enough heat is liberated in local areas of the mixture to allow the phase to be formed. No Nb_2B phase is known. We have been unable to prepare Nb_2B even by seeding a mixture of Nb + NbB with a little Ta_2B and heating rapidly to 2040°C. During every attempt melting always took place.

Three-phase equilibria: Ta_2B-Ta_3B_2-TaB.—Ta_3B_2 is unstable at high temperatures, disproportionating to Ta_2B and TaB at 2180° ± 20°C. The difficulties in establishing the temperatures at which this three-phase equilibrium occurs are not nearly as great as for the lower temperature Ta-Ta_2B-Ta_3B_2 equilibrium.

The temperature of heating will influence what phases show up in samples of composition between Ta_2B and Ta_3B_2, and plugs of composition intermediate between the two phases heated above 2040°C showed Ta_2B and Ta_3B_2 after equilibrium was established. Above 2180°C the phases Ta_2B and TaB were found in the quenched sample. More definitive experiments were as follows.

Two ½ in. diameter x ⅛ in. high plugs of composition $Ta_{1.4}B$ were pressed. About 1% cobalt was added. The plugs are designated A and B. Plug A was heated for 1 hr at 2000°C, where previous experiments indicated the reaction to form Ta_3B_2 is at least 90% complete, in the presence of cobalt, within

this time. Then, without cooling, the temperature was raised to 2195°C and left there for 1 hr. The sample was quenched by turning off the power. X-ray evidence indicated the major phases present after quenching were Ta_2B and TaB. (Very faint traces of other phases were indicated also.) Plug B was heated to 2160°C for 1 hr, quenched, and examined. Phases present were Ta_3B_2 and TaB. Plug A was repressed and heated to 2190°C within 3 min. The temperature was raised to 2210°C, then lowered to 2190°C and left there to eliminate any Ta_3B_2 formed during heat-up. The temperature was then lowered slowly to 2160° where it remained 30 min, and the sample was quenched and examined. Phases observed in the powder pattern were Ta_2B, Ta_3B_2, and TaB. The direction in which the reaction was proceeding is clearly to the low-temperature phase.

The phase diagram of Nowotny, *et al.* (5) indicating peritectic melting behavior for Ta_3B_2 around 2100°C does not appear justified.

Melting behavior.—Only two incomplete data have been obtained; however, they are of interest. Although Nowotny and co-workers (5) apparently found melting of the TaB phase at 2500°C, a bare plug heated in a concentrator to 2780°C (observed in a drilled sight hole) showed no evidence of melting. Because of the nature of the temperature measurement the actual temperature would be expected to be somewhat higher than this. Hence, the melting point of TaB must be greater than 2800°C.

A bare plug of over-all composition Ta_2B was observed to melt at 2365°C, as observed in a drilled sight hole just as the hole filled with liquid. The power was immediately shut off. On cooling the plug was shaped like a mushroom, with the bottom unmelted. Both the melted top and the unmelted bottom were x-rayed. Both films showed the following phases: Ta, Ta_2B, and TaB. In the unmelted portion the Ta_2B phase was quite spotty, apparently caused by fairly large crystallites.

Since the composition lies to the right of the $Ta_{2.4}B$ line in the phase diagram, one feels that the tantalum phase should not appear so strongly unless there were a tantalum-rich liquid or tantalum solid at the high temperature which persisted through the cooling process. If there were a melting point maximum, there would be no reason for tantalum to appear. Obviously, considerably more work is necessary in this range of the system.

Conclusions

Findings of this work are summarized in part in the phase diagram of Fig. 2. Of additional interest are the surprisingly slow rates of reaction within the Ta-TaB system and the necessity for seeding demonstrated in the neighborhood of 2000°C. This latter type of behavior has apparently not been reported previously at these temperatures.

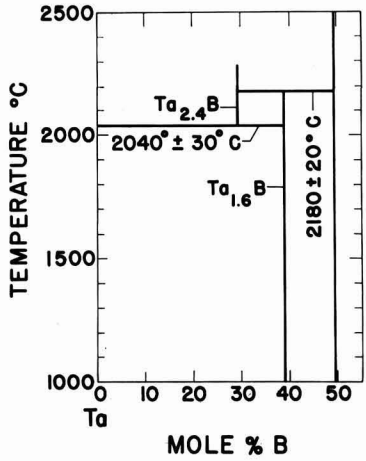

Fig. 2. The Ta-TaB phase diagram

The discrepancy between this work and that of previous authors can be ascribed in large part to failure on the part of previous authors to reach equilibrium. In the case of Nowotny, *et al.* (5) the reason is more difficult to pin-point but may lie in the fact that thoria seemed to be a contaminant in their system.

Acknowledgments

The authors are indebted to Mrs. Mary Jane Jorgensen and Mr. Bobby Lee for their assistance with numerous x-ray films, to Dr. Owen H. Kriege for his competent analytical work, and to Dr. Roy L. Petty for assistance with the IBM-704 calculational program and many helpful discussions.

Manuscript received Nov. 28, 1960. This work was done under the auspices of the AEC and abstracted in part from the doctoral thesis presented by J. M. Leitnaker to the University of Kansas.

Any discussion of this paper will appear in a Discussion Section to be published in the December 1961 JOURNAL.

REFERENCES

1. Roland Kiessling, *Acta Chem. Scand.*, **3**, 603 (1949).
2. Leo Brewer, D. L. Sawyer, D. H. Templeton, and C. H. Dauben, *J. Am. Ceram. Soc.*, **34**, 173 (1951).
3. Hans Nowotny and A. Wittmann, *Monatsh. Chem.*, **89**, 220 (1958).
4. Harry A. Eick, J. M. Leitnaker, and P. W. Gilles, Unpublished work.
5. Hans Nowotny, Friedrich Benesovsky, and Richard Kieffer, *Z. Metallk.*, **50**, 417 (1959).
6. E. F. Northrop, *Trans. Am. Electrochem. Soc.*, **25**, 69 (1919).
7. G. Babat and M. Losinsky, *J. Appl. Phys.*, **11**, 816 (1940).
8. J. B. Hess, *Acta Cryst.*, **4**, 209 (1951).
9. O. H. Kriege, "The Analysis of Refractory Borides, Carbides, Nitrides, and Silicides," Los Alamos Scientific Laboratory Report, LA-2306 (1959).
10. O. H. Kriege, Unpublished work.

Polarography of Bismuth in Molten Bismuth(III) Chloride

L. E. Topol and R. A. Osteryoung

Atomics International, A Division of North American Aviation, Inc., Canoga Park, California

ABSTRACT

A polarographic study has been carried out between 240° and 350° on solutions of bismuth in molten bismuth(III) chloride. The bismuth was introduced coulometrically by reduction of $BiCl_3$ at a graphite electrode. Polarograms yielded an anodic wave indicating the oxidation of a soluble entity; anodic limiting currents were directly proportional to the concentration of bismuth up to about 0.2 mole % Bi in $BiCl_3$. From the polarographic behavior it was concluded that the electrode reaction is probably reversible, and although a log plot analysis was not conclusive (n values of 1.5-1.8 were obtained), a subhalide BiCl is considered a probable entity. An activation energy for the current limiting process was determined as 5.8 ±1.1 kcal.

Although there have been numerous applications of polarography to fused salt systems, no application of this technique has as yet been made to metal-metal salt systems. As a portion of an electrochemical study of such systems, it was decided to investigate the polarographic behavior of bismuth in bismuth trichloride in order to determine if normal polarographic behavior would be observed and if evidence could be found relating to the species present.

Experimental

Materials.—The bismuth chloride was of reagent grade and was further purified as described elsewhere (1). Bismuth metal used in the reference half-cells was 99.99% pure; the molten metal was filtered *in vacuo* to remove any oxide present. The graphite electrodes were made from quarter-inch, ultra-high purity spectroscopic rods and were baked under vacuum and argon before use. The platinum and tungsten microelectrodes were 0.020 in. diameter high-purity wire; the tungsten electrodes were cleansed of oxide by immersion in molten sodium nitrite. The working anode was an 0.050 in. diameter tungsten wire wound into a helix at one end. The argon was purified by passage over calcium turnings at 600°C and through silica gel.

Apparatus and procedure.—The experimental cell used in the bulk of the work is shown in Fig. 1. The half-cells contained approximately equal levels of melt. The reference electrode compartment, A, usually consisted of a 0.5 mole % solution of bismuth metal in $BiCl_3$; a graphite electrode served as the inert electrode. This compartment was separated from the center cell compartment by an asbestos fiber, B. The center compartment contained the microelectrodes, C, which were made of tungsten and/or platinum, sealed into glass as indicated, and a graphite electrode, D. The lengths of the microelectrodes were measured with a binocular microscope. The graphite electrode served as the cathode in the constant current electrolysis which coulometrically introduced the reduced bismuth species into the center compartment. The third compartment, in which a tungsten spiral, E, served as the working anode for the constant current electrolysis, was separated from the center compartment by an ultrafine glass frit, F. The cell was constructed so that argon could be bled slowly over the reference and center compartments and out through a sulfuric acid bubbler and so that the chlorine generated in the third compartment could be vented. The cell was placed in a molten metal bath in a 5 in. crucible furnace, the temperature of which was regulated by a West Gardsman controller to an estimated ±1°C. The temperature of the system was read with a mercury thermometer immersed in the metal bath.

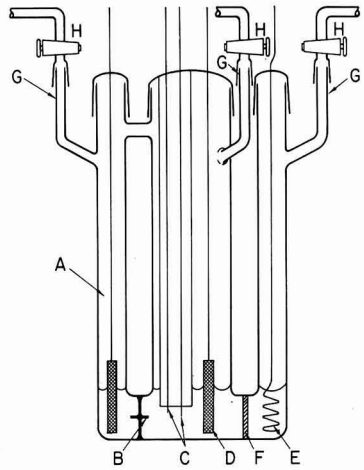

Fig. 1. Experimental cell

With the electrodes in place, the cell was filled in a dry box. Weighed amounts of purified bismuth (III) chloride and bismuth metal were added to the cell through the side arms, G. Stopcocks (H) were attached to the side arms, the cell was removed from the dry box and evacuated; argon was then admitted to the system.

The polarograms were recorded with a Sargent Model XXI polarograph. The usual polarization rate was 1.24 mv/sec. A Sargent Coulometric Source was used for the coulometric addition of bismuth to the center compartment.

Results and Discussion

Polarograms were run at both platinum and tungsten microelectrodes. The useful voltage span obtained in pure bismuth (III) chloride at 300°C with tungsten microelectrodes was about 0.8 v while with platinum microelectrodes a span of about 0.5 v was found. The cathodic limiting reaction, which occurred at about zero volts against the bismuth-bismuth (III) chloride reference, represents the reduction of bismuth (III). The anodic limiting reaction at the tungsten electrode is the evolution of chlorine, while at the platinum electrode it is presumed to be the oxidation of the platinum to the +2 state. These voltage ranges are reasonable considering the free energy of formation per chloride at 300°C of $BiCl_3$ (−21 kcal) and of $PtCl_2$ (−9 kcal) (2, 3). The difference between the chlorine evolution and platinum dissolution is also consistent with the EMF measurements of Laitinen and Liu who found that the chlorine potential in potassium chloride-lithium cholride is about 0.306 v more oxidizing than the platinum (II)-platinum potential (4).

It is not possible from these potential ranges to determine if in pure $BiCl_3$ the reduction of Bi(III) proceeds to the metal or to the subhalide, as the free energies of formation per chlorine are sufficiently close, at least for the solids, so that the reactions:

$$Bi(s) + 3/2\ Cl_2(g) = BiCl_3(s) \qquad [1]$$

$$BiCl(s) + Cl_2(g) = BiCl_3(s) \qquad [2]$$

have approximately the same standard free energy per mole of chlorine (3).

The electrolytic introduction of bismuth, as metal or subhalide, may take place by several mechanisms: (*a*) the bismuth (III) may be reduced directly to the metal, after which the metal may simply dissolve as atoms or metal polymers in the fused salt, or, it may react with bismuth (III) to form a subhalide: (*b*) the bismuth (III) may be reduced directly to the oxidation state characteristic of the subhalide. (This latter process seems more reasonable in view of the evidence to be presented.) In terms of the results herein presented, the exact reaction of the bismuth (III) in the coulometric process is unimportant, provided only that the coulombs passed may be considered to go completely into the reduction of bismuth (III); *i.e., the passage of one equivalent of* electricity is equivalent to the addition of one-third mole of bismuth metal to the center compartment.

The shape of the polarographic wave varied somewhat depending on the direction of polarization. In general, polarograms were run by starting at a potential positive to the sharp increase in current due to the anodic limiting reaction and polarizing in the negative direction.

Some typical polarographic current-voltage curves are shown in Fig. 2. Replicate polarograms are shown for several cases to give an indication of the order of reproducibility at a given concentration. The curves represent anodic waves indicating oxidation at the tungsten microelectrode of some bismuth species of oxidation state lower than plus three. Initially, the purified $BiCl_3$ melt was dark, indicating the presence of a trace of excess bismuth in solution. The polarograms also indicated this by an initial anodic current prior to the coulometric addition. This initial concentration of bismuth was of the order of 10^{-4}M, as estimated from the polarographic limiting current. Reversal of the electrolysis current, *i.e.*, making the graphite in the center compartment anodic, resulted in a decrease of the anodic limiting current at the microelectrode. (Note A and B in Fig. 2). A typical plot of the anodic limiting current at platinum and tungsten microelectrodes against microequivalents of electricity passed is given in Fig. 3. In general, the plots were linear to a coulombic input corresponding to about 0.2 mole % (0.023M) bismuth in solution. This would indicate that the efficiency of the constant current electrolysis process was 100% in this concentration range. Failure

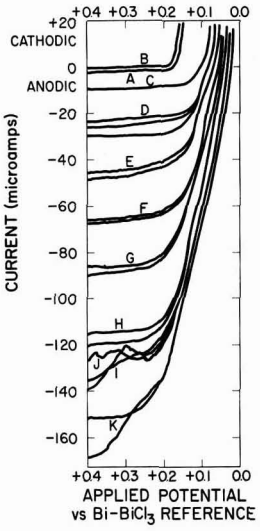

Fig. 2. Typical polarographic curves at a tungsten microelectrode: A, initial polarogram after fusion of $BiCl_3$; B, after brief anodization of graphite; C, 5.65 coulombs passed; D, 13.6 coulombs passed; E, 23.8 coulombs passed; F, 34.5 coulombs passed; G, 44.7 coulombs passed; H, 60.1 coulombs passed; I, 76 coulombs passed; J, 102 coulombs passed.

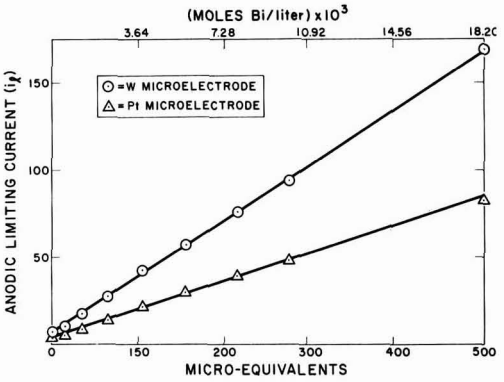

Fig. 3. Limiting current vs. microequivalents of electricity passed.

Table I. Calculation of k, the limiting current constant

Temp, °C	Electrode Material	Electrode Area, mm²	k', amp/equivalent	w, g $BiCl_3$ in center compartment	k, μa/μequiv./cm³/mm²
238	W	4.6	0.32	35.3	0.64
	Pt	2.6	0.16		0.56
270	W	2.1	0.18	47.3	1.0
	W	6.2	0.38		0.76
300	W	19.9	0.13	480	0.85
	Pt	8.7	0.86		1.5
300	Pt	2.8	0.19	66.0	1.2
300	W	3.4	0.63	24.0	1.2
	Pt	2.4	0.41		1.1
325	W	2.9	0.47	40.0	1.7
	Pt	3.9	0.80		2.2
325	W	3.6	0.59	32.0	1.4
350	W	4.8	0.64	37.2	1.4
	W	3.1	0.44		1.5

of the linear relationship between the limiting current and coulombs passed (or concentration of bismuth) at higher concentrations is not too surprising in light of similar observations in aqueous solutions.

A calculation was made of the area independent limiting current constant k, with the relations

$$i_l = k'wC/\rho \qquad [3]$$

$$= kAC \qquad [4]$$

where i_l is the measured limiting current, k' the slope of the plot of the experimental limiting current *vs.* concentration of bismuth, w and ρ the weight and density (5) of $BiCl_3$, C the formal concentration of bismuth expressed as microequivalents of electricity per cm³ of $BiCl_3$ and A the area of the electrode in mm² (Table I). The variation of k at 300°C appears to be in the same range as that reported by Laitinen, Liu, and Ferguson (6) for the reduction of Cr(III) to Cr(II) at solid microelectrodes in fused KCl-LiCl.

The equation expressing the relationship between limiting current and concentration at a solid microelectrode has been given as

$$i_l = nFADC/\delta = kAC \qquad [5]$$

where D is the diffusion coefficient of the diffusing species and δ the effective thickness of the diffusion layer (6-9). However, the work of Pavlopoulos and Strickland (10) indicated that at wire microelectrodes in aqueous solutions, where convective mass transport was operative, the limiting current was proportional to the concentration to the 1.2 power. In the present work, plots of the log of the limiting current *vs.* log of the concentration of bismuth yielded slopes ranging from 1.0 to 0.8; however, even data which gave log plot slopes of 0.8 yielded reasonably linear plots of i_l against C. It is therefore considered that, within the accuracy of the experiment, the limiting current is directly proportional to concentration. Calculation of a δ value at 300°C, using Eq. [5] above, and assuming a D value of 10^{-5} cm²/sec, yields a value for δ of about 0.1 mm, which appears to be the right order of magnitude (10). It would thus seem that Eq. [5] may be used to a first approximation to represent conditions prevailing at the electrodes in this system. If the diffusion coefficient is expressed as (11)

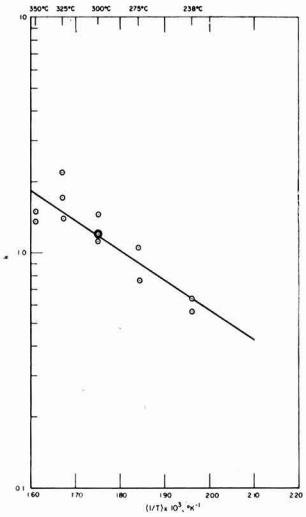

Fig. 4. Log k vs. 1/T, least squares line, slope = —(1.29 ± 0.25) x 10³.

$$D = Ae^{-E/RT} \qquad [6]$$

and if D alone in Eq. [5] is assumed to be temperature dependent, a plot of the log of the limiting current constant, k, against $1/T$ gives the activation energy, E. Such a plot is shown in Fig. 4, and a least squares treatment yields an activation energy of 5.8 ±1.1 kcal.

This value may be compared to other activation energies for current limiting processes in fused salts determined in essentially a similar manner. Thus, $NiCl_2$ in molten KCl-LiCl was found to have an activation energy for the current limiting process of 5.6 kcal (9). In molten NaCl-KCl at temperatures in the vicinity of 700°C, the activation energies for the current limiting process were determined for the reduction of the following solutes: CuCl, 6.3 kcal; $CdCl_2$, 5.9 kcal; $PbCl_2$, 4.5 kcal; $NiCl_2$, 3.0 kcal; $CoCl_2$, 4.5 kcal (12). [It is interesting to note that the activation energies (5 kcal) for self-diffusion of sodium and nitrate ions in molten sodium nitrate (13) are of the same magnitude as the activation energies for the limiting currents obtained from polarographic measurements.] Thus, the anodic polarographic current obtained on oxidation of the bismuth species may be considered as indicative of the existence in solution of discrete entities of bismuth of oxidation state lower than three.

Efforts were made to analyze the current-voltage curves by making plots of log $(i_l - i)$ against E and determining the slopes at 238°, 300°, and 325°C. The bulk of the log plots obtained were linear and the slopes (equal to 2.3 RT/nF for a reversible process) resulted in n values from 1.8 to 1; most of the n values appeared to lie between 1.5 and 1.8, and no particular trend with temperature was noted. The problems in obtaining recorded polarograms at solid microelectrodes have been discussed by Rogers,

Goodrich, *et al.* (14), and with particular reference to fused salts by Chovnyk (7), and more recently by Antipin, *et al.* (15). Although the Russian workers, in particular Chovnyk, report that the Heyrovsky-Ilkovic equation is obeyed, some evidence of the difficulties may be indicated by further reference to recent work by Delimarskii and Kuzmovich (12). For example, the authors give results for the reduction of $PbCl_2$ in molten NaCl-KCl which yields n values which vary from 3.2 to 1.4 with 5 of 6 values of n being less than 1.7. We would agree with Laitinen, Liu, and Ferguson (4) that a somewhat nonideal diffusion situation exists and that a constant-thickness Nernst diffusion layer is not strictly maintained, thus rendering difficult the efforts to obtain true n values from the log plots.

Some observations may be made in regard to the polarograms in Fig. 2. It is noted that the potential against the Bi-$BiCl_3$ reference at which the curve crosses the zero current axis shifts in the negative direction, *i.e.*, in the direction of increasing ease of oxidation, as the concentration of bismuth increases. This is as expected if consideration is given to a Nernst shift. If the Bi(III)-Bi (subhalide) couple obeys a Nernst equation of the type

$$E = \text{constant} + RT/nF \ln (Bi^{+3})/(Bi^{(3-n)}) \quad [7]$$

then, as the concentration of the reduced species increases, the equilibrium potential *vs.* the reference should shift to more negative potentials. Qualitatively, this is shown to be the case in Fig. 2 although the magnitude of the shift, calculated from the point at which the curve crosses the zero current axis, does not agree with values calculated from the equation above for integral values of n. This is not surprising since the curves for replicate runs did not cross the zero current axis at identical potentials. (Detailed potentiometric measurements are being carried out in this laboratory and will be reported in a subsequent paper.) From the observation that the current-voltage curve crosses the voltage axis at maximum slope without any observable break, it is concluded that the electrode reaction is probably reversible.

The polarographic behavior indicates that the dissolution of bismuth in $BiCl_3$ yields a species which is subject to oxidation at the electrode. It does not appear that the reduction product of Bi(III) is Bi metal which adheres to the microelectrode because running the polarogram from a region where Bi(III) reduction takes place toward positive potentials yielded the normal anodic polarographic curve rather than a curve indicative of the stripping of a metal from an electrode. We would thus conclude that the electrolytic reduction of Bi(III) at the graphite electrode involves reduction to a directly soluble species. In this connection, measurements made of the polarization of the graphite electrode during coulometric electrolysis indicated only a relatively slight apparent polarization, most of which was probably due to iR drop. This may be taken as further evidence of the reversibility of the electrode reactions involving the Bi(III)-$Bi^{(3-n)}$ couple.

Bredig (16) and Mayer, *et al.*, (17) have presented evidence that the Bi_2^{++} is the subhalide species existing in the melts. It is not possible from this work to evaluate unequivocally both the oxidation state and degree of association of the Bi species. However, it is perhaps significant that for the concentration range studied, the computed n values are closer to 2 than to 4 as would be the case for the oxidation of Bi_2^{++} to Bi^{+3} or than to 3 as would be the case for the oxidation of Bi^0 to Bi^{+3}. This suggests that perhaps Bi^+ may be the subhalide species which results when Bi is dissolved in $BiCl_3$ in the concentration and temperature range involved in this study.

Manuscript received Dec. 5, 1960; revised manuscript received March 8, 1961. This work was performed under the auspices of the Research Division of the U. S. Atomic Energy Commission.

Any discussion of this paper will appear in a Discussion Section to be published in the December 1961 JOURNAL.

REFERENCES

1. S. J. Yosim, A. J. Darnell, W. G. Gehman, and S. W. Mayer, *J. Phys. Chem.*, **63**, 230 (1959).
2. A. Glassner, " The Thermochemical Properties of the Oxides, Fluorides and Chlorides to 2500°K," ANL-5750.
3. A. J. Darnell and S. J. Yosim, *J. Phys. Chem.*, **63**, 1813 (1959).
4. H. A. Laitinen and C. H. Liu, *J. Am. Chem. Soc.*, **80**, 1015 (1958).
5. F. J. Keneshea, Jr., and D. Cubicciotto, *J. Phys. Chem.*, **62**, 843 (1958).
6. H. A. Laitinen, C. H. Liu, and W. Ferguson, *Anal. Chem.*, **30**, 1266 (1958).
7. N. G. Chovnyk, *Doklady Akad. Nauk., SSSR*, **87**, 1033 (1952); *ibid.*, **100**, 495 (1955); *Zhur. Fiz. Khim.*, **30**, 277 (1956).
8. I. M. Kolthoff and J. J. Lingane, "Polarography," Vol. 1, p. 410, Interscience Publishers Inc., New York (1952).
9. E. D. Black and T. Devries, *Anal. Chem.*, **27**, 906 (1955).
10. T. Pavlopoulos and J. Strickland, *This Journal*, **104**, 116 (1957).
11. S. Glasstone, K. Laidler, and H. Eyring, "Theory of Rate Processes," McGraw-Hill Book Co., New York (1941).
12. Yu. K. Delimarskii and V. V. Kuzmovich, *Zhur. Neorg. Khim.*, **4**, 1263 (1959).
13. E. R. Van Artsdalen, D. Brown, A. Dworkin, and F. J. Miller, *J. Am. Chem. Soc.*, **78**, 1772 (1956).
14. L. B. Rogers, H. H. Miller, R. B. Goodrich, and A. F. Stehney, *Anal. Chem.*, **21**, 777 (1949).
15. L. N. Antipin, I. Khultanskikh, and S. Vazkenin, *Zhur. Fiz. Khim.*, **30**, 1672 (1959).
16. M. A. Bredig, *J. Phys. Chem.*, **63**, 978 (1959).
17. S. W. Mayer, S. J. Yosim, and L. E. Topol, *J. Phys. Chem.*, **64**, 238 (1960).

Continuous Electrochromatography on Ion-Exchange Membranes

S. R. Caplan[1]

National Chemical Laboratory, Department of Scientific and Industrial Research, Teddington, Middlesex, England

ABSTRACT

It is shown theoretically that in continuous electrochromatography the use of an ion-exchange resin can lead to improved separations. This is because a stationary phase capable of highly selective sorption is provided, within which ions are immobilized with respect to eluant flow but not with respect to current flow. In a system of this kind, in contrast with systems employing conventional supporting media, synergy arises between electrophoresis and chromatography. Even if the ions undergoing separation do not differ greatly in their affinities for the resin, certain advantages result from its presence, particularly when the eluant contains a complexing agent.

A method of incorporating ion-exchange membranes in an electrochromatographic cell has been devised and tested with the system potassium-sodium-lithium. The cell was found to be practicable in operation, giving a sharply defined and reproducible continuous separation of the mixture. An experimental analysis of the function of the membrane has been carried out in which the electrophoretic and chromatographic components were studied separately. Some preliminary results are also reported for the system praseodymium-neodymium.

Permselective ion-exchange membranes possessing a high degree of ionic specificity, *i.e.*, the ability to discriminate between similar ions of like charge, are in the course of development in many laboratories (1, 2), and the object of the present study was to find a means of utilizing this property for the continuous separation of mixtures of closely related ions. The fractionation of any ternary or higher mixture requires, as a *sine qua non* for continuous operation, simultaneous movement of the components in two mutually transverse potential gradients. For electrolytes in solution this can be accomplished readily by continuous electrochromatography (3-6).

In principle, continuous electrochromatography depends on electrical migration transversely to the flow of a suitable eluant in a stabilizing ("anticonvection") medium. The medium almost invariably consists of vertical sheets or pads of filter paper, although porous beds packed with glass powder have also been used (7-9). The feed mixture is introduced at a convenient point along the top. The function of the medium is *solely* to ensure uniform flow of eluant. It has frequently been supposed, however, that an equally important function is to act as an adsorbent, providing a stationary phase for partition as in normal chromatography. In the entire absence of sorption by the medium the degree of separation will clearly depend only on the relative electrophoretic mobilities of the solute "zones." But with conventional media specific adsorption effects do occur, and some workers have considered that these play a part in the separation. Nevertheless the extent to which they can in fact influence it, if at all, is negligible. The adsorbed ions, being within the Stern layer, are practically immobile with respect to both electrophoretic and hydrodynamic gradients; thus the direction taken by the resultant of the two mutually perpendicular zone velocity vectors will be independent of the degree of adsorption, since each is equally affected.[2] A good demonstration of this is to be seen in the experiments with nickel and silver reported by Strain and Sullivan (3). These workers found nickel and silver to be readily separated in 4M NH_4OH by electrophoresis or chromatography alone; in the continuous procedure, however, the two metals followed the same path at different rates.

In a series of studies on ion-exchange resins in granular and membrane form (11-14), Spiegler and Coryell showed that from the point of view of electrical conductivity the wet resins, although solid in the gross physical sense, act as solutions of electrolytes. They also demonstrated that resins in both of the above forms could be used as the supporting media for electrophoretic separations. The ionic mobilities within the resins are subject to a series of modifying influences (15), but however great the affinity of an ion for a resin it is never rendered electrically immobile within the resin phase. This leads to the conclusion that improved electrochromatographic separations might be achieved by using ion-exchange membrane "curtains" rather than paper ones. In this way a stationary phase capable of highly selective sorption could be provided within which charged particles would be immobilized with respect to eluant flow but not with respect to current flow. Consequently the hydrodynamic mobility of a zone, or its rate of movement relative to that of the eluant, would be decreased to a greater extent than its electrophoretic mobility. The direction of the resultant would then no longer be independent of sorption; in other words, in this system synergy

[1] Present address: Laboratory of Physical Biology, National Institute of Arthritis and Metabolic Diseases, National Institutes of Health, Bethesda, Maryland.

[2] The general differential equation describing the concentration distribution (as a function of space and time) in terms of diffusion, adsorption, and the two velocities, has been considered by Weber (10). The solution of this equation for the stationary states does not involve an adsorption term.

arises between electrophoresis and chromatography. The factors determining the magnitude of the resulting improvement in a given separation, if any, are examined in the following section.

A suitable physical arrangement for separations of this kind consists of a pack of ion-exchange membranes interleaved with thin filter paper or similar material to act as flow stabilizer. This has the advantage over the most obvious alternative, a trough filled with fine resin granules, in that it is relatively easy in such a system to obtain uniform flow (5, 9). Moreover, membranes of high ionic specificity are likely to become more readily available than their granular counterparts. For purposes of the present discussion we define a "separation coefficient" D^1_2 as the ratio $\tan \theta_1/\tan \theta_2$, where θ is the angle through which the path of a given ionic species is swept from the vertical under the influence of an applied potential.[3] In general we are only concerned with substances sufficiently similar that negative values of D^1_2 do not arise. The coefficient D^1_2 can be evaluated without actually setting up a pack by simply carrying out separate, discontinuous, electrophoretic and chromatographic separations on narrow strips of paper or paper-membrane-paper sandwich. Providing the individual ratios of distances moved are obtained from single runs involving both substances, the value of D^1_2 is independent of voltage or rate of flow of eluant.

Theoretical

In column chromatography the combination of an ion-exchange resin with an eluant containing a complexing agent frequently gives rise to particularly favorable conditions (17, 18). The equilibria involved have been studied extensively (19): for a set of closely related cations, such as the rare earths, the advantage lies in the fact that those which are most strongly complexed have the lowest affinity for the resin and *vice versa* (20). With suitable choice of resin, ligand, and pH, the complex ions (or uncharged particles) are excluded from the resin phase, and the concentration of free metal ions in the eluant is negligibly small. The substances undergoing separation are essentially distributed between complexone and resin; the differences between their respective distribution coefficients are, accordingly, greatly magnified (as compared with a noncomplexing eluant). Complexones have been used in continuous electrochromatography to improve matters where mobility differences are small (21). The electrophoretic migration of a species under these conditions is determined by its affinity for the complexone and by the mobilities of both the complexed and uncomplexed particles.

The following considerations relate to the function of an ion-exchange medium in an electrochromatographic system, the latter operating either with or without a complexing agent. For purposes of simplification we shall neglect diffusion and assume that exchange equilibria can be regarded as instantaneous irrespective of zone velocities. Furthermore we shall assume light loading (in comparison with the total exchange capacity available in a zone), neglect sorption of complexed species and electroosmosis, and allow the formation of 1:1 complexes only. The symbols used are defined in a list at the end.

Ion-exchange material absent.—For reasons described above we ignore any specific adsorption effects due to the presence of an anticonvection medium. Thus we need only consider the electrophoretic separation. Evidently, for the cation M,

$$U^0_M = \frac{u_M[M]}{[M] + [MZ]} + \frac{u_{MZ}[MZ]}{[M] + [MZ]}$$

$$= \frac{u_M + u_{MZ} K_{MZ}[Z]}{1 + K_{MZ}[Z]}$$

Therefore, for this case,

$$D^1_2 = \frac{u_{M_1}\left(1 + \frac{u_{M_1Z}}{u_{M_1}} K_{M_1Z}[Z]\right)}{u_{M_2}\left(1 + \frac{u_{M_2Z}}{u_{M_2}} K_{M_2Z}[Z]\right)} \cdot \frac{1 + K_{M_2Z}[Z]}{1 + K_{M_1Z}[Z]} \quad [1]$$

Ion-exchange material present.—*(a) Chromatographic component.*—We have the well-known relation for the rate of movement of a zone relative to that of the eluant:

$$R_F = \frac{1}{1 + \frac{1}{v} K_d}$$

Therefore,

$$\left(\frac{x_1}{x_2}\right)_{chrom} = \frac{1 + \frac{1}{v} K_{d_2}}{1 + \frac{1}{v} K_{d_1}}$$

and using the additional relation

$$K_d = K^0_d/(1 + K_{MZ}[Z])$$

we obtain

$$\left(\frac{x_1}{x_2}\right)_{chrom} = \frac{K^0_{d_2} + v(1 + K_{M_2Z}[Z])}{K^0_{d_1} + v(1 + K_{M_1Z}[Z])} \cdot \frac{1 + K_{M_1Z}[Z]}{1 + K_{M_2Z}[Z]} \quad [2]$$

(b) Electrophoretic component.—Consideration of the mean flux of a given species through both phases within a zone leads to

$$U' = \frac{K_d \bar{u} + v U^0}{K_d + v}$$

Therefore,

$$\left(\frac{x_1}{x_2}\right)_{elec} = \frac{K^0_{d_1}\bar{u}_{M_1} + vu_{M_1}\left(1 + \frac{u_{M_1Z}}{u_{M_1}} K_{M_1Z}[Z]\right)}{K^0_{d_2}\bar{u}_{M_2} + vu_{M_2}\left(1 + \frac{u_{M_2Z}}{u_{M_2}} K_{M_2Z}[Z]\right)} \cdot \frac{K^0_{d_2} + v(1 + K_{M_2Z}[Z])}{K^0_{d_1} + v(1 + K_{M_1Z}[Z])} \quad [3]$$

(c) Continuous separation.—Dividing [3] by [2], we obtain for this case

[3] Of course, strong electro-osmotic streaming of the eluant in a medium such as glass-fiber paper can modify the direction of travel considerably, even to the extent of apparently reversing the charge of an ion (16).

$$D^1_2 = \frac{K^0_{d_1}\bar{u}_{M_1} + vu_{M_1}\left(1 + \frac{u_{M_1Z}}{u_{M_1}}K_{M_1Z}[Z]\right)}{K^0_{d_2}\bar{u}_{M_2} + vu_{M_2}\left(1 + \frac{u_{M_2Z}}{u_{M_2}}K_{M_2Z}[Z]\right)} \cdot \frac{1 + K_{M_2Z}[Z]}{1 + K_{M_1Z}[Z]} \quad [4]$$

It may be noted that if we set $\bar{u}_{M_1} = \bar{u}_{M_2} = 0$, or if v is very large, relations [4] and [1] become identical. Furthermore, if v is very small,

$$\left(\frac{x_1}{x_2}\right)_{elec} = \frac{\bar{u}_{M_1}}{\bar{u}_{M_2}}$$

An additional special case, in which D^1_2 is independent of v and [4] again becomes identical with [1], is given by

$$\frac{K^0_{d_1}\bar{u}_{M_1}}{K^0_{d_2}\bar{u}_{M_2}} = \frac{u_{M_1}}{u_{M_2}} \qquad (u_{MZ} << u_M)$$

However, it is unlikely that this relationship would hold for many real systems, since $K^0_{d_1}/K^0_{d_2}$ and $\bar{u}_{M_1}/\bar{u}_{M_2}$ may be expected to vary in the same sense with changes in resin structure.

Comparison of the two cases.—In general v will be small, and if we make the additional assumption that u_{MZ} is zero or negligibly small in comparison with u_M (if not zero it will usually be of opposite sign) we obtain the following approximate relations

Ion-exchanger absent:

$$D^1_2 = \underbrace{\frac{1 + K_{M_2Z}[Z]}{1 + K_{M_1Z}[Z]}}_{\text{complexone affinity factor}} \cdot \underbrace{\frac{u_{M_1}}{u_{M_2}}}_{\text{mobility factor}} \quad [5]$$

Ion-exchanger present:

$$D^1_2 = \underbrace{\underbrace{\frac{K^0_{d_1}}{K^0_{d_2}}}_{\text{resin affinity factor}} \cdot \underbrace{\frac{1 + K_{M_2Z}[Z]}{1 + K_{M_1Z}[Z]}}_{\text{complexone affinity factor}}}_{\text{chromatographic factor}} \cdot \underbrace{\underbrace{\frac{\bar{u}_{M_1}}{\bar{u}_{M_2}}}_{\text{mobility factor}}}_{\text{electrophoretic factor}} \quad [6]$$

the ratio of the relative affinity coefficients (20) of M_1 and M_2 with respect to hydrogen ion or whatever other ion predominates in the resin. When the mobilities of M_1 and M_2 are about equal one may achieve a separation in systems of this kind in which the chromatographic component alone is operative.

Displacement of equilibria by ion-exchange material.—For a given total concentration of the substances undergoing separation, *i.e.*, at constant $[M]_t$, and a given total concentration of complexone, the comparison of [5] and [6] is not straightforward, since the complexone affinity factor is altered by equilibria displacements resulting from the introduction of resin. Under these conditions (which are particularly likely to be encountered in exploratory strip runs) this factor is very much further from unity in Eq. [6] than in Eq. [5]. Here we have an important effect *per se*. The following calculation of the effect will be limited to the particular case studied experimentally, namely, elution of the alkali metals with uramil-diacetic acid.[4] From this discussion the general behavior can be inferred.

We have to investigate the following simultaneous equilibria, for which the constants are given:

$$M^+ \rightleftharpoons \overline{M^+} \qquad K^0_d/v$$
$$M^+ + HX^{2-} \rightleftharpoons MX^{2-} + H^+ \qquad K^a_{MX^{2-}}$$
$$HX^{2-} \rightleftharpoons X^{3-} + H^+ \qquad k_3$$
$$M^+ + X^{3-} \rightleftharpoons MX^{2-} \qquad K^a_{MX^{2-}}/k_3$$

The justification for writing K^0_d/v as the equilibrium constant for the first (exchange) reaction is the original assumption of light loading. Under these conditions we may neglect the competing ion (dimethylammonium in the present case). Figures for the various formation and dissociation constants are given by Schwarzenbach *et al.* (22), and from the values of k_1 and k_2 it is found that within the *p*H range of interest (above 7) virtually all the H_3X is present as HX^{2-}. Solving these equations for the ratio $[MX^{2-}]/[M^+]$ in terms of total concentrations of metal and complexone, we arrive at the following relation:

[4] The alkali metal separations which form the major part of the present work were based on the use of the complexone uramil-N, N-diacetic acid (22), which has been successfully employed to resolve mixtures of alkali ions on ordinary ion-exchange columns (23). It has the remarkable property of complexing lithium and sodium to a significant extent, a property not shared by the organic acids commonly used as ligands in electrophoretic studies (25).

$$\frac{[MX^{2-}]}{[M^+]} = K_{MZ}[Z] = \alpha\left(\frac{2[M]_t}{\left[\left\{\frac{\alpha}{\beta} - ([X]_t - [M]_t)\right\}^2 + \frac{4\alpha[X]_t}{\beta}\right]^{1/2} - \left[\frac{\alpha}{\beta} + ([X]_t - [M]_t)\right]} - 1\right) \quad [7]$$

Comparison of Eq. [5] and [6] shows at a glance the effect of synergy when an ion-exchanger is introduced into the system. In Eq. [6] the resin affinity factor $K^0_{d_1}/K^0_{d_2}$ (which relates essentially to chromatographic phenomena) has not disappeared, a result arising wholly as a consequence of the mobility of sorbed ions within the solid phase. In general, for a series of like ions, the greater the mobility of an ion the greater is its affinity for an ion-exchange resin and the lower the stability of its complexes (20, 24). Thus all three factors act cooperatively. The resin affinity factor may be approximately equated (for lightly loaded well-buffered systems) to

We now write

$$\rho = 1 + K_{MZ}[Z]$$

Two useful limits of ρ may be defined, and evaluated by means of Eq. [7]. They are

$$\rho^r = \lim_{\alpha\to\infty} \rho = 1 + \beta[X]_t \quad [8]$$

$$\rho^0 = \lim_{\substack{\alpha\to 1 \\ [M]_t\to[X]_t}} \rho = \left[\left\{\left(\frac{1}{2\beta[X]_t}\right)^2 + \frac{1}{\beta[X]_t}\right\}^{1/2} - \frac{1}{2\beta[X]_t}\right]^{-1} \quad [9]$$

If we ignore the first equilibrium it can be shown directly that

$$\rho^r = \lim_{\substack{\alpha \to 1 \\ [M]_f \to 0}} \rho \qquad [10]$$

It is seen that the factor ρ^r corresponds most closely to the system with resin, particularly when it is realized that even if the value of K^0_d is not very large, α can be increased without limit by diminishing the value of v. On the other hand the condition corresponding to ρ^0 is approached most closely by systems without resin (or any other material of similar sorptive capacity), unless the total concentration of M is very low relative to that of the complexone. A comparison of ρ^r and ρ^0 as functions of $\beta[X]_t$ is illuminating. (It should be borne in mind that β is a monotonic function of pH, increasing with increasing pH.) Both tend to unity with unit slope as $\beta[X]_t$ tends to zero. However, whereas ρ^r is a linear function of $\beta[X]_t$, ρ^0 rises much more slowly with a steadily decreasing slope. As $\beta[X]_t$ increases, (ρ^r_2/ρ^r_1) approaches the value $(K^a_{M_2X^{2-}}/K^a_{M_1X^{2-}})$, while (ρ^0_2/ρ^0_1) tends to $(K^a_{M_2X^{2-}}/K^a_{M_1X^{2-}})^{1/2}$.

It is now worthwhile rewriting Eq. [5] and [6] as follows:

Ion-exchanger absent ($[M]_t \approx [X]_t$):

$$D^1_2 = \frac{\rho^0_2}{\rho^0_1} \cdot \frac{u_{M_1}}{u_{M_2}} \qquad [5a]$$

Ion-exchanger present (α large):

$$D^1 = \frac{\rho^r_2}{\rho^r_1} \cdot \frac{\bar{u}_{M_1}}{u_{M_2}} \cdot \frac{K^0_{d_1}}{K^0_{d_2}} \qquad [6a]$$

The magnitude of the complexone affinity factor in the presence of ion-exchanger approaches, for the particular case considered, the square of its value in the absence of ion-exchanger. The above two equations express, of course, limiting conditions only.

Practical Consequences of the Theory

Significance of Eq. [5] and [6].—These equations furnish a direct comparison between two continuous electrochromatographic systems, one operating on a conventional medium such as paper and the other on an ion-exchange material. The most natural basis for the comparison is identity of eluant and feed. On this basis the paths of a given ionic species in the two cases are, under steady-state conditions, identical as regards liquid-phase composition, and consequently the complexone affinity factors in the equations are equal. In order to compare the separations, it is only necessary to compare the mobility factor in the first case (which can be obtained from mobilities in free solution) with the product of the affinity and mobility factors in the second (where mobilities within the resin are referred to). An estimate of the magnitude of this product, for systems incorporating membranes, should be obtainable from bi-ionic potential measurements across the membranes (29-31).

Significance of Eq. [5a] and [6a].—It is evident that the above comparison is not affected by the presence or absence of a complexing agent. However, in each case the presence of a complexing agent increases the *absolute* magnitude of the separation coefficient. Furthermore the complexone affinity factor rises on increasing the ratio of complexone to feed mixture (in terms of concentrations in the liquid phase).[5] If the mobility of a given complex is taken, as before, to be small relative to that of the uncomplexed ion, a large complexone to feed ratio entails, in the absence of ion-exchange resin, very low zone mobilities U^0. In the presence of resin the zone mobilities U^r are hardly affected by increasing this ratio, and the system may readily be operated under steady-state conditions approximating to Eq. [6a] rather than Eq. [5a]. In this way much more efficient use can be made of the complexone. It is important to remember that the substitution of an ion-exchanger (but not a simple adsorbent) for an inert supporting medium results in increased retention-times without commensurate decreases in zone mobilities, whatever the composition of the eluant. Consequently, for a given throughput a lower operating voltage is required to move a substance a predetermined distance in the direction of the electric field (the minimum for complete separation, say) before it emerges from the pack. Alternatively, if the voltage remains unchanged, the steady-state throughput of the substance will be increased.[6]

Use of resins of low ionic specificity.—The above analysis has shown that an ion-exchange medium confers advantages in practice, even if the resin affinity factor is unity. It is instructive to contrast the behavior of such a resin with that of a hypothetical adsorbent, identical in all respects except that $\bar{u} = 0$. Suppose that in a system incorporating this adsorbent the ratio of complexone to feed is large. Then the quantity $K_{MZ}[Z]$, *i.e.*, the ratio (complexed M)/(uncomplexed M), must become large in comparison with unity. Hitherto we have assumed $u_{M_1Z} \approx u_{M_2Z} \approx 0$; but if the mobilities of the complexes (which are unlikely to differ from one another appreciably) cannot be neglected, the closer they are in numerical value to the mobilities of the uncomplexed ions the closer the complexone affinity factor comes to cancelling out in the extended expression for D^1_2 (Eq. [4]). Since u_{MZ} is invariably opposite in sign to u_M, the zone mobilities themselves may approach zero. On the other hand, values of u_{MZ} large enough to become significant tend to increase D^1_2 when a resin is present.

Strip-run analyses.—The use of separate strip runs as a convenient means of evaluating D^1_2 has been described. A strict comparison between an all-paper system and an interleaved membrane system should be carried out either in the absence of complexone, or in such a manner that the composition of the zones in the paper-supported phase is constant. The basis of the comparison will then be Eq.[5] and [6]. But the most straightforward experimental technique is

[5] It rises to a limiting value—the inverse ratio of formation constants.

[6] Compared with systems incorporating a conventional supporting medium (irrespective of whether or not adsorption occurs), the throughput is increased by a factor of $1 + (K_d\bar{u}/vU^0)$. This factor is based on identical quantity and composition of liquid phases, with rates of flow suitably adjusted to elute the given substance at the predetermined position.

to load all strips with the same quantity of the ionic mixture, which leads to a comparison based on Eq. [5a] and [6a]. Even if the resin affinity factor is not perceptibly different from unity, the separation coefficient will then be higher for the interleaved membrane strips.

In the following section a series of strip runs with a mixture of Na and K is described. This series was intended primarily to establish the feasibility of operation with interleaved membranes and was carried out in conjunction with the running of an experimental laboratory-scale cell. Currently available industrial-type membranes were used showing, under the conditions of the experiments, no evidence of discrimination between the alkali ions, which were chosen for convenience in analysis. Nevertheless, the experiments constitute a preliminary test of the theory (Eq. [5a] and [6a]) as well as a demonstration of the practicability of the method.

Experimental

Electrochromatography cell.—This was similar in many respects to the paper packs described by Strain and Sullivan (3) and Sato, Norris, and Strain (4). Details are shown in Fig. 1, which is largely self-explanatory. A pack containing a dozen membranes was mounted in a simple water-cooled press. The interleaving papers (0.007 in. thick) were from sheets of "Separa DHC" (W. & R. Balston, Ltd.), a double acid-washed hardened paper of high wet strength and very low mineral content. Homogeneous membranes were employed, consisting of sulfonated polyvinyl chloride sheets (28) (see Table I, No. 1). Eluant was distributed to the recesses at the top of the press by means of a constant-level feed system, and electrolyte was gravity-fed to the two channels from Mariotte bottles. Below the lead-off strips was placed a rack of thirteen funnels leading to collecting bottles. The two large tabs for anolyte and catholyte each dipped into an end funnel, while the drip-points between were taken in pairs to the remaining eleven. Before commencing a run the pack was cycled to the desired form as if it were an ion-exchange column. At the end of this period flow of anolyte and catholyte was started, and the d-c powerpack switched on, operating under constant current conditions. After a short period to allow the pack to settle down, the feed was started.

In the examples the runs were continued for 24 hr after the commencement of feeding. In each case 75 ml of feed were pumped in at a rate of 5.6 ml/hr, that is feeding was carried on for the first 13.5 hr and then stopped. The fractions collected were numbered 1 to 13 starting with the anolyte and ending with the catholyte, the feed-point being directly above fraction 3. In general the rate of flow of eluate, per fraction, for fractions 2 to 12 was 20 ml/hr, so that about 5 l of eluant were needed for a full run. A much higher flow-rate, over 100 ml/hr, was found necessary for the anolyte and catholyte.

Separation of potasium, sodium, and lithium.—The pack was first conditioned to the dimethylammonium form, using a 0.5% solution of dimethylamine in water. Uramil-diacetic acid (Hopkin & Williams, Ltd.) was freed from sodium and other impurities by passage in aqueous solution through a column of Amberlite IR-112 resin at 60°C. In both examples the pack eluant contained 3.53 g/l UDA, adjusted to pH 9.5 with dimethylamine. The anolyte and catholyte were, respectively, 0.1*N* ammonium hydroxide and 0.1*N* hydrochloric acid. The feed was prepared in the same way as the eluant, but contained in addition potassium chloride, sodium chloride, and lithium sulfate. The composition of the feed was such as to give a total of 0.5 mg equivalents each of the alkali ions, with the exception of lithium in the first example where six times this quantity was used. Analyses of the fractions were carried out by means of an "Eel" flame photometer. Further details will be found below Fig. 2.

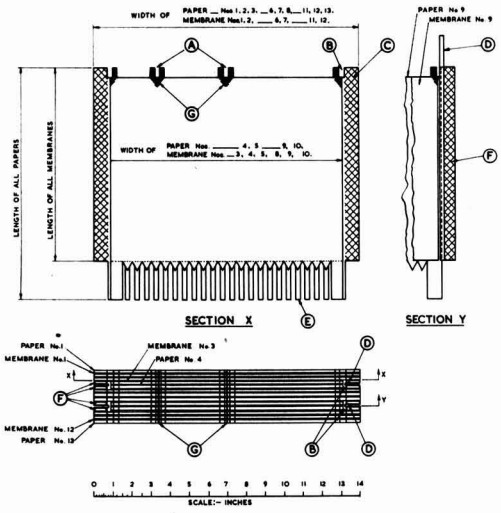

Fig. 1. Detail of interleaved pack. (Cross-hatching indicates waxed surfaces, numbers refer only to the order of assembly. Thicknesses are not to scale.) A, alternative feed-points; B, electrolyte channels; C, waxed edges; D, platinum ribbon electrodes; E, eluate lead-off strips; F, waxed paper electrode supporters; G, paper wicks.

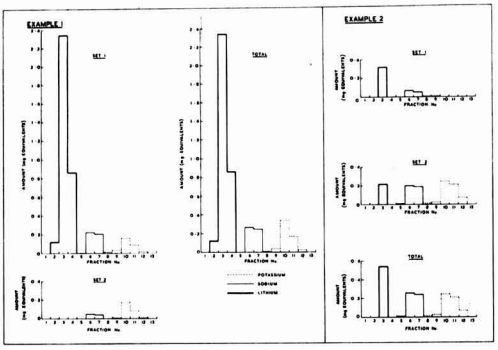

Fig. 2. Continuous separation of alkali metals. (Fractions numbered serially from 1 (anolyte) to 13 (catholyte); feed pumped in vertically above fraction 3 for first 13.5 hr.) Example 1 (216 ma, 314 v): Set 1, fractions collected after 16 hr; Set 2, fractions collected after a further 8 hr. Example 2 (212 ma, 297 v): Set 1, fractions collected after 8 hr; Set 2, fractions collected after a further 16 hr.

Table I. Properties of membranes used in strip experiments

No.	Type	Thickness,[a] in.	Specific conductance,[b] $ohm^{-1}cm^{-1} \times 10^3$	Capacity, meq./dry g	Water content, g/dry g	Remarks
1	N.C.L. SPVC	0.004	0.4	0.8	0.13	Homogeneous
2	T.N.O. C-60	0.012	7.2	1.8	0.53	Homogeneous
3	I.C.I.	0.013	11-17	c.2	c.1	Homogeneous
4	"Permaplex" C-10	0.023	2.0	3.0	0.8	Heterogeneous (Interstitial volume 13%)
5	"Permaplex" C-20	0.030	5.0	3.3	0.9	Heterogeneous (Interstitial volume 15%)

[a] Wet H-form.
[b] In 0.1M NaCl.

Strip runs with potassium and sodium.—These were carried out on single strips of membrane (3 cm wide) sandwiched between two strips of "Separa DHC" paper of the same width. A number of cation-exchange membranes were studied; details of these are given in Table I. The eluant or electrolyte solutions all contained 3.53 g/l UDA, adjusted to various pH values within the range 7-12 by varying the concentration of dimethylamine. Sodium 22 (2.6 yr) and potassium 42 (12.4 hr), as the chloride and carbonate, respectively, were used as tracers. Generally the runs were performed with about 0.5 micro-equivalents of each ion, the compositions of the 0.5M solutions having been adjusted to give an activity of about 0.1 $\mu c/\mu l$. The solutions were spotted with a micropipette on to 20 x 2 mm "loading" strips of Whatman No. 1 filter paper and allowed to dry. At the beginning of a run the loading strip was inserted with a pair of forceps into the sandwich so as to abut centrally against the "origin" end of the membrane strip. For chromatography the sandwiches were clamped between thick lengths of Perspex and mounted vertically, while for electrophoresis they were enclosed in a PVC sleeve between two horizontal copper blocks through which cooling water was circulated.

At the end of the runs the strips were dried and then scanned automatically using a ratemeter and pen recorder. Following this they were stored and rescanned a week later, by which time the potassium was no longer detectable. Only a small proportion of the activity was found on the paper strips. A set of runs on paper only, in which identical "sandwiches" were used except for the lack of a membrane filling, were carried out for comparison.

Strip runs with praseodymium and neodymium.—A number of trial runs on membrane 1 with praseodymium 142 (19.2 hr) and neodymium 147 (11.3 days) were also performed, using solutions of the oxides dissolved in hydrochloric acid. The neodymium, prior to scanning, was allowed to decay for three weeks after irradiation. During this period the activities of neodymium 149 (2.0 hr) and promethium 149 (54 hr) fell to negligibly low levels. The same quantities and activities were used as in the potassium-sodium runs. Citric acid has been studied extensively as a complexing agent for the rare earths (18, 26) and was consequently chosen as eluant. A solution containing 10% citric acid, 0.1*N* with respect to ammonium chloride, was found necessary to give a reasonable rate of chromatographic elution in the *p*H range of interest (the region in which the zones move toward the cathode). The *p*H of the eluant was adjusted by the addition of ammonia, and it was found that the "isoelectric" point of the system lay close to *p*H 2.6. At higher *p*H values the zones were anionic. The most promising results were obtained at *p*H values just below this.

Results and Discussion

Continuous Separation

The results are given in histogram form in Fig. 2. In all cases recovery was complete. It is seen that the separations are clear-cut and reproducible. It will also be seen that, under these conditions, the "breakthrough" volume of potassium (*i.e.*, volume of eluate collected prior to the first appearance of potassium) is far greater than that of lithium. These observations confirm that the interleaved pack is a practicable means of exploiting ion-exchange membranes for continuous electrochromatography.

Strip Runs with Potassium and Sodium

Since the decay of sodium 22 in one week is negligible, the position of the potassium on a given strip

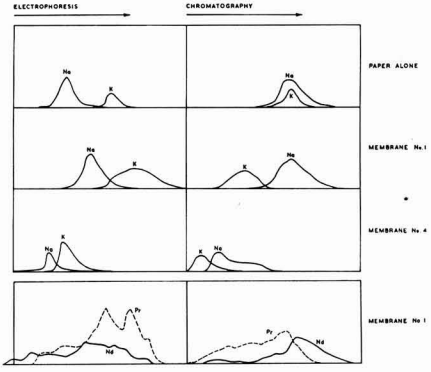

Fig. 3. Examples of strip runs (radiometric scans). In each record the origin is at the left-hand edge; in the electrophoretic cases this corresponds to the end nearest the anode. The blocks cover a length of 28 cm. The alkali metal separations shown were in uramil-diacetic acid in the vicinity of pH 11, the rare earth separations in citric acid at pH 2.5.

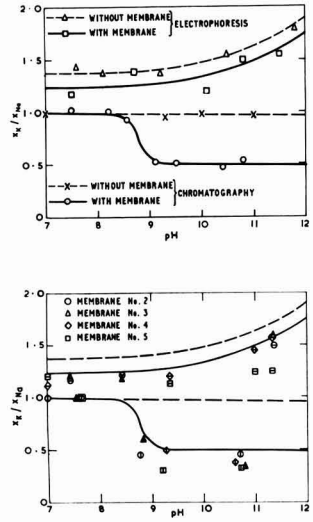

Fg. 4a. (top) Evaluation of the potassium-sodium system by means of strip experiments with membrane No. 1. Fig. 4b. (bottom) Comparison of membranes. Vertical bars denote chromatography, horizontal bars electrophoresis. Curves are from Fig. 4a.

was found easily by comparing two scans covering this interval. If separation was not complete, a plot of the potassium peak was obtained by subtraction of ordinates. Generally the chromatographic bands were unsymmetrical with flattened maxima; the ratio x_K/x_{Na} was therefore evaluated in all cases from the positions of the half-area ordinates. Some examples are shown in Fig. 3.

The results obtained in a series of experiments with membrane 1 are compared with those for paper alone in Fig. 4a. It is seen that although the mobility ratio is somewhat decreased in the presence of membrane its *p*H dependence parallels the behavior in the absence of membrane. On the other hand the corresponding chromatographic ratio, in the presence of membrane, undergoes a sharp decrease between *p*H 8 and 9. In the absence of membrane it drops only very slightly below unity at high *p*H, presumably owing to the presence of carboxyl groups in the paper.

In Fig. 4b the results are plotted for membranes 2 to 5, and compared with the curves from Fig. 4a. Ignoring for the moment the two electrophoretic points above *p*H 11 for membrane 5, it is seen that the mean electrophoretic curve would lie slightly below that of Fig. 4a, while the mean chromatographic curve would descend to a considerably lower level than that of Fig. 4a with increasing *p*H. Since the relative change in $(x_K/x_{Na})_{chrom}$ is the greater, this represents a net increase in D^K_{Na} at *p*H values above 9. The mobility ratio for membrane 5 appears to remain substantially constant throughout the range, but the values of $(x_K/x_{Na})_{chrom}$ for this membrane are the lowest of all, so that even at high *p*H D^K_{Na} calculated from the values plotted is still appreciably higher than in the case of membrane 1. The behavior of these membranes can be explained

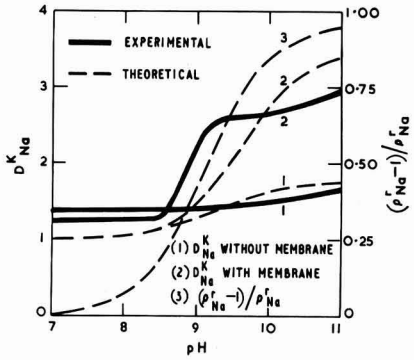

Fig. 5. Comparison of experiment with theory (see Discussion).

qualitatively by a consideration of their thicknesses (see Table I). An increase in thickness is equivalent to a decrease in the quantity v, and from Eq. [2] and [3] one would expect both $(x_K/x_{Na})_{chrom}$ and $(x_K/x_{Na})_{elec}$ to decrease with decreasing v, giving a net increase in D^K_{Na}. The thickness of membrane 5, it should be noted, is 30% greater than that of membrane 4, and it may be that we have here reached the limiting situation in which $(x_K/x_{Na})_{elec}$ is independent of *p*H and equal to $\overline{u}_K/\overline{u}_{Na}$. However, the difference in behavior between membranes 4 and 5 is remarkable at high *p*H and a possible additional factor might be the bigger void content of membrane 5 (about 25% more than that of membrane 4 on the basis g water/g dry membrane). It is highly unlikely that the large negatively charged ligand ions could penetrate to the voids, and since in the electrophoretic runs the interstitial volume represents a portion of v we have, in effect, a small sub-phase of the eluant free of complexone.

Figure 5 shows D^K_{Na} as a function of *p*H in the presence and absence of membrane, computed from the smoothed results of Fig. 4a. For comparison the *p*H dependence is also plotted of the ratio $(\rho^r_{Na}-1)/\rho^r_{Na}$, *i.e.*, the maximum possible value of the ratio (complexed Na)/(total Na). The influence of the chromatographic component of the separation, in the presence of membrane, is evident; the steep rise in D^K_{Na} at about *p*H 9 results from an alteration in the relative distribution of the two ions, which is reflected almost entirely in $(x_K/x_{Na})_{chrom}$ since the zone mobilities are dominated by the mobilities within the membrane. The value of D^K_{Na} at *p*H 9.5 in the presence of membrane is found, from the experimental curve, to be 2.61; this agrees moderately well with the value 2.14 obtained in the continuous separations, where concentrations were higher.

A qualitative comparison of theory with experiment has been attempted on the basis of Eq. [5a] and [6a] and is also shown in Fig. 5. In this calculation the mobility and resin affinity factors were taken as unity, giving the relations
membrane absent:

$$D^K_{Na} \approx \frac{\rho^0_{Na}}{\rho^0_K}$$

membrane present:

$$D^{K}_{Na} \approx \frac{\rho^{r}_{Na}}{\rho^{r}_{K}}$$

and the required values of ρ^r and ρ^0 were obtained from Eq. [8] and [9] using the known constants of uramil-diacetic acid. The limiting condition of [9] is probably approached well within a factor of 10 in the present case. We have observed that 5 μl of solution just saturate a loading strip. It is therefore reasonable to suppose that there exists at the origin, very shortly after loading, a zone of 0.1M solution (with respect to sodium and potassium). The dilution of this zone during the course of a run on paper alone is greater than 10-fold, but certainly from the degree of spreading very much less than 100-fold. So we have, at the conclusion of a run,

$$[X]_t = 1.275 \times 10^{-2}$$

$$[M]_t \approx 10^{-2} - 10^{-3}$$

However, during a good deal of the time the two concentrations will be roughly equal in magnitude.

To complete the calculation one *ad hoc* assumption has been made. A value for the apparent formation constant of the potassium complex is not known and indeed Schwarzenbach *et al.* state that no detectable potassium complex is formed. (Even the apparent formation constant of the sodium complex, 6.0 x 10^{-8}, is extremely low; this is the smallest value measured in the series of alkali metals and alkaline earths studied by these workers, with lithium next in order.) Our observations suggest that some complexing of potassium does in fact take place, to a much lesser extent than in the case of sodium but not incomparably so. Consequently we have arbitrarily assumed a value $K^a_{KX^{2-}} = 0.25\ K^a_{NaX^{2-}}$. Bearing in mind the degree of approximation involved, the theoretical behavior found is considered to be in reasonable conformity with the actual behavior. Lower values of $K^a_{KX^{2-}}$ would result in a steeper rise in the dashed curves 1 and 2.

Strip Runs with Praseodymium and Neodymium

A pair of runs at *p*H 2.5 are shown in Fig. 3. These were evaluated by means of two scans separated by an interval of 19 hr. The drop in neodymium activity over this period is only 5% and was neglected in comparison with the 50% drop in praseodymium activity. On paper alone no separation, either in chromatography or in electrophoresis, could be detected throughout the *p*H range 2.0-2.6. Sato *et al.* (27) have reported paper electrophoretic separation of these metals using lactic acid as a supporting electrolyte on Eaton-Dikeman Grade 301 paper. However, their separations depended on adsorption effects, and the neodymium zone migrated more rapidly than the praseodymium toward the cathode. It has been shown (18) that below a *p*H value of 3.2 the uncharged 1:3 complex predominates in the lanthanon-citric acid system. Consequently, from the point of view of electrophoresis the eluant in the example in Fig. 3 is an ideally stationary phase.

Conclusions

The operation of a continuous electrochromatography cell based on an interleaved pack of ion-exchange membranes has been demonstrated, and the cell shown to be a practicable arrangement whereby the synergic interaction between chromatography and electrophoresis resulting from the presence of an ion-exchange medium can be turned to good account. High-capacity membranes of high ionic specificity are desirable. For maximum over-all efficiency the volume of eluant per gram of resin in the cell should be kept as low as possible, preferably by the use of very thin interleaving material rather than thick membranes to avoid "tailing" (a trough of granular resin would require close packing of fine beads). The feed concentration should also be low, which will result in a somewhat dilute eluate.[7]

The results of the strip experiments support the contention that on the basis of these alone the optimum conditions for a given separation can be determined. They also provide a rough preliminary confirmation of the theoretical treatment. It is hoped eventually to carry out a systematic test of the latter, using selected pairs of cations or anions of approximately equal mobility (in free solution) in combination with membranes across which they are known to yield high bi-ionic potentials (32).

Acknowledgments

The author is most grateful to Mr. T. A. Gough for able technical assistance, and to Mr. D. J. McCauley for providing much of the information in Table I. The work described comprises the subject-matter of British Pat. Appl. No. 39033/58, and is published by permission of the National Research Development Corporation and the Director, National Chemical Laboratory.

Manuscript received Aug. 9, 1960; revised manuscript received Feb. 27, 1961.

Any discussion of this paper will appear in a Discussion Section to be published in the December 1961 JOURNAL.

SYMBOLS

D^i_s = separation coefficient (see introduction).

K_d = distribution coefficient for a given ionic species $= \dfrac{\text{fraction of species in resin phase}}{\text{fraction of species in eluant phase}} \times \dfrac{\text{volume of eluant}}{\text{mass of resin}}$.

K^0_d = distribution coefficient in the absence of any ligand.

$\rho = \dfrac{\text{total concentration of species in eluant}}{\text{concentration of uncomplexed species in eluant}}$ (at equilibrium). With superscripts, see Eq. [8] and [9].

$v = \dfrac{\text{volume of eluant}}{\text{mass of resin}}$ (liters/g).

x = distance moved by a zone in the horizontal or vertical direction in a given time.

[Z] = concentration of free ligand Z in eluant

[M] = concentration of free species M in eluant.

K_{MZ} = formation constant of complex MZ = [MZ]/[M][Z].

[7] This is common to all elution procedures. Concentrating the fractions would in general be carried out most easily on ion-exchange columns with suitable prior adjustment of *p*H. It is not inconceivable, however, that a displacement procedure could be developed, using an attackable anode of a metal of lower affinity and mobility than those undergoing separation, and displacing with a cation of higher affinity and mobility.

$[\overline{M}]$ = concentration of species M in resin.
$[M]_t$ = total concentration of species M in zone, *i.e.*, moles M/liter eluant including quantity in associated resin.
$u, \bar{u}$ = effective electrophoretic mobilities (uncorrected for tortuosity) of a given ionic species in eluant and resin phases, respectively, including sign.
U^r, U^o = effective zone mobilities in the presence and absence of resin, respectively.
H_3X = tribasic complexone (in particular, uramildiacetic acid).
k_1, k_2, k_3 = dissociation constants of H_3X.
$K^a_{MX^{2-}}$ = apparent formation constant of the complex MX^{2-}, where M is a monovalent cation.
$[X]_t$ = total concentration of ligand X in eluant.

In addition, the following two parameters are used:

$$\alpha = 1 + \frac{K^o_d}{v}, \qquad \beta = \frac{K^a_{MX^{2-}}}{[H^+] + k_3}$$

REFERENCES

1. D. Woermann, K. F. Bonhoeffer, and F. Helfferich, *Z. Phys. Chem.*, **8**, 265 (1956).
2. W. Slough, *Trans. Faraday Soc.*, **55**, 1036 (1959).
3. H. H. Strain and J. C. Sullivan, *Anal. Chem.*, **23**, 816 (1951).
4. T. R. Sato, W. P. Norris, and H. H. Strain, *ibid.*, **24**, 776 (1952).
5. H. H. Strain, *ibid.*, **30**, 228 (1958).
6. A. Karler, *ibid.*, **31**, 848 (1959).
7. W. Grassmann and K. Hannig, *Naturwiss.*, **37**, 397, 496 (1950).
8. W. Grassmann and K. Hannig, *Z. physiol. Chem.*, **290**, 1 (1952).
9. H. Svensson and I. Brattsten, *Arkiv Kemi Mineral. Geol.*, **1**, 401 (1950); I. Brattsten, *ibid.*, **4**, 503 (1952).
10. R. Weber, *Helv. chim. Acta*, **36**, 424 (1953).
11. K. S. Spiegler and C. D. Coryell, *Science*, **113**, 546 (1951).
12. K. S. Spiegler and C. D. Coryell, *J. Phys. Chem.*, **56**, 106 (1952).
13. K. S. Spiegler and C. D. Coryell, *ibid.*, **57**, 687 (1953).
14. K. S. Spiegler, *This Journal*, **100**, 303C (1953).
15. K. S. Spiegler, *Trans. Faraday Soc*, **54**, 1408 (1958).
16. G. Zweig, *J. Chromatography*, **2**, 202 (1959).
17. E. R. Tompkins, J. X. Khym, and W. E. Cohn, *J. Am. Chem. Soc.*, **69**, 2769 (1947).
18. E. R. Tompkins and S. W. Mayer, *ibid.*, **69**, 2859 (1947).
19. J. E. Salmon, *Revs. Pure Appl. Chem.*, **6**, 24 (1956).
20. D. Reichenberg, *Chemische Technik (Berlin)*, **10**, 454 (1958).
21. W. M. MacNevin and M. L. Dunton, *Anal. Chem.*, **29**, 1806 (1957).
22. G. Schwarzenbach, E. Kampitsch, and R. Steiner, *Helv. chim. Acta*, **29**, 364 (1946).
23. W. Busèr, *ibid.*, **34**, 1635 (1951).
24. D. Reichenberg and D. J. McCauley, *J. Chem. Soc.*, **1955**, 2741.
25. G. H. Evans and H. H. Strain, *Anal. Chem.*, **28**, 1560 (1956).
26. F. H. Spedding, *Discussions Faraday Soc.*, **7**, 214 (1949).
27. T. R. Sato, H. Diamond, W. P. Norris, and H. H. Strain, *J. Am. Chem. Soc.*, **74**, 6154 (1952).
28. H. T. Hookway, D. K. Hale, and R. G. Goldsmith (To National Research Development Corp.), British Pat. Appl. 336 (1957).
29. K. Sollner, *J. Phys. Colloid Chem.*, **53**, 1211, 1226 (1949).
30. M. R. J. Wyllie, *J. Phys. Chem.*, **58**, 67 (1954).
31. F. Bergsma and A. J. Staverman, *Discussions Faraday Soc.*, **21**, 61 (1956).
32. S. Dray and K. Sollner, *Biochim. Biophys. Acta*, **18**, 341 (1955).

Technical Note

A Modified RF Coil to Facilitate Floating Zone Techniques

S. J. Silverman[1]

Bell Telephone Laboratories, Allentown, Pennsylvania

Considerable interest has been apparent recently in utilizing floating zone techniques to get higher purity semiconductor single crystals other than silicon. It is well known that the success in growing a single crystal by this method is intimately related to the maintenance of a stable liquid zone. The two most important material parameters associated with this phenomenon are density and surface tension. Comparing the values of these parameters with those for silicon, one finds it increasingly more difficult to support sizable liquid zones of a material with a higher density and a lower surface tension. Specifically, Ge, GaAs, and GaP represent materials which have presented major difficulties in growing large diameter single crystals. In fact, Cunnell *et al.* (1) have recently commented that this diameter limitation is believed to be the main disadvantage of the zone process for GaAs. However, if one uses rf induction heating methods, then by careful consideration of coil design and coupling distance, one can create completely molten zones in material like GaAs whereby the zone height is significantly below the theoretical maximum of Heywang and Zeigler (2). Consequently, the previous diameter limitation may be removed; and, in other cases such as that of GaP, the probability of growing a completely single crystal can be enhanced materially.

The principal feature in the coil design is the concentration of power within a limited region of the work by suitable constriction of the rf field. At the same time an undetermined amount of electromagnetic levitation is always associated with the rf field. It is quite important to determine to what ex-

[1] Present address: Research Laboratory, General Electric Company, Schenectady, N. Y.

tent this phenomenon is responsible for maintaining a molten zone. The optimum conditions for levitating small molten masses had already been considered by Comenetz and Salatka (3) as well as others (4). A somewhat similar design was used in the present experiment to observe the effect in the floating zone process. It was a four-turn coil in the form of an inverted truncated cone, the smaller diameter on the bottom. When applied to a 16 mm diameter Ge crystal at a very close coupling distance, the coil failed to support the zone. Thus any subsequently successful support of a stable molten Ge zone of a similar diameter could not be attributed to levitation.

Referring to the first concept of power concentration, it can be shown from basic theory (5) that the power induced per unit length of work in a conventional solenoid is related to the impressed rf magnetic field as follows:

$$P \approx 8\pi \frac{H_o^2}{\sigma} \frac{a}{s} \text{ for } a \geqq 5s$$

where P is power induced in watts/cm, H_o, impressed rf magnetic field in oersteds, σ, electrical conductivity in Ω^{-1} cm^{-1}, a, radius of work in cm, and s, penetration depth of rf secondary current in cm.

Since the power depends on the square of the rf magnetic field, the experiments were oriented toward the appropriate coil configuration and coupling distance to constrict the field in such a way as to maximize the power concentration induced in the work.

Experimental

The present coil consists of a continuously wound four-turn pancake section in series with a top and a bottom reverse turn as shown in Fig. 1. The outer turn is the hot side, reducing the possibility of excessive electric fields between the coil and the work, which may otherwise result in voltage breakdown. On an empirical basis it has been concluded that the vertical spacing between either reverse turn and the pancake section is important. Too great a spacing causes separate heating of the work either above or below the region coplanar with the pancake. Too close a spacing allows the magnetic field lines to circumvent the reverse turns, negating the desired constriction affect.

Fig. 1. Modified rf work coil

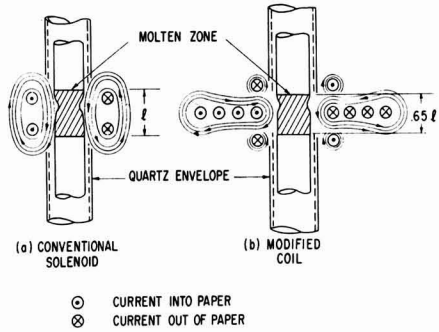

Fig. 2. Schematic representation of two different rf magnetic field configurations affecting the zone geometry of a silicon crystal.

A comparison between a conventional solenoid and the new modification is shown in the schematic of Fig. 2. The conventional coil (Fig. 2a) creates a relatively large radius of curvature of the magnetic field with consequent spreading of the molten zone, resulting in a conical liquid solid-interface. Attempts to grow a Si crystal with a conventional two turn solenoid and a large coupling distance results in a typical failure (Fig. 3a), where the sharply convex interface is revealed after the sudden spill of the molten zone. In contrast Fig. 3b shows a specimen whose interface is considerably flatter. This condition is created by utilizing the new coil. Referring to the schematic diagram (Fig. 2b) one can see that the effect of the reverse turns above and below the pancake section is to reduce the radius of curvature of the magnetic field radically in the vicinity of the work, causing a power concentration in a much smaller region than that in the conventional coil. This trend toward a more planar interface minimizes the formation of polycrystalline coring which has been frequently observed by many workers using conventional solenoids. The geometry of this interface favors an improvement in crystallographic perfection. In the course of single crystal formation a slightly convex interface has been considered quite desirable in reducing the dislocation density, as has been recently suggested by Richards (6) in connection with his observation on GaAs.

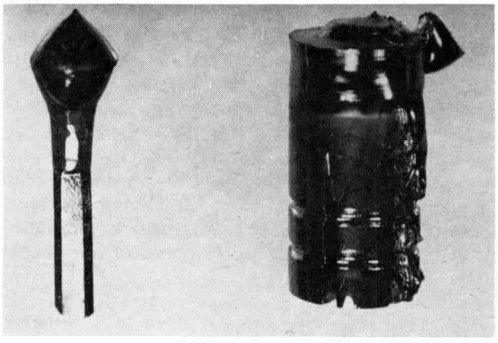

Fig. 3. Comparison of silicon interface contours as produced by (a) (left) the conventional coil and (b) (right) the modified coil.

Table I. Zone geometries of different materials subjected to conventional and modified coil designs

Material	ρ (Density in g/cc)	τ (Surface tension in dynes/cm)	Zone dimensions in mm: Δ (Coupling distance)	l (Length)	d (Diameter)	$\frac{l}{d}$
1. Si	2.3	720	6.0	~20	20	~1**
			6.0	*13*	*20*	*.65*
2. Ge	5.4	600	2.0	(Spilled)	16	—
			2.0	*7.0*	*16*	*.44*
3. GaAs	5.4	450	10	6.0	6.0	~1*
			10	*6.0*	*8.0*	*.75*
4. GaP	4.2	Unknown	5.0	6.0	6.0	1*
			5.0	*~5.0*	*6.0*	*~.8*

Conventional coil { * one turn; ** four turn } *Modified coil*

A program was inaugurated to insure that the observations on the coil's performance could be generalized for a broad category of materials rather than for one specific example. Each kind of material was represented by two samples having identical diameters and the same coupling distances. A molten zone was formed on each specimen: the first using a conventional coil, the other with the modified coil. All materials except Ge were grown in an inert gas contained in quartz envelopes having enough clearance to move vertically within the rf coil.

Silicon was studied first because of its relatively favorable values of density and surface tension, as seen in Table I. Two different frequencies were used: 450 kc and 5 mc. The results were not affected materially by this difference in operating frequencies, leading one to believe that, within these limits, frequency was a less critical parameter. After successful runs with Si, experiments were carried out on Ge, which has a density greater than that of Si by a factor of two and a surface tension lower by 16%. To obtain large diameter Ge crystals it was preferable to reduce the coupling distance as much as possible. This was achieved by surrounding the crystal with a coil at a coupling distance of 2 mm inside a large chamber which could either be evacuated or filled with an inert gaseous ambient. Relative rotation of the top and bottom chucks was used, each chuck rotating at about 50 rpm. Rotation aided the formation of a more planar interface, thereby smoothing out the asymmetry in the radial thermal gradients which was otherwise accentuated by the close proximity of the cold coil surface. As might be expected, these conditions yielded the lowest value (.44) of the length to diameter ratio as seen in Table I. A typical crystal is seen in Fig. 4. Once having demonstrated feasibility with Ge, the next logical step was to consider the crystal growing conditions for some of the III-V compounds. In addition to the material parameters similar to that of Ge, one is confronted with the adverse requirement of increasing the coupling distance to avoid condensation of the more volatile component. The condensation of As while growing GaAs has been somewhat reduced by interposing a noninductively wound strip heater between the chamber and the rf coil in a manner similar to that of Cunnell and Wickham (7). In terms of GaAs one must have P ~ .9 atm of As at T ~ 600°C; and for GaP, P ~ 25 atm of P at T ≧ 1050°C. In spite of this less favorable coupling condition, more perfect GaAs single crystals with diameters similar to the first such successful attempt shown in Fig. 5 have since been reproducibly grown. This diameter represents a 30% increase over that which has been reported to date. If one assumes a surface tension of 450 dynes/cm, for GaAs, as estimated by Weisberg *et al.* (8), then a calculation based on Heywang's (2) curve allows a maximum stable zone height of 7.1 mm for a diameter of 8 mm. In practice the zone heights have always been safely below this limit, as seen in Table I. It is anticipated that eventual modification of the furnace design to incorporate chuck rotation will permit a further increase in diameter. Frosch (9) has indicated promising progess in growing single crystal GaP by this technique, without which it would be considerably more difficult to achieve. A summary of the zone geometries for the various materials is given in Table I.

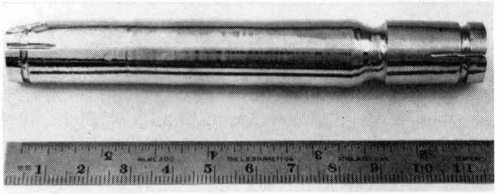

Fig. 4. Typical floating zone Ge single crystal (diameter ~16 mm).

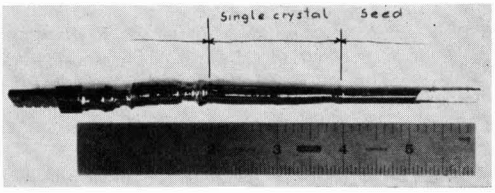

Fig. 5. Representative floating zone GaAs single crystal (diameter ~8mm).

Conclusion

A modified rf work coil incorporating two reverse turns above and below the main heating section has been responsible for concentrating the power in a restricted region of the work. By so doing we have achieved the conditions necessary to grow crystals of Ge and GaAs with larger diameters than those previously reported by the zone process.

Acknowledgment

The author wishes to thank Dr. W. C. Erdman and Mr. R. A. Porter for their invaluable contributions to this work.

Manuscript received Oct. 28, 1960. This paper was prepared for delivery before the Houston Meeting, Oct. 9-13, 1960.

Any discussion of this paper will appear in a Discussion Section to be published in the December 1961 JOURNAL.

REFERENCES

1. F. A. Cunnell, J. T. Edmond, and W. R. Harding, *Solid State Electronics*, **1**, No. 2, 97 (1960).
2. W. Heywang and G. Zeigler, *Z. Naturforsch.*, **9A**, 561 (1954).
3. G. Comenetz and J. W. Salatka, *This Journal*, **105**, 673 (1958).
4. B. Harris and A. E. Jenkins, *J Sci. Instr.*, **36**, 238 (1959).
5. G. H. Brown, C. N. Hoyler, and R. A. Bierwirth, "Radio Frequency Heating," D. Van Nostrand, New York (1948).
6. J. L. Richards, *J. Appl. Phys.*, **31**, 600 (1960).
7. F. A. Cunnell and R. Wickham, *J. Sci. Instr.*, **37**, 410 (1960).
8. L. R. Weisberg, F D. Rosi, and P. G. Heckart, AIME Meeting, Boston, Mass. (October 1959).
9. C. J. Frosch, and L. Derick, *This Journal*, **108**, 251 (1961).

Brief Communication

Photosensitive Etching of Silicon

Juergen H. Braun

Pigments Department, E. I. du Pont de Nemours and Company, Inc., Wilmington, Delaware

Brattain and Garrett (1) and, recently, Turner (2) have observed photovoltaic effects with semiconductor electrodes. Whoriskey (3) noticed that illumination affects staining of the silicon surface by solutions of nitric acid in hydrofluoric acid. Silverman and Benn (4) found that light influences chemiplating of silicon. Photoelectrolysis has been described by Uhlir (5) and was applied to device manufacture (6). Yet the effect of light on chemical etching of silicon has found only little attention; indeed, even comprehensive studies of etching phenomena fail to report lighting conditions. Experiments described below show that the impression thus created is misleading: light can have a pronounced effect on etching of silicon.

The photosensitivity of etching can be demonstrated by photoprinting (Fig. 1), performed by focusing an image onto a suitable silicon surface immersed in an etchant that attacks silicon at a moderate rate. After only a few minutes, exposure, the illuminated region of the surface changes its structure while the dark region retains its appearance. The contrast becomes more pronounced as the time of exposure increases and the image becomes permanently imprinted in the silicon.

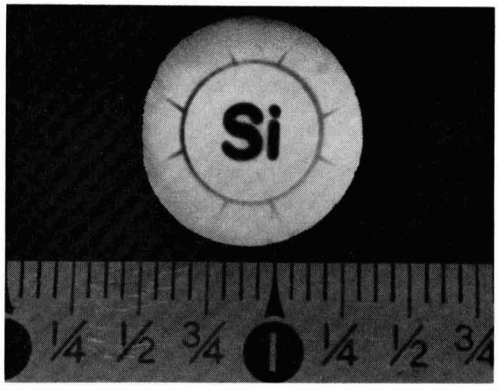

Fig. 1. Photoprinting on silicon; etched in Dash etch for 1 hr

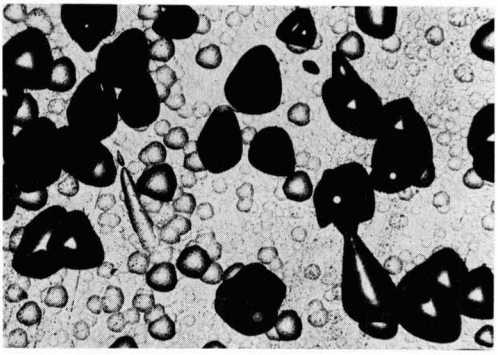

Fig. 2. Silicon surface etched in darkness; Dash etch, 16 hr. Magnification 100X. Bright field illumination.

Light accelerates the attack on n-type silicon and results in a dull and darkened surface, while a corresponding region etched in darkness dissolves at a rate that is, by orders of magnitude, slower. The "dark" surface retains its luster and develops deep etch pits of familiar appearance (Fig. 2). Etch pits on the "light" surface are barely visible and less numerous. Dark field illumination enhances visibility of the latter type of etch pit and reveals a distinctive shape (Fig. 3). For p-type silicon the effects of illumination on etching appear to be markedly less pronounced.

Experiments were conducted with n-type and p-type silicon of 0.1 to 100 ohm-cm resistivity. In most instances the silicon was etched with Dash etch (7) for periods ranging from 5 min to 2 days. Etch rates in illuminated regions were estimated at 10^3 Å/sec. The surfaces were exposed wholly or in part to illumination by 10 to 100 foot-candle of tungsten light. Printed patterns were transferred to the surface by focusing images on the silicon from lantern

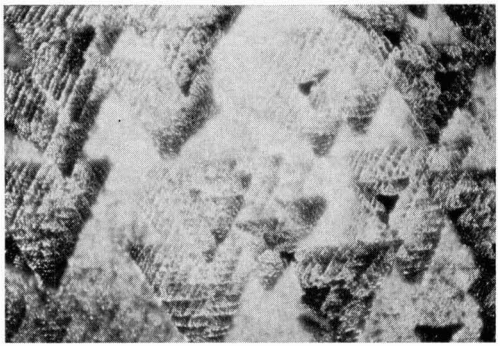

Fig. 3. Silicon surface etched in light; Dash etch, 16 hr. Magnification 100X. Dark field illumination.

slides using a simple projection system with a microscope lamp as light source. A picture began to develop on the silicon within 10 min. Optical characteristics of the projection system and not the process of photoetching itself limited resolution of the image to about 50μ. Surface preparation of the silicon had little bearing upon results. Mechanically polished, sanded, and chemically polished surfaces showed the effect equally well. Junctions in the surface were delineated clearly by a difference in etch rate of p- and n-type material.

Manuscript received March 9, 1961. This paper was prepared for delivery before the Houston Meeting, Oct. 9-13, 1961.

Any discussion of this paper will appear in a Discussion Section to be published in the December 1961 JOURNAL.

REFERENCES

1. W. H. Brattain and C. G. B. Garrett, *Bell System Tech. J.*, **34**, 129 (1955).
2. D. R. Turner, *This Journal*, **107**, 810 (1960).
3. P. S. Whoriskey, *J. Appl Phys.*, **29**, 867 (1958).
4. S. J. Silverman and D. R. Benn, *This Journal*, **105**, 170 (1958).
5. F. J. Biondi, "Transistor Technology," Vol. III, p. 134, D. Van Norstrand Co., Inc., Princeton (1958).
6. D. D. Evers (to Philco), U. S. Pat. 2,767,137, Oct. 16, 1956.
7. W. C. Dash, *J. Appl. Phys.*, **27**, 1193 (1956).

Feature

Bibliography on Electroluminescence and Related Topics, Part II

Henry F. Ivey

Research Department, Westinghouse Electric Corporation, Bloomfield, New Jersey

In 1959 a bibliography listing 720 articles or patents on electroluminescence and related effects of electric fields on solids was published in another journal (H. F. Ivey, IRE Trans. Electron Devices, *ED6*; 203). The present compilation is intended to supplement the earlier list (copies of which can be obtained from the author) and therefore entries are numbered beginning at 721. The fact that 587 new references are included indicates the intense activity in this field.

For convenience, the references have been classified into the following sections:

1. General references on electroluminescence.
2. General references on effects of electric fields in solids.
3. Electroluminescence in zinc sulfide.
4. Electroluminescence in other materials.
5. Field effects in excited phosphors.
6. Galvanoluminescence.
7. Applications of electroluminescence.
8. Patents.

It is realized that this classification scheme (or probably any other system) is not perfect, as a single paper will often contain material appropriate to more than one of the above headings; here, however, each paper has been listed only once under what is considered to be the most appropriate heading. Abstracts have not been listed if the complete paper has also been published. Since patent titles are often not very explicit, descriptive comments have been added in most cases. The new items are preceded by a listing of corrections and additions to the original bibliography. Additional corrections will be greatly appreciated.

Additions and Corrections to Previous Items

38. Add Solid-State Physics in Electronics and Telecommunications, *2*, 889 (Academic Press, 1960).
110. Change to J. Phys. Chem. Solids, *8*, 219 (1959).
116. Add Solid-State Physics in Electronics and Telecommunications, *1*, 340 (Academic Press, 1960).
120. Add Solid-State Physics in Electronics and Telecommunications, *1*, 491 (Academic Press, 1960).
125. Add Solid-State Physics in Electronics and Telecommunications, *2*, 816 (Academic Press, 1960).
128. Add Solid-State Physics in Electronics and Telecommunications, *4*, 653 (Academic Press, 1960).
172. Add Solid-State Physics in Electronics and Telecommunications, *4*, 647 (Academic Press, 1960).
195. Add Solid-State Physics in Electronics and Telecommunications, *4*, 636 (Academic Press, 1960).
232. Add Solid-State Physics in Electronics and Telecommunications, *4*, 671 (Academic Press, 1960).
265. Change to J. Appl. Phys. Japan, *11*, 594 (1957).
270. Add Solid-State Physics in Electronics and Telecommunications, *4*, 658 (Academic Press, 1960).
293. Add Solid-State Physics in Electronics and Telecommunications, *2*, 747 (Academic Press, 1960).
299. Change to J. Phys. Chem. Solids, *8*, 150 (1959).
309. Change to J. Phys. Chem. Solids, *8*, 332 (1959).
319. Change to J. Phys. Chem. Solids, *8*, 75 (1959).
342. Add J. Phys. Chem. Solids, *8*, 394 (1959).
420. Add Solid-State Physics in Electronics and Telecommunications, *4*, 598 (Academic Press, 1960).
437. Add Solid-State Physics in Electronics and Telecommunications, *4*, 611 (Academic Press, 1960).
461. Add Solid-State Physics in Electronics and Telecommunications, *4*, 594 (Academic Press, 1960).
466. Add Solid-State Physics in Electronics and Telecommunications, *4*, 602 (Academic Press, 1960).
492. Change "Gold" to "Cold".
553. Add Solid-State Physics in Electronics and Telecommunications, *4*, 762 (Academic Press, 1960).
558. Add Trans. AIEE, *78*, (Part 1), 248 (1959).
573. Change to Proc. Natl. Electr. Conf., *14*, 352 (1958); Electronic Equip. Engng., p. 34, Feb., 1959.
579. Add French Pat. 1,077,637, Nov. 10, 1954.
580. Add Australian Pat. 157,101, June 16, 1954.
581. Add Canadian Pat. 569,253, Jan. 20, 1959.
588. Add French Pat. Add. 66,222 to 1,062,791, June 5, 1956.
592. Add French Pat. Add. 63,591 to 1,062,791, Sept. 29, 1955.
594. Add French Pat. Add. 66,220 to 1,077,637, June 5, 1956, and J. O. Aicher as inventor.
613. Add U.S. Pat. 2,863,061, Dec. 2, 1958, and German Pat. 1,032,089, June 12, 1958.
615. Add German Pat. 1,007,432, May 2, 1957.
620. Add French Pat. Add. 65,871 to 1,062,791, March 22, 1956.
621. Change 2,743,249 to 2,743,239 and add French Pat. Add. 65,253 to 1,077,637, June 28, 1956.
622. Add French Pat. Add. 66,254 to 1,077,637, June 28, 1956, and German Pat. 1,014,251, Aug. 22, 1957.
623. Add French Pat. Add. 66,107 to 1,062,791, May 16, 1956.
626. Add U.S. Pat. 2,909,703, Oct. 20, 1959, and F. E. Williams as inventor.
645. Add French Pat. Add. 63,490 to 1,062,791, Sept. 28, 1955, and German Pat. 1,002,464, Feb. 14, 1957.
649. Add German Pat. 962,357, April 18, 1957.
659. Add U.S. Pat. 2,928,974, March 15, 1960.
662. Has been reissued as Re. 24,540, Sept. 23, 1958.
670. Add Canadian Pat. 575,144, May 5, 1959.
672. Add Canadian Pats. 606,135, -6, and -7, Oct. 4, 1960, and P. Zalm, H. A. Klasens, and W. Hoogenstraaten as inventors.
673. Add U.S. Pat. 2,922,892, Jan. 26, 1960, and G. Diemer and H. A. Klasens as inventors.
675. Add U.S. Pat. 2,911,553, Nov. 3, 1959, Canadian Pat. 608,655, Nov. 15, 1960, and H. J. M. Joormann and P. Zalm as inventors.
677. Add French Pat. Add. 63,873 to 1,062,791, Oct. 13, 1955.
678. Add French Pat. Add. 65,871 to 1,062,791, March 22, 1956, and German Pat. 963,172, May 2, 1957.
679. Add French Pat. 1,062,791, April 27, 1954.
680. Add U.S. Pat. 2,866,116, Dec. 23, 1958.
681. Add French Pat. Add. 63,441 to 1,062,791, Sept. 13, 1955.
682. Add Canadian Pat. 567,264, Dec. 9, 1958, and French Pat. Add. 66,166 to 1,062,791, May 17, 1956.
683. Add French Pat. Add. 63,475 to 1,062,791, Sept. 28, 1955.
685. Add French Pat. Add. 65,721 to 1,062,791, March 12, 1956.
686. Add Canadian Pat. 563,960, Sept. 30, 1958. This item is identical to #699.
694. Add R. K. Orthuber and L. R. Ullery as names of inventors.
695. Add U.S. Pat. 2,936,379, May 10, 1960, and R. K. Orthuber and L. R. Ullery as inventors.
701. Add Canadian Pat. 574,325, April 21, 1959.
703. Add U.S. Pat. 2,900,545, Aug. 18, 1959, and W. H. Drew and R. M. Rulon as inventors.
704. Add U.S. Pat. 2,952,642, Sept. 13, 1960, and A. B. Davis as inventor.
706. Add Canadian Pat. 575,169, May 5, 1959, and L. Burns as inventor.
708. Add Canadian Pat. 588,779, Dec. 15, 1959.
713. Add U.S. Pat. 2,783,407, Feb. 26, 1957.
716. Add German Pat. 1,016,860, Oct. 3, 1957.

1. General References on Electroluminescence

721. Anonymous, "Tomorrow's light," The Frontier (Armour Res. Found., Ill. Inst. Tech.), Fall, 1957.
722. Bello, F. "Light: New source in sight," Fortune, p. 138, May, 1956.

723. Butler, K. H., "Electroluminescence," Science, *129*, 544 (1959).
724. Hahn, D., "The excitation and influence of luminescence by electric fields," Ergeb. Exakt. Naturwiss., *31*, 1 (1959).
725. Henisch, H. K., and B. R. Marathe, "A note on electroluminescence due to carrier accumulation," Proc. Phys. Soc. (London), *76*, 782 (1960).
726. Ivey, H. F., "Tomorrow's light is here," Industrial Research, p. 28, Summer, 1959.
727. Jaszsczyn, P., "Certain properties of the electroluminescence of crystals," Postepy Fiz., *8*, 139 (1957).
728. Matossi, F., and S. Nudelman, "Electroluminescence," in "Methods of Experimental Physics," Vol. 6, Part B (Lark-Horovitz and Johnson, Editors), pp. 299-300, 315-331. (Academic Press, New York, 1959).
729. McKenzie, A. A., "Tomorrow's electronic light," Electronics, p. 190, Nov., 1956.
730. Oranovskii, V. E., "Electroluminescence," Priroda, Moscow, *11*, 17-22, Nov., 1958.
731. Seiler, M. R., and C. S. Peet, "Electroluminescence," Battelle Tech. Rev., p. 8, Dec., 1960.
732. Thornton, W. A., and H. F. Ivey, "Radiation, fields and electroluminescent phosphors," Westinghouse Engineer, p. 134, Sept., 1959.
733. Weiszburg, A., "On the grouping of electroluminescent effects," Acta Phys. Hungar., *10*, 337 (1959).

2. General References on Effects of Electric Fields on Solids

734. Abdullaev, G. B., G. A. Akhundov, and G. M. Aliev, "Mechanism of the effect of a strong field on p-n junctions," Doklady Akad. Nauk Azerbaidzhan SSR, *12*, 787 (1956).
735. Adirowitsch, E. I., "Influence of field emission on the distribution of strong fields in solids," Z. Phys., *155*, 195, 635 (1959).
736. Adirowitsch, E. I., "Influence of field emission on the distribution of strong fields in solids," Izvestia Akad. Nauk SSSR, *24*, 49 (1960).
737. Afanasieva, E. A., W. S. Winogradov, and E. A. Konorova, "Currents in alkali halide crystals due to electron emission from the cathode under action of an electric field," 19th M.I.T. Physical Electronics Conference, March 26-28, 1959.
738. Alfrey, G. F., and K. N. R. Taylor, "Bombardment conductivity in synthetic zinc sulfide crystals," J. Electronics Control, *8*, 301 (1960).
739. Allen, J. W., "Effect of electric fields on hydrogen-like excitons," Nature, *187*, 51 (1960).
740. Armstrong, H. L., "On avalanche multiplication in semiconductor devices," J. Electronics Control, *5*, 97 (1958).
741. Barnes, J. F., and R. H. Tredgold, "Field dependent electron mobility in ionic crystals," Proc. Phys. Soc. (London), *76*, 261 (1960).
742. Batka, V., "Emission theory of intrinsic electric breakdown," Elektrotech. Obzor, *49*, 136 (1960).
743. Bertoldi, W., and C. Kleint, "External field emission of ZnS single crystals," Ann. Phys., *4*, 388 (1959).
744. Böer, K. W., "Inhomogeneous field distribution in CdS single crystals in the region of high field strength," Z. Phys., *155*, 184 (1959).
745. Böer, K. W., "Inhomogeneous field and current distribution in semiconductors and insulators," Intntl. Conf. Semiconductors, Prague, Aug. 29-Sept. 2, 1960.
746. Böer, K. W., "Nonuniformity of field distribution and current density in CdS single crystals," Izvest. Akad. Nauk SSSR, *24*, 36 (1960).
747. Böer, K. W., "Nonuniform field distribution in electric breakdown," Izvest. Akad. Nauk SSSR, *24*, 43 (1960).
748. Böer, K. W., J. Dziesiaty, and U. Kümmel, "The electrical behavior of CdS single crystals for voltage impulses in the breakdown region," Z. Naturforsch., *13a*, 560 (1958).
749. Böer, K. W., H. J. Hänsch, and U. Kümmel, "Method for making conductivity inhomogeneities in semiconductors visible," Naturwiss., *45*, 460 (1958). (Optical effect of electric field. Also EL in CdS.)
750. Böer, K. W., H. J. Hänsch, and U. Kümmel, "Application of electro-optical effects to the analysis of electrical conductivity processes in CdS single crystals," Z. Phys., *155*, 170 (1959).
751. Böer, K. W., and U. Kümmel, "A note on the nature of dielectric breakdown," Z. Naturforsch. *9a*, 267 (1954).
752. Böer, K. W., and U. Kümmel, "Electrically excited glow curves," Arbeitstagung Festkörperphysik II (Dresden), p. 167 (Barth, Leipzig, 1955).
753. Böer, K. W., and U. Kümmel, "An experimental contribution to the problem of the electric discharge," Arbeitstagung Festkörperphysik II (Dresden), p. 171 (Barth, Leipzig, 1955).
754. Böer, K. W., and U. Kümmel, "Electrostatic charging of CdS single crystals under the influence of high fields," Z. Naturforsch., *12a*, 667 (1957).
755. Böer, K. W., and U. Kümmel, "On the electrostatic charging of CdS single crystals under the action of high electric fields," Ann. d. Phys., *2*, 217 (1958).
756. Böer, K. W., and U. Kümmel, "Contact-free excitation of electrons in CdS single crystals," Z. Naturforsch, *13a*, 698 (1958).
757. Böer, K. W., and U. Kümmel, "Influence of the contacts and of the surface on the field distribution in cadmium sulfide single crystals," Z. Phys. Chem., *214*, 127 (1960).
758. Böer, K. W., and U. Kümmel, "Processes preceding electrical breakdown in CdS single crystals," Z. Angew. Phys., *12*, 241 (1960).
759. Böer, K. W., and U. Kümmel, "On the kinetics of prebreakdown processes in solid insulation," Elektrie, *14*, 148 (1960).
760. Böer, K. W., U. Kümmel, and G. Ksoll, "Dependence of the dielectric strength on the structure of CdS single crystals," Z. Phys. Chem., *210*, 128 (1959).
761. Böer, K. W., U. Kümmel, and W. Misselwitz, "Electrical breakdown of vapor-deposited CdS films," Naturwiss., *45*, 331 (1958).
762. Böer, K. W., S. Oberländer, and J. Voigt, "On the interpretation of conductivity glow curves," Ann. d. Phys., *2*, 130 (1958).
763. Böer, K. W., and R. Rompe, "Space charge oscillations in semiconductors at high field strength," Ann. d. Phys., *5*, 200 (1960).
764. Bok, J., "Study of charge carriers in semiconductors under high electric fields," Ann. Radioelec., *15*, 120 (1960).
765. Bulyanitsa, D. S., "External electric field effect on the intrinsic absorption edge of a nonconducting crystal," Vestnik Leningrad. Univ., *14*, #10, Ser. Fiz. i Khim., #2, p. 20-4 (1959); Zhur. Eks. Teor. Fiz., *38*, 1201 (1960).
766. Burgess, R. E., "Statistical theory of avalanche breakdown in silicon," Can. J. Phys., *37*, 730 (1959).
767. Busch, G., and T. Fischer, "Field emission from semiconductors," Brown Boveri Rev., *45*, 532 (1958).
768. Chatkarov, M. L., "Variations of ionization energy in impurity semiconductors," (Effect of electric field), Zhur. Tekh. Fiz., *28*, 962 (1958); Soviet Phys.-Tech. Phys., *3*, 895 (1958).
769. Chuenkov, V. A., "Behavior of valence crystals of the germanium type in a strong electric field," Izvest. Akad. Nauk SSSR, *22*, 363 (1958); Zhur. Tekh. Fiz., *28*, 470 (1958).
770. Chuenkov, V. A., "Deduction of a criterion for dielectric breakdown in ionic crystals from a kinetic equation," Izvest. Akad. Nauk SSSR, *22*, 369 (1958).
771. Chynoweth, A. G., "Electrical breakdown in p-n junctions," Semiconductor Products, *1*, 33 (1958).
772. Chynoweth, A. G., "Field ionization in narrow p-n junctions," Intntl. Conf. Semiconductors, Progue, Aug. 29-Sept. 2, 1960.
773. Chynoweth, A. G., "Internal field emission," Progress in Semiconductors, *4*, 95 (1960) (John Wiley, New York).
774. Chynoweth, A. G., "Uniform silicon p-n junctions. II. Ionization rates for electrons," J. Appl. Phys., *31*, 1161 (1960).
775. Chynoweth, A. G., W. L. Feldmann, C. A. Lee, R. A. Logan, G. L. Pearson, and P. Aigrain, "Internal field emission at narrow silicon and germanium p-n junctions," Phys. Rev. *118*, 425 (1960).
776. Chynoweth, A. G., and R. A. Logan, "Internal field emission at narrow p-n junctions in indium antimonide," Phys. Rev., *118*, 1470 (1960).
777. Chynoweth, A. G., and K. G. McKay, "Internal field emission in silicon p-n junctions," Phys. Rev. *106*, 418 (1957).
778. Dilworth, C. C., "The influence of surface films on the electrical behavior of contacts," Proc. Phys. Soc. (London), *60*, 315 (1948).
779. Distad, M. F., "Equilibrium currents induced in zincblende by electron bombardment of negative electrode," Phys. Rev., *80*, 879 (1950).
780. Elinson, M. I., "The influence of internal electric fields in a semiconductor on its field emission," Radiotekh. i Elektronika, *4*, 140 (1959).
781. Elinson, M. I., and D. V. Zernov, "The mechanism of electron emission from thin dielectric layers due to a strong electric field (the Malter effect)," Radiotekh. i Elektronika, *2*, 75 (1957).
782. Esaki, L., "New phenomenon in narrow germanium p-n junctions," Phys. Rev., *109*, 603 (1958).
783. Fomin, N. V., "Absorption of infrared radiation by semiconductors in an electric field," Fiz. Tverdogo Tela, *2*, 605 (1960).
784. Franz, W., "Dielectric breakdown," Handbuch der Physik, *17*, 155 (Springer Verlag, 1956).
785. Franz, W., "Influence of an electric field on an optical absorption edge," Z. Naturforsch., *13a*, 484 (1958).
786. Franz, W., "The theory of the inner field emission from the valence band," Z. Naturforsch., *14a*, 415 (1959).
787. Fröhlich, H., and B. V. Paranjape, "Dielectric breakdown in solids," Proc. Phys. Soc. (London), *69B*, 21 (1956).
788. Fröhlich, H., and J. H. Simpson, "Intrinsic dielectric breakdown in solids," Advances in Electronics, *2*, 185 (1950).
789. Geppert, D. V., "Internal field emission and low temperature thermionic emission into vacuum," Proc. IRE, *48*, 1644 (1960).
790. Goetzberger, A., and W. Shockley, "Metal precipitates in silicon p-n junctions," J. Appl. Phys., *31*, 1821 (1960).
791. Goffaux, R., "Electronic emission of p-n junctions," J. Phys. Rad., *21*, 94 (1960).
792. Gordeev, G. V., "Ionization by collision at n-p junctions," Fiz. Tverdogo Tela, *1*, 851 (1959).

793. Gribnikov, Z. S., and E. I. Rashba, "Exciton diffusion in a nonhomogeneous electric field," Zhur. Tekh. Fiz., *28*, 1948 (1958); Fotoelek. i Opt. Yavleniya v Poluprovod., Trudy Pervogo Vsesoyuz. Soveshchaniya, Kiev, p. 123 (1959).
794. Gross, E. F., and B. P. Zakharchenia, "Ionization of excitons in Cu_2O crystals by an electric field," Zhur. Tekh. Fiz., *28*, 231 (1958); Soviet Physics-Tech. Phys., *3*, 206 (1958).
795. Harrick, N. J., "Metal to semiconductor contacts: Injection or extraction for either direction of current flow," Phys. Rev., *115*, 876 (1959).
796. Harrick, N. J., "Rectification without injection at metal-to-semiconductor contacts," Phys. Rev., *118*, 986 (1960).
797. Kallmann, H. P., B. Kramer and G. M. Spruch, "Alternating-current impedance measurements on insulated cadmium sulfide crystals," Phys. Rev., *116*, 628 (1959).
798. Kamphusmann, J., "On the theory of internal field emission," Z. Naturforsch., *14a*, 165 (1959).
799. Kane, E. O., "Zener tunneling in semiconductors," J. Phys. Chem. Solids, *12*, 181 (1960).
800. Keldysh, L. V., "Effect of crystal lattice vibrations on electron-hole pair production in a strong electric field," Zhur. Eks. Teor. Fiz., *34*, 962 (1958).
801. Keldysh, L. V., "Kinetic theory of impact ionization in semiconductors," Zhur. Eks. Teor. Fiz., *37*, 713 (1959); Soviet Phys.-JETP, *37*, 509 (1960).
802. Keldysh, L. V., V. S. Vavilov, and K. Britzin, "The effect of strong electric fields on the absorption edge in silicon," 20th M.I.T. Physical Electronics Conf., Cambridge, Mass., March 25, 1960.
803. Keldysh, L. V., V. S. Vavilov, and K. I. Britzin, "The influence of a strong electric field on the optical properties of semiconductors," Intntl. Conf. Semiconductors, Prague, Aug. 29-Sept. 2, 1960.
804. Koenig, S. H., "Inter-electron collisions and the 'temperature' of hot electrons," Proc. Phys. Soc. (London), *73*, 959 (1959).
805. Lüty, F., "Field emission from excited color centers," Z. Phys., *153*, 247 (1958).
806. Maserjian, J., "Determination of avalanche breakdown in p-n junctions," J. Appl. Phys., *30*, 1613 (1959).
807. Mead, C. A., "The tunnel-emission amplifier," Proc. IRE, *48*, 359 (1960).
808. Merz, W. J., "Some photoelectronic properties of ZnS single crystals," in Solid State Physics in Electronics and Telecommunications, *2*, 811 (Academic Press, 1960).
809. Muss, D. R., and R. F. Greene, "Reverse breakdown in In-Ge alloy junctions," J. Appl. Phys., *29*, 1534 (1958).
810. O'Dwyer, J. J., "Dielectric breakdown in solids," Adv. Physics, *2*, 349 (1958).
811. Patrick, L., and W. J. Choyke, "Electron emission from breakdown regions in SiC p-n junctions," Phys. Rev. Letters, *2*, 48 (1959).
812. Petrov, A. N., G. G. Talyts, and M. S. Giterman, "Stark effect on excitons in ionic crystals," Fiz. Metal. i Metalloved, Akad. Nauk SSSR, *9*, 327 (1960).
813. Price, P. J., and J. M. Radcliffe, "Esaki tunneling," IBM J. Res. Dev., *3*, 364 (1959).
814. Ridley, B. K., "The effect of an electric field on the decay of excess carriers in semiconductors," Proc. Phys. Soc. (London), *75*, 157 (1960).
815. Rose, F. W. G., "A comparison of the theory of impact ionization with measurements on silicon p-n junctions," J. Electronics Control, *6*, 70 (1959).
816. Rother, H., "The mechanism of the diffusion-determined field instabilities in semiconductors at high field strengths," Ann. Phys., *5*, 203 (1960).
817. Rothstein, J., "Enhancement of photographic speed and sensitivity by electric fields," Photographic Sci. Engng., Jan.-Feb., 1960.
818. Ruppel, W., "Space-charge-limited currents in ZnS single crystals," Helv. Phys. Acta, *31*, 311 (1958).
819. Senitzky, B., "Electron emission from silicon p-n junctions," Phys. Rev., *116*, 874 (1959).
820. Senitzky, B. and J. L. Moll, "Breakdown in silicon," Phys. Rev., *110*, 612 (1958).
821. Shotov, A. P., "Collision ionization in germanium p-n junctions," Zhur. Tekh. Fiz., *28*, 437 (1958), Soviet Phys.-Tech. Phys., *3*, 413 (1958).
822. Sillars, R. W., "The effect of field emission on the behavior of semiconductor contacts," Proc. Phys. Soc. (London), *68B*, 881 (1955).
823. Simon, R. E., and W. E. Spicer, "Field-induced photoemission and hot-electron emission from germanium," J. Appl. Phys., *31*, 1505 (1960).
824. Simon, R. E., and W. E. Spicer, "Photoemission from Si induced by an internal electric field," Phys. Rev., *119*, 621 (1960).
825. Snitko, O. V., "Influence of an external electric field on the surface recombination and condenser photoelectromotive force of n-type silicon," Fiz. Tverdogo Tela, *1*, 980 (1959).
826. Sohm, J. C., "Impact ionization of impurities in silicon at low temperatures," Compt. rend., *249*, 2737 (1959).
827. Steele, M. C., "Collision ionization in n-indium arsenide," Bull. Am. Phys. Soc., *4*, 28 (1959).
828. Steele, M. C., and M. Glicksman, "Properties of p-type InSb in pulsed high electric fields," Phys. Rev., *118*, 474 (1960).
829. Steele, M. C., L. Pensak, and R. D. Gold, "Pulse amplification using impact ionization in germanium," Proc. IRE, 47, 1109 (1959).
830. Steinberger, I. T., "Further experimental evidence on majority carrier injection in CdS single crystals," J. Phys. Chem. Solids, *15*, 354 (1960).
831. Stöckmann, F., "The dependence of photoelectric currents on electric field intensity," Z. Phys., *147*, 544 (1957).
832. Stratton, R., "Field emission from semiconductors," Proc. Phys. Soc. (London), *B68*, 746 (1955).
833. Stratton, R., "The effect of field emission on the behavior of semiconductor contacts," Proc. Phys. Soc. (London), *69B*, 491 (1956).
834. Stratton, R., "The hot-electron effect in n-type germanium," J. Electronics Control, *5*, 157 (1958).
835. Thielemann, W., "Field effect on CdS single crystals," Z. Naturforsch, *14a*, 92 (1959).
836. Ukhanov, Y. I., and S. G. Shul'man, "Effect of strong electric field on the transparency of a germanium diode," Zhur. Tekh. Fiz., *27*, 2507 (1957); Soviet Phys.-Tech. Phys., *2*, 2332 (1957).
837. Vermeer, J., "The electrical conduction of glass at high field strengths," Physica, *22*, 1257 (1957).
838. Von Hippel, A., "Electronic conduction in insulating crystals under very high field strength," Phys. Rev., *54*, 1096 (1938).
839. Whitehead, S., "Dielectric breakdown of solids" (Oxford Univ. Press, 1951).
840. Williams, R., "Electric field induced light absorption in CdS," Phys. Rev., *117*, 1487 (1960).
841. Wul, B. M., "On the breakdown in p-n junctions in germanium," in "Semiconductors and Phosphors," p. 647 (Interscience Publishers, 1958).
842. Wul, B. M., and A. P. Shotov, "Impact ionization in silicon p-n junctions," Fiz. Tverdogo Tela, Suppl. *1*, 150 (1959).
843. Yamaguchi, J., and Y. Hamakawa, "High electric field effects in germanium p-n junctions," J. Phys. Soc. Japan, *14*, 15 (1959).
844. Yamashita, J., "Theory of avalanch multiplication in nonpolar semiconductors," Progress in Semiconductors, *4*, 63 (John Wiley, New York 1960).
845. Yashukova, I. M., "The dependence of the electrical conductivity of polycrystalline CdSe on the electric field intensity," Fiz. Tver. Tela, *1*, 388 (1959); Soviet Phys. Solid State, *1*, 349 (1959).
846. Zverev, L. P., M. M. Noskov, and M. Y. Shur, "Influence of an electric field on the spectral dependence of the internal photoeffect in cuprous oxide," Izvest. Vysshikh Ucheb. Zavedenii Fiz., No. 2, p. 39-42 (1959).

3. Electroluminescence in Zinc Sulfide

847. Antonov-Romanovskii, V. V., "Electroluminescence of zinc sulfide powder layers," Czech. J. Phys., *9*, 146 (1959) (in English).
848. Antonov-Romanovskii, V. V., "On relaxation of electroluminescence for small departures from the stationary state," Optika i Spektros., *6*, 229 (1959); Optics and Spectros., *6*, 146 (1959).
849. Aso, T., K. Nakamura, and K. Hashimoto, "Functions of copper impurities in zinc sulfide," Rep. Liberal Arts. Sci. Fac. Shizuoka Univ., Nat. Sci., *2*, 53 (1958).
850. Ballentyne, D. W. G., "Crystal structure and electroluminescence in ZnS," J. Phys. Chem. Solids, *10*, 242 (1959).
851. Ballentyne, D. W. G., "Electroluminescence—A disorder phenomena," J. Electrochem. Soc., *107*, 807 (1960).
852. Bodo, Z., and J. Weiszburg, "Light patterns of electroluminescent panels," Acta. Phys. Hungar., *10*, 341 (1959).
853. Bonch-Bruevich, A. M., "On electroluminescent phenomena when an electric field is switched on and off," Optika i Spektros., *6*, 256 (1959); Optics and Spectros., *6*, 165 (1959).
854. Bonch-Bruevich, A. M., and O. S. Marenkov, "Polarization phenomena in electroluminors," Optika i Spektros., *8*, 855 (1960); Optics and Spectros., *8*, 449 (1960).
855. Bukke, E. E., L. A. Vinokurov, and M. V. Fok, "Effect of the sum of the stored light on the intensity of electroluminescence of ZnS:Cu, Al phosphors," Optika i Spektros., *5*, 172 (1958).
856. Damaskova, S., "Course of electroluminescence of ZnS:Cu, Mn," Czech. J. Phys., *9*, 529 (1959).
857. Destriau, G., "Some new technical aspects of electroluminescence," Bull. Soc. Franc. Electr., *9*, 383 (1959).
858. Diemer, G., and P. Zalm, "The role of exhaustion barriers in electroluminescent powders," Physica, *25*, 232 (1959) (Short note only).
859. Dreeben, A., "Effect of CdS on the electroluminescence of ZnS:Cu, halide phosphors," Meeting Electrochem. Soc., Chicago, May 4, 1960.
860. Favorin, V. N., G. S. Kozina, and L. K. Tikhonova, "Spectral characteristics of electroluminescence of some electroluminophors in the case of the simultaneous action of constant and alternating fields," Optica i Spektros., *7*, 703 (1959); Optics and Spectros. 7, 420 (1959).
861. Favorin, V. N., and L. P. Poskacheyeva, "Voltage dependence of the spectral composition of the radiation from certain electroluminophors in an alternating field," Optika i Spektros., *7*, 706 (1959); Optics and Spectros., *7*, 422 (1959).
862. Fredericks, W. J., "Very low frequency excitation of electroluminescence," Bull. Am. Phys. Soc., *5*, 187 (1960) (Abstract).

863. Fujisaki, H., T. Matsumura, and Y. Tanabe, "The electrical character and the electroluminescence of ZnS crystals with various metal electrodes," Tohoku Daigaku Kagakukeisoku Kenkyusho Hokoku, *7*, (1958) (Translation 59-17899, The John Crerar Library).
864. Georgobiani, A. N., and M. V. Fok, "Relaxation processes in electroluminescence," Optika i Spektros., *5*, 167 (1958).
865. Goffaux, R., "Electronic properties of electroluminescent ZnS powders," J. Phys. Rad., *20*, 18A (1959).
866. Goldberg, P., "Particle size effects and the distribution of barriers in electroluminescent zinc sulfide phosphors," J. Electrochem. Soc., *106*, 34 (1959).
867. Goldberg, P., "The action of nickel and cobalt in electroluminescent zinc sulfide phosphors," J. Electrochem. Soc., *106*, 498 (1959).
868. Goldberg, P., "Etch pits on electroluminescent zinc sulfide crystallites," Meeting on Color Centers and Crystal Luminescence, Turin, Sept. 8-11, 1960.
869. Goldberg, P., and S. Faria, "On the physical characteristics and chemical composition of electroluminescent phosphors," J. Electrochem. Soc., *107*, 521 (1960).
870. Greguss, P., and J. Weiszburg, "The electroluminescent panel in an ultrasonic field," Acustica, *9*, 183 (1959).
871. Halpin, A. T., and P. Goldberg, "Effects of interaction among particles in electroluminescent layers," Meeting Electrochem. Soc., Chicago, May 3, 1960.
872. Hoffmann, G. R., and D. H. Smith, "The light output waveform emitted from electroluminescent cells energized by square waves and pulses of voltage," J. Electronics Control, *9*, 161 (1960).
873. Huzimura, R., and T. Sidei, "Effect of impurities and (firing) temperature on the spectra of electroluminescence," J. Phys. Soc. Japan, *13*, 1064 (1958).
874. Jaffe, P. M., "Influence of Mg and Cd on the electroluminescence of ZnS:Cu phosphors," Meeting Electrochem. Soc., Chicago, May 4, 1960.
875. Jaffe, P. M., "Influence of halogen coactivator on the electroluminescence of ZnS:Cu phosphors," Meeting Electrochem. Soc., Chicago, May 4, 1960.
876. Johnson, J. E., "Microsecond response of electroluminescent cells," Meeting IRE Prof. Group on Electron Devices, Washington, Oct. 28, 1960.
877. Kazankin, O. N., F. M. Pekerman, and L. N. Petoshina, "Electroluminescent sulfide and selenide phosphors," Optika i Spektros., *6*, 672 (1959); Optics and Spectros., *6*, 435 (1959).
878. Kazankin, O. N., F. M. Pekerman, and L. M. Petoshina, "Electroluminescence of ZnS:Cu,Mn phosphors in a constant field," Optika i Spektros., *7*, 776 (1959); Optics and Spectros., *7*, 458 (1959).
879. Kazankin, O. N., and L. N. Petoshina, "Influence of temperature on the electroluminescence of powder phosphors," Optika i. Spektros., *4*, 76 (1958).
880. Koller, L. R., and H. D. Coghill, "Formation of phosphor films by evaporation," J. Electrochem Soc., *107*, 973 (1960).
881. Kozina, G. S., V. N. Favorin, and I. D. Anisimova, "Electroluminescence light pulses under the simultaneous action of DC and AC voltages," Optika i Spektros., *8*, 218 (1960); Optics and Spectros., *8*, 112 (1960).
882. Kozina, G. S., and L. P. Poskacheeva, "Total luminescence brightness of ZnS:Cu and ZnS:Cu,Mn electroluminophors in a pulsating field," Optika i Spektros., *8*, 214 (1960); Optics and Spectros., *8*, 110 (1960).
883. Kremheller, A., "Microscopic observations on electroluminescent phosphors," J. Electrochem. Soc., *107*, 8 (1960).
884. Kuchar, K., "Remarks on the theory of electroluminescence in ZnS crystals," Czech. J. Phys., *9*, 679 (1959).
885. Larach, S., and R. E. Shrader, "Electroluminescence of polycrystallites," RCA Rev., *20*, 532 (1959).
886. Lehmann, W., "Voltage dependence and particle size distribution of electroluminescent phosphors," J. Electrochem. Soc., *107*, 20 (1960).
887. Lehmann, W., "Microscopic observations on electriluminescent ZnS:Cu phosphors," J. Electrochem. Soc., *107*, 657 (1960).
888. Liamichev, I. Y., and I. N. Orlov, "The influence of the electrical prehistory of an electroluminescent phosphor on the characteristics of its emission when excited by short voltage pulses," Optika i Spektros., *7*, 398 (1959); Optics and Spectros., *7*, 258 (1959).
889. Lochinger, R. B., "Electroluminescence at high excitation frequencies," Scientia Electrica, Vol. 4, #4 (1958).
890. Lozykowski, H., and M. Rozwadowski, "Effect of ultrasonic waves on electroluminescence of ZnS:Cu phosphor," Bull. Acad. Polon. Sci., Ser. Sci. Math. Astron. Phys., *7*, 651 (1959).
891. Maeda, K., "Origin of local high electric field in electroluminescence," Physica, *25*, 721 (1959).
892. Maeda, K., "Electroluminescence of insulated particles," J. Phys. Soc. Japan, *13*, 1352 (1958); *15*, 2051 (1960).
893. Matsumura, T., H. Fujisaki, and Y. Tanabe, "Preparation of zinc sulfide single crystals," Sci. Rep. Res. Inst. Tokoku Univ., *A10*, 459 (1958) (also ac and dc electroluminescence).
894. Matsumura, T., and Y. Tanabe, "Electroluminescence of ZnS single crystals," Tokoku Daigaku Kagakukeisoku Kenkyusho Hokoku, *7*, 175 (1958) (Translation 59-17900, The John Crerar Library).
895. Miyamoto, T., "Electroluminescence of thin films of ZnS containing $MnCl_2$," Oyo Butsuri, *28*, 594 (1959).
896. Mujashita, K., T. Takahashi, and M. Wada, "Brightness and firing atmosphere in preparation of electroluminescent ZnS (Cu,Al) phosphors," Rep. Res. Inst. Elec. Comm., Tohoku Univ., *10*, 125 (1958).
897. Morehead, F. F., "The mechanism and efficiency of electroluminescence in ZnS phosphors," J. Electrochem. Soc., *107*, 281 (1960).
898. Mudar, J., S. Nudelman, and K. Kamyszek, "Electroluminescent time average light output of a ZnS:Se phosphor," Meeting Electrochem. Soc., Chicago, May 4, 1960.
899. Nakajima, S., S. Yasuoka, and W. Ichise, "Electroluminescence of ZnS:Cu,Mn phosphors," Toshiba Review (Japan), *15*, 622 (1960).
900. Nakamura, K., "The electroluminescence and the electrophotoluminescence of ZnS phosphors," Oyo Butsuri, *27*, 528 (1958).
901. Naraoka, K., and Y. Kotera, "Electroluminescence of ZnS:Cu,Mn phosphors," Oyo Butsuri, *29*, 116 (1960).
902. Narita, S., "Electroluminescence in ZnS single crystals," J. Phys. Soc. Japan, *15*, 128 (1960).
903. Neumark, G. F., "Efficiency of electroluminescence in ZnS," Phys. Rev., *116*, 1425 (1959).
904. Nudelman, S., and J. Mudar, "Fatigue in electroluminescent phosphors," Bull. Am. Phys. Soc., *5*, 70 (1960) (Abstract).
905. Oranovskii, V. E., and B. A. Khmelinin, "Study of electroluminescence of ZnS:Cu single crystals," Optika i Spektros., *7*, 542 (1959); Optics and Spectros., *7*, 336 (1959).
906. Oranovskii, V. E., E. I. Panasiuk, and V. T. Fediushin, "Electroluminescence of ZnS single crystals," Inzh. Fiz. Zhur. Akad. Nauk Belorus SSR, *2*, 39 (1959).
907. Oranovskii, V. E., and Z. A. Trapeznikova, "Spectra of electro- and photoluminescence of phosphors activated by rare earth elements," Optika i Spektros., *5*, 302 (1958).
908. Patek, K., "Temperature dependence of secondary peak of electroluminescence of ZnS:Cu," Czech. J. Phys., *9*, 460 (1959).
909. Patek, K., "The electroluminescence of single crystals of ZnS:Cu excited with pulses of alternating polarity," Czech. J. Phys., *10*, 452 (1960).
910. Patek, K., "The influence of a small electric perturbation on the electroluminescence curve of ZnS:Cu," Czech. J. Phys., *10*, 679 (1960).
911. Rabotkin, V. L., and V. A. Sokolov, "Anisotropy of the light pulses from a polarized electroluminescent cell," Optika i Spektros., *8*, 276 (1960); Optics and Spectros., *8*, 144 (1960).
912. Ratner, M., "Capacitative measurements on zinc sulfide electroluminescent cells," Bull. Am. Phys. Soc., *4*, 370 (1959) (Abstract).
913. Ratner, M., "Ionic properties of electroluminescent zinc sulfide," Bull. Am. Phys. Soc., *5*, 70 (1960) (Abstract).
914. Sidei, T., and R. Huzimura, "Electroluminescence of ZnS. Dependence on voltage and variation with time," Oyo Butsuri (Japan), *28*, 14 (1959).
915. Sloyan, T. J., "Electroluminescent emission under pulse excitation," IRE-AIEE Solid-State Device Research Conf., Ithaca Univ., June 17-19, 1959.
916. Smith, I. L., R. M. Potter, and M. Aven, "Mechanism of depreciation of electroluminescent phosphors," Meeting Electrochem. Soc., Chicago, May 3, 1960.
917. Solomon, A. L., and P. Goldberg, "Copper-chloride relationships in photoluminescent and electroluminescent zinc sulfide," Meeting Electrochem. Soc., Chicago, May 4, 1960.
918. Stauer, E. V., and V. P. Izotov, "Dielectric and optical properties of some zinc sulfides." Izvest. Akad. Nauk SSSR, *24*, 224 (1960).
919. Stauer, E. V., and M. G. Rosenblat, "Influence of crushing on the optical and electrical properties of some ZnS electroluminors," Optika i Spektros., *7*, 570 (1959); Optics and Spectros., *7*, 351 (1959).
920. Steinberger, I. T., "A direct proof for a carrier multiplication process during electroluminescence," Solid State Physics in Physics and Telecommunication, *4*, 646 (Academic Press, 1960).
921. Steinberger, I. T., V. Bar, and E. Alexander, "Electroluminescence of zinc sulfide single crystals," Meeting on Color Centers and Crystal Luminescence, Turin, Sept. 8-11, 1960; Phys. Rev., *121*, 118 (1961).
922. Strock, L. W., "Temperature-induced color shifts in electroluminescence," Meeting Electrochemical Society, Chicago, May 2, 1960.
923. Strock, L. W., "Phosphors for electroluminescent lamps," Illum. Engng., *55*, 24 (1960).
924. Strock, L. W., "Color of electroluminescent phosphors," Meeting Opt. Soc. Am., Boston, Oct. 14, 1960.
925. Tanaka, S., "Electroluminescence of ZnS phosphors excited by short field pulses," J. Phys. Soc. Japan, *41*, 1123 (1959).
926. Thornton, W. A., "ac-dc electroluminescence," Phys. Rev., *113*, 1187 (1959).
927. Thornton, W. A., "Electroluminescence at low voltages," Phys. Rev., *116*, 893 (1959).
928. Thornton, W. A., "Electroluminescent thin films," J. Appl. Phys., *30*, 123 (1959).

929. Thornton, W. A., "DG electroluminescence of zinc sulfide films," IRE-AIEE Solid-State Device Research Conf., Pittsburgh, June 13, 1960.
930. Thornton, W. A., "Electroluminescence maintenance," J. Electrochem. Soc., *107*, 895 (1960).
931. Trofimov, V. S., "Dependence of the brightness of electroluminescence on voltage," Optics i Spektros., *4*, 113 (1958).
932. Vlasenko, N. A., "The effect of temperature on the electroluminescence of a sublimed ZnS:Mn phosphor," Optika i Spektros., *8*, 414 (1960); Optics and Spectros., *8*, 215 (1960).
933. Vlasenko, N. A., and I. A. Popkov, "Study of the electroluminescence of a sublimed ZnS:Mn phosphor," Optika i Spektros., *8*, 81 (1960); Optics and Spectros., *8*, 39 (1960).
934. Wachtel, A., "ZnS:Cu,Cl and (Zn,Cd)S:Cu,Cl electroluminescent phosphors," J. Electrochem. Soc., *107*, 602 (1960).
935. Wachtel, A., "(Zn,Hg)S and (Zn,Cd,Hg)S electroluminescent phosphors," J. Electrochem. Soc., *107*, 682 (1960).
936. Wada, M., T. Takahashi, and M. Fukuda, "An apparatus for measurement of the waveform of electroluminescence," Oyo Butsuri (Japan), *28*, 26 (1959).
937. Weiszburg, J., "Light patterns of electroluminescent panels," Acta Phys. Hungar., *10*, 341 (1959).
938. Weiszburg, J., and P. Greguss, Jr., "The effect of ultrasonic radiation on electroluminescent panels," Acta Phys. Hungar., *11*, 185 (1960).
939. Weiszburg, J., J. Schanda, and Z. Bodo, "Time-dependent spectra of electroluminescent ZnS:Cu,Pb," Phil. Mag., *4*, 830 (1959).
940. Wendel, G., and G. Richter, "Electroluminescence of copper-activated zinc sulfides," Z. Phys. Chem., *214*, 253; *215*, 80 (1960).
941. Zallen, R., W. T. Eriksen, and H. Ahlburg, "Electroluminescence under pulsed square-wave excitation," J. Electrochem. Soc., *107*, 288 (1960).

4. Electroluminescence in Other Materials

942. Adams, I., J. W. Mellichamp, and G. A. Wolff, "Luminescence of AlN," Meeting Electrochem. Soc., Chicago, May 2, 1960.
943. Allen, J. W., and P. E. Gibbons, "Breakdown and light emission in gallium phosphide diodes," J. Electronics Control, *7*, 518 (1959).
944. Astafurov, A. U., "Electric breakdown of thick ice layers during pulsing," Izvest. Akad. Nauk SSSR, *22*, 419 (1958).
945. Batdorf, R. I., A. G. Chynoweth, G. C. Dacey, and P. W. Foy, "Uniform silicon p-n junctions. I. Broad area breakdown," J. Appl. Phys., *31*, 1153 (1960).
946. Benoit a là Guillaume, C., "Recombination of excess carriers in germanium," Ann. Phys., *4*, 1187 (1959).
947. Benoit a là Guillaume, C., and O. Parodi, "Zeeman effect on the intrinsic recombination emission in germanium," J. Electronics and Control, *6*, 356 (1958).
948. Benoit a là Guillaume, C., and O. Parodi, "Radiative recombination of free carriers with carriers trapped at impurity centers," Solid-State Physics in Electronics and Telecommunications, *1*, 294 (Academic Press, 1960).
949. Benoit a là Guillaume, C., and O. Parodi, "Radiative rebination in germanium and silicon," Intntl. Conf. Semiconductors, Prague, Aug. 29-Sept. 2, 1960.
950. Brill, P. H., and R. F. Schwarz, "Radiative recombination in germanium," Phys. Rev., *112*, 330 (1958).
951. Chynoweth, A. G., and H. K. Gummel, "Photon emission from avalanche breakdown in germanium p-n junctions," J. Phys. Chem. Solids, *16*, 191 (1960).
952. Chynoweth, A. G., and K. G. McKay, "Light emission and noise studies of individual microplasmas in silicon p-n junctions," J. Appl. Phys., *30*, 1811 (1959).
953. Davies, L. W., "Recombination radiation from hot electrons in silicon," Phys. Rev. Letters, *4*, 11 (1960).
954. DeNobel, D., "Phase equilibria and semiconducting properties of cadmium telluride," Philips Res. Rep., *14*, 361, 430 (1959).
955. Eagles, D. M., "Optical absorption and recombination radiation in semiconductors due to transitions between hydrogen-like acceptor impurity levels and the conduction band," J. Phys. Chem. Solids, *16*, 76 (1960).
956. Elinson, M. I., G. F. Vasil'ev, and A. G. Zhdan, "Autoelectronic emission of dielectrics containing impurities," Radiotekh. i Elektron., *4*, 1718 (1959), (Electroluminescence of corundum, Al_2O_3).
957. Eriksen, W. T., "Minority carrier lifetime by carrier injection electroluminescence in SiC," Silicon Carbide, p. 376 (Pergamon Press, 1960).
958. Frerichs, R., and R. Handy, "Electroluminescence in cuprous oxide," Phys. Rev., *113*, 1191 (1959).
959. Frerichs, R., and I. Liberman, "Electroluminescence at point Contacts in cuprous oxide and the mobility of Cu^+ ions at room temperature," Phys. Rev. Letters, *3*, 214 (1959).
960. Goetzberger, A., "Investigation of crystal imperfections by means of avalanche breakdown patterns of very thin junctions in silicon," Intntl. Conf. Semiconductors, Prague, Aug. 29-Sept. 2, 1960.
961. Goetzberger, A., "Uniform avalanche effect in silicon three-layer diodes," J. Appl. Phys., *31*, 2260 (1960).
962. Gorton, H. C., J. M. Swartz, and C. S. Peet, "Radiative recombination in gallium phosphide point-contact diodes," Nature, *188*, 303 (1960).
963. Gosnet, A., O. Parodi, and C. Benoit a là Guillaume, "Light due to recombination by means of impurities in germanium," Compt. Rend. *248*, 1628 (1959).
964. Greebe, C. A. A. J., and W. F. Knippenberg, "Grown p-n junctions in silicon carbide," Philips Res. Repts., *15*, 120 (1960).
965. Grimmeiss, H. G., W. Kischio and A. Rabenau, "Preparation and electrical and optical properties of AlP," J. Phys. Chem. Solids, *16*, 302 (1960).
966. Grimmeiss, H. G., and H. Koelmans, (EL in GaN), Z. Naturforsch., *14a*, 264 (1959).
967. Grimmeiss, H. G. and H. Koelmans, "P-N luminescence and photovoltaic effects in GaP," Philips Res. Repts., *15*, 290 (1960).
968. Haynes, J. R., "Production and detection of recombination radiation" in Methods of Experimental Physics, Vol. 6, Part B, 321-324 (Lark-Horovitz and Johnson, Editors), (Academic Press, New York, 1959).
969. Haynes, J. R., "Experimental proof of the existence of a new electronic complex in silicon," Phys. Rev. Letters, *4*, 361 (1960).
970. Imai, T., Y. Mizushima, and Y. Igarashi, "New cold cathode using magnesium oxide," J. Phys. Soc. Japan, *14*, 979 (1959).
971. Kikuchi, M., "Visible light emission from metal-silicon contact," J. Phys. Soc. Japan, *14*, 682 (1959).
972. Kikuchi, M., and S. Iizima, "Avalanche electroluminescence in CdS single crystals," J. Phys. Soc. Japan, *14*, 852 (1959).
973. Kikuchi, M., and T. Iizuka, "Observation of microplasma pulses and electroluminescence in gallium phosphide single crystal," J. Phys. Soc. Japan, *15*, 935 (1960).
974. Kikuchi, M., and K. Tachikawa, "Visible light emission from germanium diffused p-n junction," J. Phys. Soc. Japan, *14*, 1830 (1959).
975. Kikuchi, M., and K. Tachikawa, "Visible light emission and microplasma phenomena in a silicon p-n junction," J. Phys. Soc. Japan, *15*, 835 (1960).
976. Koenig, S. H., and R. D. Brown, III, "Far infrared electron-ionized donor recombination radiation in germanium," Phys. Rev. Letters, *4*, 170 (1960).
977. Krumme, J. B., and W. J. Leivo, "Luminescence in semiconducting diamond," Bull. Am. Phys. Soc., *5*, 187 (1960). (Abstract).
978. Lehfeldt, W., (Electroluminescence in AgCl containing CuCl), Nachr. Ges. Wiss. Gottingen, Math-Phys. Kl., p. 270 (1933).
979. Loebner, E. E., and I. G. Hegyi, "On the origin of complex brightness waveforms in A.C. electroluminescence," Meeting Electrochem. Soc., Philadelphia, May 4, 1959.
980. Loebner, E. E., and E. W. Poor, Jr., "Bimolecular electroluminescent transitions in GaP," Phys. Rev. Letters, *3*, 23 (1959).
981. Lozykowski, H., and H. Meczynska, "Electroluminescence of CdS-Ag with and Ag_2S layer," Bull. Acad. Polon. Sci., Ser. Sci. Math. Astron. Phys., *6*, 595 (1958) (in English).
982. Male, J. C., and J. R. Prior, "Intrinsic recombination radiation in diamond," Nature, *186*, 1037 (1960).
983. Mandelkorn, J., "Electrical characteristics of some GaP devices," Proc. IRE, *47*, 2012 (1959).
984. Mayer, D. W., "Self-sustained electron emission from aluminum and beryllium oxides," Fifth Natl. Conf. Tube Techniques, New York City, Sept. 15, 1960.
985. Moll, J. L., A. Uhler, Jr., and B. Senitsky, "Microwave transients from avalanching silicon devices," Proc. IRE, *46*, 1306 (1958).
986. Moss, T. S., "Emission of radiation from semiconductors," in "Optical Properties of Semiconductors," pp. 91-98 (Academic Press, New York, 1959).
987. Müller, S., "Recombination light emission and electron multiplication in silicon," Z. Naturforsch., *13a*, 240 (1958).
988. Nagy, E., and J. Weiszburg, "Electrical properties of electroluminescent silicon carbide," Acta Phys. Acad. Sci. Hung., *8*, 235 (1957).
989. Namba, S., M. Yoshizawa, and H. Tamura, "Electroluminescence of organic fluorescent compounds," Oyo Butsuri, *28*, 439 (1959).
990. Nelson, J. T., and J. C. Irvin, "Visible light from a germanium reversed-bias p-n junction," J. Appl. Phys., *30*, 1847 (1959).
991. Pankove, J. I., "Radiative surface effect in germanium," J. Phys. Chem. Solids, *6*, 100 (1958).
992. Pankove, J. I., "Influence of degeneracy on recombination radiation in germanium," Phys., Rev. Letters, *4*, 20 (1960).
993. Patrick, L., and W. J. Choyke, "Impurity bands and electroluminescence in SiC p-n junctions," J. Appl. Phys., *30*, 236 (1959); "Silicon carbide," p. 281 (Pergamon Press, 1960).
994. Pearson, G. L., "Photoprocesses in elemental semiconductors" in "Photochemistry of the Liquid and Solid State," pp. 157-66 (1957).
995. Pettsol'd, E. G., "Some electroluminescent properties of zinc oxide with addition of bismuth oxide," Izvest. Akad. Nauk SSSR, *24*, 104 (1960).
996. Rompe, R., "Discussion of problems of the electric discharge," Arbeitstagung Festkörperphysik II (Dresden), p. 163 (Barth, Leipzig, 1955). (Electroluminescence in CdS).

997. Rücker, D., "The electroluminescence of silicon carbide," Z. Angew. Phys., *10*, 254 (1958).
998. Saby, J. S., "Limits for junction rectifier electroluminescence," IRE-AIEE Solid-State Device Research Conf., Pittsburgh, June 14, 1960.
999. Schleimann-Jensen, A., "Generation of submillimeter waves by an avalanching semiconductor," Proc. IRE, *47*, 1376, 1378 (1959).
1000. Simpson, O., "Some optical properties of semiconductors," Research, *12*, 127 (1959).
1001. Skellett, A. M., B. G. Firth, and D. W. Mayer, "The magnesium oxide cold cathode and its application in vacuum tubes," Proc. IRE, *47*, 1704 (1959).
1002. Tauc, J., "The share of thermal energy taken from the surroundings in the electroluminescent energy radiated from a p-n junction," Czech. J. Phys., *7*, 275 (1957).
1003. Uchida, I., "Infrared radiation from silicon grown junction," J. Phys. Soc. Japan, *14*, 1831 (1959).
1004. Ukhanov, Y. I., "Modulation of infrared radiation in germanium at low temperatures," Zhur. Tekh. Fiz., *27*, 1652 (1957); Soviet Phys.-Tech. Phys., *2*, 1536 (1957) (Also electroluminescence).
1005. Vavilov, V. S., "Recombination emission in semiconductors," Uspekhi Fiz. Nauk, *68*, 247 (1959).
1006. Vavilov, V. S., A. A. Gippius, M. M. Gorshkov, and B. D. Kopylovskii, "Radiative recombination in germanium crystals subjected to bombardment by fast electrons," Zhur. Eks. Teor. Fiz., *37*, 23 (1959).
1007. Vereshchagin, I. K., "Influence of gas adsorption on electroluminescence," Optika i Spektros., *8*, 420 (1960); Optics and Spectros., *8*, 219 (1960), (ZnO).
1008. Vereshchagin, I. K., "The connection between the luminescent, electric, and chemical properties of zinc oxide," Izvest. Vysshikh Ucheb. Zavedenii Fiz., No. 2, 31-6 (1960).
1009. Vereshchagin, I. K., and V. S. Teslyuk, "Electroluminescence of zinc oxide and its dependence on thermal treatment conditions," Izvest. Vysshikh Ucheb. Zavedenii Fiz., No. 6, pp. 114-17 (1958).
1010. Vorob'ev, A. A., and V. D. Kuchin, "Emission from liquid and solid dielectrics in strong electric fields," Izvest. Tomsk. Politekh. Inst., *91*, 385 (1956) (Alkali halides and organic materials).
1011. Wachtel, A., "CaS:Cu,Eu electroluminescent phosphors," J. Electrochem. Soc., *107*, 199 (1960).
1012. Weinstein, M. A., "Thermodynamic limitation on the conversion of heat into light," J. Opt. Soc. Am., *50*, 597 (1960) (Recombination electroluminescence).
1013. Weiszburg, J., "On the electroluminescence of insulated SiC crystals," Acta. Phys. Hungar., *11*, 95 (1960).
1014. Williams, F. E., "Irreversible thermodynamics of injection electroluminescence," Bull. Am. Phys. Soc., *5*, 70 (1960) and Meeting Electrochem. Soc., Chicago, May 2, 1960.
1015. Wolff, G. A., I. Adams, and J. W. Mellichamp, "Electroluminescence of AlN," Phys. Rev., *114*, 1262 (1959).
1016. Wolff, P. A., "Theory of optical radiation from breakdown avalanches in germanium," J. Phys. Chem. Solids, *16*, 184 (1960).
1017. Yamashita, H., S. Ibuki, M. Yoshizawa, and H. Komiya, "Electroluminescence of CdS single crystal," J. Phys. Soc. Japan, *15*, 2366 (1960).

5. Field Effects in Excited Phosphors

1018. Bleil, C. E., and D. D. Snyder, "Some effects of low fields on luminescence of CdS," J. Appl. Phys., *30*, 1699 (1959).
1019. Coche, A., and R. Henck, "Effect of alternating and direct electric fields on the luminescence of certain zinc sulfides excited by alpha rays," J. Phys. Rad., *20*, 827 (1959).
1020. Cusano, D. A., "Photoelectroluminescence, electroluminescence, and related high field effects in zinc sulfide phosphor layers," Doctoral Thesis, Physics Dept., Rensselaer Polytechnic Institute, Jan., 1959; Univ. Microfilms 59-2925.
1021. Cusano, D. A., "Single-layer image intensifying screens with high resolution," Image Intensifier Symposium, Fort Belvoir, Va., pp. 185-199, Oct. 6-7, 1958.
1022. Déjardin, G., and J. Janin, "X-ray photoconductivity of some sulfide phosphors," Bull. Am. Phys. Soc., *5*, 47 (1960) (abstract only).
1023. Destriau, G., "A general effect of coactivators of Mn in ZnCdS:Mn,X phosphors showing the electroenhancement effect," Meeting Electrochem. Soc., Philadelphia, May 4, 1959.
1024. Destriau, G., "Energy limit of the electroenhancement and electroextinction effects," Compt. Rend., *249*, 245 (1959).
1025. Fridkin, V. M., "Some effects observed in an investigation of the luminescence of ZnS electrets," Doklady Akad. Nauk. SSSR, *131*, 290 (1960) (Effect of field on luminescence).
1026. Gobrecht, H., and H. E. Gumlich, "On the enhancement and quenching of the luminescence of manganese-activated ZnS by electric fields," Z. Phys., *156*, 436 (1959).
1027. Gobrecht, H., and H. E. Gumlich, "On the influence of the excitation wavelength on electrophotoluminescence," Z. Phys., *158*, 226 (1960).
1028. Gobrecht, H., H. E. Gumlich, and J. Zum Bruch, "On the influence of temperature on electrocathodoluminescence," Intntl. Conf. Semiconductors, Prague, Aug. 29-Sept. 2, 1960.
1029. Golovin, B. M., N. T. Kashukeev, I. N. Orlov, and V. M. Fridkin, "Photoelectret state in zinc sulfide and two new electrophotographic processes," Fiz. Tverdogo Tela, *2*, 1004 (1960).
1030. Gumlich, H. E., "The enhancement and quenching of the luminescence of manganese-activated zinc sulfide by electric fields," Doctoral Thesis D83, Technical University of Berlin, 1958.
1031. Haering, R. R., "Luminescence and conductivity induced by field ionization of traps," Canadian J. Phys., *37*, 1374 (1959).
1032. Halsted, R. E., "Electrophotoluminescent amplification," J. Appl. Phys., *29*, 1706 (1958).
1033. Henck, R., "Action of electric fields on the luminescence of certain zinc sulfides excited by α- and β-rays," Thesis, University of Strasbourg, May 25, 1960.
1034. Hershinger, L. W., and M. E. Lasser, "Very low voltage DC electroquenchable phosphors," Meeting Electrochem. Soc., Philadelphia, May 3-7, 1959.
1035. Jaffe, P. M., "Electric field enhancement of cathodoluminescence (cathodoelectroluminescence)," J. Electrochem. Soc., *106*, 667 (1959).
1036. Kotera, Y., and K. Naraoka, "The Gudden-Pohl effect of ZnS:Cu," J. Electrochem. Soc., *106*, 1066 (1959).
1037. Kotera, Y., and K. Naraoka, "Electrophotoluminescence of zinc sulfide phosphors," Bull. Chem. Soc., Japan, *33*, 721 (1960).
1038. Matossi, F., "Quenching of photoconductivity and lifetime of conduction electrons," Z. Phys., *151*, 5 (1958).
1039. Mattler, J., "Variation of the electroenhancement effect with the frequency of the electric field," Compt. Rend., *249*, 2051 (1959).
1040. Mattler, J., "Field enhancement of the light emitted by alpha scintillations," Meeting Electrochem. Soc., Philadelphia, May 4, 1959.
1041. Messier, J., and J. Mattler, "Action of electric fields on the luminescence of α-scintillations," Compt. Rend., *250*, 3822 (1960).
1042. Patek, K., "On the photoelectroluminescence of ZnS:Cu," Czech. J. Phys., *8*, 612 (1958) (in Russian) and *9*, 161 (1959) (In English).
1043. Pingault, F., "Sensitization to x-rays of luminescent materials of the type ZnCdS:Mn by infrared radiation," Compt. Rend., *249*, 248 (1959).
1044. Pingault, F., and G. Destriau, "Some new features of phosphors showing the electroenhancement effect," Meeting Electrochem. Soc., Philadelphia, May 4, 1959.
1045. Steinberger, I., and V. Bar., "Gudden-Pohl effect in single crystals of ZnS," Meeting on Color Centers and Crystal Luminescence, Turin, Sept. 8-11, 1960.
1046. Vinokurov, L. A., and M. V. Fok, "The simultaneous effect of light and electric fields on electroluminescent phosphors," Optika i Spektros., *7*, 241 (1959); Optics and Spectros., *7*, 152 (1959).
1047. Wendel, G., "On field enhancement in ZnS/CdS:Mn phosphors," Monatsber. Deutsch. Akad. Wiss. Berlin, *2*, 490 (1960).

6. Galvanoluminescence

1048. Audubert, R. and E. T. Verdier, "Emission of ultraviolet radiation on electrolysis of solutions of hydrazoic acid and sodium azide," Compt. Rend., *208*, 1984 (1939).
1049. Audubert, R., and O. Viktorin, "Emission of ultraviolet light by anodic oxidation of aluminum," J. Chim., Phys., *34*, 18 (1937).
1050. Dakin, T. W., and D. Berg. "Luminous spots on electrodes in insulating oil gaps," Nature, *184*, 120 (1959).
1051. Darveniza, M., "Light emission from insulating liquids due to excitation by D.C. fields near breakdown," Nature, *183*, 743 (1959).
1052. Gee, A., "Electrochemiluminescence at a silicon anode in contact with an electrolyte," J. Electrochem. Soc., *107*, 787 (1960).
1053. Lewowski, T., "Excitation of photostimulated co-exoelectron emission by anodic oxidation of aluminum," Z. Naturforsch., *15a*, 90 (1960).
1054. Sasaki, Y., "p-i-n junction in the anodic oxide film of tantalum," J. Phys. Chem. Solids, *13*, 177 (1960).
1055. Smith, A. W., "The impedance, rectification, and electroluminescence of anodic oxide films on aluminum," Can. J. Phys., *37*, 591 (1959).

7. Applications of Electroluminescence

1056. Anonymous, "Cast in a new light," Steelways, p. 10, Nov., 1960.
1057. Anonymous, "Electroluminescence. Area light source solving cockpit illumination problems," Vectors (Hughes Aircraft Co.), 2, #3, 14 (1960).
1058. Anonymous, "Electroluminescence at work," Illum. Engng., *55*, 10 (1960).
1059. Anonymous, "Cyanoethylation makes electrical magic," Chemical Week, p. 103, May 28, 1960; Electronic Design, May 25, 1960.
1060. Batailler, G., "Frequency multipliers for operation of electroluminescent cells," J. Phys. Rad., *21*, 72S (1960).
1061. Blazek, R. J., R. W. Wollentin, and H. R. Bullinger, "Multilayer and flexible single-layer electroluminescent lamps,"

Illum. Engng. Soc. Conference, Pittsburgh, Sept. 12-16, 1960.
1062. Boyd, S. H., "Control of persistence in electroluminescent panels," Meeting IRE Prof. Group on Electron Devices, Washington, D.C., Oct. 30, 1959.
1063. Bray, T. E. "An electro-optical shift register," IRE Solid-State Circuits Conference, Philadelphia, Feb., 1959.
1064. Buck, I. E., Jr., "Ceramic multilayer multicolor electroluminescent lamp," Illum. Engng. Soc. Conference, Pittsburgh, Sept. 12-16, 1960.
1065. Callahan, J. M., "New lighting for '60 dashboards. Cars to introduce radical lighting," Automotive News, April 27, 1959.
1066. Caywood, W. P. Jr., "Bistable and low-voltage ferroelectric-control configurations for electroluminescent display devices," National Electronics Conf., Chicago, Oct. 10-12, 1960.
1067. Cerulli, N. F., "Zinc borate glasses as dielectrics in electroluminescent lamps," Doctoral Thesis, Ceramics Dept., Rutgers Univ., June, 1958. University Microfilms #58-5677.
1068. Chamberlin, R. R., "An improved electroluminescent display panel," Meeting Electrochem. Soc., Philadelphia, May 6, 1959.
1069. Coerdt, R. J., "Analysis of characteristics of electroluminescent lamps with conductive grid structures," Meeting Electrochem. Soc., Philadelphia, May 6, 1959.
1070. Destriau, G., and P. Destriau, "Electroluminescence, electrophotoluminescence, and future prospects in radiology," Ann. Radiologie, *1*, 767 (1958).
1071. Diemer, G., "Power amplifiers using electro-optical effects," Electronics, p. 71, Feb. 26, 1960.
1072. Diemer, G., and J. G. Van Santen, "New applications of electro-optical phenomena," Nederl. Tijd. voor Natuurk., *25*, 265 (1959).
1073. Diemer, G., and J. G. Van Santen, "Power amplifiers based on electro-optical effects: A survey," Philips Res. Repts., *15*, 368 (1960).
1074. Eastman Kodak Co., "Electroluminescent safelights for photographic darkrooms," Illum. Engng., *55*, 201 (1960).
1075. Evans, L. W., "Electroluminescent display devices," Meeting IRE Prof. Group on Electron Devices, Washington, Oct. 28, 1960.
1076. Gardner, A. R., "Electroluminescence," Product Engng., p. 74, Sept. 15, 1958.
1077. Gardner, W. L., "Bright steady electroluminescent displays under development," Natl. Res. Council Publ. 595, p. 189 (1958).
1078. Ghandhi, S. K., "Photoelectronic circuit applications," Proc. IRE, *47*, 4 (1959).
1079. Hadley, C. P., and R. W. Christensen, "Solid-state image intensifier under dynamic operation," RCA Rev., *20*, 670 (1959).
1080. Hamburger, T., "Electroluminescent typewriter," Natl. Electronics Conf., Chicago, Oct. 12-14, 1959.
1081. Hamburger, T., "Electroluminescent alpha-numeric display," Electronics, p. 49, Jan. 22, 1960.
1082. Harris, J. M., "New developments in electroluminescent lighting," Meeting Opt. Soc. Am., Boston, Oct. 14, 1960.
1083. Harris, J. M., and P. J. Blinkilde, "Electroluminescent sources in automotive instrument lighting," Illum. Engng., *55*, 32 (1960).
1084. Henderson, S. T., "Electroluminescence and its possible application to radiology," Brit. J. Radiology, p. 313, June, 1958.
1085. Hoffmann, G. R., D. H. Smith, and D. C. Jeffreys, "High-speed light output signals from electroluminescent storage systems," Proc. IEE, *107B*, 599 (1960).
1086. Hook, H. O., "Optical feedback type storage light intensifiers," RCA Rev., *20*, 744 (1959).
1087. Isborn, C., "Photoconductor optical encoders for in-line readout devices," IRE Convention, New York, March 21, 1960.
1088. Ivey, H. F., "The effects of electrode resistance in electroluminescent cells," IRE Trans. Electron Devices, *ED6*, 335 (1959).
1089. Ivey, H. F., "Problems and progress in electroluminescent lamps," Illum. Engng. *55*, 13 (1960).
1090. Ivey, H. F., W. Lehmann, and W. A. Thornton, "Electroluminescent phosphors for display devices," 20th M.I.T. Physical Electronics Conference, March 25, 1960.
1091. Josephs, J. J., "A review of panel-type display devices," Proc. IRE, *48*, 1380 (1960).
1092. Jurgen, R. K., "Solid-state panels for display or storage," Electronics, p. 46, Jan. 30, 1959.
1093. Kazan, B., "Description and properties of the panel x-ray amplifier," Nondestructive Testing, *16*, 438 (1958).
1094. Kazan, B., "A feedback light-amplifier panel for picture storage," Proc. IRE, *47*, 12 (1959).
1095. Lack, A., "The new miracle in lighting," Science Digest, p. 44, August, 1957.
1096. Linden, B. R., "New techniques in low level fluoroscopy," IRE Trans. Nuclear Sci., *NS5*, 104 (1958).
1097. Lochinger, R. B., and M. J. O. Strutt, "Applications of electroluminescent cells as electrical circuit elements," Scientia Electrica, *5*, #3, 77 (1959).
1098. Lochinger, R. B., and M. J. O. Strutt, "Electroluminescent cell applications," Electronic Radio Engr., *36*, 398 (1959).
1099. Loebner, E. E., "Solid-state opto-electronics," RCA Rev., *20*, 715 (1959).
1100. Lyman, R. C., "An electroluminescent symbolic indicator," Meeting Electrochem. Soc., Philadelphia, May 6, 1959.
1101. Lyman, R. C., and C. I. Jones, "Electroluminescent panels for automatic displays," Electronics, p. 44, July 10, 1959.
1102. Marko, A. J., and A. L. Solomon, "Code translation by an electroluminescent photoconductive panel array," Meeting IRE Prof. Group on Electron Devices, Washington, D.C., Oct. 29, 1959.
1103. Manchester, H., "Electroluminescence. A new kind of light," Building Products, Feb., 1958; Readers' Digest, p. 96, Feb., 1958.
1104. Mann, M., "The light that won't burn out," Popular Science, p. 115, Jan., 1957.
1105. Mash, D. H., "An electroluminescent digital indication with a silicon carbide coding matrix," J. Sci. Instr., *37*, 47 (1960).
1106. Matarese, J., and M. S. Wasserman, "Crossed grid electroluminescent panel displays with sequential and random access," Meeting IRE Prof. Group on Electron Devices, Washington, D.C., Oct. 29, 1959.
1107. Nicoll, F. H., "Properties of a single-element light amplifier using sintered CdSe photoconductive material," RCA Rev., *20*, 658 (1959).
1108. Nicoll, F. H., and A. Sussman, "Two-color input—two-color output image intensifier panel," Proc. IRE, *48*, 1842 (1960).
1109. Nudelman, S., J. Lambe, J. Mudar, and G. Trytten, "Electroluminescent-piezoelectric flat panel displays," Meeting Electrochem. Soc., Chicago, May 4, 1960.
1110. Patek, K., "Design of an electroluminescent light amplifier," Slaboproudy Obzor, *19*, 876 (1958).
1111. Rose, A., and R. H. Bube, "The role of space-charge currents in light amplifiers," RCA Rev., *20*, 648 (1959).
1112. Ross, S. H., "Where can you use electroluminescence?" Consulting Engineer, p. 126, July, 1959.
1113. Sack, E. A., "The ELF screen," Research (London), *12*, 54 (1959).
1114. Sack, E. A., Jr., "Advances in screen structure and data distribution for the ELF display system," IRE Convention, New York, March 21, 1960.
1115. Siddall, G., "The preparation of electroluminescent panels," Vacuum, *7/8*, 61 (1957/58) (Published April, 1959).
1116. Stürmer, W., "X-ray image amplification with semiconductors," Siemens-Reiniger-Werke Nachrichten, *10*, 2 (1960).
1117. Toulon, P., "New applications of electroluminescence," Bull. Soc. Franc. Elect., *9*, 4 (1959).
1118. Troup, P. B., "Best illumination for instrument dials," Product Engineering, p. 41, Oct. 3, 1960.
1119. Uehara, Y., "The solid-state light amplifier," Toshiba Review (Japan), *15*, 619 (1960).
1120. Vincent, G. L., "How Sylvania produces first electroluminescent PE units," Ceramic Industry, p. 108, May 1959.
1121. Whetstone, A., "Millimicrosecond light source," Rev. Sci. Instr., *30*, 447 (1959). (Si p-n junction).
1122. Wollentin, R. W., S. R. Goldfarb, and D. C. Bell., "Electroluminescent lamp brightness measurement," Illum. Engng. Soc. Conference, Pittsburgh, Sept. 12-16, 1960.

8. Patents

1123. Anderson, A. E., and E. A. Sack, Jr., "Cathode ray tube," U.S. Pat. 2,888,593, May 26, 1959. (Electroluminescent elements controlled by ferroelectric elements charged by electron beam).
1124. Arnott, E. G. F., and H. F. Ivey, "Cathode-ray device," U.S. Pat. 2,863,084, Dec. 2, 1958. (Cathodoluminescence enhanced by alternating field).
1125. Bain, G. W., "Polarized electroluminescent phosphors and dielectrics," U.S. Pat. 2,887,601, May 19, 1959. (Particles aligned in field).
1126. Ballard, K. H., "Method of producing electroluminescent lamps," U.S. Pat. 2,887,402, May 19, 1959. (Ceramic type lamp made on temporary base; phosphor in contact with one electrode).
1127. Bartels, B. E., "Electroluminescent lamp," U.S. Pat. 2,928,015, March 8, 1960. (Grooved base with both electrodes on side opposite to phosphor; may be flexible).
1128. Bell, K. L., "Electrical illuminating devices," U.S. Pat. 2,790,936, April 30, 1957. (Radiofrequency excited electroluminescent phosphor).
1129. Berkley, C., "Video display device," U.S. Pat. 2,909,599, Oct. 20, 1959. (Electroluminescent layer with delay-line scanning and light valve).
1130. Bowerman, E. R., Jr., "Electroluminescent device," U.S. Pat. 2,958,009, Oct. 25, 1960. (Digital display lamp with photoconductive control).
1131. Braun, F. A., "Device for inversion of photographic negatives," German Pat. 1,030,581, May 22, 1958. (Electroluminescent phosphor and photoconductor).
1132. Butler, K. H., H. H. Homer, and R. M. Rulon, "Electroluminescent phosphors," U.S. Pat. 2,919,249, Dec. 29, 1959. (ZnS:Cu fired in 3% H_2 + 97% N_2).

1133. Butler, K. H., and R. M. Rulon, "Method of making electroluminescent phosphors," U.S. Pat. 2,919,250, Dec. 29, 1959. (Two-step process for ZnS or ZnSe activated by Cu and Pb with or without Mn).

1134. Caserio, M. J., and H. C. Stuerzl, "Panel illumination," U.S. Pat. 2,858,632, Nov. 4, 1958. (Instrument lighting).

1135. Cerulli, N. F., "Method of electrophoretic deposition of luminescent materials and product resulting therefrom," U.S. Pat. 2,851,408, Sept. 9, 1958; Canadian Pat. 568,290, Dec. 30, 1958.

1136. Cheney, R. H., "Electroluminescent light construction," U.S.Pat. 2,958,762, Nov. 1, 1960. (Overlay illuminated by lamp).

1137. Cohen, I. A., "Electroluminescent telephone dial," U.S. Pat. 2,908,806, Oct. 13, 1959.

1138. Compagnie Générale de Télégraphie sans Fils, "Arrangement for measuring electric intensity by electroluminescence," French Pat. 1,225,064, June 29, 1960.

1139. Croft, W. C., "Combination panel lighting and ventilating apparatus," Canadian Pat. 593,938, March 8, 1960.

1140. Curey, French Pat. 1,204,806, Aug. 10, 1959. (Electroluminescent advertising sign).

1141. Cusano, D. A., "Field enhanced luminescence system," U.S. Pat. 2,909,692, Oct. 20, 1959. (Thin film excited by x-rays, ultraviolet, or visible light with unidirectional field).

1142. Cusano, D. A., "Projection color television with photoelectroluminescent screen," U.S. Pat. 2,957,940, Oct. 25, 1960.

1143. Davis, D. W., "Image reproducing device," U.S. Pat. 2,925,-525, Feb. 16, 1960. (Electroluminescent display controlled by cathode-ray beam).

1144. Degenhardt, H., "Electroluminescent materials based on zinc sulfide," German Pat. 1,046,806, Dec. 18, 1958. (ZnS:Cu, Pb prepared with tartaric acid or in CO).

1145. Destriau, G., "X-ray system," U.S. Pats. 2,885,558-59, and -60, May 5, 1959. (Application of phosphors showing enhancement of x-ray excited luminescence upon application of alternating field).

1146. Destriau, G., "Electroluminescent cell," U.S. Pat. 2,901,651, Aug. 25, 1959; Canadian Pat. 585,050, Oct. 13, 1959. (Phosphor particles rotated in field).

1147. Destriau, G., "Phosphor," U.S. Pat. 2,951,814, Sept. 6, 1960. [(Zn,Cd) S:Mn,Au for field enhancement of x-ray images].

1148. Diemer, G., and J. G. Van Santen, "Image reproducing device," U.S. Pat. 2,882,419, April 14, 1959. (Cascade image intensifiers operated at different frequencies).

1149. Dombrowski, J. A., "Method of manufacturing electroluminescent lamps," U.S. Pat. 2,851,374, Sept. 9, 1958; British Pat. 830,225, March 9, 1960. (Silk screen method for ceramic-embedded phosphors).

1150. Elliott, J. F., and R. E. Halsted, "Electroluminescent device and networks," U.S. Pat. 2,904,696, Sept. 15, 1959. (Photoconductive-electroluminescent device to increase Q of tuned circuit).

1151. Etzel, E. P., and C. K. Lui-Wei, "Thin sheet of phosphor embedded glass and method of preparing," U.S. Pat. 2,857,541, Oct. 21, 1958. (Lead tellurite dielectric with protective layer on phosphor particles).

1152. Evans, H. J., "Display device with storage," U.S. Pat. 2,920,232, Jan. 5, 1960. (Photoconductor-electroluminor type).

1153. Evans, W. G., "Illuminating and heating and cooling panel member," U.S. Pat. 2,932,954, April 19, 1960. (Electroluminescent and thermoelectric elements).

1154. Faria, S., and P. Goldberg, "Electroluminescent lamp," U.S. Pat. 2,951,169, Aug. 30, 1960. [Phosphor particles coated with nonconductor (SiO_2) for better efficiency].

1155. Fiore, J. P., and C. S. Czegho, "Color image reproducers," U.S. Pat. 2,861,206, Nov. 18, 1958. (Electroluminescent strips with photoconductor or material showing bombardment-induced conductivity).

1156. Fischer, A., "Apparatus for producing projected positive image of a photographic negative," German Pat. 1,069,902, Nov. 26, 1959. (Infrared quenching of ultraviolet-excited luminescence enhanced by electric field).

1157. Fischer, A. G., "Electroluminescent lamp," U.S. Pat. 2,938,136, May 24, 1960. (p-i-n structure for recombination electroluminescence).

1158. Fridrich, E. G., "Electroluminescent lamp construction," U.S. Pat. 2,901,652, Aug. 25, 1959. (Flexible lamp).

1159. Fridrich, E. G., "Variable color electroluminescent lamp," U.S. Pat. 2,918,594, Dec. 22, 1959. (Parallel conductors coated with different phosphors).

1160. Fridrich, E. G., and P. A. Dell, "Electroluminescent lamp and manufacture thereof," U.S. Pat. 2,945,976, July 19, 1960. (Laminated construction using thermoplastic material).

1161. Froelich, H. C., "Preparation of electroluminescent phosphors," U.S. Pat. 2,950,257, Aug. 23, 1960. (ZnS:ZnO:Cu phosphor heated in reducing atmosphere at 300°C after preparation).

1162. Fromm, K. N., and T. Miller, "Tricolor television picture tube," U. S. Pat. 2,795,730, June 11, 1957. (Field quenching of luminescence).

1163. Garwin, R. L., H. A. Reich, and S. Triebwasser, "Memory devices," U.S. Pat. 2,897,399, July 28, 1959. (Electroluminescent-photoconductive type).

1164. Gillson, J. L., Jr., "Apparatus for generating visible light by photoelectroluminescence," U.S. Pat. 2,933,602, April 19, 1960; British Pat. 810,872, March 25, 1959. (Ultraviolet or x-rays; AC; ZnS:Mn with or without Cu or Fe).

1165. Goldberg, P., and A. K. Levine, "Process for producing electroluminescent phosphors," U.S. Pat. 2,957,830, Oct. 25, 1960. (ZnS:Cu fired, milled, and then refired at lower temperature).

1166. Halsted, R. E., "Improvement in electrophotoluminescent signal amplifiers," British Pat. 827,555, Feb. 10, 1960. (Electrophotoluminescent phosphor plus photosensitive element as electrical amplifier).

1167. Hanlet, J. M. N., "Electroluminescence device," U.S. Pat. 2,883,582, April 21, 1959; British Pat. 851,079, Oct. 12, 1960. (Improved display panel).

1168. Hanlet, J. M. N., "Method of making electroluminescent layers," U.S. Pat. 2,917,442, Dec. 15, 1959; French Pat. 1,141,523, Sept. 3, 1957; British Pat. 851,076, Oct. 12, 1960. (Electroluminescent oxide films).

1169. Hanlet, J. M. N., "Electroluminescent materials," French Pat. 1,139,169, June 26, 1957; British Pat. 850,592, Oct. 5, 1960; German Pat. 1,023,820, Feb. 6, 1958. (ZnO,CdO,BaO or CaO activated by Cu,Pb,Mn,Ag,Tl,Se or Ge).

1170. Hanlet, J. M. N., "Preparation of layers of electroluminescent materials," U.S. Pat. 2,936,252, May 10, 1960. (Films of ZnS, CdS, ZnO or CdO).

1171. Hanlet, J. M. N., "Electroluminescent element and method of fabrication," French Pat. 1,196,188, Nov. 23, 1959. (P-N junction of BN formed by doping with Zn and Te).

1172. Hanlet, J. M. N., "Electroluminescent cell," French Pat. 1,196,189, Nov. 23, 1959. (p-i-n SiC junction).

1173. Hanlet, J. M. N., "Electroluminescent devices," U.S. Pat. 2,929,950, March 22, 1960; British Pat. 851,077, Oct. 12, 1960. (AC-operated electroluminescent phosphor plus DC-operated photoconductor-electroluminescent phosphor combination).

1174. Hanlet, J. M. N., "Electronic anticoincidence device," U.S. Pat. 2,964,638, Dec. 13, 1960. (Photoconductor-electroluminescent type).

1175. Harmon, G. G., Jr., "Electroluminescent microwave reviewer," U.S. Pat. 2,928,937, March 15, 1960.

1176. Heinsohn, G., German Pat. 1,079,737, April 14, 1960. (Base of electroluminescent layer roughened to improve adherence).

1177. Henisch, H. K., "Electroluminescent display device," U.S. Pat. 2,856,553, Oct. 14, 1958. (Use of infrared generated by electroluminescence to quench visible electroluminescence).

1178. Hoffmann, G. R., and R. E. Hayes, "Electroluminescent display devices," U.S. Pat. 2,947,912, Aug. 2, 1960. (Elimination of cross-talk in x-y panels by resistive biasing).

1179. Jay, T., Jr., "Electroluminescent device," U.S. Pat. 2,931,915, April 5, 1960. (Photoconductive-electroluminescent light amplifier with separate electroluminescent input).

1180. Jay, T., Jr., "Electroluminescent device," U.S. Pat. 2,932,746, April 12, 1960. (Like U.S. 2,931,915 but with x-y electrodes).

1181. Jenny, D. A., and E. E. Loebner, "Light inverters," U.S. Pat. 2,883,556, April 21, 1959. (Uses infrared quenching of electroluminescent phosphors).

1182. Joormann, H. J. M., "Tuning indicator," U.S. Pat. 2,790,161, April 23, 1957.

1183. Kalfaian, M. V., "Color image tube utilizing electroluminescent screen," U.S. Pat. 2,813,223, Nov. 12, 1957. (Cathode-ray scanning).

1184. Kalfaian, M. V., "Color image screen utilizing electroluminescence," U.S. Pat. 2,872,613, Feb. 3, 1959. (Scanned by electron beam).

1185. Kallmann, H. P., and B. Rosenberg, "Voltage responsive screen control methods and systems," U.S. Pat. 2,892,968, June 30, 1959. (Use of diodes to prevent cross-talk in x-y display device).

1186. Kazan, B., "Flying spot scanner," U.S. Pat. 2,851,634, Sept. 9, 1958. (Delay line for signal distribution).

1187. Kazan, B., "Electroluminescent image reproduction," U.S. Pat. 2,858,363, Oct. 28, 1958. (Photoconductor plus electroluminescent layer. Optical input provides scanning. Adapted to color reproduction; see also #641).

1188. Kazan, B., "Electroluminescent device," U.S. Pat. 2,873,380, Feb. 10, 1959. (Electroluminescent phosphor controlled by variable reactance device such as a saturable reactor or ferroelectric material).

1189. Kazan, B., "Steroscopic x-ray intensification," U.S. Pat. 2,884,528, April 28, 1959. (Photoconductor-electroluminor type. Two colors or directions of polarization used for stereoscopy).

1190. Kazan, B., "Picture producing devices," U.S. Pat. 2,884,566, April 28, 1959. (Array of electroluminescent strips and of voltage-controlled light-valve strips at right angles).

1191. Kazan, B., "Half-tone image production," U.S. Pat. 2,896,087, July 21, 1959. (Regenerative photoconductor-electroluminescent image amplifier with pulsed voltage supply).

1192. Kazan, B., "Electroluminescent device," U.S. Pat. 2,900,574, August 18, 1959. (Series of photoconductor-electroluminor elements, each controlled by preceding set).

1193. Kazan, B., "Light amplifying device," U.S. Pat. 2,905,830, Sept. 22, 1959. (Ferroelectric-electroluminescent combination controlled by photoconductor).

1194. Kazan, B., "Storage tube," U.S. Pat. 2,905,830, Sept. 22, 1959. (Ferroelectric-electroluminescent combination controlled by photoconductor).

1195. Kazan, B., "Electroluminescent device," U.S. Pat. 2,914,678, Nov. 24, 1959. (Two photoconductive elements in series with each electroluminescent element to prevent cross-talk in x-y display device. Photoconductors excited by x-y electroluminescent strips).

1196. Kazan, B., "Electroluminescent device," U.S. Pat. 2,919,352, Dec. 29, 1959. (Double photoconductor-electroluminor type with controllable optical feedback).

1197. Kazan, B., "Picture storage device," U.S. Pat. 2,926,263, Feb. 23, 1960. (Two photoconductive elements in series with each electroluminescent element, with only one receiving optical feedback).

1198. Kazan, B., "Electroluminescent storage device," U.S. Pat. 2,942,120, June 21, 1960. (Photoconductor-electroluminescence device with two separate electroluminescent sections, one for viewing and one for feedback).

1199. Kazan, B., and J. E. Berkeyheiser, Jr., "Radiant energy control apparatus," U.S. Pat 2,943,205, June 28, 1960. (Current through photoconductive-electroluminescent type x-ray image intensifier used to control x-ray exposure).

1200. Klasens, H. A., and H. J. M. Joormann, "Electroluminescent element," U.S. Pat. 2,964,666, Dec. 13, 1960; British Pat. 810,918, March 25, 1959. (Use of photoluminescent material to achieve desired emission color).

1201. Koury, F., "Light amplifier and storage device," U.S. Pat. 2,878,394, March 17, 1959. (Photoconductor-electroluminescent type).

1202. Kruse, P. W., "Image intensifiers," U.S. Pat. 2,892,096, June 23, 1959. (Color reproduction using an array of prisms, photoconductors and three electroluminescent phosphors of different emission color).

1203. Kruse, P. W., "Radiation amplifier," U.S. Pat. 2,928,006, March 8, 1960; British Pat. 845,391, Aug. 24, 1960. (Photoconductor-electroluminor type with input and output on same side).

1204. Larach, S., "Electroluminescent devices and materials and methods of preparation thereof," U.S. Pat. 2,859,367, Nov. 4, 1958. (ZnSe:Cu,Br and (Zn,Cd)Se:Cu,Br).

1205. Larach, S., "Light intensifier," U.S. Pat. 2,898,475, Aug. 4, 1959. (Ultraviolet emission from cathodoluminescent phosphor excites phosphor showing electroenhancement effect).

1206. Larach, S., "Polychromatic electroluminescent means," U.S. Pat. 2,925,532, Feb. 16, 1960. (Image panel with three different phosphors in lines or dots).

1207. Larach, S., and R. E. Shrader, "Electroluminescent devices," U.S. Pat. 2,921,218, Jan. 12, 1960. (Use of ultraviolet-emitting BN with or without photoluminescent material).

1208. Lehmann, W., "Method for making an electroluminescent phosphor which is not photoluminescent," Canadian Pat. 579,564, July 14, 1959. (ZnS:Cu with Ni, Fe, or Co).

1209. Lehmann, W., "Phosphor," Canadian Pat. 579,685, July 14, 1959. (ZnS:Cu fired in sulfur vapor).

1210. Lehmann, W., "Method of preparing three-color electroluminescent phosphor," Canadian Pat. 579,686, July 14, 1959; U.S. Pat. 2,937,150, May 17, 1960. (ZnS:Cu,Mn).

1211. Lehmann, W., "Area-type light source," U.S. Pat. 2,974,732, Feb. 9, 1960. (Electroluminor plus photoluminescent phosphor).

1212. Lehmann, W., French Pat. 1,229,283, April 29, 1960. (Separation of small particles of ZnS for high electroluminescence efficiency).

1213. Lempicki, A., "Image converter," U.S. Pat. 2,890,350, June 9, 1959. (Electroluminor plus infrared-quenchable photoconductor).

1214. Lewis, C. W., "Electrical apparatus and solid dielectric therefore," U.S. Pat. 2,920,256, January 5, 1960. (Cyanoethyl cellulose as dielectric).

1215. Lieb, A., German Pat. 1,078,667, March 31, 1960. (Limited electroluminescent area varies with applied voltage due to varying thickness or resistive voltage drop; used with photoconductor).

1216. Liebson, S. H., "Flat picture screen and methods and means for operating the same," U.S. Pat. 2,928,993, March 15, 1960. (Photoconductor-electroluminor type with external light source).

1217. Lindsay, H. R., "Improvements in and relating to apparatus embodying electroluminescent devices," British Pat. 842,242, Nov. 25, 1959. (Display device employing electroluminescent phosphor whose color of emission depends upon applied frequency).

1218. Livingston, D. C., "Electroluminescent device," U.S. Pat. 2,874,308, Feb. 17, 1959; British Pat. 855,425, Nov. 30, 1960. (Use of photoconductor to give storage in display device).

1219. Livingston, D. C., "Electroluminescent device," U.S. Pat. 2,881,360, April 7, 1959. (Frequency or phase difference indicator).

1220. Livingston, D. C., "Electroluminescent device," U.S. Pat. 2,930,897, March 29, 1960. (Elimination of cross-talk in x-y panel by resistive biasing).

1221. Livingston, D. C., "Electroluminescent device," U.S. Pat. 2,932,770, April 12, 1960. (Matrix of photoconductor-electroluminor elements with selective extinction).

1222. Loebner, E. E., "Information handling systems," U.S. Pat. 2,907,001, Sept. 29, 1959. (Electroluminescent-photoconductive logic circuits).

1223. Loebner, E. E., "Wavelength selective radiation responsive systems and devices," U.S. Pat. 2,914,679, Nov. 24, 1959. (Two photoconductors of different spectral response in series with one electroluminescent element).

1224. Lui-Wei, C. K., "Electroluminescent cell," Canadian Pat. 569,170, Jan 20, 1959. (Nylon as embedding material for phosphors).

1225. MacIntyre, A. J., Jr., and R. A. Martel, "Electroluminescent device," U.S. Pat. 2,894,854, July 14, 1959. (Barium titanate mixed with phosphor or as separate layer).

1226. MacIntyre, A. J., Jr., and R. A. Martel, "Electroluminescent devices and methods therefore," U.S. Pat. 2,900,271, Aug. 18, 1959; British Pat. 851,101, Oct. 12, 1960. (All-plastic lamp).

1227. Mager, E. L., "Electroluminescent lamp," U.S. Pat. 2,866,118, Dec. 23, 1958. (Phosphor embedded in glass).

1228. Mager, E. L., "Electroluminescent lamp," Canadian Pat. 588,340, Dec. 8, 1959. (Maintenance improved by plastic layer devoid of phosphor).

1229. Marshall, T. G., Jr., "Logical circuit element," U.S. Pat. 2,885,564, May 5, 1959. (Electroluminescent-photoconductive type).

1230. Marzocchi, A., A. W. Brown, and H. C. Blankmeyer, "Luminescent panels," U.S. Pat. 2,959,701, Nov. 8, 1960. (Use of glass fibers to increase light output).

1231. Mash, D. H., "Closed-circuit television systems," U.S. Pat. 2,866,182, Dec. 23, 1958. (Photoconductor, superlinear resistor and electroluminescent phosphor with superimposed ac and dc).

1232. Mash, D. H., "Improvements in and relating to combined electroluminescent and photoconductive devices," U.S. Pat. 2,918,582, Dec. 22, 1959; British Pat. 809,380, Feb. 25, 1959. (Uses superlinear resistor).

1233. Mash, D. H., "Devices employing electroluminescence," British Pat. 815,089, June 17, 1959. (Photoconductor-electroluminescent image device with automatic scanning).

1234. Mash, D. H., "Electroluminescent devices," U.S. Pat. 2,919,366 Dec. 29, 1959; British Pat. 829,247, March 2, 1960. (Method for exciting only selected areas).

1235. Mash, D. H., "Improvements in and relating to the manufacture of translucent electrically-conducting layers," British Pat. 828,720, Feb. 24, 1960. (Glass beads plus conducting paint. Used in electroluminescent cells).

1236. Matarese, J., "Commutator," U.S. Pat. 2,866,922, Dec. 30, 1958. (For use with electroluminescent display device).

1237. Matarese, J., "Oscillator," U.S. Pat. 2,898,556, Aug. 4, 1959. (Photoconductive-electroluminescent device).

1238. Matarese, J., "Electroluminescent device," U.S. Pat. 2,951,-970, Sept. 6, 1960. (Diode matrix for signal distribution to crossed-grid display).

1239. Michlin, H. A., "Electroluminescent color lamp," U.S. Pat. 2,867,739, Jan. 6, 1959. (Multilayer multicolor lamp).

1240. Michlin, H. A., "Producing luminescent images by electroluminescence," U.S. Pat. 2,881,353, April 7, 1959. (Phosphor excited simultaneously by cathode rays and ultraviolet radiation).

1241. Miller, J. D., "Indicia bearing electroluminescent panel and method of manufacture," U.S. Pat. 2,922,912, Jan. 26, 1960.

1242. Nagy, E., and J. Szabo, "Electroluminescent cell and method of making same," U.S. Pat. 2,941,103, June 14, 1960. (Powder with high dielectric constant added to phosphor/dielectric mixture).

1243. Neugass, E. A., U.S. Pat. 2,791,050, May 7, 1957; British Pat. 829,588, March 2, 1960. (Electroluminescent illumination of signs, instruments, etc.).

1244. Neugass, E. A., "Instrument lighting devices," U.S. Pat. 2,945,145, July 12, 1960.

1245. Nicoll, F. H., "Electroluminescent device and systems," U.S. Pat. 2,855,531, Oct. 7, 1958. (Electroluminescent cell responsive to mechanical motion or sonic or ultrasonic energy).

1246. Nicoll, F. H., "Electroluminescent image device," U.S. Pat. 2,884,541, April 28, 1959. (Photoconductor-electroluminescent device with interdigital electrodes and auxiliary conductors).

1247. Nicoll, F. H., "Electroluminescent device to give negative pictures," U.S. Pat. 2,891,169, June 16, 1959. (Photoconductor in parallel with phosphor).

1248. Nicoll, F. H., and B. Kazan, "Electroluminescent device," U.S. Pat. 2,880,346, March 31, 1959. (Cell operated on dc protected from breakdown by resistive layer).

1249. Orthuber, R. K., "Radiation intensifier with photoconductive and electroluminescent material," German Pat. 1,004,301, March 14, 1957. (AC on phosphor and DC on photoconductor).

1250. Orthuber, R. K., and C. C. Larson, "Image device," U.S. Pat. 2,892,095, June 23, 1959. (Electroluminor combined with material showing electron bombardment induced conductivity).

1251. Orthuber, R. K., and C. C. Larson, "Image device," U.S. Pat. 2,909,667, Oct. 20, 1959. (Cathode-ray controlled photoconductive-electroluminescent device).

1252. Orthuber, R. K., C. C. Larson, and G. W. Bain, "Information display device," U.S. Pat. 2,877,371, March 10, 1959; British Pat. 839,375, June 29, 1960. (Electroluminescent phosphor with ferroelectric or polaristor material).

1253. Orthuber, R. K., and L. R. Ullery, "Radiation amplifier construction," U.S. Pat. 2,875,350, Feb. 24, 1959. (Photoconductor in grooves of rigid base; electroluminescent phosphor on flexible base pressed on).

1254. Orthuber, R. K., L. R. Ullery, and C. L. Day, "Radiation amplifier," U.S. Pat. 2,837,661, June 3, 1958. (Photoconductor-electroluminor type).

1255. Philips Electrical Industries, Belgian Pat. 575,947, Feb. 20, 1959. (Sealing of electroluminescent lamp).

1256. Piper, W. W., "Method of improving the activation of electroluminescent single crystals," French Pat. 1,163,905, Oct. 2, 1958.

1257. Piper, W. W., "Single crystal electroluminescence," U.S. Pat. 2,932,879, April 19, 1960. (Single oriented crystals of ZnS, ZnSe, CdS, CdSe and mixtures thereof).

1258. Piper, W. W., "Electroluminescent cell and method of making the same," U.S. Pat. 2,944,177, July 5, 1960; British Pat. 844,589, Aug. 17, 1960; French Pat. 1,228,480, April 22, 1960. (Electroluminescent phosphor in discrete particles of glass in plastic dielectric).

1259. Putkovich, R. P., and T. M. Corry, "Electrical power supplies," U.S. Pat. 2,937,298, May 17, 1960. (Transistor inverter for electroluminescent cells).

1260. Rajchman, J. A., "Electrical display device," U.S. Pat. 2,928,894, March 15, 1960; British Pat. 838,624, June 22, 1960. (Transfluxor-controlled electroluminescent panel).

1261. Rajchman, J. A., "An electrical display device," British Pat. 839,003, June 29, 1960. (Electroluminescent panel controlled by ferroelectric "transchargers").

1262. Reis, C. S., "Solid state network," U.S. Pat. 2,900,522, Aug. 18, 1959. (Photoconductor-electroluminor counter).

1263. Reis, C. S., "Display apparatus," U.S. Pat. 2,950,418, Aug. 23, 1960. (Digital lamp with photoconductive switching).

1264. Rindone, G. E., "High dielectric constant glass," U.S. Pat. 2,906,631, Sept. 29, 1959; British Pat. 809,099, Feb. 18, 1959. (For use in electroluminescent devices).

1265. Rosenberg, B., "Electroluminescent device," U.S. Pat. 2,916,630, Dec. 8, 1959. (Photoconductor-electroluminor device operated on d.c. with commutator).

1266. Rothschild, G. N., "Electroluminescent display device," U.S. Pat. 2,915,641, Dec. 1, 1959. (Photoconductor-electroluminor type with matched photoconductor and electroluminor).

1267. Rothschild, S., "Improvements and relating to photocopying," British Pat. 815,466, June 24, 1959. (Use of electroluminescent source).

1268. Sack, E. A., Jr., "Display systems," U.S. Pat. 2,917,667, Dec. 15, 1959. (Electroluminescent phosphor controlled by ferroelectric capacitor).

1269. Sack, E. A., Jr., "Display device," U.S. Pat. 2,922,993, Jan. 26, 1960; French Pat. 1,224,914. (Digital display lamp).

1270. Sack, E. A., Jr., and J. A. Asars, "Display device," U.S. Pat. 2,922,076, Jan. 19, 1960. (Electroluminescent-ferroelectric structure).

1271. Schröter, F., "Phosphor layer with increased persistence," German Pat. 1,079,220, April 7, 1960. (Cathode ray tube with double-layer screen; field enhancement of luminescence of second layer which is ultraviolet-excited by first cathodoluminescent layer).

1272. Skellet, A. M., "Cold cathode vacuum lamp," U.S. Pat. 2,925,511, Feb. 16, 1960. (Uses electroluminescence to start).

1273. Solomon, A. L., and G. J. Goldsmith, "Ferroelectric compositions and devices," U.S. Pat. 2,944,200, July 5, 1960. (Thiourea and its isomorphs used in electroluminescent systems).

1274. Standard Telephones and Cables, Ltd., "Electroluminescent light amplifier or image converter and method of manufacturing same," British Pat. 838,902, June 22, 1960. (Photoconductor-electroluminor type constructed on metallic mesh).

1275. Strange, J. W., "Improvements in and relating to the illumination of dials and the like," British Pat. 799,142, Aug. 6, 1958; U.S. Pat. 2,872,567, Feb. 3, 1959.

1276. Stürmer, W., "Image converter," German Pat. 968,667, April 17, 1958. (Electroluminescent phosphor plus photoconductor).

1277. Swindells, F. E., "Electroluminescent structures," U.S. Pat. 2,941,104, June 14, 1960. (Organic dielectrics for flexible lamps).

1278. Sylvania Electric Products, Inc., "Electroluminescent display systems," British Pat. 748,834, May 9, 1956. (Radar or television display device. See also #700).

1279. Sylvania Electric Products, Inc., "Electroluminescent lamp," British Pats. 815,720 and 815,721, July 1, 1959. (Two separate phosphor-dielectric layers with nonuniform phosphor distribution, particularly ceramic type).

1280. Sylvania Electric Products, Inc., "Preparation of improved electroluminescent phosphors," British Pat. 843,907, Aug. 10, 1960. (Two-step firing process for (Zn,Cd) (S,Se)).

1281. Sylvania Electric Products, Inc., "Electroluminescent lamp," British Pat. 844,377, Aug. 10, 1960. (Including layer of material with dielectric constant greater than 1000).

1282. Sylvania Electric Products, Inc., "Electroluminescent device," British Pat. 849,387, Sept. 28, 1960. (Photoconductive-electroluminescent light amplifier with photoconductor on surface of transparent rods which are bundled together).

1283. Tauc, J., "Semiconductor cooling element," French Pat. 1,184,217, July 17, 1959. (P-N junctions with radiative recombination).

1284. Thorington, L., "Cold cathode light source," U.S. Pat. 2,955,221, Oct. 4, 1960. (Uses electroluminescence to start).

1285. Thornton, W. A., German Pat. 1,087,698, Aug. 25, 1960. (AC-DC electroluminescence).

1286. Thurlby, L. T., and J. B. Collins, "Radiation detection and indicating devices," U.S. Pat. 2,909,668, Oct. 20, 1959. (Photoconductor-electroluminescent type).

1287. Tomlinson, T. B., "Improvements in or relating to arrangements including electroluminescent and photoconductive elements," British Pat. 820,800, Sept. 23, 1959. (Photoconductor and phosphor in parallel, combination in series with fixed impedance).

1288. Tomlinson, T. B., "Improvements in or relating to electroluminescent display devices," British Pat. 845,213, Aug. 17, 1960. (Use of nonlinear material in x-y panel to reduce crosstalk).

1289. Toulon, P. M. G., "Display systems," U.S. Pat. 2,875,380, Feb. 24, 1959. (Electroluminescent phosphor controlled by nonlinear capacitors).

1290. Toulon, P. M. G., "Solid-state display device," U.S. Pat. 2,938,135, May 24, 1960. (Method of construction for electroluminescent-ferroelectric screen).

1291. Ullery, L. R., "Display amplifier and method of making same," U.S. Pat. 2,773,992, Dec. 11, 1956. (Photoconductor-electroluminescent amplifier with photoconductor on perforated support).

1292. Valverde, R., "Electric switch with electroluminescent signal," U.S. Pat. 2,901,582, Aug. 25, 1959.

1293. VanSanten, J. G., and G. Diemer, "Solid-state image intensifier," U.S. Pat. 2,948,816, Aug. 9, 1960. (Bridge-type circuit for photoconductive-electroluminescent amplifier elements).

1294. Wachtel, A., "Phosphor," U.S. Pat. 2,874,128, Feb. 17, 1959. (ZnS:Cu, Cl fired in closed container with free sulfur).

1295. Wachtel, A., "Phosphor," U.S. Pat. 2,951,813, Sept. 6, 1960; Canadian Pat. 579,687, July 14, 1959. (ZnS:Cu, Cl fired in S_2Cl_2 vapor).

1296. Wahlig, C. F., "Method of image storage and release," U.S. Pat. 2,939,029, May 31, 1960. (Gudden-Pohl effect).

1297. Walker, C. H., and M. G. Clarke, "Electroluminescent panel," U.S. Pat. 2,866,117, Dec. 23, 1958; British Pat. 821,543, Oct. 7, 1959. (Phosphor in glass on slab of $BaTiO_3$ or TiO_2).

1298. Walker, C. H., and M. G. Clarke, "Devices for amplifying or converting radiation," U.S. Pat. 2,870,342, Jan. 20, 1959. (Sheet of $BaTiO_3$ or TiO_2 as base for photoconductor-electroluminor light amplifier).

1299. Walker, C. H., and J. N. Knutton, "Improvements relating to electroluminescent devices," British Pat. 850,846, Oct. 12, 1960. (Lead connections to multisegment lamp).

1300. Wasserman, M., "Electroluminescent device," U.S. Pat. 2,948,823, Aug. 9, 1960. (Different electrode areas for photoconductive and electroluminescent elements in photoconductor-electroluminor device).

1301. Wendel, G., East German Pat. 18,774, April 5, 1960. (Electroluminescent phosphor activated at second firing at lower temperature than first).

1302. Williams, F. E., "Image intensification apparatus," U.S. Pat. 2,645,721, July 14, 1953. (Use of electroluminescent cell with large-area photosurface to give uniform source of photoelectrons).

1303. Williams, F. E., "Color information presentation system," U.S. Pat. 2,928,975, March 15, 1960. (Combination of photoelectroluminescent layers of different emission color with electroluminescent display panel or cathodoluminescent phosphor).

1304. Woods, J., "Improvements in or relating to fluorescent material," Brit. Pat. 821,677, Oct. 14, 1959. (Single crystals of ZnS showing field enhancement of ultraviolet or x-ray excited luminescence).

1305. Yando, S., "Electroluminescent device," U.S. Pats. 2,917,669, Dec. 15, 1959; 2,922,923, Jan. 26, 1960; and 2,951,168, Aug. 30, 1960. (Piezoelectric scanning).

1306. Zalm, P., H. A. Klasens, and J. C. Michielsen, "Method of producing an electroluminescent substance," Canadian Pat. 606,168, Oct. 4, 1960. ((Zn, Cd)S with addition of alkali or alkaline earth sulfide activated by Cu, Au, or Mn. See also #674).

1307. Zappacosta, J. A., "Electronic display apparatus," U.S. Pat. 2,886,731, May 12, 1959. (Electroluminescent display with delay-line scanning; screen thickness varied to account for decrease in signal amplitude along delay line).

Discussion Section

This Discussion Section includes discussion of papers appearing in the JOURNAL of The Electrochemical Society, Vol. 106, No. 9 and 12 (September and December, 1959) and Vol. 107, No. 5, 6, 7, 9, 10, 11, and 12 (May, June, July, September, October, November, and December, 1960). Discussion not available for this issue will appear in the Discussion Section of the December 1961 JOURNAL.

Overvoltage and Catalysis

Paul Rüetschi (pp. 819-827, Vol. 106, No. 9)

L. G. Austin[1]: Dr. Rüetschi's derivation of his Eq. [5] is at fault for the following reason. The energy or heat of adsorption which has relevance in deriving adsorption isotherms or kinetic equations is the differential energy change.[2] The differential energy change per unit charge on charging a condenser is not $\frac{1}{2} CV^2/q$ as used in the paper, but $\left[\frac{\partial(\frac{1}{2} CV^2)}{\partial q}\right]_q = V$. Thus, the structural factor α, by Rüetschi's reasoning, should be 1 not ½.

Similarly, for electrochemical rate processes, α cannot have the meaning ascribed to it by Rüetschi. We must return to the classical concept that the activation energy for adsorption is changed by an amount proportional to V but not equal to V; α is the proportionality constant, lying between 0 and 1. The usual physical models explaining this appear to be quite reasonable.

Paul Rüetschi: The remarks of Dr. Austin reflect the views held by the majority of electrochemists during recent decades. However, the conventional interpretation of the transfer coefficient α on the basis of geometrical pictures of linearized potential energy curves, yielding a more or less "symmetrical" barrier and the value $\alpha = \frac{1}{2}$, is not satisfactory from various points of view. It was the object of the paper "Overvoltage and Catalysis" to treat this problem.

The interpretation of α on the basis of symmetrical energy barriers, which has been accepted widely in the past, is at fault because of the following reasons:

(A) It does neglect interaction (in particular, electrostatic interaction) of species in the double layer and, therefore, the change of energy with coverage or charge.

(B) It does not explain the "coincidence" that the value of $\alpha = \frac{1}{2}$ is found so frequently for a variety of different reactions and surfaces.

(C) It does not describe the influence of specifically adsorbed foreign ionic species on the reaction rate.

The paper gives the rudiments of a theory which I subsequently worked out in greater detail, and which gives a satisfactory interpretation of α.

It was Volmer[3] who first introduced the transfer coefficient. He did it in a formal manner without explanation, for both the forward and the backward reaction of the hydrogen electrode, in order to satisfy the Nernst relation at equilibrium. Volmer explained hydrogen overvoltage in the following manner: "The reason for hydrogen overvoltage is without any doubt the fact that protons arriving at the surface of the electrode by current transport are not immediately transferred into gaseous hydrogen, but rather remain in some form at the electrode, and in this manner increase the potential difference electrode-electrolyte." Furthermore: "The potential depends in a linear manner on the surface concentration of adsorbed protons and the electrode interface behaves like a condenser." This is precisely the picture used in the paper "Overvoltage and Catalysis."

Starting out with the very simplest model of a condenser, having on the solution side of the interface a charge layer consisting of statistically identical charged species, *e.g.*, protons, and on the electrode side a charge layer of opposite sign consisting also of statistically identical species (*e.g.*, electrons), then the total energy of this condenser is

$$E = QV/2 = CV^2/2 = Q^2/2C$$

This energy must be distributed uniformly among all the dipoles consisting, *e.g.*, of an electron in the electrode and a proton in solution. Therefore, the energy per unit dipole charge is $V/2$, and not V.

The fallacy in Dr. Austin's argument, according to which the differential energy should be considered, becomes evident from the fact that, in a condenser, voltage and charge are invariably dependent on each other. How then can one differentiate with respect to Q the function $CV^2/2 = Q^2/2C$ at constant Q?

The fact is simply that (because of electrostatic interaction) each charge, even infinitesimally small, added to the condenser will in turn change the potential of the condenser by a similar infinitesimal amount. This means that all the other charges which previously were on the condenser will also get a little "lift" by the small additional charge. The energy expended to put the "last" infinitesimal charge e_o on a condenser is, of course, $e_o \times V$, but this energy cannot be ascribed solely to the "last" particle added, but is equally shared by all the statistically identical particles in the double layer.

The differential energy, obtained by differentiating $E = CV^2/2 = Q^2/2C$ with respect to Q is naturally V, but it is not equal to the energy difference per unit charge between bulk and surface for a given *constant* surface state, and is therefore *not* pertinent to the question of the energetic states of particles in interfaces.

One must compare the difference in energy per particle between bulk and surface for a *constant* state, that is for *constant voltage and charge* on the electrode surface. If one tries to evaluate the difference beween bulk and surface energy by a process which itself changes the surface energy, one is necessarily at fault. To demonstrate this more clearly,

[1] Dept. of Fuel Technology, Pennsylvania State University, University, Park, Pa.
[2] B. M. W. Trapnell, "Chemisorption," pp. 11, 110, Butterworths Scientific Publications, London (1955).
[3] Volmer, *Z. physik. Chem.*, 150A, 203 (1930).

one could imagine, for instance, a case where the particle to be considered has an exceedingly high charge. As one transfers this particle from the bulk to the interface, one then would change the total charge and voltage of the interface condenser greatly, and the energy expended in tranferring the particle to the interface would not be equal to the energy difference between bulk and surface for a given *constant* surface condition.

In an actual electrochemical interface, held at a given *constant* potential, statistically an equal number of charges are entering and leaving the interface per unit time. For each particle entering, one will also leave the interface; and the single step of adding an individual charge to the interface is meaningless (because it is not repetitive without changes of the surface state). One has to consider the simultaneous leaving of the charges as well.

That the treatment of the energetics of particles in interfaces, as given in the paper "Overvoltage and Catalysis," is correct becomes very transparent by consideration of the electric field in the condenser. The energy of the condenser $E = CV^2/2$ must be considered to be "stored" uniformly in the electric field between the charged particles of the condenser. The energy density (energy per cm^3) is given by $\epsilon_o \mathcal{E}^2/2$ where $\mathcal{E}$ is the electric field strength and $\epsilon_o = 8.854 \cdot 10^{-12}$ amp sec $volt^{-1}$ m^{-1}. If one now subdivides the interface into sections containing just one dipole, then the energy per dipole is $(1/2)\ \epsilon_o \mathcal{E}^2\ a\ d$, where a is the area per dipole and d the distance between the charge layers. Considering that the charge per interface section and the capacity per interface section are related by $q^* = c^*V = \epsilon_o Va/d$ and, furthermore, that $\mathcal{E} = V/d$, one obtains immediately for the energy per particle with the charge q^* the expression

$$Vq^*/2$$

which is identical to the equation used in my paper.

The electrostatic energy stored in the electric field around the particles must be contributing to the local short range chemical (vibrational or thermal) energy to overcome the total energy required for reaction. Due to the electrostatic energy stored in the electric field around each dipole, the average energy per particle in the surface is raised, compared to the energy per particle in the bulk, by the amount $q^*V/2$.

In analogy to the principle of Born and Oppenheimer, the "relatively slow" thermal motion can be separated from the "immediate" electrostatic forces, and for each thermal configuration the energy is increased by the average electrostatic contribution, which in turn helps the particles to overcome the necessary local activation energy. Therefore, in the statistical treatment of reaction rates, the electrostatic energy per particle is added to the short range thermal energy in the exponential term, which leads immediately to the Volmer equation with $\alpha = ½$.

Following publication of the paper "Overvoltage and Catalysis," I have refined the theory of electrostatic interaction to include foreign nonreacting ions in the double layer and to interpret deviations of α from the value of one half.

The Fuel Cell and the Carnot Cycle

H. A. Liebhafsky (pp. 1068-1071, Vol. 106, No. 12)

John M. Matsen[4]: The ultimate efficiency of fuel cell systems is not as low as one might think from a superficial examination of Dr. Liebhafsky's paper. His calculations of thermodynamic efficiencies are correct for the conditions assumed, but he is concerned only with the simplest cases and excludes auxiliary devices which might be used to increase efficiencies.

The key to the disadvantages which Dr. Liebhafsky demonstrates for operating the hydrogen-oxygen cell at high temperatures lies in his statement, ". . . the potential advantage of this fuel cell over the steam plant will disappear unless the rejected heat is properly used." His calculations are based on the assumption that the rejected heat, $T_1\Delta S$, is entirely wasted. Actually, this heat could be used just as efficiently as the heat from an ordinary combustion, ΔH, simply by including a heat engine in the fuel cell system. The work then obtainable from the system would be not the negative free energy change ($-\Delta G = T_1\Delta S - \Delta H$) but the change in availability ($\Delta B = T_2\Delta S - \Delta H$). It is shown easily that ΔB is always greater than $-\Delta H(T_1 - T_2)/T_1$, which is the maximum work available from a combustion process.

$$0 > \Delta H - T_1\Delta S = \Delta G \text{ (The reaction is spontaneous)}$$

$$\Delta S > \Delta H/T_1$$

$$T_2\Delta S > \Delta HT_2/T_1$$

$$T_2\Delta S - \Delta H > -\Delta H(T_1 - T_2)/T_1$$

Therefore, with the available heat being used in the same way in each case, the fuel cell system is always more efficient than a combustion process.

In evaluating the efficiency of a fuel cell cycle in combination with a nuclear reactor, it was concluded that this efficiency would be less than that of a Carnot cycle unless ΔCp was zero, permitting reversible heat flow. For any ΔCp, however, the heat exchange between products and reactants can be made reversible by the addition of auxiliary heat engines to the system. (These engines may be fuel cell cycles as well as Carnot cycles.) In such a case, the fuel cell cycle would be as efficient as a Carnot cycle no matter what the magnitude of ΔCp. This admittedly is an idealized mode of operation, but the Carnot cycle itself represents a highly idealized case, so that comparison on this basis is valid.

It should be emphasized that Carnot efficiency is a limit only when the fuel consumed in the cell is produced in a thermal cycle. Such is not the case for cells which consume primary fuels, *e.g.*, a coal-consuming redox cell.

Exception must be taken to two items in Dr. Liebhafsky's paper, although they are relatively minor and not essential to the development of his argument. First, the sign of ΔS is erroneously equated with the sign of ΔCp on the grounds that this follows from the identity:

$$d(\Delta S) = \Delta Cp d(\ln T)$$

Integration of this equation requires knowledge of (*a*) ΔCp as a function of T, down to $T = 0$; (*b*) ΔS at

[4] Dept. of Chemical Engineering, Columbia University, New York 27, N. Y.

$T = 0$; (c) temperatures and latent heats of phase changes of reactants and products. Note that ΔCp cannot be assumed to be a constant $\neq 0$ for this integration, since this would give an infinite ΔS at $T = 0 + dT$. There are many cases where ΔS and ΔCp are of opposite sign, *e.g.*, the reaction:

$$H_2 + Cl_2 = 2HCl$$

At 25°C, $\Delta Cp = -1.08$ cal/°K, while $\Delta S = +4.737$ cal/°K. Secondly, the worth of the statement, "The sign and magnitude of ΔCp are determined primarily by the change in the number of gaseous molecules during reaction," is questionable. Picking 1200°K (as an average temperature for the range 400°K to 2000°K discussed in the paper), the following data exist for representative gaseous oxidations:

Reaction	Δn	ΔCp
$C_2H_6 + 3.5O_2 = 2CO_2 + 3H_2O$	$-\frac{1}{2}$	-3.60
$H_2 + \frac{1}{2}O_2 = H_2O$	$-\frac{1}{2}$	-1.071
$CO + \frac{1}{2}O_2 = CO_2$	$-\frac{1}{2}$	$+1.24$
$SO_2 + \frac{1}{2}O_2 = SO_3$	$-\frac{1}{2}$	$+3.18$
$CH_4 + 2O_2 = CO_2 + 2H_2O$	0	-0.98
$H_2 + Cl_2 = 2HCl$	0	$+0.80$
$C_2H_4 + 3O_2 = 2CO_2 + 2H_2O$	0	$+2.17$

H. A. Liebhafsky: My paper was written to emphasize that a fuel cell alone (A) is not Carnot-cycle limited (Conclusion 1, obvious and well known); and that an isolated system (B) containing only a heat source (nuclear reactor as example), a fuel cell, and a single connecting heat exchanger is Carnot-cycle limited (Conclusion 2, obvious but less well known). Consideration of System B led to the subordinate conclusions that reversible operation of this system to produce electricity in finite amounts could entail irreversible heat transfer when ΔCp differs from zero (Conclusion 3), and that such irreversibility did cause the efficiency to fall below the Carnot efficiency in the example cited (Conclusion 4).

In reaching these four conclusions, I deliberately restricted discussion to A and B (Imposed Restriction) and—again deliberately—made certain approximations in thermodynamics.

Mr. Matsen now points out that the heat rejected by A can be usefully employed in a heat engine. Of course it can, but in contravention of the Imposed Restriction. The proper employment of such rejected heat long has been recognized as essential to economically successful generation of electricity in fuel cells on a central-station scale.[5-8]

Dr. Matsen further points out that heat flow always can be made reversible. Of course it can. He also points out that heat flowing because ΔCp differs from zero could be converted to work by adding appropriate components to B. This certainly would increase the efficiency above that given by Eq. [6] of the discussed paper, but again it is in contravention of the Imposed Restriction.

[5] E. Gorin, U.S. Pat. 2,570,543, Oct. 9, 1951; 2,581,650, Jan. 8, 1952; and 2,581,651, Jan. 8, 1952.
[6] E. Gorin and H. L. Recht, *Chem. Eng. Progr.*, 55, No. 8, 51 (1959).
[7] H. A. Liebhafsky and D. L. Douglas, "The Fuel Cell," *Mech. Eng.*, 81, No. 8, 64 (1959).
[8] D. L. Douglas and H. A. Liebhafsky, "Fuel Cells. History, Operation, and Applications," *Physics Today*, 13, No. 6, 26-30 (1960).

Mr. Matsen appears to agree that the thermodynamic approximations do not vitiate any of the four conclusions given above. I wish to thank him for citing data showing that these approximations are in certain cases (not all important for the fuel cell) poorer than I had thought them.

Finally, I wish to thank Professor A. J. deBethune for pointing out that 71.7% is the correct efficiency in Eq. [9]. The incorrect value, 73.3%, resulted because 20,500 was used in place of 20,050.

Effect of Hydrogen Pressure on the Hydrogen Overvoltage on Bright Rhodium

Sigmund Schuldiner (pp. 452-457, Vol. 107, No. 5)

A. M. Peers[9]: It is interesting that the method of Schuldiner gives much lower values for the surface coverage by atomic hydrogen than do charging curve methods. Schuldiner's suggestion that his method measures only a fraction of the total adsorbed hydrogen is consistent with (and lends weight to) a mechanism which I have proposed recently to account for the time-dependence of the hydrogen overvoltage on electrodeposited nickel.[10] This mechanism assumes, in agreement with gas-phase adsorption studies, that a fraction of the adsorbed hydrogen is weakly bound (type A, say) and the remainder strongly bound (type B) to the metal surface. It is further assumed that the type A bond is a necessary precursor to the type B bond and that the rate of combination of type B atoms is negligible, owing to their large adsorption energy. The usual partial reactions, simple discharge, ion + atom (electrochemical) and combination are then written,

$$H^+ + e \rightarrow H_A;\ H^+ + H_B + e \rightarrow H_2;\ 2H_A \rightarrow H_2$$

(The second is favored by the negative charge on the strongly bound hydrogen.) It may be noted that the mechanism proposed by Schuldiner for hydrogen evolution on rhodium (discharge followed by combination) involves only the weakly bound, type A atoms.

Sigmund Schuldiner: I am very grateful for Dr. Peers' comments and, needless to say, am glad that we are in agreement that atomic hydrogen can exist both as a weakly and strongly bonded species. This also is in accord with a recent study of hydrogen adsorption on platinum by Pliskin and Eischens.[11] In a very recent investigation[12] at this laboratory of the hydrogen reaction on platinum, we have been able to confirm the existence of these two species of hydrogen atoms. In fact, our work strongly indicates that a significant amount of hydrogen can also be absorbed in the outermost layers of a platinum electrode and that this hydrogen, which probably exists as a Pt-H alloy similar to Pd-H alloys, also contributes to the total amount of hydrogen determined by anodic charging curve methods.

[9] Institut du Radium, Laboratoire Curie, 11 rue Pierre-Curie, Paris 5e, France.
[10] A. M. Peers, *J. chim. phys.*, 58, 336 (1961).
[11] W. A. Pliskin and R. P. Eischens, *Z. Phys. Chem. N. F.*, 24, 11 (1960).
[12] C. H. Presbrey, Jr., and S. Schuldiner, Paper submitted to *This Journal*.

Preparation of Solid Electrodes for Hydrogen Overpotential Studies

A. C. Makrides and M. T. Coltharp (pp. 472-473, Vol. 107, No. 5)

A. M. Peers[13]: Makrides and Coltharp have prepared nickel cathodes having an activity (*i.e.*, current density for a given overpotential) about 40 times that of the nickel wire cathodes of Bockris and Potter.[14] Nickel cathodes about 400 times as active as those of Bockris and Potter have been prepared in this laboratory by electrodeposition from very pure nickel chloride-boric acid solution. Activities comparable with those reported in earlier studies of hydrogen overpotential on nickel[14-18] were obtained only by deliberate contamination of the electrodeposit, particularly by mercury vapor. Further details of this work will appear in the *Journal de Chimie Physique*.

An Investigation of the Reaction between Aluminum and Water

W. J. Bernard and J. J. Randall, Jr. (pp. 483-487, Vol. 107, No. 6)

D. G. Altenpohl[19]: The authors are to be congratulated on their fine investigation. There are a number of open questions, and here are a few suggestions on how to investigate further the properties of hydrated oxides, generated by reaction between aluminum and distilled water at temperatures between approximately 70°-100°C.

In Bernard's and Randall's work, no evidence was obtained on the form in which the water is combined in the oxide generated at the surface. Infrared spectral analysis and DTA[20] are two methods to obtain information on this.[21] Corresponding results are shown in Fig. 1 and 2 of this discussion.

The behavior of hydrated films, generated at temperatures between 70°-100°C, is in the results of these two methods very similar to trihydrates, although by x-ray diffraction no crystalline trihydrates are to be detected in these films. But, at temperatures around approximately 150°C or above, the hydrated oxide crystallizes according to these two methods fairly similarly to the mineralogical boehmite and could therefore be called pseudo-boehmite.[22]

The existence of an inhibition period (mentioned on p. 486 of the discussed paper) has been reported previously.[23] The inhibition period does not depend on the purity of the metal, which has a strong in-

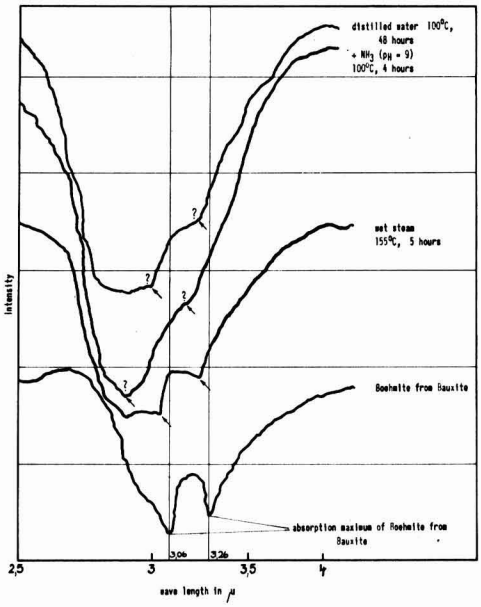

Fig. 1. Infrared spectrum of various hydrated aluminum oxides (Weak maximum is marked by arrow.) Corresponding oxide films were, in Case 1, 2, and 3, made by reaction of 99.99% Al with H_2O. (In Case 2, a small amount of ammonium was added to the distilled water.)

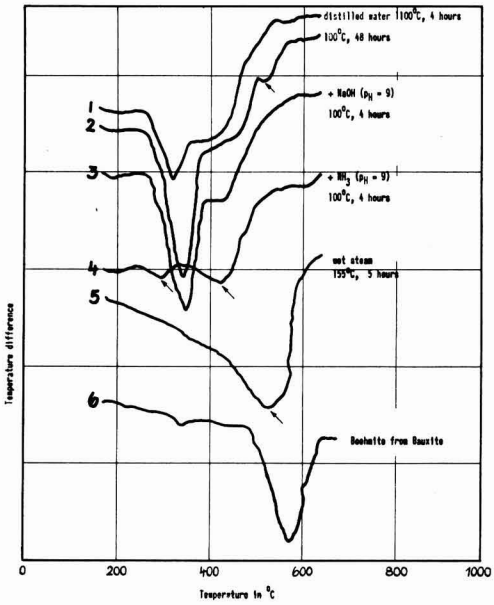

Fig. 2. Differential thermoanalyses (DTA) of hydrated oxide from various origins. (No. 1-5 made by reaction between 99.99% Al and H_2O; in No. 2 and 3 additions have been made to the distilled water used for reaction.) Arrow marks weak heat evolution. (Note: Curves 1-6 are shifted vertically for better reproduction.)

fluence on the growth of the film after several hours' reaction time (Fig. 3 of this discussion).

One must distinguish between the inhibition of hydrogen evolution and of film growth: in boiling

[13] Institut du Radium, Laboratoire Curie, 11 rue Pierre-Curie, Paris 5e, France.
[14] J. O'M. Bockris and E. C. Potter, *J. Chem. Phys.*, **20**, 614 (1952).
[15] F. Bowden and E. Rideal, *Proc. Roy. Soc.*, **A120**, 80 (1928).
[16] P. Lukowzew, S. Levina, and A. N. Frumkin, *Acta Physicochim., U.S.S.R.*, **11**, 21 (1939).
[17] Y. Kolotyrkin and A. N. Frumkin, *Compt. rend. acad. sci. U.R.S.S.*, **33**, 445 (1941).
[18] R. Jeffereys *et al.* (1956), quoted by J. Yeager, J. P. Cels, E. Yeager, and F. Hovorka, *This Journal*, **106**, 328 (1959).
[19] Aluminium-Industrie-Aktien-Gesellschaft, Feldeggstrasse 4, Zurich 8, Switzerland.
[20] DTA = Differential thermoanalysis (heating of a dead burned Al_2O_3 sample together with the test sample and checking of the temperature difference).
[21] D. Altenpohl, "Ueber das Verhalten von Korn- und Subkorngrenzen bei der Reaktion zwischen Aluminium und Wasser," *Z. Metallk.*, **48**, 305 (1957).
[22] R. M. Haag, Report KAPL-1739, AEC, Knolls Laboratory (1957).
[23] D. Altenpohl, "Das Verhalten von Reinaluminium und Reinstaluminium in kochendem Wasser," *Aluminium*, **9**, 361 (1953).

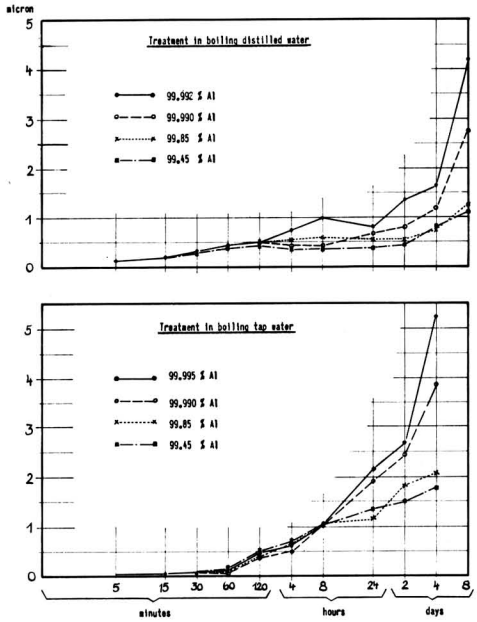

Fig. 3. Thickness of hydrated oxide film for various times of treatment in boiling distilled water of 98°C. Thickness was determined by dissolution of the aluminum brommethanol and by weighing of the film.

tap water, the hydrogen evolution is, within the first 30 min of reaction, considerably less than in boiling distilled water, and the growth of the oxide film is related to the evolution of hydrogen (Fig. 3). After approximately 3-4 hr of reaction at 100°C, the films in tap water grow faster than in distilled water, without detectable difference in hydrogen evolution. This indicates that, in the first stages of reaction, a different mechanism takes place than after the reaction was going on for a longer time. After several hours of reaction at 100°C, the generated hydrated aluminum oxide becomes more and more insoluble in the CrO_3-H_3PO_4 stripping solution, and at the same time the x-ray lines of boehmite become sharper.[21,23,24]

There has been some controversy on the nomenclature of hydrated aluminum oxides.[24-26]

Ginsberg[25,26] expresses the opinion that the term "hydrated aluminum oxides" should be removed from literature as being misleading. In boehmite or bayerite and in the water containing films generated in boiling or superheated water, according to Ginsberg, water is never present as hydrate, but these compounds form a true hydroxide lattice. Therefore, Ginsberg wants to replace the term "hydrated oxides" with the term "hydroxides" or "oxide-hydroxides."

According to our present knowledge, the films, generated by reaction between aluminum and boiling distilled water, consist of a mixture of poorly crystallized boehmite (pseudo-boehmite) in a matrix of amorphous hydroxides and superhydroxides. This hydroxide matrix has a water content between 30-60%.[27] With increased reaction time, more and more boehmite crystallizes out in this matrix. This "pseudo-boehmite" gives the x-ray pattern of boehmite but, in infrared analysis, can be clearly distinguished from the mineralogical boehmite as being less properly crystallized.

The determination of a film thickness on superpurity aluminum by checking weight increase is fairly uncertain because a considerable amount of oxidation occurs at the grain boundaries.[28,29] At the lower purities (below 99.85% Al), the oxidation occurs predominantly as a film parallel to the surface at temperatures below 160°-200°C.

Walter J. Bernard and John J. Randall, Jr.: The hypothesis that the product of the reaction between aluminum and water consists of poorly crystallized boehmite in a matrix of amorphous hydroxide seems to us to be a reasonable and attractive one. Unfortunately, no direct experimental evidence is yet available to support this idea, and it only can be conjectured from the composition of the film and x-ray data. Altenpohl's work with infrared and differential thermal analysis, which was earlier presented in his footnote 21, does not give unambiguous structural information.

There appears to be some difference in interpretation of the term "inhibition period." In our paper, we used this expression to describe the short time lapse (the order of seconds) which occurs before aluminum and water show visible evidence of reaction, i.e., evolution of hydrogen. In footnote 23, Altenpohl does not explicitly describe this phenomenon nor use a comparable expression for any other effect. He does indicate in his Fig. 3 a very slow rate for the first stage of the reaction (the order of hours), but this has no relationship to the inhibition period as defined by us. Furthermore, it is difficult to see what connection with our paper there is with the relative rates of growth of films on aluminum in pure water and in contaminated water. If one discusses the growth of films of the same composition, the rate of evolution of hydrogen is *directly* related to film growth; observations of another nature are irrelevant here.

We believe that weight measurements permit a reasonably accurate estimate of film thickness. Intergranular oxidation is known to occur with aluminum at elevated temperatures but is probably negligible at 100°C in the time interval studied.[30]

High Current Electronic Interrupter for the Study of Electrode Processes

W. E. Richeson and M. Eisenberg (pp. 642-647, Vol. 107, No. 7)

D. N. Staicopoulos[31]: Richeson and Eisenberg have disclosed the design of a very versatile electronic interrupter intended for use in the study of electrode

[24] D. Altenpohl, "Zur Frage des Auftretens von Böhmit bei der Reaktion zwischen Aluminium und kochendem oder überhitzten Wasser," *Aluminium*, 8, (Augustt 1960).
[25] H. Ginsberg, *Aluminium*, 36, 16 (1960).
[26] H. Ginsberg, *Z. Erzbergbau und Metallhüttenwesen*, 13, 5 (1960).
[27] W. Tragert, Paper delivered at Symposium of the Electrochemical Society, May 2, 1960, Chicago, Ill.
[28] K. Videm, Kjeller Report KR2 (1959); P. Lelong and J. Jerenguel, *J. of Nuclear Mat.*, 1, 58 (1959).
[29] G. Faschinger, Unpublished results.
[30] V. H. Troutner, *Corrosion*, 15, 9t (1959).
[31] Engineering Research Lab., Engineering Dept., E. I. du Pont de Nemours & Co., Inc., Wilmington, Del.

processes. It is similar in several respects to an instrument described by Staicopoulos, Yeager, and Hovorka in 1951.[32] Features common to these two instruments are as follows: (*a*) Circuitry for handling currents higher than a few tenths of an ampere is provided via a parallel connection of any desirable number of interrupter valves; (*b*) both instruments utilize pulse-generating circuitry to achieve the electronic-switching function of the interrupter.

These instruments differ, however, in one important respect: The Richeson and Eisenberg interrupter utilizes an oscilloscope to display the time variation of the polarization and depends on the voltage calibration on the screen of the cathode-ray tube to determine the value of this polarization. The instrument described in 1951 features a gated-bridge null detector, with which accurate measurements of the instantaneous potential can be made. Furthermore, the pulse-generating and pulse-delay circuitry of this interrupter permit the measurement of the polarization potential at any given time (within 5 μsec) following current interruption. In a modified version of this instrument, at present in operation at the writer's laboratory, currents of the order of 0.8 amp and interruption and/or potential-measuring periods as short as 2.2 ± 0.2 μsec are available.

M. Eisenberg: I find the remarks of D. N. Staicopoulos interesting. The major performance differences between our interrupter and that by D. N. Staicopoulos, *et al.*, (*see* footnote 32) is in the current carrying capacity and response speed. Our interrupter had a current carrying capacity of 5 amp and a minimum interrupter period of 1.6 μsec. Upon interruption, depending on the experimental conditions, "ringing" obscured the decay for a period ranging from 0.3 to 0.6 μsec. To the best of our knowledge, such an interrupter performance has not been reported before.

In recent investigation, the use of solid-state devices also has been considered and found to be too slow for the purpose of a high-speed interrupter. It is important to distinguish between the time of interruption and the minimum time for resolution, *i.e.*, the minimum time it takes until the decay curve is free of disturbances so that polarization and the slope of its decay can be measured at this point. For such purposes, the use of an oscilloscope is necessary. In a recent version of this interrupter design, interruptions as short as 1 μsec have been achieved with the "ringing" disturbance limited to 0.3 μsec.

Discharge of a Lead-Acid Cell through an R-L Circuit

J. J. Lander and E. E. Nelson (pp. 722-725, Vol. 107, No. 9)

E. Willihnganz[33]: Lander and Nelson conclude that polarization does not occur during a short-pulse discharge of a lead acid battery because they could explain the transient voltages without it. This conclusion disagrees with our own[34] and we believe that the cause of the disagreement is experimental.

Lander and Nelson used a large cell with a high inductance, and studied the voltage during discharge. We used a series of small cells and studied the voltage both during discharge, and after the discharge was interrupted. It is our conclusion that polarization is present, and that it develops so rapidly that it is difficult to observe in the presence of a large inductance, during discharge, but is easily observed immediately after a discharge pulse ends.

If we take our data on the small cells, extrapolate them to the larger cells, and make an allowance for the difference in separator thickness, we conclude that the "resistance" reported by Lander and Nelson is about 20% high because of polarization.

This amount of polarization would pass unnoticed in the experimental work of Lander and Nelson because the polarization develops in a few thousandths of a second, and it appears to level off at a voltage which is proportional to the current. With these properties, polarization would have almost the same effect on cell voltage as internal resistance and would, therefore, be regarded as a resistance by Lander and Nelson. However, it could have been distinguished from a resistance voltage had oscilloscope readings been taken as the discharge current was interrupted.

J. J. Lander: Dr. Willihnganz makes the point that the experimental work treated in the paper precluded finding a type of polarization characterized by a voltage which is proportional to current. Our technique is presumed to prevent observation because the large inductance of the cell (actually, better, the inductance of the total circuit) slowed down current rise time so the polarization of which he speaks can easily keep up with the rate of establishment of *IR* loss.

He also concludes that our internal resistance is too high by a factor of 20%. This result is arrived at by making a long extrapolation from data probably obtained on an automobile battery and scaling it up to submarine cell size. It also seems to be inherent in his estimate of our error that he has correctly measured the internal resistance of his own cell combination. Perhaps he has, but, even if he has, it would be surprising indeed for such an extrapolation to produce such an accurate estimate of our error.

However, Dr. Willihnganz's first point may be well taken and might, indeed, cast doubt on the validity of our conclusions and, so, it seems in order to attempt to obtain some independent estimate of polarization values.

NRL Report 4347, "Polarization Studies of the Lead-Acid Storage Cell," which is the basis for the paper under discussion, contains data which indicate that polarization at the positive plate is an extremely slow process (by comparison) and probably could contribute no more than 0.01 v in 0.1 sec by the time 9000 amp were flowing in the submarine cell under test. (The positive element reached 0.05 v polarization at 2 sec.) The positive plates in this cell are 0.317

[32] D. N. Staicopoulos, E. Yeager, and F. Hovorka, *This Journal*, 98, 68 (1951).

[33] C & D Batteries, Div. of The Electric Autolite Co., Conshohocken, Pa.

[34] E. Willihnganz, *This Journal*, 102, 99 (1955); *Trans. Am. Inst. Elec. Engrs.*, 78, 259 (September 1959).

cm thick and have a gross area of 69,000 cm^2 (one side only), so gross current density was 0.065 amp/cm^2 (counting two sides per positive plate). Unpublished work at NRL by one of the authors (J. J. Lander) has shown that polarization at the positive plate is, indeed, such a slow process. *IR* free polarizaion data obtained during discharge of an 0.013 cm thick PbO_2 plate at a current density of 0.144 amp/cm^2 showed 0.04 v polarization at 0.1 sec. At 0.024 amp/cm^2, it polarized to 0.005 v in 0.1 sec. In view of the 24 X factor in plate thickness, the latter current density situation would appear to be more nearly representative of the submarine cell at 9000 amp, to say nothing of the fact that, in the cell, current built up from 0 to 9000 amp in 0.1 sec or so while, in the unpublished work quoted, it was applied instantly.

In the paper under discussion, for the 9000-amp discharge, the total measured voltage loss was 0.44 v in 0.1 sec, so it is concluded that positive plate polarization contributes no more than about 1.1% to the voltage decay at 0.1 sec and correspondingly less at the lower rate discharges.

In looking at negative plate polarization on discharge, we have recourse to data obtained by Beck, Lind, and Wynne-Jones[35] which are not corrected for *IR* loss. In this work, they measured stable polarization values at lead-plated electrodes of known area and found:

I (amp/cm^2)	ΔV (volts)
0.00056	0.013
0.0023	0.025
0.0058	0.032
0.0206	0.052
0.034	0.07
0.0508	0.100

If we use the value 138,000 cm^2 for the area of the negative plates in our cell (counting both sides of the plates), then the polarization, based on the above data would be:

I (amperes)	ΔV (volts)
7000	0.1
2800	0.05

However, because of the porous nature of the plates, if we estimate surface area to be (conservatively) 100 X greater than 138,000, the corresponding polarization values would be 0.01 and 0.005, and we still have not corrected for Beck's, *et al.*, *IR* losses. In further unpublished work at NRL, the senior author has essentially checked Beck's, *et al.*, data on flat Pb sheets.

Therefore, it seems that polarization of the negative plate contributes even less than that of the positive plate at the discharge currents involved in our work. Consequently, we think we are justified in stating that the reported values of internal resistance are not significantly affected by polarization contributions from other than *IR* losses.

It seems to me that in battery technology, at least, the simpler, more direct approaches may be preferred.

[35] Beck, Lind, and Wynne-Jones, *Trans. Faraday Soc.*, 50, 147 (1954).

Inhibition of Acid Attack on Steel by Heavy Metal Ions

J. A. Shropshire (pp. 740-744, Vol. 107, No. 9)

E. L. Koehler[36]: Hoar and Havenhand[37] likewise have noted a relationship between sulfur and inhibition by dissolved tin. They noted that, in acid solutions, corrosion is accelerated by sulfur in the metal or in the solution owing to stimulation of the anodic processes. They suggest that the diminished anodic polarization of iron is brought about by hydrogen sulfide due to a specific adsorption on the iron surface, which assists the anodic electron transfer process. They further considered it likely that tin ions act by removing hydrogen sulfide from its sphere of action on the anodic process. The data in the current paper are presented in such a fashion that it is not possible to evaluate such a possibility, and I wonder if the author would care to comment.

It would appear necessary to do a little more than just to describe the inhibiting effect as due to a protective coating of tin sulfide. The author himself points out that the inhibiting effect is immediately apparent and not dependent on any film thickening process. With this picture, we further have to explain why the inhibiting effect of dissolved tin should be purely anodic in nature, since dissolved tin has little if any effect on the hydrogen overvoltage curve for the steel at potentials more noble than where tin starts to plate out.

J. A. Shropshire: The author does not object to the suggestion, as outlined above, that tin ions act by removing hydrogen sulfide from its sphere of action on the anodic process. However, in what manner is this accomplished? If it is by the continuous formation of a stable complex of Sn^{++} and H_2S, this is tantamount to suggesting the formation of SnS. If the species were soluble and diffused away from the surface, inhibition would be strongly dependent on diffusion of fresh Sn^{++} to the surface, since production of H_2S would continue. The author does not believe the extreme inhibition could be accounted for in this manner.

On the other hand, it seems more reasonable to assume that the removal of H_2S from its sphere of action is by precipitation of the insoluble species at the surface. This inhibition is by definition restricted to anodic sites if we postulate that the anodic stimulation is due to the presence of sulfide. It does not seem unreasonable to postulate higher quantities of sulfur at grain boundaries and dislocations, which would be expected to have higher anodic activity. (A comparable suggestion recently has been put forth by Buck and Leidheiser.[38]) In the absence of metal ion plating, then, no effect on the cathodic hydrogen evolution reaction is to be expected.

The author feels that the significant points to be considered in comparing the results of this study with data obtained in other investigations are (*a*)

[36] Central Research and Engineering Div., Continental Can Co., Inc., 7622 S. Racine Ave., Chicago 20, Ill.

[37] T. P. Hoar and D. Havenhand, "Factors Influencing the Rate of Attack of Mild Steel by Typical Weak Acid Media, "*Tech. Publ.*, Int. Tin Res. and Dev. Council, Series A, No. 36—Reprinted from *J. Iron Steel Inst.*, Vol. 133 (1936).

[38] W. R. Buck, III, and H. Leidheiser, Jr., *This Journal*, **108**, 203 (1961).

the identity of inhibition obtained with Sn^{++} and Pb^{++} and (b) the remarkable decrease in inhibition in going from 1*N* to 3*N* HCl. This latter point alone suffices to rule out most electrochemical mechanisms that one can imagine.

Identification of the Diffusion Species in Uranium Oxidation

J. G. Schnizlein, J. D. Woods, J. D. Bingle, and R. C. Vogel (pp. 783-785, Vol. 107, No. 9)

M. W. Mallett[39]: The authors have given a good description of how markers (both inert and radioactive) may be used to identify the diffusing species in uranium oxidation. However, the tests are applicable only in the case where there exists a species diffusing through a protective film. A parabolic oxidation rate is evidence of such protection. The authors indicate that when samples were "oxidized at 200°C in 200 mm oxygen" . . . "an essentially linear rate is achieved after a brief, very much lower initial rate." The fact that the oxidation rate is linear shows that the oxide under test is nonprotective and obviates the use of the tests. It appears that application of the tests would be legitimate only for the film formed during the brief initial period of slow oxidation.

It is incidental that the tests do show that uranium is not diffusing. However, this negative result cannot be used as proof that oxygen is diffusing through the lattice structure or its interstices. Oxygen is, of course, diffusing as molecular gas through the pores of the oxide but this is not a part of the problem.

J. G. Schnizlein: Perhaps it should have been stated more explicitly that the marker experiments, which demonstrate the absence of uranium diffusion, do not distinguish between oxygen ion migration through a compact oxide and oxygen molecules going through a porous oxide. The fact that new oxide is produced at the metal surface is the important conclusion.

We note that other investigators associate a linear rate law with either porous scale or a surface reaction with constant area. Haycock[40] states, "Linear rate laws generally are associated with one of two mechanistic features. Surface reactions occurring at either the metal-scale or scale-gas interface can be considered in some cases to be slow and therefore rate determining. If the interface has a constant area throughout the reaction, then an over-all linear rate law would be expected. The second mechanism giving rise to linear kinetics depends on the formation of an 'open' or porous scale structure."

Electroluminescence—A Disorder Phenomenon

D. W. G. Ballentyne (pp. 807-810, Vol. 107, No. 10)

W. Lehman[41]: The author attempts to correlate the effect of electroluminescence of ZnS phosphors with coexistence of the cubic and the hexagonal crystal

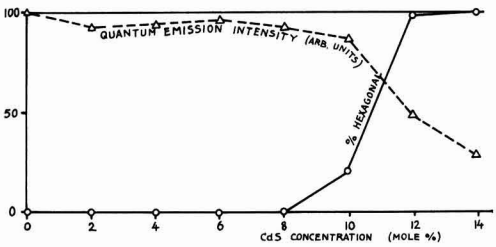

Fig. 1. Correlation between the electroluminescent emission intensities of a series of (Zn,Cd)S:Cu,Br phosphors and the lattice structure.

modifications in comparable intensities (*i.e.*, detectable by the usual x-ray analysis). This idea also has been discussed previously in the literature.[42-44] Such correlation may exist in certain cases but it is fairly easy to show that it does not exist in general. For instance, one may prepare a phosphor which contains both cubic and hexagonal phases but which is not electroluminescent. Hence, the presence of both cubic and hexagonal phases is not a sufficient condition to make the phosphor electroluminescent. On the other hand, one may prepare excellent electroluminescent phosphors which are only cubic in structure, at least as far as is detectable by normal x-ray powder diffraction patterns.[45] Hence, the presence of both, cubic and hexagonal, phases in comparable concentrations is not even a necessary condition.

The general experience in this laboratory regarding the correlation of electroluminescence with the lattice structure is demonstrated in Fig. 1 of this discussion. It shows the emission intensity of electroluminescence (in terms of quanta/cm²/sec) of a series of (Zn,Cd)S:Cu,Br phosphors prepared and excited under standard conditions. The lattice is cubic within the detectable limit (~1%) up to 8% CdS, changes from cubic to hexagonal between 8 and 14% CdS, and is completely hexagonal for 14% or more CdS. The range between about 8 and 14% CdS (where the lattice contains both cubic and hexagonal structure) is by no means characterized by an especially good electroluminescence. Further, the concentration of the hexagonal phase decreases very rapidly with decreasing CdS concentration between 14 and 8% CdS. It is already below 1% (the detectable limit) at 8% CdS so that it seems to be fairly certain that is is very, very small (if present at all) at zero CdS.

One gains a deeper insight into the situation by careful examination of the phosphors under a microscope. This requires a high resolution because the interesting objects are mostly of a size of about 1 μ or somewhat below. The particles of a cubic phosphor tend to form faults (visible as striations on the particles) even when no hexagonal phase is present in noticeable concentration. They also contain many inclusions of Cu_2S if there was an excess of copper (*i.e.*, not compensated by a coactivator) present

[39] Consultant, Thermal Chemistry Group, Battelle Memorial Institute, 505 King Ave., Columbus 1, Ohio.

[40] E. W. Haycock, "Transitions from Parabolic to Linear Kinetics in Scaling of Metals," *This Journal*, 106, 771 (1959).

[41] Research Dept., Westinghouse Electric Corp., Bloomfield, N. J.

[42] L. W. Strock, *Illum. Eng.*, 55, 24 (1960).

[43] M. A. Short, E. G. Steward, and T. B. Tomlinson, *Nature*, 177, 240 (1956).

[44] A. H. McKeag and F. G. Steward, *This Journal*, 104, 41 (1957).

[45] The writer has sent two phosphor samples representing these two examples to Dr. Ballentyne for examination.

during firing. The dark Cu_2S inclusions and their correlation with the emitting "spots" inside the particles can be seen directly by microscope.[46] Dark Cu_2S inclusions are also indirectly indicated by the somewhat darker body color of the phosphor, which cannot be lightened even by a very thorough cyanide wash. These cubic particles also are well electroluminescent. On the other hand, the particles of a hexagonal phosphor are highly perfect; *i.e.*, there are no (or very few) visible striations, no (or very few) dark Cu_2S inclusions, and no (or very few) emitting "spots" inside the particles. For this reason, the hexagonal phosphors generally are weaker in electroluminescence than cubic phosphors are. The intermediate stage where cubic and hexagonal structures are simultaneously present in the same phosphor is characterized by an intermediate concentration of lattice faults and, therefore, of Cu_2S segregations inside the particles, and by an electroluminescence intensity intermediate to those of the cubic and the hexagonal ranges.

It is obvious that the occurrence of Cu_2S segregations in ZnS particles is facilitated by the presence of lattice faults, *e.g.*, by stacking faults between cubic and hexagonal. However, the observations indicate that the electroluminescence of ZnS phosphors is not directly due to a mixed cubic-hexagonal lattice but to the presence of an electrically well-conducting second phase (Cu_2S in most practical cases) in intimate contact with the ZnS crystals. This also is shown by the fact that nonelectroluminescent ZnS phosphors can be made electroluminescent if a well-conducting second phase is artificially provided, *e.g.*, by admixing a fine metal powder to the phosphor[47] or by overcoating the phosphor particles with a thin layer of Cu_2S.[48] It is difficult to understand how such means should be able to introduce stacking (or any other) faults in the crystal structure of the phosphor; yet the phosphors become electroluminescent.

D. W. G. Ballentyne: It is asserted in the discussion that the presence of an electron-rich layer and a cubic phase gives rise to good electroluminescence. In the paper, it has been shown that it is possible to prepare a phosphor containing no copper which is electroluminescent. Zinc sulfide crystals grown from the vapor in high temperature are not electroluminescent when indium electrodes are applied and these crystals are hexagonal. Doping these crystals by refiring in copper activated material leads to electroluminescence. Such treatment causes a mixture of phases. The light does not appear to be associated with inclusions in the crystal but to be emitted under the electrode or at striations in the body of the crystal.

In general, the author has not found that all zinc sulfide phosphor coated with copper sulfide becomes electroluminescent. Such treatment of phosphors containing mixed phases, or which are predominantly cubic is *sometimes* successful; in general, the method does not in our experience work.

To summarize, however, the author believes that the concept of an electron-rich layer in contact with a semiconducting phosphor does not explain the occurrence of electroluminescence.[49] More recent experiments such as those reported by W. A. Thornton[50] on the lack of threshold and by P. Goldberg and S. Faria[51] on the maintenance of brightness on solution of the crystallites, tend to undermine still further this simple explanation. The evidence appears to indicate that it is possible to make a poor electroluminescent phosphor by disordering zinc sulfide, but that, in general, the addition of copper greatly increases the efficiency. X-ray analysis cannot resolve the problem as to whether the effect occurs in cubic materials or materials which are disordered, because 5% of another phase would not be detected. Work is continuing in order to resolve this problem on ZnTe, ZnS and ZnSe, ZnS mixtures as the pure telluride and selenide is cubic.

[46] W. Lehmann, *This Journal*, **107**, 657 (1960).
[47] W. Lehmann, *This Journal*, **104**, 45 (1957).
[48] P. Zalm, G. Diemer, and H. A. Klasens, *Philips Research Repts.*, **9**, 81 (1954).
[49] M. A. Short, E. G. Steward, and T. B. Tomlinson, *Nature*, **177**, 240 (1956).
[50] W. A. Thornton, *Phys. Rev.*, **116**, 4, 894 (1959).
[51] P. Goldberg and S. Faria, *This Journal*, **107**, 521 (1960).

Fuel Cell Thermodynamics

A. J. deBethune (pp. 937-939, Vol. 107, No. 11)

John M. Matsen[52]: The fuel cell cycle as analyzed by Professor deBethune will not be as efficient as a Carnot cycle operating between the temperatures T_h of the heat source and T_l of the sink. He has only shown it to be the equivalent of a reversible cycle which accepts $T_h\Delta S_c$ heat units at T_h and $\int_l^h \Delta C_p dT$ heat units at lower temperatures (from T_h down to T_l). This result is to be expected, since within the cycle represented in his Eqs. [A], [B], [C], and [D] there is no heat conduction, friction, or other irreversible process. The point is that since no device is provided to supply the heat $\int_l^h \Delta C_p dT$ reversibly from either T_h or T_l, it must flow irreversibly from T_h down to the temperature at which it is accepted by the cycle. (If ΔC_p is negative, the heat will flow from the temperature at which it is rejected by the cycle down to T_l.) The theoretical work which the amount of heat Q_h available at T_h can do may be calculated from the equation $W = Q_h(T_h - T_l)/T_h$, and in this case it is equal to

$$(T_h - T_l)\left(-\Delta S_c - \int_l^h \Delta C_p d\ln T\right) + [(T_h - T_l)/T_h]\int_l^h \Delta C_p dT$$

This exceeds the work of the fuel cell cycle, given in his Eq. [7], by

$$T_l \int_l^h \Delta C_p d\ln T - (T_l/T_h)\int_l^h \Delta C_p dT$$

In order to operate at theoretical efficiency, the heat $\int_l^h \Delta C_p dT$ must be transferred between T_h or T_l and the temperature at which it is accepted or rejected by the fuel cell cycle by means of an auxiliary heat engine. If this engine operates with an isothermal at T_h, the heat absorbed by it at T_h will be

$$T_h \int_l^h \Delta C_p d\ln T$$

The work done by this auxiliary cycle will be

$$T_h \int_l^h \Delta C_p d\ln T - \int_l^h \Delta C_p dT$$

The following heat and work terms will be involved in the operation of the two cycles:

[52] Dept. of Chemical Engineering, Columbia University, New York 27, N. Y.

Term	Fuel cell cycle	Auxiliary cycle	Total
Q_h	$-T_h(\Delta S_a + \int_l^h \Delta C_p d \ln T)$	$T_h \int_l^h \Delta C_p d \ln T$	$-T_h \Delta S_a$
Q_l	$T_l \Delta S_a$	0	$T_l \Delta S_a$
W	$-\Delta S_a(T_h - T_l) + \int_l^h \Delta C_p dT - T_h \int_l^h \Delta C_p d \ln T$	$T_h \int_l^h \Delta C_p d \ln T - \int_l^h \Delta C_p dT$	$-(T_h - T_l)\Delta S_a$

In addition, the heat $\int_l^h \Delta C_p dT$ is exchanged between the two cycles. Since, for the combination, $W/Q_h = (T_h - T_l)/T_h$, it is obvious that Carnot efficiency has been attained. Different combinations of auxiliary engines or refrigerators might be used. These would alter the heat and work terms for auxiliary and over-all cycles but not the over-all efficiency.

In the cases where the heating and cooling processes are not done reversibly, the work of the fuel cell cycle is still given by deBethune's Eq. [7] rather than by Eq. [10] and [11].

The various processes in question may be represented on temperature-entropy coordinates. Fig. 1 of this discussion shows the properties of the working fluid at each step in the cycle. With heat exchange between steps B and D, the over-all process may be represented by Fig. 2. The enclosed area is equal to the work done by the cycle. Since in the step B + D the cycle accepts heat at temperatures below T_h, there is a loss of efficiency if this heat is supplied at T_h. This loss can be eliminated by transferring the heat via an auxiliary cycle, one possibility being shown in Fig. 3. The combination of the two cycles is then the equivalent of a Carnot cycle operating between T_h and T_l.

Andre J. deBethune: To evaluate the work output of a four-step regenerative fuel cell cycle involving (A) an electrochemical reaction such as M + X = MX at a low temperature T_l, (B) heating of MX to a higher temperature T_h, (C) decomposition of MX at T_h, and (D) cooling of the regenerated M + X to T_l,

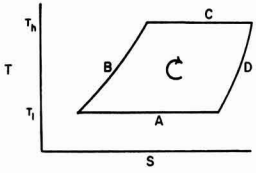

Fig. 1

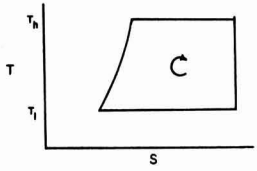

Fig. 2

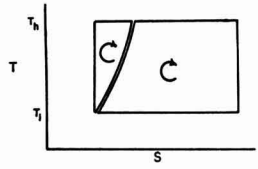

Fig. 3

it is necessary to distinguish two cases, *i.e.*, either (*a*) ΔC_p for the fuel cell reaction A is zero, or (*b*) ΔC_p is not zero.

If ΔC_p is zero, the heating-cooling steps combined are adiabatic, and the fuel cell cycle becomes energetically a simple Carnot cycle whose reversible work output is given by Carnot's theorem in its usual integral form

$$W_u(\text{cycle}) = Q_h(T_h - T_l)/T_h \qquad [1]$$

as shown by Liebhafsky.[53] The *T-S* diagram reduces to a perfect rectangle[54] whose area is equal to Eq. [1].

If ΔC_p is not zero, the fuel cell cycle, even if reversible, is not a simple Carnot cycle, and its *T-S* diagram is not rectangular (*see* Mr. Matsen's Fig. 1 and 2, above). Its useful work output is then not given by Eq. [1]. Reversible operation, in this case, demands the availability of an infinite number of heat reservoirs of infinite heat capacity, whose temperatures differ by dT, such as are always postulated theoretically in the reversible heating and cooling of substances.[55] The reversible work output will now be given by Carnot's theorem in differential form

$$W_u(\text{cycle}) = \int_l^h dQ(T - T_l)/T \qquad [2]$$

By the first law, this is also equal to $\oint dQ$. The integration of [2] yields (*cf.* Eq. [7] of discussed paper)

$$W_u(\text{cycle}) = \oint dQ = -\Delta G_A - \Delta G_C$$
$$= -\Delta S_A(T_h - T_l) + \int_l^h \Delta C_p dT - T_h \int_l^h \Delta C_p d \ln T \qquad [3]$$
$$= \Delta S_C(T_h - T_l) + \int_l^h \Delta C_p dT - T_l \int_l^h \Delta C_p d \ln T \qquad [4]$$

where $G = H - TS$ is the "free enthalpy" (Gibbs free energy) of the cell. The reversible work output is equal to the area of the *T-S* diagram for the cycle. Mr. Matsen's Fig. 1 and 2 illustrate the *T-S* diagram for a fuel cell cycle in which ΔC_p is positive.

If only *two* heat reservoirs are available, the cycle of processes involving the fuel cell and its surroundings cannot be fully reversible unless an auxiliary heat engine is supplied to transfer heat between temperatures reversibly, as suggested by Mr. Matsen. The role of the auxiliary engine is to transform the reversible, but non-Carnot, cycle of the fuel cell into a reversible cycle which is also a Carnot cycle. The extra work output from the auxiliary engine, equal to the *T-S* area of the extra "triangle" in Mr. Matsen's Fig. 3, means also a gain in the reversible efficiency of energy conversion since all the reversible heat is now derived from a single high-temperature source.

Eqs. [3] and [4] (discussed paper, Eq. [7]) give *the theoretical work output* of a *fuel cell cycle alone* that is operated *reversibly throughout*. For irreversible operation, the loss in work output (energy dissi-

[53] H. A. Liebhafsky, *This Journal*, 106, 1068 (1959).
[54] J. Willard Gibbs, "Graphical Methods in the Thermodynamics of Fluids" (1873) in "Collected Works, Vol. I—Thermodynamics," pp. 9-12, Longmans Green & Co., New York (1928).
[55] K. S. Pitzer and L. Brewer, "Lewis and Randall's Thermodynamics," 2nd Ed., Chapter 10, McGraw-Hill Book Co., New York (1961).

pation) will depend on the actual extent of the irreversibility. As a most favorable case, consider a cycle with reversible isothermal steps and reversible heat exchange between steps (B) and (D), in which the only irreversibility lies in the heat fluxes between the fuel cell at an intermediate temperature T and the heat reservoirs at T_h and T_l. The seat of the irreversibility lies now, not in the working substance of the cell, but in the surrounding walls. The cycle of the working substances remains at least "quasi-reversible," and the work output is still virtually given by the reversible expressions [3] and [4] (discussed paper, Eq. [7]), as pointed out above by Mr. Matsen (and contrary to a statement by the writer in the discussed paper). The only energy dissipation in this case is that of extra work output from the auxiliary engine.

Irreversibility within the cycle of the working substances gives rise to energy dissipation that should reduce the work output to below the reversible amount Eqs. [3] and [4]. This can occur by pumping losses in the transfer of the working substances around the cycle, and by polarization losses in the electrochemical operation of the isothermal steps. If, by hypothesis, this energy dissipation can be assumed equal to the T-S area of the "triangular point" on the left hand end of Mr. Matsen's Fig. 2, *i.e.,* if the potential work output of the heat absorbed (or released) in heating (or cooling) is supposed to be dissipated by pumping or polarization, the work output of the cycle would be given by Eqs. [10] or [11] in the discussed paper. However, if the energy dissipation is either less than or greater than supposed above, the work output of the cycle would then be greater than or less than Eqs. [10] and [11] in the discussed paper, but in any case, always less than Eqs. [3] and [4] above.

Dissolution of Copper in Sulfuric Acid Solutions

D. P. Gregory and A. C. Riddiford (pp. 950-956, Vol. 107, No. 12)

N. Ibl[56]: I would like to make a few comments on the part of this interesting paper dealing with the study of disks whose surface is partly blocked off. If a circular patch at the center of the disk is inactive, the average mass transfer rate j (moles cm^{-2} sec^{-1}) at the active parts is larger than if the whole surface is available for the dissolution process. Boundary layer theory leads to the following relationship for j [57]

$$j = j_o \frac{(R^3 - r^3)^{2/3}}{R^2 - r^2} \qquad [1]$$

with $j_o = 0.62\, C_o D^{2/3}\, \nu^{-1/6}\, \omega^{1/2}$

which can be derived in a similar manner as Levich's equation for the full disk (without blocking off). j_o is the mass transfer rate for the full disk according to Levich's equation. R is the radius of the whole disk, and r the radius of the blocked off patch. $\pi(R^2 - r^2)$ is the area of the active part of the disk. It is seen from Eq. [1] of this discussion that j increases with increasing radius r of the blocked off patch.

[56] Dept. of Industrial and Engineering Chemistry, Swiss Federal Institute of Technology, Zurich 6, Switzerland.

[57] Levich, Physico-Chemical Hydrodynamics, Moscow (1959). *See* also A. Frei and N. Ibl, To be published in *Helv. Chim. Acta.*

Let us now consider the mass transfer rate j_w referred to the sum of the active and inactive areas (*i.e.,* the mass transfer rate per unit area of the whole disk). We have

$$j_w = j \frac{\pi(R^2 - r^2)}{\pi R^2} = j_o \left(1 - \frac{r^3}{R^3}\right)^{2/3} = j_o(1 - f^{3/2})^{2/3} \qquad [2]$$

where f is equal to r^2/R^2 and is thus the ratio of the blocked off area to the total area of the disk. In contrast to j, j_w decreases with increasing r (or f). However, a substantial decrease of j_w takes place only at relatively large values of f. For instance, for $f < 0.1$ j_w differs from j_o by less than 2%. In this range, the loss of active area is almost completely compensated by the increase in the mass transport rate j at the active parts of the disk.

It is of interest to compare Eq. [2] of this discussion with the experimental results of Gregory and Riddiford. In their Fig. 11, k_1, which differs from j_w by a constant factor only, is plotted against the percentage of the blocked off area, *i.e.,* against 100 f. At 25° for $f < 0.1$, k_1 is seen to be virtually the same as for the full disk. At $f = 0.1$ it has decreased by *ca.* 1%. This is in reasonable agreement with Eq. [2] of this discussion, which predicts a decrease of 2%. However, at 45°, k_1 remains constant up to $f = 0.15$, whereas, according to Eq. [2], at $f = 0.15$ it should have decreased by 4%. In this case, k_1 is thus larger than the value for mass transfer control. This makes it difficult to explain by a kinetic effect the fact that k_1 breaks down at a larger value of f at the higher, than at the lower, temperature.

On the other hand, at high values of f, k_1 becomes somewhat smaller than predicted by Eq. [2]. According to the authors' Fig. 11, if 49% of the area of the disk is blocked off, k_1 is 1.44 smaller than for the full disk, whereas according to Eq. [2] it should be 1.32 times smaller. As mentioned by the authors, owing to the dissolution process, a step develops at the edge of the blocked patch. It is possible that such factors have caused to some extent deviations from the theoretical behavior. In another connection, A. Frei of our laboratory is now measuring limiting currents at partly blocked off disks with redox systems so that no step is formed at the edge of the patch. It is hoped that these experiments will help to clarify the reasons for the discrepancies observed.

A. C. Riddiford: This is a most interesting suggestion. Dr. Gregory and I had realized that a complete treatment of the effect of blocking off part of the working surface would necessitate consideration of the radial convective and diffusive components of mass transport, and we are glad to see that Dr. Ibl has treated the matter both theoretically and experimentally.

Without wishing to anticipate Dr. Ibl's derivation of his equations, it should be noted that the mass-transport equation takes the form

$$v_y \frac{\partial c}{\partial y} + v_r \frac{\partial c}{\partial r} = D\left(\frac{\partial^2 c}{\partial y^2} + \frac{\partial^2 c}{\partial r^2} + \frac{1}{r}\frac{\partial c}{\partial r}\right) \qquad [3]$$

where v_y, v_r are, respectively, the normal and radial components of the fluid velocity, D is the diffusion coefficient of the species of bulk concentration c, and y, r are, respectively, the normal and radial coordi-

Table I

f (observed)	j_w/j_o (observed)	$(1 - f^{3/2})^{2/3}$	$(1-f^{3/2})^{3/4}$
		25°C	
0.037	0.99	0.995	0.995
0.054	1.00	0.992	0.991
0.096	0.98	0.980	0.978
0.152	0.95	0.960	0.955
0.217	0.92	0.931	0.923
0.289	0.87	0.894	0.881
0.484	0.69	0.761	0.735
		45°C	
0.055	0.99	0.991	0.990
0.153	0.99	0.960	0.955
0.253	0.93	0.913	0.903
0.383	0.85	0.835	0.816

nates. On one approach to the problem, it is convenient to introduce a new variable z, defined as

$$z = \text{const.}\,(ry)^{1/2p} \qquad [4]$$

where the constant and exponent are independent of the coordinates, and $0 < p < 1$. This together with a second variable, x, defined according to the value chosen for p, permits equation [3] to be written

$$\frac{\partial^2 c}{\partial z^2} + \frac{1-2p}{z}\frac{\partial c}{\partial z} = \frac{\partial c}{\partial x} \qquad [5]$$

when, from Sutton's work,[58] the generalized form of Dr. Ibl's second equation becomes

$$j_w = j_o(1 - f^{3/2})^{1-p} \qquad [6]$$

in the same notation.

In their treatment of the similar case of a disk having an active center, separated by inert material from an annular active ring, Ivanov and Levich[59] chose $p = 1/3$ which, with equation [6], gives Dr. Ibl's second equation. The choice of $p = 1/3$ is, however, an approximation. A less drastic approximation can be achieved by setting $p = 1/4$.

A comparison between our experimental data and the alternatives $p = 1/3$ and $p = 1/4$ is given in the following Table I. It will be noted that the experimental values are not sufficiently precise to distinguish with certainty between the two cases, although from the more extensive data at 25°C, $p = 1/4$ would seem to give rather closer agreement. It is to be hoped that the experiments of Frei and Ibl will clarify the situation.

Dr. Ibl rightly points out that it is difficult to accept our kinetic explanation of the different behavior of k_1 at 45°C. A more probable explanation lies in the fact that the approximations made in transforming equation [3] into [5] are temperature-dependent. Again, more precise experimental data would be desirable.

Thermoelectric and Crystallographic Properties of Ag_2Se

J. B. Conn and R. C. Taylor (pp. 977-982, Vol. 107, No. 12)

Charles Wood[60]: It is emphasized in this paper that Ag_2Se is nondegenerate, but a different definition from the one generally accepted is used. A material is degenerate if classical statistics cannot be applied, *i.e.*, if the Fermi-level is less than about 2 kT away from the conduction or valance band edge. From the value of the energy gap published by Busch and Junod,[61] one would expect the material to be degenerate. 0.075 ev is only 3 kT at room temperature. Results presented at "The Symposium on Thermoelectric Energy Conversion", Dallas,[62] suggest that the energy gap in Ag_2Se is even smaller than this (0.05 ev), with even a greater probability of degeneracy at room temperature.

In quoting a value for the carrier concentration (n) at room temperature in Table I of this paper, it is assumed that conduction by electrons is predominant and that the contribution of holes can be neglected. If this assumption is correct, and some experimental evidence has been obtained in support of this viewpoint,[62] then the position of the Fermi-level (η^*) can be obtained simply from the general expression for Seebeck coefficient[63]:

$$\alpha = \pm\frac{k}{e}\left[\frac{r+2}{r+1}\frac{F_{r+1}(\eta^*)}{F_r(\eta^*)} - \eta^*\right]$$

Inserting the value of the Seebeck coefficient from Table I, it is found that, for the most common forms of charge carrier scattering, *i.e.*, atomic lattice ($r = 0$), impurity ion ($r = 2$), or ionic lattice ($r = 1$), the Fermi-level lies above the bottom of the conduction band, and therefore the material is degenerate. This is in agreement with the results on Ag_2Se in footnote 62, where the mobility *vs.* temperature curve showed an approximate relationship of $\mu \propto T^{-1/2}$, corresponding to ionic lattice scattering, *i.e.*, $r = 1$, giving a value of $n^* = +3$ kT above the conduction band edge. Thus, Ag_2Se appears to be highly degenerate.

Lastly, the scatter of the points in Fig. 2 of the paper is such that a straight line could be drawn parallel to the curve for metals or degenerate semiconductors (Line 2) with a deviation from a straight line taking place in the low electrical conductivity region, possibly due to an ambipolar contribution.

The Structure of Cryolite-Alumina Melts

P. A. Foster, Jr., and W. B. Frank (pp. 997-1001, Vol. 107, No. 12)

E. W. Dewing[64]: The conclusion that solutions of alumina in molten cryolite contain predominantly AlO_2^- ions is in conflict with the facts[65,66] that alumina is insoluble in pure sodium fluoride and that the solubility passes through a maximum as aluminum fluoride is added.

If one considers anions containing O:Al ratios of 1:1, 2:1 and 3:1, these must be formed by the reactions

$$Al_2O_3 + 3(x-1)\,NaF + AlF_3 = 3Na_{(x-1)}\,AlOF_x \qquad [1]$$

[58] W. G. L. Sutton, *Proc. Roy. Soc.*, **A182**, 48 (1943).
[59] Yu. Ivanov and V. Levich, *Doklady Akad. Nauk S.S.S.R.*, **126**, 1029 (1959).
[60] Kearfott Div., General Precision, Inc., 1500 Main Ave., Clifton, N. J.
[61] G. Busch and P. Junod, *Helv. Phys. Acta*, **30**, No. 6, 420 (1957).
[62] P. F. Taylor and C. Wood, Symposium on Thermoelectric Energy Conversion, Dallas, Texas, January 1961.
[63] A. F. Ioffe, "Semiconductor Thermoelements and Thermoelectric Cooling" (Infosearch, 1957).
[64] Electrometallurgical Div., Aluminium Laboratories Ltd., Arvida, Que., Canada.
[65] P. P. Fedotiev and V. Ilyinskii, *Z. anorg. Chem.*, **80**, 113 (1913).
[66] N. W. F. Phillips, R. H. Singleton, and E. A. Hollingshead, *This Journal*, **102**, 690 (1955).

$$2Al_2O_3 + 3(1 + y)\ NaF = 3Na_{(1+y)}\ AlO_2F_y + AlF_3 \quad [2]$$

$$Al_2O_3 + 3NaF = Na_3AlO_3 + AlF_3 \quad [3]$$

Probable values for x are 2 or 4, and for y are 0 or 2. From the respective equilibrium constants, and with $a_{Al_2O_3} = 1$ throughout,

$$a_{Na_{(x-1)}AlOF_x} = K_1(a_{AlF_3})^{1/3}\ (a_{NaF})^{x-1} \quad [1a]$$

$$a_{Na_{(1-y)}AlO_2F_y} = K_2\ (a_{NaF})^{1+y}/(a_{AlF_3})^{1/3} \quad [2a]$$

$$a_{Na_3AlO_3} = K_3(a_{NaF})^3/(a_{AlF_3}) \quad [3a]$$

It is obvious that only the first of these expressions becomes zero when $a_{AlF_3} = 0$, the other two becoming infinite. Thus, if AlO_2^- were in fact the important species, one would expect a large solubility of alumina in NaF. (Liquid NaF actually converts Al_2O_3 to solid $NaAlO_2$, but this, in turn, is insoluble.[67])

From the Gibbs-Duhem relationship for the binary NaF-AlF_3 system (*i.e.*, without added alumina), it follows that the product $(a_{AlF_3})^{1/3}\ (a_{NaF})^{x-1}$ which appears in Eq. [1a] is a maximum for a molar ratio NaF:AlF_3 of $3(x-1):1$. One would expect the solubility of alumina to be a maximum in the vicinity of this composition, exact correspondence being improbable owing to varying activity coefficients. The measurements of Phillips, Singleton, and Hollingshead[66] show a maximum solubility (expressed in wt %) at a molar NaF:AlF_3 ratio around 4.7:1. This is in the range expected if the average value of x lies between 2 and 4. Any attempt to interpret further the position of the maximum would be extremely hazardous.

Polymeric ions with Al:O atom ratios of 1:1 meet the above conditions equally well.

Although Foster and Frank state that "Transport number determinations[68] in cryolite-alumina melts . . . suggest the existence of the aluminate ion," reference to the original work shows this not to be the case. There we find the statement, "The cathode to anode migration of fluorine and aluminum in the equivalent ratio of essentially 2 to 3, or atom ratio of 2 to 1, is evidence for the presence of $NaAlOF_2$ in the molten electrolyte." It goes on to say that although $AlO_2F_2^{---}$ is not ruled out, the quantitative data fit $AlOF_2^-$ better. This would be fully in line with the considerations above.

Perry A. Foster, Jr. and William B. Frank: The conclusion that solutions of alumina in fused cryolite contain AlO_2^- ions does not conflict with the fact that (*a*) insoluble aluminate is formed in the reaction of alumina with molten sodium fluoride and (*b*) a maximum "alumina solubility" is attained in a sodium fluoride enriched cryolite base melt. On the contrary, these facts, when combined with other experimental observations, tend to confirm the mechanism proposed for the dissolution of alumina in molten cryolite.

Recent work in the sodium fluoride-alumina system[69] is in accord with the findings of Fenerty[70] and others[71,72] that an insoluble aluminate phase is produced when these mixtures are fused. Bonnier[72] and Seyyedi and Petit[73] have indicated that sodium aluminate is insoluble in molten sodium fluoride. However it is also true and quite important that sodium aluminate is very soluble in cryolite.[72]

The x-ray diffraction pattern of the residue obtained by leaching with water, a sodium fluoride-alumina sample quenched from above the melting point of sodium fluoride, proved to be entirely cryolite. Since the excess sodium fluoride and the sodium aluminate are both soluble in water and there was no evidence of alumina in the residue, the following reaction must proceed quantitatively

$$6NaF + 2Al_2O_3 = 3NaAlO_2 + Na_3AlF_6 \quad [1]$$

Samples that were quenched in the composition range of 0-5.4% alumina revealed that the melt became doubly saturated with respect to sodium fluoride and sodium aluminate. The freezing point of sodium fluoride was slightly depressed in this composition interval. At higher weighed-in alumina content, the melt became doubly saturated with respect to beta-alumina and sodium aluminate. Hence, some solubility of the sodium aluminate produced must occur in the resulting liquid phase. The observed shallow freezing point depression of sodium fluoride and the limited "alumina solubility" are related to the cryolite formed by reaction [1].

It is the generally held view that molten salts are ionic in nature. Therefore, the high solubility of sodium aluminate in molten cryolite, the small solubility of sodium aluminate in NaF-Al_2O_3 melts, and the insolubility of sodium aluminate in molten sodium fluoride suggest that the AlO_2^- solubility is related to the activity of AlF_6^{3-} in the melt. The reaction proposed for the solution of alumina in cryolite (Scheme VI), it seems, takes place between alumina and melts of the NaF-AlF_3 system from pure sodium fluoride to aluminum fluoride-rich cryolite base melts. The solubility of the aluminate in the resulting liquid phase varies from low values in pure sodium fluoride to a maximum near the cryolite composition, decreasing in aluminum fluoride-rich fusions. The alumina or aluminate phase precipitating from the melt is also dependent upon the composition of the solvent.[74]

Calculations show that the initial addition of sodium fluoride to cryolite-alumina melts leads to an increase in AlF_6^{3-} activity. Further addition of sodium fluoride decreases the AlF_6^{3-} activity. Hence, the experimentally determined maximum in "alumina solubility" as the cryolite-alumina melts are enriched with sodium fluoride is not unexpected. The addition of aluminum fluoride to molten cryolite or cryolite-alumina fusions decreases the AlF_6^{3-} activity, and lower solubilities are predicted.

Transport experiments did not exclude the possibility of the anion AlO_2^- in cryolite-alumina melts. Equilibria involving $NaAlO_2$ are discussed in the original publication.[75] In light of present knowledge of the extent of dissociation of molten cryolite and

[67] A. Fenerty, Unpublished work in this laboratory.
[68] W. B. Frank and L. M. Foster, *J. Phys. Chem.*, 61, 1531 (1957).
[69] P. A. Foster, Jr., To be published.
[70] A. Fenerty, Unpublished work, Aluminium Laboratories, Ltd., Arvida, Que., Canada.
[71] P. P. Fedotieff and W. Iljinsky, *Z. anorg. Chem.*, 80, 113-154 (1913).
[72] E. Bonnier, *Ann. Phys.*, 8, (12), 258-312 (1953).
[73] A. Seyyedi and G. Petit, *J. phys. radium*, 20, 832-833 (1959).
[74] P. A. Foster, W. B. Frank, and L. M. Foster, "The Mechanism of Alumina Solution in the Aluminum Producing Electrolyte," XVIIIth International Congress of Pure and Applied Chemistry, Montreal, August, 1961.
[75] W. B. Frank and L. M. Foster, *J. Phys. Chem.*, 61, 1531 (1957).

consideration of the mobility of postulated aluminate and oxyfluoroaluminates, all the anionic transference observed for fluorine should be attributed to free fluoride ions. The small anionic migration observed for aluminum must therefore be assigned to an anion containing no fluorine.

On the Role of the Oxygen Concentration Cell in Crevice Corrosion and Pitting

G. J. Schafer, J. R. Gabriel, and P. K. Foster
(pp. 1002-1004, Vol. 107, No. 12)

U. R. Evans[76]: The suggestion early in the paper that Hoar's acid theory and Evans' Differential Aeration Theory are rival explanations may convey the idea of a controversy which does not exist.

The accumulation of acid at anodic points has been emphasized in my work with Edeleanu,[77] who measured the fall of *p*H with passage of anodic current, and that with Farmery[78] on the stress corrosion of alloys. Edeleanu's views in particular have always been in close accord with those of Hoar, which had been carried out in the same laboratory as Edeleanu's earlier work. Edeleanu's latest work[79] on pitting mechanism, which introduces crystallographic factors, deserves study.

However, acid production cannot be essential for pitting, since rows of pits have been produced on zinc placed in pure water along the two crevices set up by stretching a nylon thread over the surface—as shown by Eurof Davies.[80] Probably the mechanism is that any invisible oxide film keeps breaking down spontaneously; at places where oxygen is replenished, it is at once repaired, but, at places where replenishment is slow, discontinuities will remain, so that these places will be anodic in relation to the rest.

Probably the spontaneous cracking is due to the fact that any metal which has been deformed, superficially worked, or abraded carries tensional and compressional forces in equilibrium; if the surface layer is oxidized, the equilibrium is upset, so that, in certain geometrical situations, the film is ruptured. Work with Faerden on the anodic behavior of nickel[81] showed that the location of the pitting (which often led to perforation) was what would be expected on this view. However, in other cases, different factors may determine the sites of the pits.

G. J. Schafer, J. R. Gabriel, and P. K. Foster: We thank Dr. Evans for his comments and the interest he has shown in our work.

We had no intention of implying that the differential aeration and acid mechanisms were rival explanations for localized corrosion. Our main argument is that when steady-state conditions exist it is impossible to have one mechanism without the other, although either mechanism may predominate in a particular case.

We feel that in the early literature it was not sufficiently emphasized that localized corrosion has both an initiation and (usually) a steady-state phase. Crevice corrosion is so obviously initiated by oxygen or inhibitor shortage due to geometry, whereas pitting may be initiated by a large variety of agencies. Here, crevice corrosion differs from pitting. Once steady state is attained, however, we contend that pitting and crevice corrosion are two names for the same phenomenon, which arose because it was not recognized that the steady-state mechanisms differed in degree rather than in principle.

With regard to the pitting on zinc in pure water observed by Evans and Davies, we agree that anodic acid production would not be expected under these conditions, but we do not see that the case cited in any way vitiates our theory. We hold that *steady-state* localized corrosion cannot be sustained without the conjoint action of the differential aeration and acid mechanisms. The non-steady-state behavior observed (viz., initiation of pitting followed by a decay in corrosion rate to zero) would therefore be expected from our theory. We agree that pitting of zinc in pure water is *initiated* by differential aeration, but subsequently the attack falls off because no acid accumulates at anodes and the differential aeration cannot be maintained, as shown in our mathematical proof.

We did perhaps commit the sin of omission by not stating more explicitly in the original paper that our arguments applied to steady-state localized corrosion only.

We are not concerned with the different theories propounded about factors determining the sites of pitting corrosion. Our concern is entirely with established pits or crevices which continue to corrode.

We feel that Dr. Evans' remarks have shown the need for some discussion of the term "steady-state" and this is at present under consideration.

[76] University Dept. of Metallurgy, Pembroke St., Cambridge, England.
[77] C. Edeleanu and U. R. Evans, *Trans. Faraday Soc.*, 47, 1121 (1951).
[78] H. K. Farmery and U. R. Evans, *J. Inst. Met.*, 84, 413 (esp. p. 422), (1955-56).
[79] C. Edeleanu, *J. Inst. Met.*, 89, 90 (1960-61).
[80] U. R. Evans, and D. Eurof Davies, *J. Chem. Soc.*, 1951, 2607.
[81] A. Faerden and U. R. Evans, Summary of work given in U. R. Evans' "Corrosion and Oxidation of Metals," pp. 110-113, Edward Arnold & Co., London (1960).

FUTURE MEETINGS OF
The Electrochemical Society

Detroit, Mich., October 1, 2, 3, 4, and 5, 1961
Headquarters at the Statler Hotel
Sessions probably will be scheduled on Batteries, Corrosion (including a Symposium on Surface Structure vs. Corrosion Behavior), Electrodeposition (including symposia on Addition Agents and on Electrodeposited Magnetic Films), Electronics (Semiconductors), Electro-Organics, and Electrothermics and Metallurgy

★ ★ ★

Los Angeles, Calif., May 6, 7, 8, 9, and 10, 1962
Headquarters at the Statler Hilton Hotel
Sessions probably will be scheduled on Electric Insulation, Electronics (including Luminescence and Semiconductors), Electrothermics and Metallurgy, Industrial Electrolytics, and Theoretical Electrochemistry

★ ★ ★

Boston, Mass., September 16, 17, 18, 19, and 20, 1962
Headquarters at the Statler Hilton Hotel

★ ★ ★

Pittsburgh, Pa., April 14, 15, 16, 17, and 18, 1963
Headquarters at the Penn Sheraton Hotel

★ ★ ★

New York, N. Y., September 29, 30, and October 1, 2, and 3, 1963
Headquarters at the New Yorker Hotel

★ ★ ★

Toronto, Ont., Canada, May 3, 4, 5, 6, and 7, 1964
Headquarters at the Royal York Hotel

Papers are now being solicited for the meeting to be held in Los Angeles, Calif., May 6-10, 1962. Triplicate copies of each abstract (*not exceeding 75 words in length*) are due at Society Headquarters, 1860 Broadway, New York 23, N. Y., *not later than December 15, 1961* in order to be included in the program. *Please indicate on abstract for which Division's symposium the paper is to be scheduled, and underline the name of the author who will present the paper.* No paper will be placed on the program unless one of the authors, or a qualified person designated by the authors, has agreed to present it in person. An author who wishes his paper considered for publication in the JOURNAL should send triplicate copies of the manuscript to the Managing Editor of the JOURNAL, 1860 Broadway, New York 23, N.Y.

Presentation of a paper at a technical meeting of the Society does not guarantee publication in the JOURNAL. However, all papers so presented become the property of The Electrochemical Society, and may not be published elsewhere, either in whole or in part, unless permission for release is requested of and granted by the Editor. Papers already published elsewhere, or submitted for publication elsewhere, are not acceptable for oral presentation except on invitation by a Divisional program Chairman.

Current Affairs

ECS Section News

Indianapolis Section

The Indianapolis Section held its third technical meeting of the current season on Friday, March 10, at Butler University in Indianapolis. The Section was honored to have Ralph Schaefer, Society President, as the speaker for the evening.

Dr. Schaefer first reported on the current status of the Society and its varying activities. He illustrated the relationship between costs of publishing the JOURNAL and the recent increase in membership dues, and indicated that advertising income is diminishing steadily. Following this, Dr. Schaefer discussed "General Characteristics of Electrodeposits." After indicating the general area which electrodeposition occupies in the broad electrochemical field, he delineated some of the characteristics and parameters of the process and of electrodeposits—with emphasis on some of the key items which influence their uniformity and structure. This presentation was concluded with a discussion session.

The fourth technical meeting of the Indianapolis Section, a joint affair with the Indiana Section of the American Chemical Society, was held on Thursday, March 16, at Butler University. Charles H. Huggins from the General Electric Research Laboratory, Schenectady, N. Y., spoke on "The Chemistry, Physics, and Biophysics of Organic Semiconductors."

Dr. Huggins' talk was concerned with both theoretical and experimental intercomparisons of the three classes of organic molecular solids which currently are considered the most interesting with respect to electrical properties. These materials then were compared with the valence crystal semiconductors, such as silicon and germanium, to show similarities and differences.

T. C. O'Nan, *Sec.-Treas.*

News from India

Electrochemistry Seminar. — The Second Seminar on Electrochemistry was held at the C.E.C.R.I., Karaikudi, from December 17 to 20, 1960. Eighty-three papers were presented in eight sessions: electrode kinetics and electrochemical equilibria, electroanalysis, electro-organic products, electro-inorganic products, electrothermics and electrometallurgy, metal finishing and electrodeposition, corrosion, miscellaneous. Scientists from Australia, Austria, France, Japan, Poland, the United Kingdom, and the United States of America participated in the Seminar. Abstracts of the papers have been published as a booklet by the C.E.C.R.I.

Exhibition of Scientific and Technical Publications.—During December 1960 at New Delhi, the National Institute of Sciences of India arranged an exhibition of scientific and technical publications published in India in English and in regional languages since 1935. This was part of the Silver Jubilee Celebrations of the Institute. The India Section of The Electrochemical Society participated in the Exhibition by displaying copies of the *Bulletin*, as well as the Special Symposium Numbers.

Indian Science Congress. — The 48th session of the Indian Science Congress was held at Roorkee, U.P., from January 3 to 9, 1961. The program covered sectional meetings, symposia, popular and special lectures, visits to institutions and other places of interest, and social functions. An exhibition of scientific and laboratory equipment was arranged. Delegates from many foreign countries participated in the deliberations. Several papers on electrochemistry and allied branches were presented. The following were among the topics for the symposia: cooperation between the instrument industry and the scientists; role of impurities in metals and inorganic compounds; ferroalloys; science, technology, and social changes in India; standardization of engineering education in India.

Symposium on Redox Processes.—A Symposium on Redox Processes was held in the Dept. of Chemistry, University of Allahabad, Allahabad, on February 1 and 2, 1961, under the auspices of the Chemical Research Committee, Council of Scientific and Industrial Research, India. There were 52 papers under the following sections: electrode processes, reactions in solution, and analytical applications. Scientists from the U.S.S.R. and the U.S.A. contributed four papers. The program included special lectures and social functions. The organizers have plans to publish the proceedings. T. L. Rama Char (India Section) and I. I. Vasu, Bangalore, presented a paper on "Electrolytic Reduction of Aqueous Tungstate Solutions."

Training Course in Storage Battery Technology.—The Second Course of training in Storage Battery Technology was held by the C.E.C.R.I., Karaikudi, for seven weeks, commencing from February 1, 1961. The main intention was to provide training to technical personnel representing battery manufacturers, large consumers of batteries, and organizations engaged in the testing of batteries according to ISI specification.

Symposium on Light Metal Industry in India.—The National Metallurgical Laboratory held a Symposium on "Light Metal Industry in India" at Jamshedpur from February 14 to 17, 1961. Twenty-seven papers were presented covering various aspects of light metals: beryllium, titanium, aluminum, magnesium, light alloys; production, physical metallurgy, application in nuclear engineering, corrosion resistance. There were contributions from France, Japan, Switzerland, United Kingdom, U.S.A., and West Germany. The program included lectures, visits, film shows, and social gatherings. Abstracts of the papers have been published in the *NML Technical Journal* (Vol. 3, No. 1, 1961). The NML is publishing the proceedings of the Symposium. K. G. Sheth, J. Sundararajan, and T. L. Rama Char (India Section) presented a paper on "Corrosion of Aircraft Aluminum Alloys in Acid Solutions and Its Prevention by Inhibitors."

Conference on Defense Problems in Electrochemistry.—A Conference on "Defense Problems in Electrochemistry" was held by the Electronics Research and Development Establishment (LRDE) at Bangalore on March 13, 1961. The object of the

Conference was to discuss some of the pressing defense problems pertaining to electrochemistry. The following topics were covered: (*a*) Increasing the output of dry cells by the use of better-grade manganese dioxide, (*b*) Optimization of constructional technique for achieving maximum size and weight reduction in defense batteries, (*c*) Scope for adoption of mercuric-oxide-type primary batteries for reducing size and weight, (*d*) Problems connected with the development of a field-type, light-weight secondary battery for defense application, (*e*) Scope for application of alkaline-type secondary batteries like the silver-zinc for maximum size and weight reduction, (*f*) Tantalum capacitors. (*g*) Plating through holes in printed circuitry, and (*h*) Photoconductive cells. There were representatives from the Defense Services, LRDE, ILE, ADE, CSIR, IISc, government departments, industries, and scientific societies (India Section). The following members of the India Section, ECS, participated in the Conference: K. S. G. Doss, H. V. K. Udupa, and V. Aravamuthan (C.E.C.R.I.); T. L. Rama Char (IISc and India Section), S. Ramaswamy (Mettur Chemical and Industrial Corp.); R. L. N. Sastry, R. C. Misra, and R. Raman (LRDE). The participants also included Patrons of the India Section. The delegates were entertained at lunch by Amco Batteries Ltd., Bangalore.

T. L. Rama Char,
India Correspondent

New York Metropolitan Section

The March 1 meeting of the Metropolitan Section was held at the Robert Treat Hotel, Newark, N. J. The guest speaker was Adolph Blicher of the Radio Corp. of America, Semiconductor and Materials Division. The topic for the evening was "Tunnel Diodes."

Dr. Blicher pointed out that the tunnel diode is the newest addition to the family of solid-state devices. Its importance, however, is not limited to the fact that it gives a circuit designer unusual new possibilities, but, also, that it blazes a new trail in the understanding of semiconductor materials and dramatizes, together with the solid-state maser, the onset of a new era—that of Quantum Electronics.

Dr. Blicher presented the tunnel diode as a quantum-mechanical device which had many important advantages as a circuit element for switching, amplifier, and oscillator applications. He also discussed methods of fabricating tunnel diodes, as well as some of the current research at RCA on these new high-speed devices.

Richard Glicksman

Ontario-Quebec Section

The third meeting of the Ontario-Quebec Section was held in Montreal on April 14. The following two papers were presented: "Special Refractories — New Developments, Properties, and Uses" by Charles R. Landback, Carborundum Co., Refractories Division, Perth Amboy, N. J., and "Platinized Titanium Electrodes" by Harold B. Berman, Engelhard Industries Inc., Chemicals Division, Newark, N. J. Ralph S. Miller, Quebec Iron and Titanium Corp., Sorel, Que., acted as Technical Chairman.

The following were elected officers of the Section for the 1961-1962 season:

Chairman—R. A. Ritchie, Electric Reduction Co. of Canada, Ltd., Toronto, Ont., Canada

Vice-Chairman (Programs)—R. A. Campbell, Dept. of Mines & Technical Surveys, Ottawa, Ont., Canada

Vice-Chairman (Membership)—Andre Hone, Ecole Polytechnique, Montreal, Que., Canada

Secretary-Treasurer — Tom Pezzack, Union Carbide Canada Ltd., Toronto, Ont., Canada

Committeemen—G. M. Mason, Aluminum Co. of Canada Ltd., Montreal; P. G. Walker, Union Carbide Canada Ltd., Montreal; H. U. Ross, University of Toronto, Toronto; W. C. Cooper, Canadian Copper Refiners, Montreal; E. A. Planche, Canadian Industries Ltd., Montreal

Local Section Councilors—Tom Pezzack and L. G. Henry

L. G. Henry, *Chairman*

Washington-Baltimore Section

The March 16 meeting of the Washington-Baltimore Section was held at the National Bureau of Standards in Washington, D. C.

Clarence M. Shepherd of the U.S. Naval Research Laboratory discussed the problems associated with "Battery Design."

If there is adequate basis for describing battery performance in terms of design parameters, it is in principle possible to optimize the design for a specific end-use in terms of any of a number of properties such as weight, volume, or cost. Mr. Shepherd demonstrated the principle with a computation of the optimum design of a silver-oxide zinc-alkaline cell for minimum weight.

S. Schuldiner, *Secretary*

Manuscripts and Abstracts for Spring 1962 Meeting

Papers are now being solicited for the Spring Meeting of the Society, to be held at the Statler Hilton Hotel in Los Angeles, Calif., May 6, 7, 8, 9, and 10, 1962. Technical Sessions probably will be scheduled on Electric Insulation, Electronics (including Luminescence and Semiconductors), Electrothermics and Metallurgy, Industrial Electrolytics, and Theoretical Electrochemistry.

To be considered for this meeting, triplicate copies of abstracts (*not exceeding 75 words in length*) must be received at Society Headquarters, 1860 Broadway, New York 23, N. Y., *not later than December 15, 1961. Please indicate on abstract for which Division's symposium the paper is to be scheduled and underline the name of the author who will present the paper.* No paper will be placed on the program unless one of the authors, or a qualified person designated by the authors, has agreed to present it in person. An author who wishes his paper considered for publication in the JOURNAL should send triplicate copies of the manuscript to the Managing Editor of the JOURNAL, 1860 Broadway, New York 23, N. Y.

Presentation of a paper at a technical meeting of the Society does not guarantee publication in the JOURNAL. However, all papers so presented become the property of The Electrochemical Society, and may not be published elsewhere, either in whole or in part, unless permission for release is requested of and granted by the Editor. Papers already published elsewhere, or submitted for publication elsewhere, are not acceptable for oral presentation except on invitation by a Divisional program Chairman.

ECS Membership Statistics

The following three tables give breakdown of membership as of Apr. 1, 1961. The Secretary's Office feels that a regular accounting of membership will be very stimulating to membership committee activities. In Table I it should be noted that the totals appearing in the right-hand column are *not* the sums of the figures in that line since members belong to more than one Division and, also, because Sustaining Members are not assigned to Divisions. But the totals listed are the total membership in each Section. In Table I, Sustaining Members have been credited to the various Sections.

Table I. *ECS Membership by Sections and Divisions*

Section	Division: Battery	Corrosion	Electric Insulation	Electro-deposition	Electronics	Electro-Organic	Electrothermics & Met.	Industrial Electrolytic	Theoretical Electrochem.	No Division	Total as of 1/1/61	Total as of 4/1/61	Net Change
Boston	18	36	12	35	83	5	23	10	27	5	177	174	— 3
Chicago	23	34	10	37	31	17	17	13	36	7	148	146	— 2
Cleveland	53	28	1	45	42	8	30	28	36	6	192	184	— 8
Columbus, Ohio	5	14	2	17	14	2	31	5	11	2	60	64	+ 4
Detroit	25	21	4	51	18	8	11	9	39	6	104	108	+ 4
India	10	9	2	21	7	6	5	8	15	3	42	39	— 3
Indianapolis	32	11	12	12	25	7	14	6	15	2	69	70	+ 1
Midland	10	16	1	5	4	3	9	16	10	—	43	45	+ 2
Mohawk-Hudson	12	27	19	9	20	2	13	3	23	5	76	79	+ 3
New York	111	114	31	176	186	40	102	76	129	35	618	621	+ 3
Niagara Falls	13	19	2	23	28	5	66	57	11	10	168	163	— 5
Ontario-Quebec	5	19	2	12	7	1	37	25	12	4	92	85	— 7
Pacific Northwest	5	8	1	8	1	—	7	9	12	3	38	34	— 4
Philadelphia	38	21	7	41	78	7	28	23	45	16	210	209	— 1
Pittsburgh	5	45	5	29	40	6	33	20	36	1	133	131	— 2
San Francisco	15	14	1	28	33	3	16	19	22	2	98	94	— 4
S. Calif.-Nevada	24	23	4	42	72	5	30	22	43	3	150	154	+ 4
Texas	5	24	2	14	43	3	9	26	30	1	103	104	+ 1
Washington-Baltimore	37	35	8	35	25	4	14	6	24	2	144	138	— 6
U. S. Non-Section	57	67	11	73	70	31	62	48	78	24	349	333	—16
Foreign Non-Section	66	66	16	70	40	33	48	65	85	85	302	312	+10
Total as of Jan. 1, 1961	558	660	153	790	855	197	633	506	743	220	3316		
Total as of Apr. 1, 1961	569	651	153	783	867	196	605	494	739	222		3287	—29
Net Change	+11	—9	0	—7	+12	—1	—28	—12	—4	+2			

Table II. *ECS Membership by Grade*

	Total as of 1/1/61	Total as of 4/1/61	Net Change
Active	2895	2576	—319
Faraday (Active)	33	37	+ 4
Deutsche Bunsen Gesellschaft (Active)	17	20	+ 3
Delinquent	84	354	+270
Active Representative Patron Members	10	10	0
Active Representative Sustaining Members	107	99	— 8
Total Active Members	3132	3096	— 36
Life	16	16	0
Emeritus	65	78	+ 13
Associate	39	49	+ 10
Student	43	41	— 2
Honorary	7	7	0
Total	3316	3287	— 29

The figures pertaining to Patron and Sustaining Member Representatives, and Faraday and Deutsche Bunsen Gesellschaft members subscribing to the JOURNAL, have been added to reflect reclassifications and changes in membership status.

Table III. *ECS Patron and Sustaining Membership*

	Total as of 1/1/61	Total as of 4/1/61	Net Change
Patron Member Companies	5	5	0
Sustaining Member Companies	157	145	— 12

Personals

S. Ghosh of Karaikudi, India, has left for France for specialized training in applied science at the Faculté des Sciences, Strasbourg.

Herman S. Preiser, formerly with the Bureau of Ships, U.S. Navy Dept., has been elected president and technical director of Chemionics Engineering Labs., 1 Bala Ave., Bala-Cynwyd, Pa. The company will be engaged in the manufacture of cathodic protection and other electrochemical equipment and will provide general consulting services in the corrosion control and industrial electrochemical field.

T. L. Rama Char, Bangalore, India, has been elected vice-chairman of the Deccan Section of the Royal Institute of Chemistry, London.

John W. Rhyne, Jr., has been appointed chief electrochemist of Telecomputing Corp's Power Sources Division, Denver, Colo. In his new position, Mr. Rhyne is responsible for all electrochemical design of Power Sources projects in advanced silver-oxide-zinc and silver-oxide-cadmium batteries. He also directs all electrochemical research and development. Prior to joining the Telecomputing division, Mr. Rhyne was senior research electrochemist for the Delco-Remy Division of General Motors.

Zachary D. Sheldon has joined the Carborundum Co., Niagara Falls, N. Y., as associate director of the Research and Development Division. He will assist in supervising Carborundum's expanding research and development programs. Formerly, he was manager, Advanced Materials Development, General Engineering Lab., General Electric Co., Schenectady, N. Y.

S. Soundararajan has been appointed Lecturer in the Dept. of Inorganic and Physical Chemistry, Indian Institute of Science, Bangalore, India.

Joseph H. Brennan

Joseph H. Brennan, chief metallurgist for Union Carbide Metals Co., Niagara Falls, N. Y., died on April 19, 1961 after a lengthy illness. He was 58 years old.

He was born in Minneapolis, Minn., in 1902, and received his early education there. He attended the University of Minnesota.

Mr. Brennan began his association

with Union Carbide Corp. in 1920 as a chemist, and was connected with the ferroalloy industry during his entire career. He held many patents, both in the United States and abroad, on the purification and production of metals and alloys. One of his major contributions in his field was the development of a process for the production of ferrochrome of very low carbon content. He was the co-inventor of a process for treating low-grade tungsten ores, which was used for the larger part of America's production during World War II. He collaborated on the design, construction, and operation of the cobalt refinery which supplied most of the U.S. cobalt requirements during the war years.

Mr. Brennan served as a consultant to the National Research Council on the design of processes for complex rare metal ores and was associated in a consulting capacity with the Manhattan Project and the Atomic Energy Commission.

A long-time member of The Electrochemical Society, he held various offices in the Niagara Falls Local Section. In addition, he was a Fellow of the Institute of Chemistry, and a member of the American Society for Metals, American Association for the Advancement of Science, Prospectors and Developers Association (Ontario), and the Society of the Chemical Industry (Britain). In 1950, he was the recipient of the Schoellkopf Medal, awarded annually by the Western New York Section of the American Chemical Society, and, in 1958, received the Frank J. Tone Medal.

Mr. Brennan is survived by his wife, Anne, three sons, and a brother.

Book Reviews

The Surface Treatment and Finishing of Aluminium and Its Alloys, 2nd, Ed., by S. Wernick and R. Pinner. Published by Robert Draper Ltd., 85 Udney Park, Teddington, Middlesex, England, 1959. 607 pages; $13.00.

This British book is quite up to date in its descriptions of mechanical, chemical, and electrochemical processes for the finishing of aluminum and its alloys. The subject matter is well organized and interestingly presented. The illustrative material greatly increases the interest and value of the work. This includes many excellent photographs of industrial operations and equipment, informative graphs relating process variables to practical results, and electron micrographs of electrolytic aluminum-oxide coatings.

Subjects covered include mechanical surface treatments, chemical and electrolytic polishing, chemical oxide coatings, decorative and protective anodizing, hard anodizing, electrodeposition on aluminum, organic finishing, vitreous enameling, and metal spraying. Coverage of these topics is complete and accurate. Very little attention is given to the production of aluminum-oxide films for electrolytic capacitors.

In the chapter on Physical and Chemical Properties of Anodic Oxide Coatings, both nondestructive and destructive methods are described for the evaluation of the oxide films. The descriptions and illustrations of these tests are quite detailed.

This book would be a useful addition to the library of anyone working in the expanding field of light metals.

Henry S. Myers

Physical Chemistry, 2nd Ed., by Farrington Daniels and Robert A. Alberty. Published by John Wiley & Sons, Inc., 440 Park Ave. South, New York, N. Y., 1961. 744 pages; $8.75.

This second edition of Daniels and Alberty is an excellent readable outline of elementary physical chemistry at the college level. It is easy to teach from and to learn from.

Some new material has been added, chiefly on the kinetic theory of gases, atomic and molecular orbitals, spectroscopy, and statistical mechanics. However, the major revisions consist of rearrangement of topics and rewriting of some loosely knit portions. For example, the new chapter on statistical mechanics consists of material taken from the old chapter on quantum theory and then expanded. Instead of a separate chapter on electrolytic conductance, there is now a chapter entitled "Irreversible Processes in Liquids," covering viscosity, diffusion, and electrolytic conductance as being related phenomena.

There are some new problems and illustrations, especially for the newer material, but many of the old problems still remain from as far back as the Getman and Daniels "Outlines of Physical Chemistry" which was the successor in this series to the 1913 Getman "Outlines of Theoretical Chemistry." The approach is phenomenological rather than mathematical. The device of putting derivations, such as that of the Debye-Hückel equation and the Maxwell-Boltzman equation, into an appendix is to be commended. There could, however, be more description of experimental methods.

The text makes no pretense of being comprehensive and rigorous. It definitely is not a source book, a reference book, or a graduate text. It is, however, a very, very good textbook for students wishing to obtain a general understanding of basic physical chemistry.

H. W. Salzberg

Notice to Members and Subscribers

(Re Changes of Address)

To insure receipt of each issue of the JOURNAL, please be sure to give us your old address, as well as your new one, when you move. Our records are filed by states and cities, not by individual names. The Post Office does not forward magazines.

We should have this information *by the 16th of the month* to avoid delays in receipt of the next issue.

News Items

New ECS Sustaining Member

North American Aviation, Inc., Rocketdyne Division, Canoga Park, Calif., recently became a Sustaining Member of The Electrochemical Society.

Back Issues of ECS Journal Available from Walter J. Johnson, Inc.

The Electrochemical Society has concluded an agreement with Walter J. Johnson, Inc., of New York City, giving them reprint rights to out-of-print volumes of the JOURNAL and authorizing them to handle the sale of back volumes and single issues, with the exception of the current calendar year.

Anyone interested in obtaining back copies of volumes or single issues of the JOURNAL should correspond direct with Walter J. Johnson, Inc., 111 Fifth Ave., New York 3, N. Y.

Sixth Annual Appalachian Underground Corrosion Short Course

The 1961 Appalachian Underground Corrosion Short Course will be held June 6, 7, and 8, 1961, at West Virginia University, School of

Mines, Morgantown, W. Va. Advance registration is not required.

The course covers basic, intermediate, and advanced education of corrosion control practices as related to underground pipe, cable, and water systems. Approximately 69 papers are scheduled, plus field illustrations. A copy of all papers presented, in book form, is sent to all persons attending the course.

Additional information can be obtained from Mr. John H. Alm, Publicity Chairman, Dearborn Chemical Co., 2 Gateway Center, Pittsburgh 22, Pa.

IRE Symposium on Electronic Systems Reliability

The Kansas City IRE Section will sponsor a symposium on "Electronic Systems Reliability" to be held on November 14, 1961 in Kansas City, Mo.

Papers are planned on MTF prediction, reliability evaluation, and process and fabrication techniques to improve reliability. The Technical Program Chairman is Dr. Arthur Goldsmith, director of engineering for Wilcox Electric.

Symposium proceedings will be published and mailed to pre-registrants at least two weeks before the symposium. Speakers will present only an abstract of their papers; about half of each session will be devoted to discussion. An addendum to the proceedings, on the discussion, also is being planned.

Conference on Magnetism and Magnetic Materials

The Seventh Annual Conference on Magnetism and Magnetic Materials will be held in Phoenix, Ariz., November 13-16, 1961, at the Hotel Westward Ho. This conference is sponsored jointly by the American Institute of Electrical Engineers and the American Institute of Physics, in cooperation with the Office of Naval Research, the Institute of Radio Engineers, and the Metallurgical Society of the A.I.M.E.

The deadline for submission of abstracts is August 18. Further details can be obtained from the Local Chairman, Peter B. Myers, Motorola Semiconductor Products Div., 5005 E. McDowell Rd., Phoenix, Ariz.

Yardney Electric Enters Seawater Battery Field

Yardney Electric Corp., which pioneered the development of silver-zinc and silver-cadmium batteries, has entered the seawater battery field, the company announced recently. The battery is expected to find wide use in torpedoes and such antisubmarine warfare applications as sonar and sono buoys.

A Yardney seawater battery was shown for the first time at the Institute of Radio Engineers Convention in New York City, March 20-23. It is a primary (one-shot) unit with silver-chloride and magnesium duplex electrodes. According to Yardney Electric, it will be made available in sizes, ranging from 1 amp-hr to 100 amp-hr capacity, and any voltage, depending on requirements.

The Yardney seawater battery is capable of energy outputs up to 30 whr/lb and 2.5 whr/in.^{3}, and, with proper packaging, can be stored indefinitely and kept in the dry condition.

Semiconductor Wafers Polished Electrochemically

A new electrochemical technique for rapid, scratch-free polishing of germanium and silicon wafers for transistors recently was revealed by M. V. Sullivan of Bell Telephone Laboratories, Murray Hill, N. J. The new polishing method is much faster and more efficient than conventional polishing methods. In addition to the anticipated savings of more than 50% of the polishing cost, there is a distinct improvement in the electrical characteristics of certain types of devices.

One of the major problems in the manufacture of transistors is maintaining an undamaged surface on the semiconductor slice used for the active element of the device. In conventional manufacturing practice, these slices are prepared in four steps. First, they are sawed from a cylindrical single crystal, then they are lapped with coarse abrasive, and polished on optical lapping machines. These three operations produce a smooth, flat surface. In the final step, the slices are etched to remove all the residual mechanical damage to the crystal face caused by abrasive action.

When there are deep scratches from lapping and polishing, the etchant cannot remove all the damage, and poor-quality transistors result. In contrast, electrochemical polishing does not introduce new damage during processing.

In the technique Mr. Sullivan described, semiconductor slices are mounted on a nonconducting disk. After electrical contact is made to the slices, they are placed on a polishing wheel over which an electrolyte flows. When the polishing wheel rotates, a film of electrolyte, whose thickness is determined principally by the viscosity of the electrolyte, separates and automatically maintains the semiconductor at a relatively constant distance from the wheel.

Dilute potassium hydroxide is the electrolyte used for the electropolishing of germanium, and dilute hydrofluoric acid is used for silicon. For n-type material, either germanium or silicon, it is desirable to illuminate the semiconductor surface during electroetching.

The smoothness of the surface obtained by this method is apparent through study of photomicrographs of comparative surfaces. A mechanically polished surface shows distinct scratches when magnified 500 times. These scratches are caused by broken pieces of abrasive and semiconductor, which are ground into the face of the polished slice. On the other hand, semiconductor slices polished by this new technique show no texture that can be associated with surface roughness even under electron-microscope examination at 53,000 power.

December 1961 Discussion Section

A Discussion Section, covering papers published in the January-June 1961 JOURNALS, is scheduled for publication in the December 1961 issue. Any discussion which did not reach the Editor in time for the June 1961 Discussion Section will be included in the December 1961 issue.

Those who plan to contribute remarks for this Discussion Section should submit their comments or questions in triplicate to the Managing Editor of the JOURNAL, 1860 Broadway, New York 23. N. Y., *not later than September 1, 1961.* All discussion will be forwarded to the author(s) for reply before being printed in the JOURNAL.

Announcements from Publishers

"Electrode Processes," Faraday Society Discussions No. 1, 1947. Published by Butterworths, London, 1961. 338 pages; $12.00.

This is a hard-cover reprint of the 1947 General Discussion. Although many of the ideas and statements have been outstripped by events over the last 14 years, this collection of papers and free and uninhibited discussion contains much valuable material for theoretical electrochemists.

"Gmelins Handbook of Inorganic Chemistry, 8th Ed." Published by Verlag Chemie, GmbH., Weinheim/Bergstr., West Germany, 1960. The four volumes reported below all have the German-English table of contents and English heads and subheads for each subdivision. The cutoff date is 1949 with some later references.

Oxygen, Section 4, Air, Active Oxygen, and Ozone. System No. 3. XV + 366 pages, 76 graphs; $53.00—The contents include the physical properties of air; a chapter on atomic oxygen subdivided into formation and preparation, phosphorescence spectrum, and chemical reactions; a section on ozone which includes preparation, physical and chemical properties. The literature on mechanical-thermal properties is reported as late as 1956 in footnotes inserted after type was set.

Sulfur, Part B. Section 2, Sulfur-Oxygen Acids. System No. 9. XXXVIII + 758 pages, 146 graphs; $111.00.—The volume starts with oxoacids of sulfur, with the greatest emphasis on sulfurous and sulfuric acids. The lower sulfur oxygen acids are included, as are the higher acids such as thiosulfuric acid, and di- and polythionic acids. The volume concludes with a section on the SO_2-H_2O system, and the hydrate of SO_2. Although the cutoff date was 1949 for the rest of this 8th Edition, the literature for this volume is covered up to early 1960 for some sections.

Lithium, Supplement Volume. System No. 20. XXXVIII + 525 pages, 73 graphs; $77.50.—This volume surveys the literature from 1926 to 1959. The major subdivisions are occurrence; preparation, with a special section on isotope enrichment; physical and chemical properties, with a special section on electrochemical behavior; and a section on alloys and compounds.

Mercury, Section 1. System No. 34. XVII + 466 pages, 53 graphs; $67.50.—This first section on the mercury system treats occurrence, preparation, and physical properties. Some references are as late as 1952.

"Rare Earth Elements." Published by Academy of Sciences of the U.S.S.R. Translated for the N.S.F. by the Israel Program for Scientific Translation. 356 pages.

This is mainly the collected papers presented at the June 1956 Conference on Rare Earth Elements, at the Institute of Geochemistry and Analytical Chemistry of the Academy of Sciences of the U.S.S.R. The topics covered are primarily the occurrence, separation, and production of the R.E.E., the analysis of these elements, and finally, industrial applications. JOURNAL readers may be interested in the paper entitled "Comparison of Electrochemical Methods of Obtaining Ytterbium."

"Progress in Inorganic Chemistry, Vol. 2." Edited by F. Albert Cotton. Published by Interscience Publishers, Inc., 250 Fifth Ave., New York City, 1960. 399 pages; $10.50.

The second volume in this annual series of review articles covers the following topics: radioactivation analysis in inorganic geochemistry; halides and oxyhalides of elements of groups Vb and VIb; extraction of inorganic compounds into organic solvents; some fluorine compounds of the transition metals; intensities of spectral bands in transition metal complexes; unusual oxidation states of some actinide and lanthanide elements; metal alkoxides.

"An Introduction to Transition-Metal Chemistry: Ligand-Field Theory," by Leslie F. Orgel. Published by John Wiley & Sons, Inc. 440 Park Ave. South, New York City, 1960. 180 pages; $4.50.

The book is a nonmathematical treatment of ligand-field theory for the experimental chemist with little training in quantum mechanics. The first part covers ionic solids and classical coordination chemistry. The second part covers carbonyls, dicyclopentadienyls, etc.

"Cobalt—Chemistry, Metallurgy, and Uses. ACS Monograph 149." Edited by Roland S. Young. Published by Reinhold Publishing Corp., 430 Park Ave., New York City, 1961. VII + 424 pages; $15.00.

This is a reference book broken down into self-contained chapters on various topics. The chapters of possible interest to JOURNAL readers would include those on extractive metallurgy; chemical and physical properties (which includes some data on passivity and corrosion); magnetic, electrical, and electronic applications; and electroplating. Each chapter has its separate bibliography. References and statistics are through 1959.

"Boron—Synthesis, Structure, and Properties." Edited by J. A. Kahn, W. F. Nye, and G. K. Gaule. Published by Plenum Press, Inc., 227 W. 17 St., New York City, 1960. VI + 189 pages; $8.50.

This contains the proceedings of the September 1951 Conference on Boron, sponsored by the U. S. Army Signal Research and Development Agency. The papers concentrate mainly on crystallization, purification, and crystal growth, crystal structure and bonding, and the fundamental physical properties. The papers of interest to JOURNAL readers would include those on preparation of high-purity boron by the hot-wire technique, utilization of boron filaments in vapor-phase distillation of boron, zone methods, zone purification, floating zone melting, semiconductor properties, optical and electrical properties, and oxidation of boron in air at temperatures between 400° and 1300°C.

"Diffused Coatings on Iron and Steel," by N. S. Gorbunov. Published by Academy of Sciences of the U.S.S.R., Moscow, 1958. 165 pages.

The book discusses general conditions for formation of diffusion coatings and the various experimental methods of forming and analyzing diffusion coatings on iron and its alloys, and gives results for various alloys. The experimental results are broken down into chapters, each concerned with a group in the periodic classification. The experimental data concern thickness of layers, corrosion rates, wear hardness, microhardness, etc. There are 110 tables, 116 figures (mostly graphs), and 192 references, most of which refer to early work. The latest references to Russian work are for the year 1957.

"Mathematical Handbook for Scientists and Engineers," Definitions, Theorems, and Formulas for Reference and Review, by Granino A. Korn and Theresa M. Korn. Published by McGraw-Hill Book Co., New York City. 960 pages, 110 tables; $20.00.

"Precision Measurement and Calibration," National Bureau of Standards Handbook 77, issued Feb. 1, 1961. Vol. I—"Electricity and Electronics," 845 pages; $6.00.

Vol. III—"Optics, Metrology, and Radiation," 1025 pages; $7.00. Available from Superintendent of Documents, U. S. Govt. Printing Office, Washington 25, D. C.

"Research Highlights of the National Bureau of Standards," Annual Report 1960. National Bureau of Standards Miscellaneous Publication 237, 189 pages; 65 cents. Available from Superintendent of Documents, U. S. Govt. Printing Office, Washington 25, D. C.

"Design and Construction of a Unit for Measuring Metal Skin Temperatures—Phase I, Theoretical Analysis and Design," Dec. 1960. AEC Report (SC-4461(RR),* 48 pages; $1.50.

"Thermoelectric Refrigerator for the Line Recorder Mass Spectrometer," (Theoretical design), Nov. 1960. AEC Report (GAT-365),* 24 pages; 50 cents.

"Surface Phenomena in Semiconductors and Growth of Semiconductor Crystals," W. A. Albers, Jr., and others, Wayne State University, for Air Force Office of Scientific Research, March 1960. Report PB 161 867,* 35 pages; $1.25.

"The Arc Image Furnace for Growing Semiconductor Crystals," R. P. Poplawsky and J. E. Thomas, Jr., Wayne State University, for Air Force Office of Scientific Research, March 1960. Report PB 161 868,* 106 pages; $2.50.

"Status Report on Thermoelectricity," J. W. Davisson and J. Pasternak, U. S. Naval Research Lab., in collaboration with B. B. Rosenbaum, Bureau of Ships, and P. Maycock, Office of Naval Research, Aug. 1960. Report PB 161 977,* 64 pages; $1.75.

* Order from Office of Technical Services, Business and Defense Services Administration, U. S. Dept. of Commerce, Washington 25, D. C.

"Thermoelectricity Abstracts," U. S. Naval Research Lab., Aug. 1960. Report PB 161 714,* 94 pages; $2.25.

"Ultra-High Resistance Measurements of Plastics," A. R. Blanck, Picatinny Arsenal, U. S. Army, Aug. 1960. Report PB 161 784,* 14 pages; 50 cents.

"Research on New High-Temperature Semiconducting Materials," S. S. Devlin and others, Clevite Corp., for Wright Air Development Div., U. S. Air Force, June 1960. Report PB 161 938,* 157 pages; $3.00.

"Investigation of Physical Properties of Semiconductors," M. E. Caspari, University of Pennsylvania, for Wright Air Development Div., U. S. Air Force, April 1960. Report PB 161 903,* 42 pages; $1.50.

"Research on High-Temperature Ferroelectric Storage Media," G. F. Pulvari, The Catholic University of America, for Wright Air Development Div., U. S. Air Force, April 1960. Report PB 161 805,* 123 pages; $2.75.

"High-Temperature Insulation for Wire," K. N. Harris and J. D. Walton, Jr., Engineering Experiment Station of the Georgia Institute of Technology, for Wright Air Development Div., U. S. Air Force, March 1960. Report PB 161 788,* 40 pages; $1.00.

"Oxidation Behavior and Protective Coatings for Columbium and Columbium-Base Alloys (DMIC Report 123)," W. D. Klopp, Defense Metals Information Center, Jan. 1960. Report PB 151 080,* 97 pages; $2.25.

"High Temperature Oxidation of Iron-Chromium Binary Alloys in Water Vapor. Part 1—A Preliminary Study of the Mechanism of Iron-Chromium Binary Alloys in Water Vapor," C. T. Fujii and R. A. Meussner, U. S. Naval Research Lab., Sept. 1960. Report PB 161 696,* 24 pages; 75 cents.

* Order from Office of Technical Services, Business and Defense Services Administration, U.S. Dept. of Commerce, Washington 25, D. C.

"Corrosion of Metals in Tropical Environments. Part 5—Stainless Steels," B. W. Forgeson and others, U. S. Naval Research Lab., Sept. 1960. Report PB 161 749,* 19 pages; 75 cents.

"Physical Metallurgy of Tungsten and Tungsten Base Alloys," R. H. Atkinson and others, Westinghouse Lamp Div., for Wright Air Development Div., U. S. Air Force, May 1960. Report PB 161 978,* 251 pages; $4.00.

"An Improved DC Current-Interrupter Unit," C. H. Presbrey, Jr., and S. Schuldiner, U. S. Naval Research Lab., July 1960. Report PB 161 437,* 19 pages; 75 cents.

"Measurement of the Thermal Properties of Metals at Elevated Temperatures," R. L. Rudkin and others, U. S. Naval Radiological Defense Lab., May 1960. Report PB 171 185,* 24 pages; 75 cents.

"Organic Semiconductor Study," J. B. Rust and others, Hughes Aircraft Co., for Wright Air Development Div., U. S. Air Force, June 1960. Report PB 171 177,* 58 pages; $1.75.

"Investigation of Organic Semiconductors," G. P. Brown and S. Afterbut, General Electric Co., for Wright Air Development Div., U. S. Air Force, Sept. 1960. Report PB 171 340,* 76 pages; $2.25.

"Ion Exchange Separation and Coulometric Titration of Plutonium in Irradiated Fuel Element Solutions," June 1960. AEC Report HW-66441,* 21 pages; 50 cents.

* Order from Office of Technical Services, Business and Defense Services Administration, U.S. Dept. of Commerce, Washington 25, D. C.

Brief Communications

The JOURNAL accepts short technical reports having unusual importance or timely interest, where speed of publication is a consideration. The communication may summarize results of important research justifying announcement before such time as a more detailed manuscript can be published. Consideration also will be given to reports of significant unfinished research which the author cannot pursue further, but the results of which are of potential use to others. Comments on papers already published in the JOURNAL should be reserved for the Discussion Section published biannually.

Submit communications in triplicate, typewritten double-spaced, to the Editor, Journal of The Electrochemical Society, 1860 Broadway, New York 23, N. Y.

Literature from Industry

Metex T-103, a highly efficient alkaline metal cleaner that provides excellent penetration into deep recesses, rapid wetting of oily surfaces, fast softening and displacing of grease deposits, and complete and rapid emulsification of oily soils, is designed for use on steel, copper, and brass.

Data Sheet No. 40 is available from MacDermid Inc., Waterbury, Conn.

Electro-Gleam 55, a liquid acid electropolish material that works equally well on carbon steel, aluminum, and stainless steel, produces a bright, smooth finish, removes weld burns, deburrs and removes sharp edges, removes stress from metals, improves corrosion resistance, and reduces friction in the finished part. Parts may be used as electropolished or further plated, chromated, or anodized.

Data Sheet No. 81 is available from MacDermid Inc., Waterbury, Conn.

Metex Nickel Activator M-668, an organic activator for nickel that can be used by immersion only or with cathodic current, is a dark, straw-colored liquid which is used in the acid dip before chrome plating. It eliminates nickel passivity, a prominent cause of "clouds" forming under chrome plate.

Data Sheet No. 118 is available from MacDermid Inc., Waterbury, Conn.

Aluminum Etch Compounds. A wide selection of aluminum etch compounds which produce a variety of etched results from coarse grain to extremely fine are fully described in Technical Data Sheets No. 109 and 109-1. Rates of metal removal vary so that an aluminum etch compound can be selected to give any desired result, from soil removal to deep attack for chemical milling.

The data sheets are available from MacDermid Inc., Waterbury, Conn.

Metal Stripping Compounds. New metal stripping compounds that effectively strip electroless nickel coatings from steel, magnesium base alloys, nickel phosphorous, copper, brass, and copper base alloys by immersion only are fully described in a new series of Technical Data Sheets, No. 119, 120, and 121. Called Metex Stripper IN-SP, IN-S, IN-CA, and IN-CB, the products are in dry powder form which is dissolved in water to remove electroless nickel coatings.

The data sheets are available from MacDermid Inc., Waterbury, Conn.

Copperoid M, a complete process for preparing and copper-plating printed circuit boards which require through-hole plating, produces a thin, homogenous copper coating on all plastic and copper surfaces and may be used on all types of copper-clad plastic laminates. It may also be used for metallizing other nonconductors, and for electroforming, electrotyping, electronic, and other such applications.

Data Sheet No. 122 is available from MacDermid Inc., Waterbury, Conn.

New Products

Semiconductor Alloy Kit. A semiconductor alloy kit, catalog No. Z-100, priced at $100, contains over 25,000 semiconductor preforms including the latest alloys used in the industry. Unique new clad metals, such as indium-clad aluminum, are included. There are 24 different alloys for use in both germanium and silicon diodes, rectifiers, and transistors. Other alloys include tin-antimony, lead-silver, indium-germanium, tin-lead-antimony, 99.999% pure indium, aluminum-boron.

The kit is available from Accurate Specialties Co., Inc., 345 Lodi St., Hackensack, N. J.

One-Dip Cadmium Conversion Process. Hanson-Van Winkle-Munning Co., has announced the introduction of Chem-Rite C-55, an inexpensive single-dip chromate conversion coating process for cadmium. It enhances the brightness of the cadmium deposit, produces a clear chromate surface, and is extremely easy to operate. No subsequent leaching is necessary.

Full information is contained in the "Instruction Manual for Chem-Rite C-55," available free on request from Hanson-Van Winkle-Munning Co., Church St., Matawan, N. J.

Glass Microminiature Transistor Enclosure. A new all-glass enclosure for micro-transistors, developed by Corning Glass Works, Corning, N. Y., assures high reliability because of its simplicity. Hermetic seals between the case and cover are ob-

tained with ease by device manufacturers, using a glaze with a low melting point already applied by Corning to the rim of the case. The new package is 60 mils high and only 150 mils in diameter.

Low-Temperature Fluxless Solder, TIN-A-LUM, which melts at extraordinarily low temperature thus eliminating the danger of metal destruction under heat, has been developed for use on aluminum and its alloys, zinc, tin, pewter, magnesium, and other metals, as well as castings. It has good machineability, can be polished and chromium plated, and is an excellent conductor of heat and electricity.

Metals for Industry, Inc., 299 Pavonia Ave., Jersey City N. J., which is placing the product on the market in the United States, has been appointed sole agent for America.

Employment Situations

Positions Available

Consulting Physicist with thorough knowledge of single crystals, float zoning, semiconductor materials, wanted by established Western European company. Annual retainer, daily or project compensation. Work by mail. Indicate background in confidence to *Box A-287, c/o The Electrochemical Society, 1860 Broadway, New York 23, N. Y.*

Four challenging research positions for experienced surface chemists, in fully-equipped laboratory devoted to research and development on aluminum and copper alloys, involving: A. Electrochemical kinetics, adsorption, and oxide film structure investigations related to finishing processes. B. Studies of interfacial surface reactions between polymeric resins and metal oxide surfaces relating to strength and permanence of joints in the adhesive bonding of metals. C. Mechanisms relating to surface phenomena, associated with liquid metal-solid metal inter-action as applied to soldering and brazing. D. Surface and electrochemical reactions effecting the kinetics of general, localized, and stress corrosion processes. Pleasant living, with access to major university. Send reply to R. H. Endriss, Personnel Manager, Olin Mathieson Chemical Corp., 125 Munson St., New Haven, Conn.

Solid-State Chemists — Research and development group seeks chemist or chemical physicist for solid-state work on cathodoluminescent and electroluminescent materials, photoconductors, and chemicals for electronic applications. Candidates should have Ph.D. or equivalent and be capable of independent work. Unexperienced as well as experienced candidates will be considered. Modern and well-equipped laboratories, in northeastern Pennsylvania. Publication of work encouraged. Send résumé to: D. F. Fortney, Technical Services, Chemical and Metallurgical Division, Sylvania Electric Products Inc., Towanda, Pa.

Advertiser's Index

THE ELECTROCHEMICAL SOCIETY, INC.

The Electrochemical Society is an international organization of individuals and companies concerned with or interested in Electrochemistry and allied subjects.

The Society is dedicated to the advancement of the theory and practice of Electrochemistry and related subjects, as shown in the following divisions:

Battery	Electro-Organic
Corrosion	Electrothermics and Metallurgy
Electric Insulation	Industrial Electrolytic
Electrodeposition	Theoretical Electrochemistry
Electronics	

Among the means to this end are the holding of meetings for the reading and discussion of professional and scientific papers on these subjects, the publication of such papers, discussions, and communications as may seem appropriate, and cooperation with chemical, electrical, and other scientific and technical societies.

It is an incorporated society without capital stock. The affairs of the Society are managed by a Board of Directors under a Constitution and Bylaws. Officers are nominated by a nominating committee appointed by the Board of Directors and elected by the members.

Direct all general correspondence and inquiries regarding membership to Society headquarters at 1860 Broadway, New York 23, N. Y.

Officers of the Society

President ..... H. B. Linford
Past President ..... R. A. Schaefer
Vice-President ..... F. L. LaQue
Vice-President ..... W. J. Hamer
Vice-President ..... L. I. Gilbertson
Treasurer ..... E. G. Enck
Secretary ..... I. E. Campbell

The Electrochemical Society

Patron Members

Aluminum Co. of Canada, Ltd.,
Montreal, Que., Canada

International Nickel Co., Inc.,
New York, N. Y.

Olin Mathieson Chemical Corp.,
Chemicals Div., Industrial Chemicals
Development Dept., Niagara Falls, N. Y.

Union Carbide Corp.
Divisions:
Union Carbide Metals Co.,
New York, N. Y.
National Carbon Co., New York, N. Y.

Westinghouse Electric Corp., Pittsburgh, Pa.

Sustaining Members

Air Reduction Co., Inc.,
New York, N. Y.

Ajax Electro Metallurgical Corp.,
Philadelphia, Pa.

Allen-Bradley Co., Milwaukee, Wis.

Allied Chemical Corp.
Solvay Process Div., Syracuse, N. Y.
General Chemical Div., Morristown, N. J.

Alloy Steel Products Co., Inc., Linden, N. J.

Aluminum Co. of America,
New Kensington, Pa.

American Metal Climax, Inc.,
New York, N. Y.

American Potash & Chemical Corp.,
Los Angeles, Calif. (2 memberships)

American Smelting and Refining Co.,
South Plainfield, N. J.

American Zinc Co. of Illinois,
East St. Louis, Ill.

American Zinc, Lead & Smelting Co.,
St. Louis, Mo.

American Zinc Oxide Co., Columbus, Ohio

M. Ames Chemical Works, Inc.,
Glens Falls, N. Y.

Armco Steel Corp., Middletown, Ohio

Basic Inc., Maple Grove, Ohio

Bell Telephone Laboratories, Inc.,
New York, N. Y. (2 memberships)

Bethlehem Steel Co., Bethlehem, Pa.
(2 memberships)

Boeing Airplane Co., Seattle, Wash.

Burgess Battery Co., Freeport, Ill.
(4 memberships)

Canadian Industries Ltd., Montreal, Que.,
Canada

Carborundum Co., Niagara Falls, N. Y.

Catalyst Research Corp., Baltimore, Md.

Columbian Carbon Co., New York, N. Y.

Columbia-Southern Chemical Corp.,
Pittsburgh, Pa.

Consolidated Mining & Smelting Co. of
Canada, Ltd., Trail, B. C., Canada
(2 memberships)

Continental Can Co., Inc., Chicago, Ill.

Cooper Metallurgical Associates, Cleveland,
Ohio

Corning Glass Works, Corning, N. Y.

Diamond Alkali Co., Painesville, Ohio

Dow Chemical Co., Midland, Mich.

Wilbur B. Driver Co., Newark, N. J.
(2 memberships)

E. I. du Pont de Nemours & Co., Inc.,
Wilmington, Del.

Eagle-Picher Co., Chemical Div., Joplin, Mo.

Eastman Kodak Co., Rochester, N. Y.

Thomas A. Edison Research Laboratory, Div.
of McGraw-Edison Co., West Orange, N. J.

Electric Auto-Lite Co., Toledo, Ohio
C & D Division, Conshohocken, Pa.

Electric Storage Battery Co., Yardley, Pa.

Englehard Industries, Inc., Newark, N. J.
(2 memberships)

The Eppley Laboratory, Inc., Newport, R. I.
(2 memberships)

Exmet Corp., Tuckahoe, N. Y.

Fairchild Semiconductor Corp., Palo Alto,
Calif.

Food Machinery & Chemical Corp.
Becco Chemical Div., Buffalo, N. Y.
Westvaco Chlor-Alkali Div., South
Charleston, W. Va.

Foote Mineral Co., Paoli, Pa.

Ford Motor Co., Dearborn, Mich.

General Electric Co., Schenectady, N. Y.
Chemistry & Chemical Engineering
Component, General Engineering
Laboratory
Chemistry Research Dept.
General Physics Research Dept.
Metallurgy & Ceramics Research Dept.
Aircraft Accessory Turbine Dept.,
West Lynn, Mass.

General Instrument Corp., Newark, N. J.

(Sustaining Members cont'd)

General Motors Corp.
Delco-Remy Div., Anderson, Ind.
Guide Lamp Div., Anderson, Ind.
Research Laboratories Div., Warren, Mich.
General Telephone & Electronics Laboratories Inc., Bayside, N. Y. (2 memberships)
Gillette Safety Razor Co., Boston, Mass.
Globe-Union, Inc., Milwaukee, Wis.
Gould-National Batteries, Inc., Minneapolis, Minn.
Grace Electronic Chemicals, Inc., Baltimore, Md.
Great Lakes Carbon Corp., New York, N. Y.
Hanson-Van Winkle-Munning Co., Matawan, N. J. (2 memberships)
Harshaw Chemical Co., Cleveland, Ohio (2 memberships)
Hercules Powder Co., Wilmington, Del.
Hewlett-Packard Co., Palo Alto, Calif.
Hill Cross Co., Inc., West New York, N. J.
Hoffman Electronics Corp., Semiconductor Div., El Monte, Calif. (2 memberships)
Hooker Chemical Corp., Niagara Falls, N. Y. (3 memberships)
Hughes Aircraft Co., Culver City, Calif.
International Business Machines Corp., Yorktown Heights, N. Y.
International Minerals & Chemical Corp., Skokie, Ill.
ITT Federal Laboratories, Div. of International Telephone & Telegraph Corp., Nutley, N. J.
Jones & Laughlin Steel Corp., Pittsburgh, Pa.
K. W. Battery Co., Skokie, Ill.
Kaiser Aluminum & Chemical Corp.
Div. of Chemical Research, Permanente, Calif.
Div. of Metallurgical Research, Spokane, Wash.
Kawecki Chemical Co., Boyertown, Pa.
Kennecott Copper Corp., New York, N. Y.
Libbey-Owens-Ford Glass Co., Toledo, Ohio
Mallinckrodt Chemical Works, St. Louis, Mo.
P. R. Mallory & Co., Indianapolis, Ind.
Merck & Co., Inc., Rahway, N. J.
Metal & Thermit Corp., Detroit, Mich.
Miles Chemical Co., Div of Miles Laboratories, Inc., Elkhart, Ind.
Minnesota Mining & Manufacturing Co., St. Paul, Minn.
Monsanto Chemical Co., St. Louis, Mo.
Motorola, Inc., Chicago, Ill.
National Cash Register Co., Dayton, Ohio
National Lead Co., New York, N. Y.
National Research Corp., Cambridge, Mass.
National Steel Corp., Weirton, W. Va.
North American Aviation, Inc., Rocketdyne Div., Canoga Park, Calif.
Northern Electric Co., Montreal, Que., Canada
Norton Co., Worcester, Mass.
Ovitron Corp., Long Island City, N. Y.
Peerless Roll Leaf Co., Inc., Union City, N. J.
Pennsalt Chemicals Corp., Philadelphia, Pa.
Phelps Dodge Refining Corp., Maspeth, N. Y.
Philco Corp., Philadelphia, Pa.
Philips Laboratories, Inc., Irvington-on-Hudson, N. Y
Potash Co. of America, Carlsbad, N. Mex.
Radio Corp. of America
Tube Div., Harrison, N. J.
RCA Victor Record Div., Indianapolis, Ind.
Ray-O-Vac Co., Madison, Wis.
Raytheon Co., Waltham, Mass.
Reynolds Metals Co., Richmond, Va.
Rheem Semiconductor Corp., Mountain View, Calif.
Schering Corporation, Bloomfield, N. J.
Shawinigan Chemicals Ltd., Montreal, Que., Canada
Speer Carbon Co.
International Graphite & Electrode Div., St. Marys, Pa.
Sprague Electric Co., North Adams, Mass.
Stackpole Carbon Co., St. Marys, Pa.
Stauffer Chemical Co., New York, N. Y.
Tennessee Products & Chemical Corp., Nashville, Tenn.
Texas Instruments, Inc., Dallas, Texas
Metals and Controls Corp., Attleboro, Mass.
Three Point One Four Corp., Yonkers, N. Y.
Titanium Metals Corp. of America, Henderson, Nev.
Tung-Sol Electric Inc., Newark, N. J.
Udylite Corp., Detroit, Mich. (4 memberships)
Universal-Cyclops Steel Corp., Bridgeville, Pa.
Upjohn Co., Kalamazoo, Mich.
U. S. Steel Corp., Pittsburgh, Pa.
Victor Chemical Works, Chicago, Ill.
Western Electric Co., Inc., Chicago, Ill.
Wyandotte Chemicals Corp., Wyandotte, Mich.
Yardney Electric Corp., New York, N. Y.